ESTIMATING HYDRAULIC CONDUCTIVITIES THROUGH THE MEASUREMENT OF STREAMING POTENTIALS

Jemias Clifford Mazibuko

Submitted in fulfilment of the requirements for the degree

Magister Scientiae in Geohydrology

in the

Faculty of Natural and Agricultural Sciences

(Institute for Groundwater Studies)

at the

University of the Free State

Supervisor: Dr Francois Fourie

January 2019

DECLARATION

I, Clifford Jemias Mazibuko, hereby declare that the dissertation hereby submitted by me to the Institute for Groundwater Studies in the Faculty of Natural and Agricultural Sciences at the University of the Free State, in fulfilment of the degree of Magister Scientiae, is my own independent work. It has not previously been submitted by me to any other institution of higher education. In addition, I declare that all sources cited have been acknowledged by means of a list of references.

I furthermore cede copyright of the dissertation and its contents in favour of the University of the Free State.

Jemias Clifford Mazibuko

31 January 2019

ACKNOWLEDGEMENTS

The product of this work is a special dedication to my pillars of joy, the women part of my life, my wife Patience Mazibuko and my angelic daughters Zinhle, Zandile and Zipho.

The following persons and institutions are greatly appreciated for their contribution towards the investigations and eventual completion of this study:

- My supervisor and mentor, Dr Francois Fourier for his guidance, insightful advice and patience, without which that integral part of the research would have not been a success. The equipment and part of the resources used were made available by the Institute of Groundwater Studies (IGS) through his organisation.
- Dr Modreck Gomo for all your expositions in groundwater hydraulics and general guidance. Contacts with you, were a motivation to complete the study.
- My employer Water Resources Consultants Pty Ltd, Botswana and Zambia for availing me with time to carry out the study amid busy schedules of professional work.
- My relatives who played a role during the period of this research work: my parents Phildah and Krispin Mazibuko, sister Mercy Mazibuko and family, borthers Tawanda, Edward and Themba Mazibuko and their families. Your moral, spiritual and financial guidance is greatly appreciated.
- Dr Emmanuel Sakala, my long-time friend, colleague and pace setter, your encouragement fuelled the quest to complete this research and hopefully until PHD qualification.

Much appreciation goes to Prof Heinson Graham, whose first contact with me in 2008 via emails instilled the research interest in characterizing groundwater flow using streaming potentials. Self- Potential method is regarded as the ugly duckling of geophysics but the scientific expositions made by Revil Andre and Prof Jardani Abderrahim, and Revil in modern self-potential theory through their book called “The self-potential theory” made me to fall in love with this non-invasive flow sensor. I have never met these folks but their work is an encouragement and is felt from a continental distance.

TABLE OF CONTENTS

LIST OF APPENDICES

LIST OF FIGURES

LIST OF TABLES

CHAPTER 1:
INTRODUCTION

1.1 RESEARCH FRAMEWORK

Over the last few decades, the availability of surface water in rivers has dropped to levels that have threatened water supply security due to low surface water recharge, over usage of water and pollution of surface water sources. Dennis & Dennis (2012) stated that South Africa is currently facing high levels of water stress due to increasing levels of water scarcity and water quality problems. Climate change effects have imposed additional stresses on water resources (Makwiza, et al., 2018). Roberts (2010) predicted that water demand will overshoot supply in South Africa by 2025. This increase in water scarcity has caused water experts to shift their focus from surface water to groundwater as the primary source of water.

The total amount of water on planet Earth occurs on or near the Earth's surface in many forms, as listed in Table 1.1. Unfortunately, of the amount of water available to human life, only 2.5% of the total volume of water is classified as fresh water. Fresh water is inarguably the most important basic need for the existence of human life as most life activities revolve around the supply of fresh water (from consumption to industry). The demand for fresh water supply has increased rapidly over the past years due to expansion in industrialization and more commercial farming activities. These economic activities have heavily relied on surface water resources (such as rivers, dams and lakes), and have resulted in depletion of the surface water resources to their limits. However, according to Fitts (2002) the fortunate part is that of the 30.2% of fresh water volume available for productive extraction, surface water constitutes only 2.5% and the remaining 97.5% occurs as groundwater. This implies that groundwater forms the largest source of fresh water available for consumption.

The problem is that, it is difficult to most water users to quantify the amount of groundwater resources for reliable water budgets, especially in Karoo aquifers. According to Woodford & Chevallier (2002), the general perception of water experts and users is that there is limited groundwater storage in Karoo aquifers. However, it was observed that the Karoo aquifers contain considerable amount of water and therefore the problem

is more of identification and management of groundwater resources, rather than the yield of Karoo aquifers.

Table 1.1: Distribution of Water in Earth's Reservoirs

Reservoir	Percentage of all Water	Percentage of Fresh Water	Percentage of Fresh Water Available for Human Use
Oceans	96.5	-	-
Glacial ice	1.8	69.6	-
Groundwater	1.68	29.4	30.16
Surface water	0.018	0.76	
Others	0.002	0.24	-

Fitts (2002)

Management of groundwater resources demands a better understanding of aquifer characteristics. However, the subsurface heterogeneity introduced by fracturing mechanisms in Karoo aquifers presents challenges to understanding aquifer characteristics. These problems include the assessment of groundwater supply and sustainability and numerical modelling of groundwater flow and contaminant transport (Ball *et al.,* 2010). The effort from many research scientists in having a better understanding of aquifer characteristics has propelled an increase in the need to develop alternative techniques for hydrogeological investigations.

1.1.1 Problem Statement

It is difficult to estimate the hydraulic parameters, especially hydraulic conductivity of near-surface sediments or a fractured media because of their heterogeneous nature. Heterogeneous aquifers require high resolution measurements of parameters used in estimating aquifer behaviour or characteristics.

The primary parameter used for characterising aquifers is the hydraulic conductivity. In-situ hydraulic conductivity is estimated through measurements of aquifer drawdown induced during pumping from a borehole; this procedure is called a pumping test. The common practice is to conduct the drawdown measurements in a single well test and extrapolate the measurements to a greater volume of the aquifer because only a few wells are available for a given field test. This results in a limited amount of information being obtained to infer the pattern of groundwater flow or the distribution of hydraulic parameters. Over the years, this form of measurement has been giving reliable point estimations for groundwater flow in homogeneous media, but in principle it is not

accurate to extrapolate single measurements to a greater volume because the fractured rock systems are heterogeneous.

The best way in this in-situ approach is to monitor drawdown in observation boreholes, however, it is costly to install observation boreholes. When many observation wells are installed into the aquifer, they disturb the natural setup of the hydrological system as they act as highly permeable vertical drains (Titov *et al.*, 2005). In addition, even if observation boreholes are available, the information obtained is usually not enough to provide a volumetric distribution of hydraulic head with time, therefore there is need for additional data to fill in the gap of missing spatial information.

1.1.2 Study Motivation

In hydrogeological investigations, geophysical techniques have been widely used to obtain large volumes of information on the subsurface at low cost and these methods are non-intrusive. In the last two decades, geophysical approaches have intensely been used to estimate groundwater flow parameters.

When water moves through pores and fractures in the aquifer, it produces an electric potential, called the streaming potential (S_tP), commonly referred to as self-potentials (SP) along the flow path (Birch, 1993; Doussan *et al.*, 2002; Maineult *et al.*, 2005; Sill, 1983). Birch (1998) demonstrated that digital filtering of self-potential anomalies can produce images of the water table. Therefore, streaming potential measurements offer an alternative method for characterizing hydrological systems. Measurement of streaming potentials associated with groundwater flow for hydrologic characterization of the subsurface is cheap and allows for non-invasive and spatially dense grids for system state measurements (which is not the case with observation wells). The streaming potential method remains the only non-invasive method that can simultaneously characterise the geometry and the dynamics of ground water flow in real time (Rizzo *et al.*, 2004).

Many researches have shown the possibility of using this electrical signal for the quantitative estimation of the hydrogeological parameters of a porous medium. They have demonstrated that there is a correlation between the self-potential signals and the values of the hydraulic head (Revil *et al.*, 2003). Rizzo *et al.* (2004) and Jardani *et al.* (2008) further demonstrated a successful integral approach to real time hydrological parameter investigations using a combination of hydraulic and geophysical measurements during pumping tests. Other experiments have gone further to compute semi-analytical solutions

for the transient streaming potential response of an unconfined and a confined aquifer during continuous constant rate pumping. These efforts reveal that, where observation wells are unavailable for estimation of hydraulic parameters, streaming potential data recorded at land surface are usable for preliminary estimates of aquifer hydraulic conductivity and specific storage.

Several of these studies have been performed by different scholars and researchers in Europe, Australia, Asia and America but according to the author's knowledge no similar studies have to date been done in Africa. This has motivated the author to apply the techniques of streaming potential with locality in an African hydrogeological setting.

1.2 AIM AND OBJECTIVES

The fundamental physical principles guiding the link between groundwater flow and streaming potential have been demonstrated by many researchers in laboratory environments of limited volume scale, mostly representative of only a porous medium.

In this research, the main aim is to demonstrate the applicability of estimating the hydraulic conductivity using streaming potentials in fractured and porous Karoo aquifers.

The objectives of the study are:

i. To review literature on the interaction of fluids with porous and fractured media at the grain boundary scale, and the relationship with electric potentials.

ii. To understand further the relationship between streaming potential and hydraulic head.

iii. To review and understand the characteristic hydraulic behaviour of Karoo aquifers

iv. To develop the equipment which can measure streaming potentials around a pumping well.

v. To measure streaming potential signals around a pumping well during a constant rate drawdown test.

vi. To interpret electrokinetic signals in terms of hydraulic conductivity within the cone of depression.

1.3 RESEARCH METHODOLOGY

The approach of the study is structured in five research steps summarised as:

1. **Theory review:** The self-potential theory is reviewed in relation to Darcy's law from Poisson's equation to coupled flow problem which is a governing relationship between the S_tP and hydraulic head is developed to guide the interpretation of SP data in hydrogeological context. The resultant is a derivation of analytical solutions for radial coupled flow, for both steady state and un-steady steady conditions.
2. **Site characterization:** A review of the geology and geohydrology of the study test sites complimented with a physical borehole inventory and hydraulic tests is performed with the aim of understanding the geometry and behaviour of the aquifer systems. The resultant is a geohydrological framework which facilitated the planning of streaming potential field measurements.
3. **Field measurements:** Constant rate tests and recovery tests (drawdown-time measurements) are performed on a pumping borehole and monitored in the neighbouring boreholes and piezometers. Streaming potential is monitored with spatial reference on selected monitoring points during the pumping tests at two study sites. The sites represent a fractured Karoo aquifer and porous Karoo aquifer.
4. **Data interpretation:** The measured streaming-potential signal is analysed in order to find a spatial drawdown distribution. When spatial drawdown has been determined, these data are interpreted in a hydrogeological context. Hydraulic conductivity is estimated using both measured drawdown and streaming potential data. Estimation of hydraulic conductivity from streaming potential and computation of drawdown are performed using the governing coupled flow analytical solutions derived in the theory review.
5. **Method validation:** In order to validate the efficiency of the streaming-potential method for estimation of hydraulic conductivity during pumping test, the computed drawdown from SP data are compared to the measured drawdown. The second level of validation compares the hydraulic conductivity values estimated from streaming potential to the hydraulic conductivity values estimated from measured drawdown.

The general study framework showing the research work flow from the objectives to the research output is summarised in Figure 1.1.

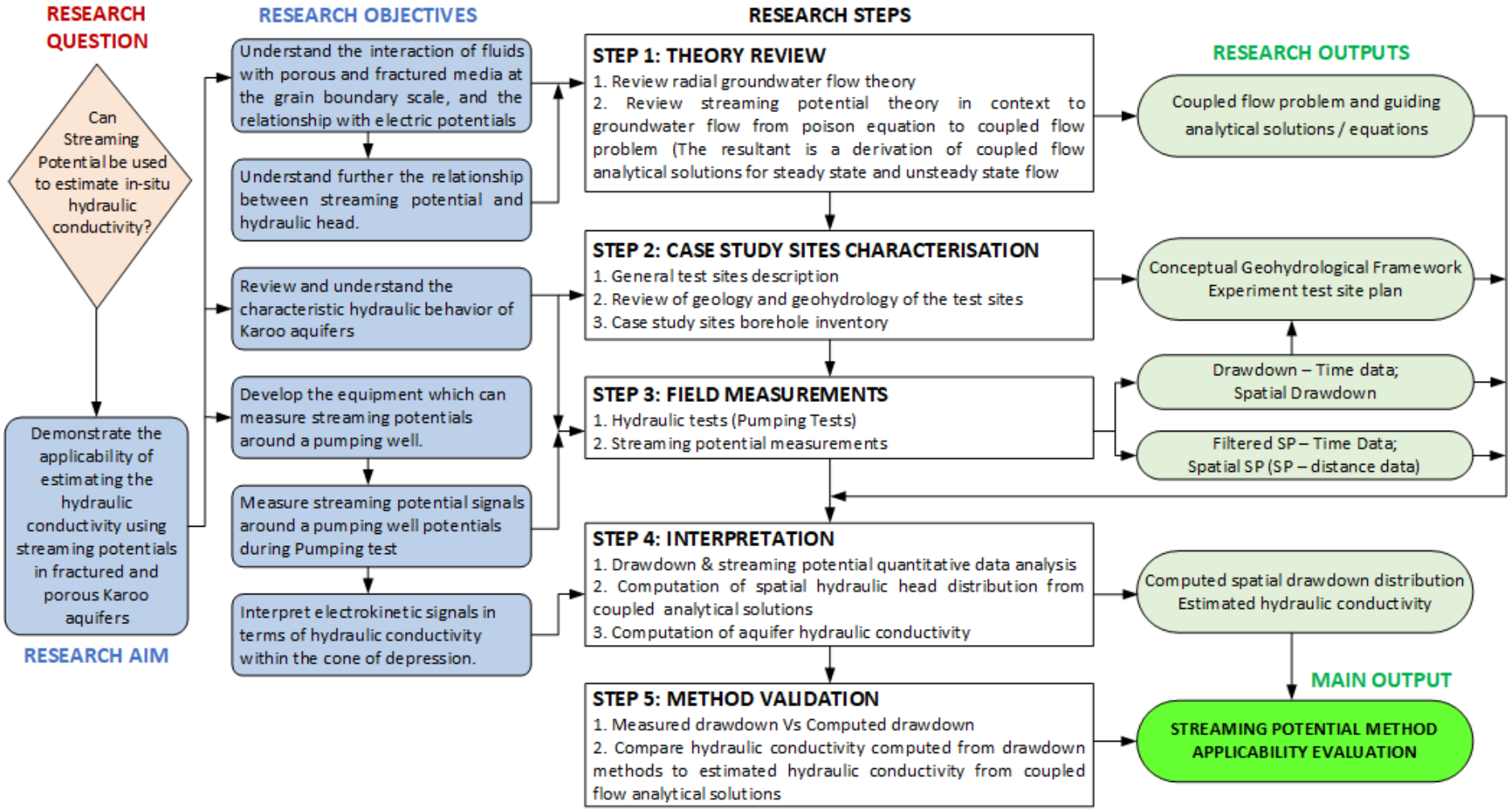

Figure 1.1: Research study approach

1.4 LOCATION OF THE STUDY AREA

The research was performed in two case study sites representing a fractured Karoo aquifer and a porous Karoo aquifer, located in Bloemfontein, Free State Province of South Africa. The first case study site is a fractured aquifer located at the University of Free State in Bloemfontein at a test site popularly known as the Campus Test Site. The second case site is a porous alluvial aquifer in the catchment of Modder River downstream of Krugersdrift Dam, which is situated about 35 km north-west of the city of Bloemfontein. This site is referred to as the Krugersdrift Test Site. The locations of these two test sites are shown in Figure 1.2.

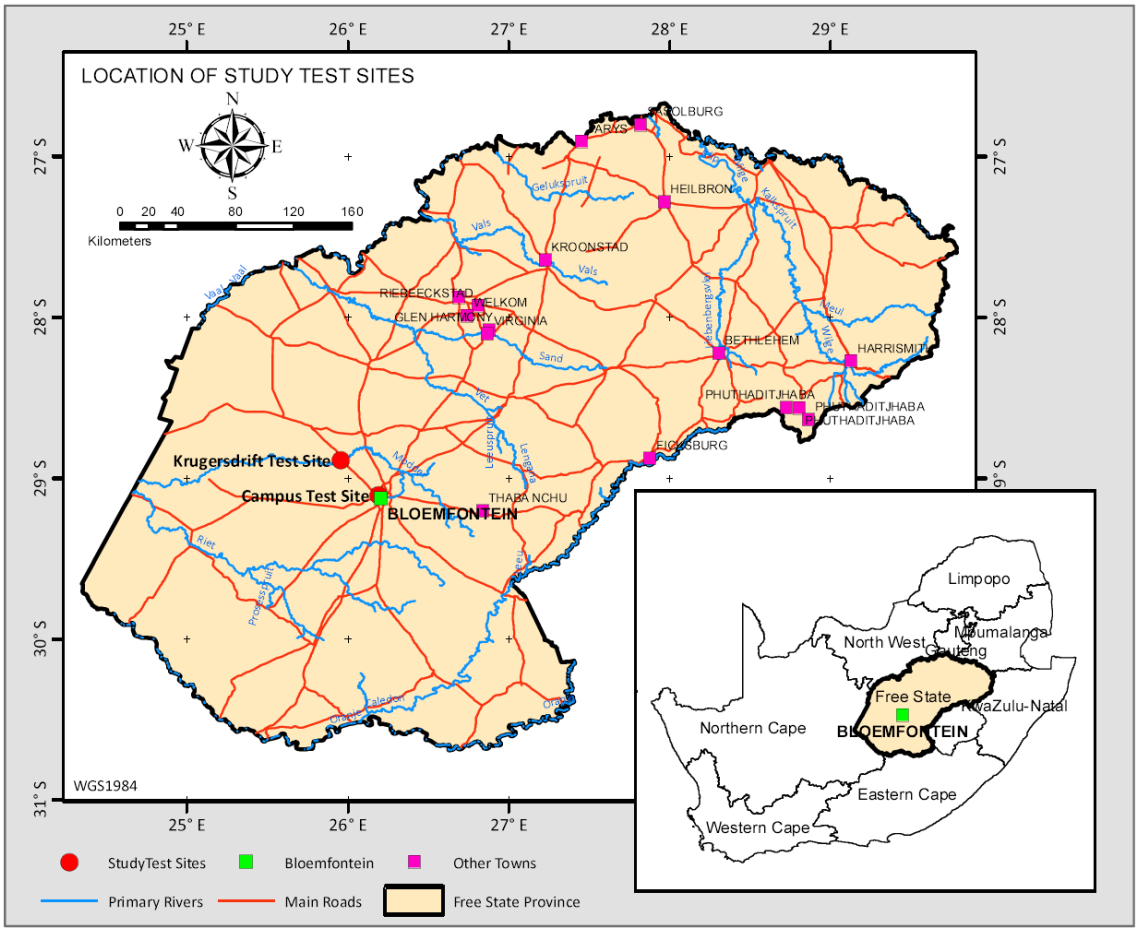

Figure 1.2: Locations of the study test sites

Since the research is purely experimental, the sites were chosen primarily because observation boreholes are already installed within the research sites, which allows for comparison of drawdown measurements with streaming potential estimations.

1.5 OUTLINE OF THE DISSERTATION

This dissertation is composed of six chapters that are briefly discussed below.

Chapter 1: Introduction

Chapter one highlights the gaps and limitations that exist in determining the in-situ hydraulic conductivity using pumping test and the need of adding in fill data through additional or alternative measurements of streaming potentials around a pumping well. It introduces the study research by highlighting its aim, objectives, general research methodology and outlining the location of the study area. The chapter concludes by giving a synopsis of the structure of the dissertation.

Chapter 2: Characteristics of the Study Area

This chapter introduces the study area by giving a general description of its climate, drainage, regional geology and geohydrology of the Supergroup within which the study area is located. A critical review of the geological and geohydrological characteristics of the Karoo Supergroup is performed in this chapter. The presentations used are extracted from reports of previous work conducted to investigate Karoo aquifers by different researchers particularly Botha *et al*. (1998) and Woodford & Chevallier (2002).

Chapter 3: Groundwater Flow and Streaming Potential Theory

This chapter reviews groundwater flow and streaming potential theory in context to a pumping well. The goal is to provide an understanding of the relationship between electro-kinematic signals and hydraulic head during a pumping test. In order to afford interpretation framework of streaming potential in relation to hydraulic parameters, groundwater flow theory for steady-state flow and unsteady-state flow is also reviewed and the resultant is a presentation of derivation of a coupled groundwater flow analytical solution as provided by Rizzo *et al.* (2004).

Chapter 4: Methods and Materials

The approach, methods and materials used in conducting the research experiments are described in this chapter. It explains how the experimental data was collected and the instruments used, highlighting all precautions taken and challenges encountered. It lastly scripts the processing and interpretation techniques that were adopted to facilitate interpretation of streaming potential signals in relation to groundwater flow.

Chapter 5: Site Characterisation

The chapter begins by exposing the conditions influencing the geohydrology character of each study site. It concludes by discussing the aquifer flow regimes of each study site. The desk work performed in this chapter forms is a guide and a build-up on the data set interpretation framework.

Chapter 6: Results and Discussion

The results and discussion of the field experiments conducted at the two study sites are presented in this chapter. The results include the raw data from drawdown and streaming potential measurements performed during pumping tests at the study test sites, the processing procedure and analysis of these datasets. A critical analysis of streaming potential is performed to compute the hydraulic conductivity using two approaches: the coupled flow problem and the analytical solutions derived by Rizzo *et al.* (2004). This is the chapter where the primary datasets of the study are interpreted in relation to groundwater flow problem. Validation of the data is performed by generation of the spatial drawdown using the analytical solutions and comparing to the drawdown measured during the pumping tests. The chapter concludes by performing an applicability analysis of the streaming potential in estimating hydraulic conductivity.

Chapter 7: Conclusion and Recommendations

A summary of the findings obtained from the applicability analysis of the method to geohydrology investigations is presented. It ends by making recommendations for future work in order to develop a more workable approach of streaming potential method for both research and commercial reasons.

CHAPTER 2:
CHARACTERISTICS OF THE STUDY AREA

2.1 INTRODUCTION

This chapter introduces the study area by giving a general description of its climate, drainage, regional geology and geohydrology of the Supergroup within which the study area is located. A review of the geology and geohydrological setting is important to provide an early opportunity of understanding the groundwater system of the study area. A conceptual understanding of the geology provides a best means of characterising groundwater flow and its storage. The research area is located within the Karoo Supergroup in South Africa, therefore this chapter discusses the geology of the Karoo Supergroup and its geohydrological properties.

2.2 GENERAL CHARACTERISTICS

2.2.1 Climate

Climate plays a role in influencing water resources and Southern Africa is under threats of climate change. The effects being low rainfall, high temperatures, prolonged dry seasons resulting in less recharge in aquifer and surface water bodies. Prolonged dry seasons complimented with high temperatures (evaporation) will promote the emergence of evaporates resulting in salinity. Therefore, it is important to highlight the climatic characteristic of the study area. South Africa has a wider variety of climates than most other countries in sub-Saharan Africa. The country has been divided into 24 climate regions, as listed in Table 2.1.

Bloemfontein falls in the region of the Dry Highveld Grassland. It receives predominantly summer rainfall (October-April) with mean annual precipitation of approximately 548 mm (Figure 2.1). The warmest month of the year is January, with an average temperature of 22.7°C and July is the coldest month with an average temperature of 8.3°C, (Figure 2.2). Evaporation in this quaternary catchment is estimated to be in the range of 1 800 mm to 2 000 mm (Pitman, *et al.,* 1998).

Table 2.1: The climatic region of South Africa

1. Northern Arid Bushveld	13. South-Eastern Coast Grassland
2. Central Bushveld	14. Eastern Mountain Grassland
3. Lowveld Bushveld	15. Alpine Heathland
4. South-Eastern Thornveld	16. Great and Upper Karoo
5. Lowveld Mountain bushveld	17. Eastern Karoo
6. Eastern Coastal Bushveld	18. Little Karoo
7. KwaZulu-Natal Central Bushveld	19. Western Karoo
8. KwaZulu Bushveld	20. West Coast
9. Kalahari Bushveld	21. North-Western Cape
10. Dry Highveld Grassland	22. South-Western Cape
11. Moist Highveld Grassland	23. Southern Cape
12. Eastern Grassland	24. Southern Cape Forest

Figure 2.1 and Figure 2.2 respectively show the rainfall and temperature pattern of Bloemfontein.

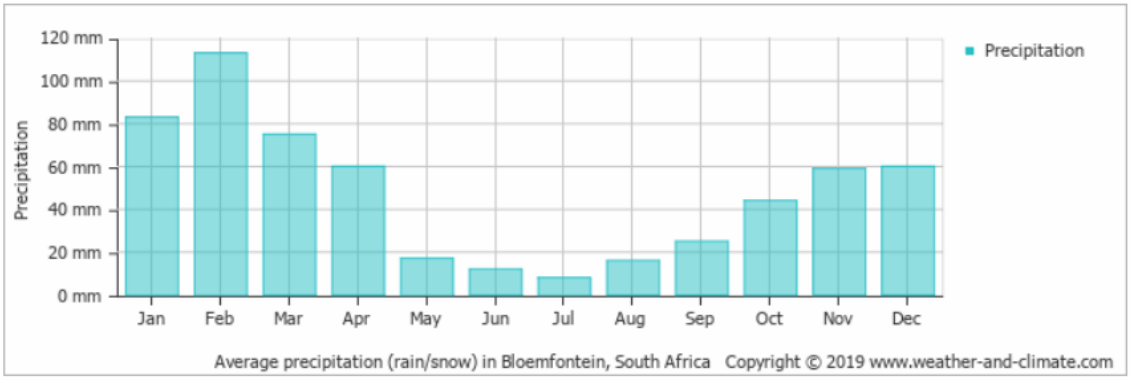

Figure 2.1: Rainfall pattern of Bloemfontein

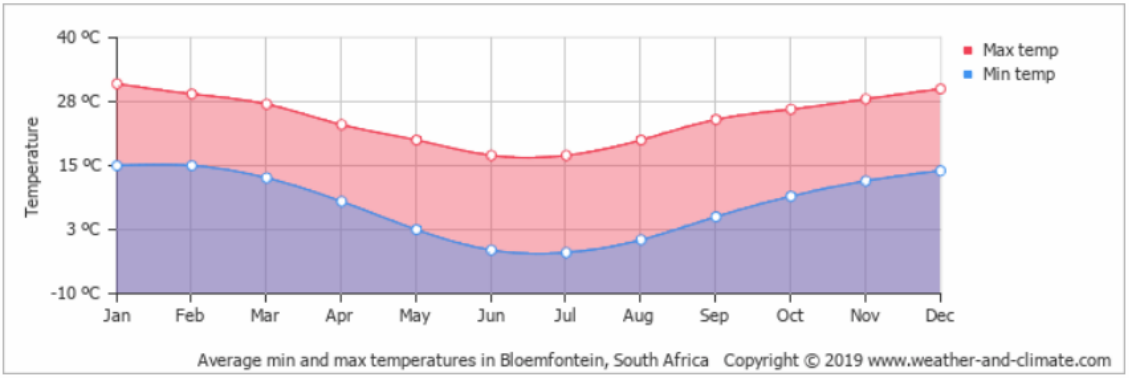

Figure 2.2: Temperature variations in Bloemfontein

2.2.2 Topography and Drainage

The two test sites chosen for the study are within the Modder River catchment and therefore its drainage pattern is mainly influenced by the westward draining Modder River (Figure 2.3). The main tributaries of Modder River in the surrounding areas of Bloemfontein are north-westerly draining Kaal Spruit and northward draining Renoster Spruit. Further down Krugersdrift Dam in the Bloemfontein Nature Reserve site, Modder River flows through a very low gradient terrain where numerous pans are found.

Bloemfontein is characterised by a wide spread flat topography with elevations varying from 1 100 to 1 450 metres above mean sea level (mamsl) (Figure 2.3).

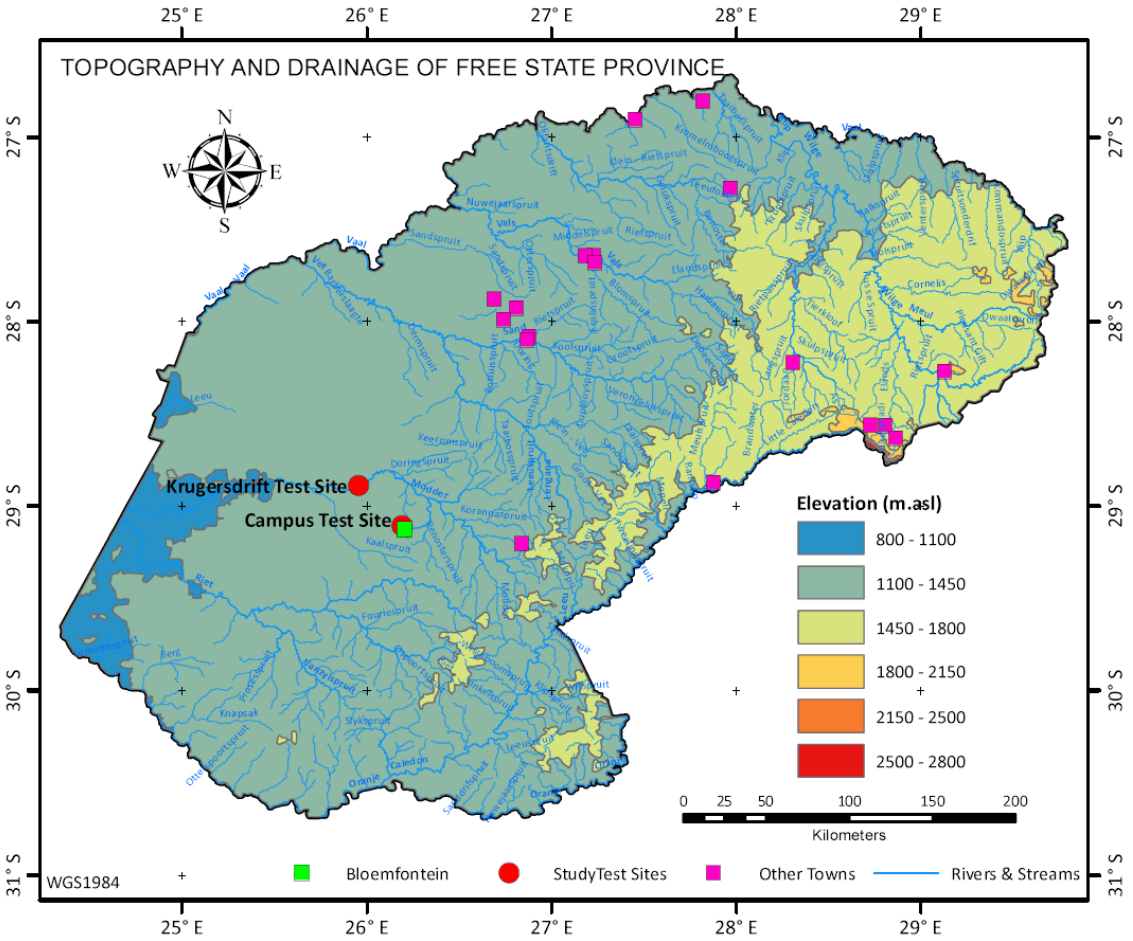

Figure 2.3: Topography and drainage of the Free State Province

The topographic contours of the Campus Test Site gently slope towards the north-east with elevations varying from 1410 to 1413 metres above mean sea level as shown in Figure 2.4 (Botha *et al.*, 1998). The topography at Krugersdrift Test Site slopes towards Modder River, influencing the groundwater flow direction at the test site (Figure 2.5).

Boreholes 1 to 9 are located on a gently sloping terrain just before the steep surface drops into the riverbed height.

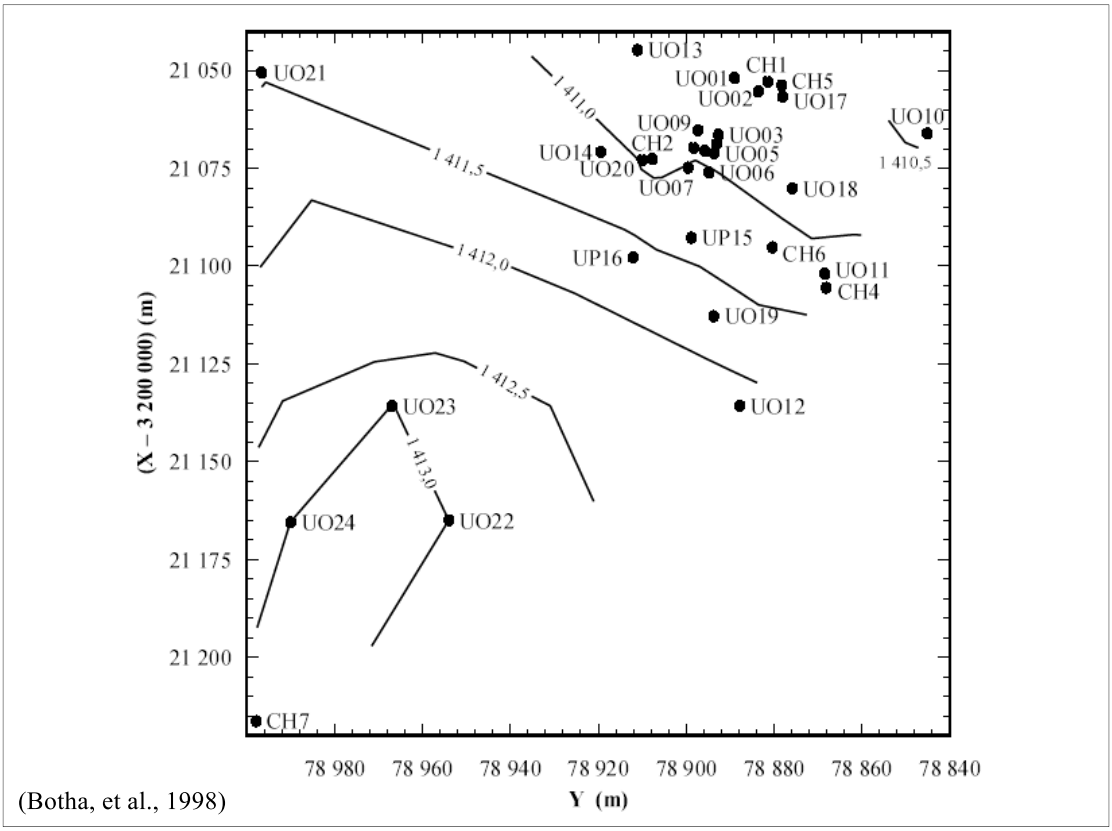

(Botha, et al., 1998)

Figure 2.4: Topographic contours of the Campus Test Site

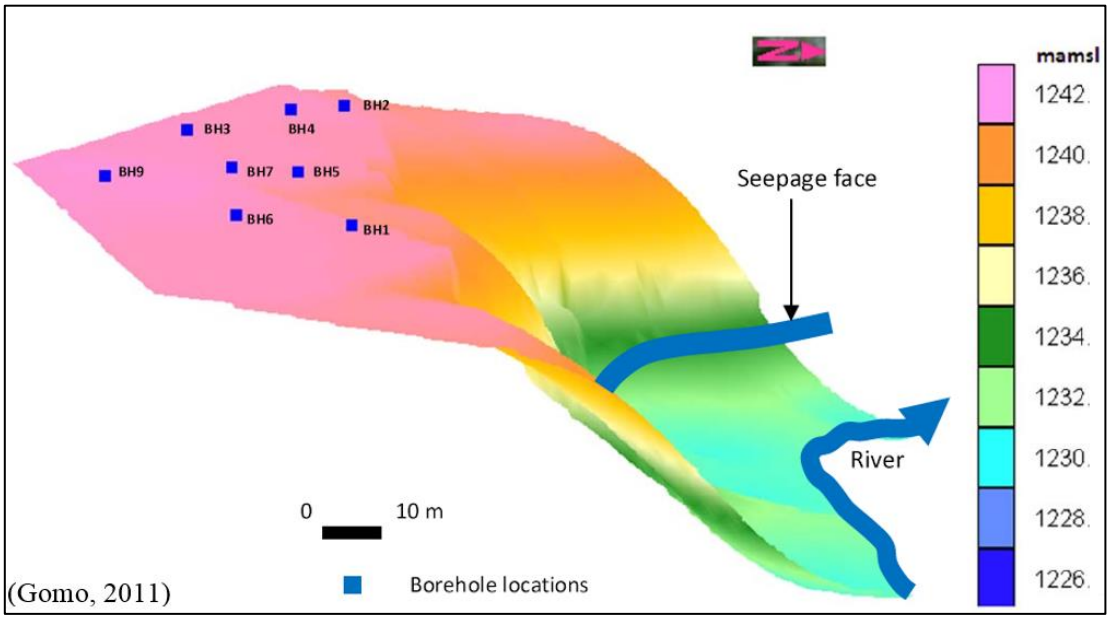

(Gomo, 2011)

Figure 2.5: Topography at the Krugersdrift Test Site from the riparian zone to the river

2.2.3 Vegetation

The vegetation of the study area is part of the Grassland Biome and the Nama Karoo Biome. Bloemfontein and its surrounding areas are dominated by a single layer of grasses and its amount of cover depends on rainfall and the degree of grazing. In most areas, trees are absent, except in a few localized habitats such as the river banks and along the dolerite structures (Gomo, 2011). In siting for water supply wells, geohydrologists have approximated the position of dolerite intrusion structures by analysing the type, physical appearance and the density of the vegetation. The Campus Test Site is located within the campus in a built-up area, therefore its natural vegetation has been transformed by urbanisation, while the Krugersdrift Dam test site still has its natural and preserved appearance.

The riparian vegetation alongside the Modder River banks comprises of tall thorn trees, small Bushveld shrubs and thick grasses which is the characteristic vegetation of the Krugersdrift Dam test site (Gomo, 2011).

2.3 REGIONAL GEOLOGY OF THE STUDY AREA

The study area falls in the Main Karoo Basin, therefore the regional geology of the study area is controlled by the geology of the Karoo Supergroup. The geology of the Karoo Supergroup will be discussed in detail using text mainly from Woodford & Chevallier (2002).

The Main Karoo Basin covers an area of about 630 000 km^2, approximately 50% of South Africa as shown in Figure 2.6. The Karoo Supergroup comprises of thick successions of dominantly sedimentary strata that were deposited in an intracratonic, foreland basin on Gondwanaland during the Carboniferous, Permian, Triassic and early Jurassic ages, 300 to 160 million years ago (Woodford & Chevallier, 2002). Sediments of this supergroup are divided into the Dwyka, Ecca, Beaufort, Stormberg and Drakensberg Groups (Geel, 2014). These groups are distinguished clearly in terms of their own physical properties within the supergroup because the sedimentation occurred under different depositional environment.

The Karoo Basin is a retro-arc foreland basin (Catuneanu *et al*., 2005) which is situated behind a magmatic arc in front of the Cape Fold Belt. The Cape Fold Belt is a thrust belt which was created by the northern subduction of the oceanic lithosphere situated in the south of the arc (Catuneanu & Bowker, 2001). It overlies the central and eastern parts of

South Africa and deepens in the Southern part of Northern Cape Province. It is bounded by a fold-thrust belt (Cape Fold Belt) lying along the southern margin, the cratonic basement to the west, north and northeast, and the Indian Ocean to the southeast. Surface altitudes of the Karoo Supergroup range between 800 and 3 650 mamsl. The generally flat to undulating topography is broken by the up-warped plateau edges and the escarpment, most prominent in the Drakensberg region (Golder Associates, 2011).

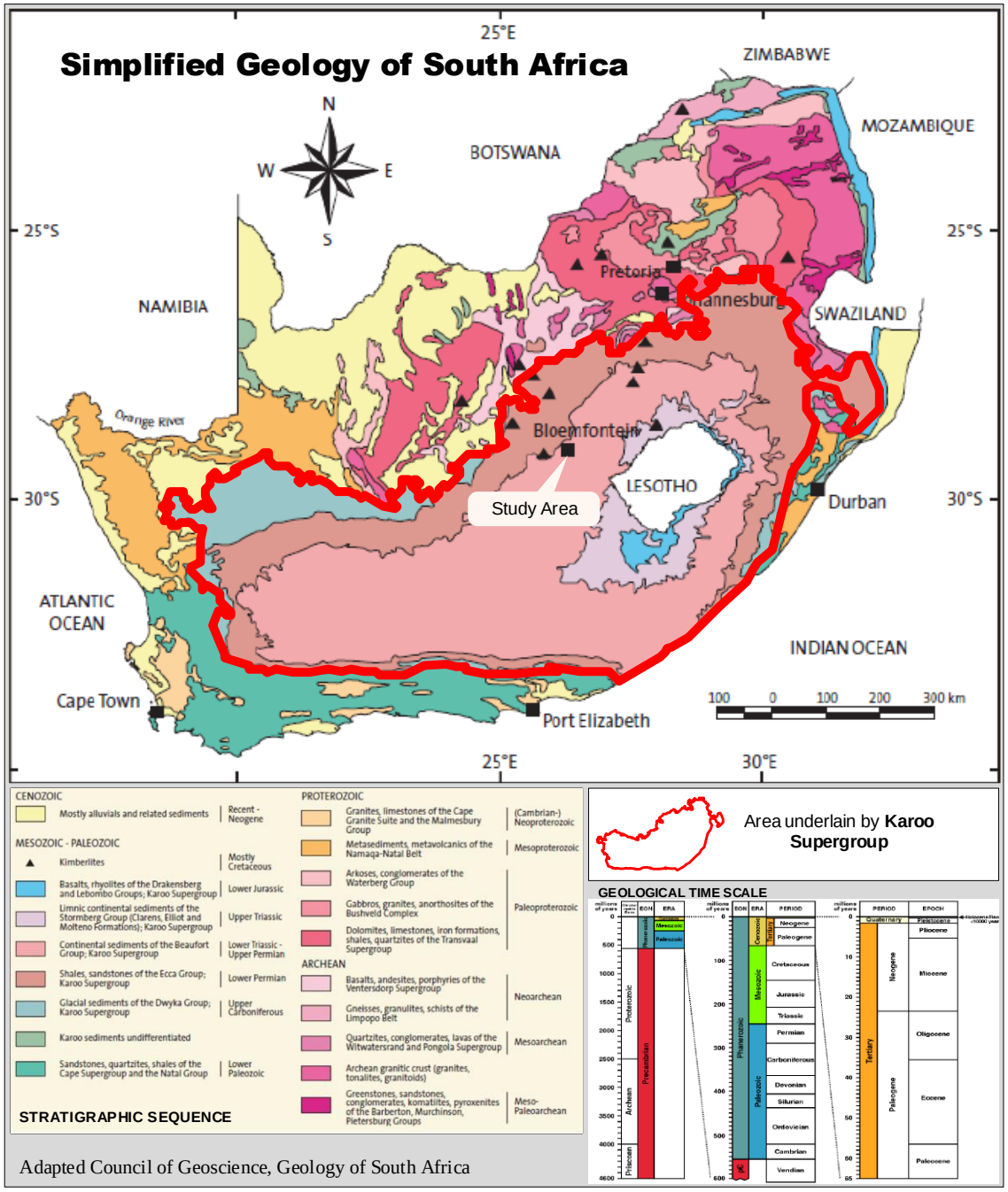

Figure 2.6: Geology of South Africa and the occurrence of Karoo Supergroup

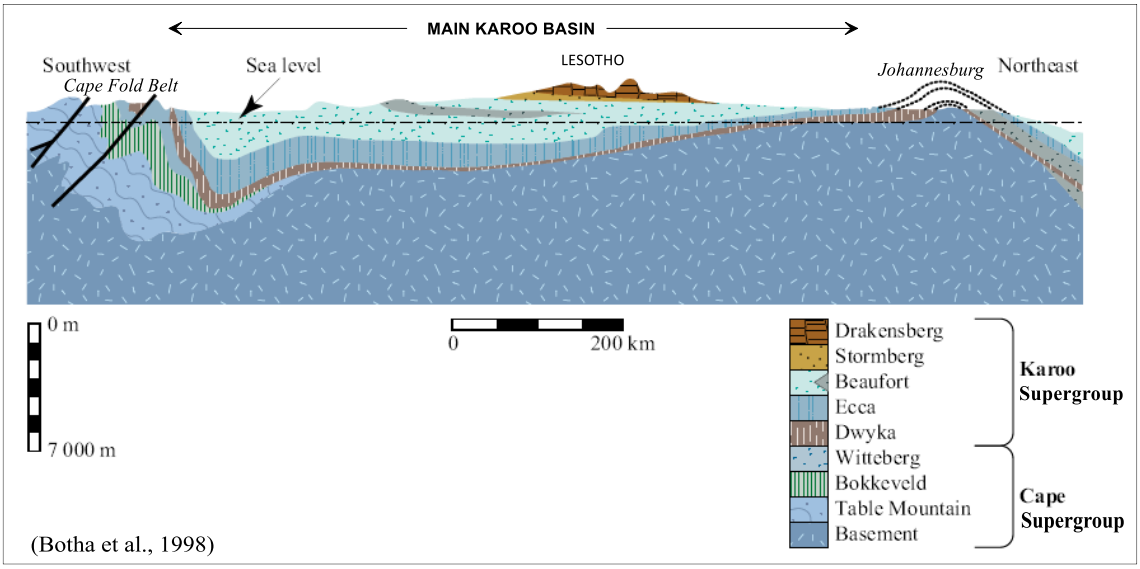

Figure 2.7: Schematic cross-section of the Karoo basin

2.4 LITHOSTRATIGRAPHY OF THE KAROO SUPERGROUP

2.4.1 Geological Sequence of the Karoo Supergroup

The geological sequence of the Karoo stratigraphic groups, formations and lithology, is shown in Table 2.2. The lithostratigraphic units of the Karoo Supergroup outcrop concentrically around the Main Karoo Basin (Figure 2.8).

Table 2.2: Lithostratigraphy of the Karoo Supergroup (Adapted from Tankard *et al.*, 1982)

Drakensberg Volcanics		Basalt	**Jurassic**
Stormberg Group	Clarens	Cross-bedded sandstone	**Triassic**
	Elliott	Red mudstone and sandstone	
	Molteno	Sandstone, conglomerate and mudstone	
Beaufort Group	Tarkastad Subgroup	Burgersdorp Formation	
		Katberg Sandstone	
	Adelaide Subgroup	Green, grey and purple mudstones	**Permian**
		Sandstone	
Ecca Group		Shale and sandstone	
Dwyka Group		Tillite and diamictite	**Carboniferous**

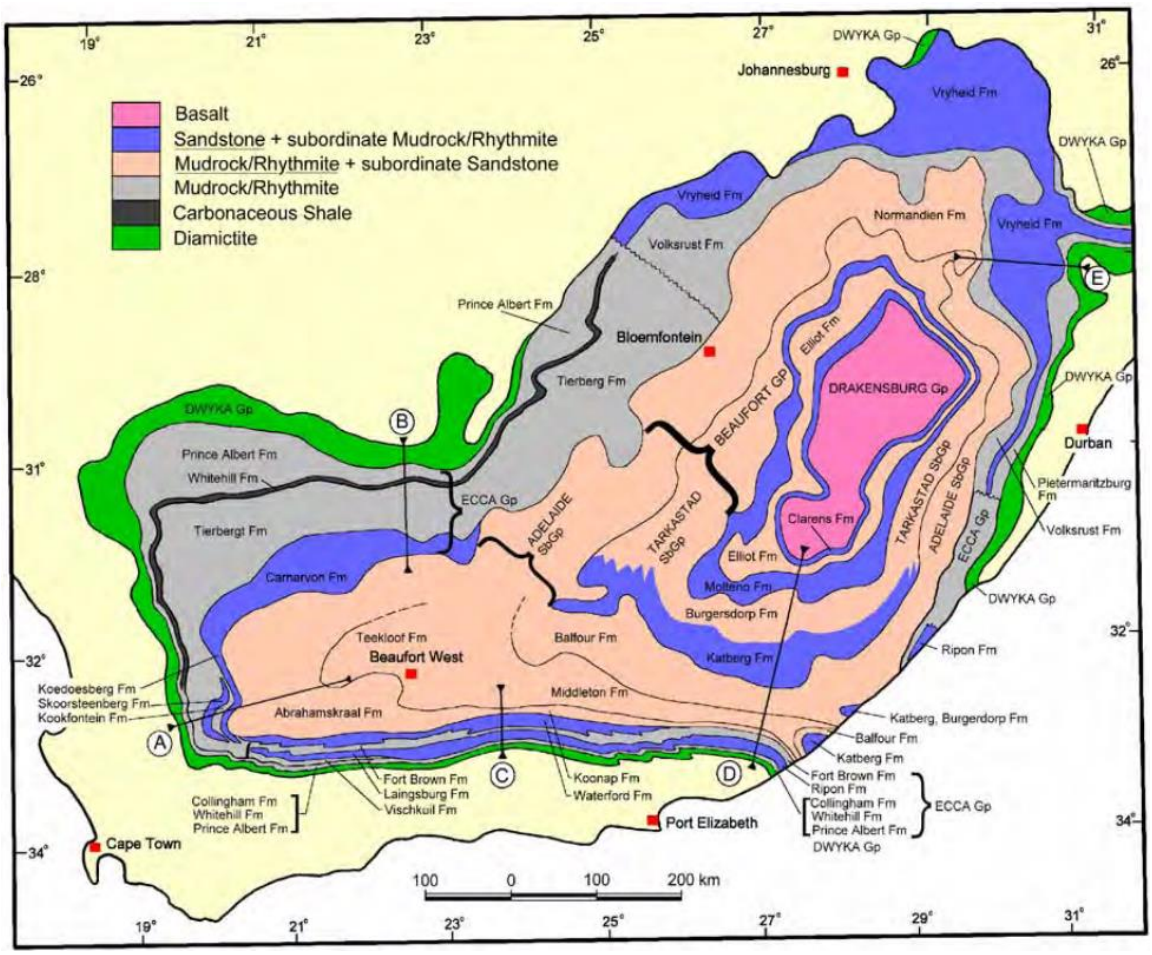

Figure 2.8: Areal extent of the lithostratigraphic units of the Main Karoo Basin (Johnson *et al*., 1997)

2.4.2 Dwyka Group

The Dwyka group is the oldest and lowermost group of the Karoo Supergroup, sitting on the Precambrian granitic rocks in the north and the Cape Fold Belt sedimentary rocks in the south. It was formed when the Gondwanaland migrated over the South Pole during Carboniferous age approximately 350 Ma (Geel, 2014). The Dwyka Group consists mainly of the clast-rich diamictite / tillite, which are angular to rounded fine grained, blue to grey clasts of the basement rocks, cemented in a clay and silt matrix. The subordinate rock types are conglomerate, sandstone, rhythmite and mudstone.

2.4.3 Ecca Group

The Ecca Group was formed by marine deposition over the Dwyka Group, as a result of the further northwards drifting of the Gondwanaland in the Permian Age (approximately 286-248 Ma). The Ecca Group rocks are consisting of clastic sequence of sediments comprising mudstone, siltstone, sandstone, minor conglomerate and coal. These clastic

sediments are divided into 16 formations, which reflect the lateral facies changes that characterise the succession.

2.4.4 Beaufort Group

The Beaufort Group overlays the Ecca Group and the Ecca-Beaufort boundary is generally defined by the first occurrence of red and purple mudstones (Turner, 1981). The rocks were deposited through fluvial processes by large, northward flowing, meandering rivers. The subgroups are lower Adelaide Subgroup and an upper Tarkastad Subgroup. The late Permian Adelaide Subgroup typically consists of green, grey and red mudstones, shale, siltstone, and fine to medium grained lithofeldspathic sandstone that form thick lens-shaped units (McCathy & Rubidge, 2005). Coarse to very coarse sandstone is common in the northern part of the basin and in general sandstone constitute about 20 to 30% of the thickness of the Adelaide Subgroup. These sandstone units normally form upward fining cycles. Johnson *et al*. (1997) recognise that the mudstone units are a result flood plain and lacustrine environment deposition.

Tarkastad Subgroup exhibits richer sandstones and mudstones. It was formed in the early Triassic age and the sediments of the Tarkastad Subgroup tend to form fining upward cycles. It is comprised of the following major four formations namely: the Katberg, Burgersdrop, Verkykerskop and Driekoppen Formations.

2.4.5 Stormberg Group

Stormberg Group is subdivided into three geological sedimentary formations which were deposited in the Late Triassic and the Jurassic Period namely, the Molteno, Elliot and Clarens Formations. The Molteno Formation comprises of medium to coarse grained sandstones and grey mudstones. The sandstone in the Molteno Formation has a unique glittering. In some parts, the formation hosts irregular coal seams and well-preserved plant fossils (Woodford & Chevallier, 2002). The Elliot Formation is comprised of an alternating sequence of marron to green-grey mudrock and fine to medium grained yellowish sandstone. The formation has a lower arenaceous unit with upward fining cycles, reflecting meandering river sedimentation and an upper mudstone dominated unit which hosts vertebrate fossils in some parts.

The Clarens Formation is the youngest of the Karoo sedimentation formed in the middle Jurassic age (Catuneanu *et al*., 1998). It consists mainly of wind-blown, fine-grained sandstone and siltstone which are white to cream in colour. The upper most part of the

formation contains some minor basaltic lava flows interlayered with sandstone, which mark the beginning of magmatic activity that led to the end of Main Karoo Basin sedimentation.

2.5 KAROO DOLERITE MAGMATISM

The end of Karoo sedimentation was marked by the widespread early Jurasic Volcanism, (Tankard *et al.*, 1982). Karoo magmatism is associated with huge, possibly plume-related magmatism that occurred approximately 183 Ma ago. It is also related to the subsequent break-up of the Gondwana supercontinent during the Early-Middle Jurassic period. The Karoo volcanic rocks generally overlie and intrude through various sedimentary formations of the Karoo Supergroup. These volcanic rocks consist mainly of tholeiitic to picritic lava flows, felsic pyroclastic rocks, and related dyke swarms and sills, emplaced prior to the break-up of Gondwana and the opening of Indian Ocean (Manninen, *et al.*, 2008).

2.6 GEOHYDROLOGY OF THE KAROO BASIN

2.6.1 Dwyka Formation

The Dwyka Group sediments are dominated by diamactite and shale which have very low hydraulic properties often tend to form aquitards (Woodford & Chevallier, 2002). The paleo marine depositional environments have influenced the quality of water in the Dwyka Group aquifers to be often saline. Production of water in these low hydraulic aquifers is enhanced by narrow discontinuities such as jointing and fracturing. In general, the Dwyka Group is not an ideal unit for the large-scale development of groundwater.

2.6.2 Ecca Group

The Ecca Group Formations are dominated by shales with very low porosities and hydraulic conductivity. Tiny fractures and weathering within the shales and mudrock enhance their potential for storing and transmitting water into the main bedding plane fractures (Gomo, 2011). Since the shales are very dense, they are often overlooked as significant sources of groundwater.

The hydraulic properties become enhanced within the sedimentary deposits which often form multi-layered sandstone porous aquifers. According to Rowsell & De Swardt (1976) the sandstones are poorly sorted with very low permeability and that their primary

porosities have been lowered considerably by diagenesis. However, the contacts between the sedimentary beds form the preferential ground water flow paths raising the potential for groundwater exploration targets.

2.6.3 Beaufort Group

The Beaufort Group consists of coarse-grained sedimentary deposits along the braided stream environment and fine-grained sediments away from the meandering river basins. These promote aquifers which are multi-layered and multi-porous due to the lateral migration of meandering streams over a floodplain (Woodford & Chevallier, 2002). Since the sedimentary beds are multi-layered, multi-porous and in most cases, lens shaped, the aquifers in the Beaufort Group exhibit a complex behaviour due to discontinuities in the hydraulic properties. The alluvial fan and braided stream environment near the Cape Fold Belt comprising of coarse-grained sandstone has higher primary permeabilities while more distal central and northern portion dominated by finer sandstone and mudstone has very low primary permeabilities. However, according to Botha *et al.* (1998), the upper formations of the Beaufort Group are characterised by sub-horizontal bedding, with parallel, orthogonal and diagonal fractures which usually enhances the yields of boreholes especially if the borehole intersects a bedding-parallel fracture.

2.6.4 Stormberg Group

The Molten Formations forms the most ideal aquifers consisting of medium to coarse grained and well sorted and persistent sandstone beds. The Elliot formation is dominated by red mudstone which gives it characteristics more of an aquitard than aquifer. The Clarens Formation has well sorted medium to fine grained sandstones with very high and uniform porosities of the order of 8%. However, the Clarens Formation is poorly fractured and has a very low permeability. This makes it to have less economic value in terms of groundwater extraction using boreholes.

2.6.5 Geohydrology of Dolerite Intrusion

Most water supply borehole in Karoo formations are sited next to a linear or sub-vertical dolerite dyke. This is because the fracturing intensity increases near the dolerite where the formation has been disturbed as compared to the area where the formation is undisturbed. Vertical intrusion tends to promoted vertical and sub-vertical fracture zone

around the dyke area which are easily delineated with magnetic, resistivity tomography and electromagnetic geophysical methods.

2.6.6 Hydraulic Character of the Karoo Rocks

i. The Southern Karoo Basin sandstones have extremely low primary porosity and permeability. The primary porosity and permeability of the Middle Ecca sandstones improves from south to north of the Main Karoo Basin.

ii. The porosity of the Karoo beds decreases with depth with higher porosities within the first 30m of the earth's surface (Vegter, 1992). This is attributed to weathering and leaching of rocks within the upper 30m and increase in the lithostatic pressures and temperature with depth.

iii. According to Woodford & Chevallier (2002) the shale porosity and bulky density in the northern Karoo Basin varies between 2-10% and 2400-2600 kg/m^3 and decreases to less than 2% in the southern part.

iv. The Karoo aquifers are multi-layered and multi-porosity with significant secondary fracture porosity present at depth.

v. The Karoo rock matrix store considerable amount of water while the bedding fractures act as main conduits of water to boreholes. This implies that the yield of boreholes in Karoo aquifers is enhanced when the boreholes intersects a bedding-parallel fracture. The bedding parallel fractures have small apertures which may be of considerable extent though they have low frequency of occurrence and weak connectivity.

vi. Woodford & Chevallier (2002) resolved that there are two major flow regimes in Karoo aquifers when stressed. The flows are vertical matrix flow and horizontal bedding-parallel fracture flow. This make the flow in a productive Karoo aquifer to be regarded as three dimensional.

CHAPTER 3:
GROUNDWATER FLOW AND STREAMING POTENTIAL THEORY

3.1 INTRODUCTION

The literature covered under this chapter describes guiding fundamentals in estimating hydraulic conductivity using pumping test theory. It starts by discussing basic groundwater flow principles from Darcy law to groundwater flow equations for steady state and unsteady-state flow in confined aquifers. As will be revealed in Chapter 5 the two test sites chosen for this study are confined aquifers, therefore discussion in this section are limited to the analytical solutions in confined aquifers.

The second part of the chapter proceeds by reviewing the fundamental theory of streaming potential method in relation to groundwater flow towards a production well. It provides an understanding of the relationship between streaming potential and hydraulic head. The resultant is a presentation of a coupled groundwater flow equation of hydraulic parameters and streaming potential.

3.1.1 Darcy Law and Hydraulic Conductivity

In 1856, Henri Philibert Gaspard Darcy formulated a law that describes the rate of flow of water in a porous media. It is therefore necessary to highlight the law he formulated, before discussion on the modern descriptions of groundwater flow in an aquifer.

Darcy law states that, the rate of flow through a porous medium is directly proportional to the loss of head and the cross-sectional area through which the flow is occurring, and inversely proportional to the length of the flow path (Dennis *et al*., 2008). The law is summarized in a relationship as:

$$Q = \frac{KA(h_1 - h_2)}{L} = -KA\frac{dh}{dl} \qquad 3.1$$

Where Q is the volume rate of flow or discharge (Length^3/Time), h_1 and h_2 are two hydraulic heads between the flow length *(L)* and $^{dh}/_{dl}$, is the hydraulic gradient or *grad h*, negative in the direction of flow (representing a head loss) and *A* is the cross-sectional area normal to the direction of flow. *K* is introduced as the constant of proportionality.

Equation 3.1 is simplified to:

$$q = \frac{Q}{A} = -K\frac{dh}{dl} = -K\nabla h \qquad 3.2$$

Where q is the specific discharge also known as Darcy velocity or flux (Length /Time) and ∇h is the gradient of the hydraulic head, h.

The constant of proportionality, K, introduced in Darcy law is called hydraulic conductivity. Hydraulic conductivity is the volume of water that will move through a porous medium in unit area perpendicular to the direction of flow. It is an indication of the ease with which water moves through the subsurface and is expressed in the units of Length/Time, usually metres per day *(m/d),* (Kruseman & De Ridder, 1990). In Table 3.1 Kruseman and De Ridder (1990) shows the orders of magnitude of K for different rock types. In a fractured rock, hydraulic conductivity is affected by fracture density and width of their apertures. Fractures increase K of the solid rock by larger magnitudes.

Table 3.1: Orders of magnitude of K for different materials kinds of rocks

Geological classification	**Hydraulic conductivity *K* (m/d)**	
Unconsolidated materials:		
Clay	10^{-8}	- 10^{-2}
Fine sand	1	- 5
Medium sand	5	- 2×10^{1}
Coarse sand	2×10^{1}	- 10^{2}
Gravel	10^{2}	- 10^{3}
Sand and gravel mixes	5	- 10^{2}
Clay, sand and gravel mixes (e.g. till)	10^{-3}	- 10^{-1}
Rocks:		
Sandstone	10^{-3}	- 1
Carbonate rock with secondary porosity	10^{-2}	- 1
Shale	10^{-7}	
Dense solid rock	$< 10^{-5}$	
Fractured and weathered rock (core sample)	Almost 0	- 3 x 10^{-2}
Volcanic rock	Almost 0	- 10^{3}

Fetter (2001) recalls that hydraulic conductivity is a function of both the properties of the medium and the fluid. To separate the dependency of K on both the medium and fluid, Nutting (1930) factored K as:

$$K = \frac{k\rho g}{\mu} \qquad 3.3$$

Where ρ is the density of the fluid, μ is the dynamic viscosity of the fluid and g is the acceleration due to gravity and k is the permeability of the porous medium which is independent of the fluid properties. It has dimension of Length^2.

Most aquifers are heterogeneous in nature, meaning that their hydraulic parameters vary in magnitude with position. It will mean that *K* is usually a function of spatial direction and time, therefore there exists a possibility of transforming Darcy law (Equation 3.2) to include *K* under the gradient operator, such that:

$$q = -\nabla(Kh) \qquad 3.4$$

In the situation where the *K* is dependent on the directional orientation of the matrix pores the aquifer is said to be anisotropic in nature. Hydraulic conductivities and permeabilities of anisotropic formations are therefore tensors and not scalars. The scope of this study limits itself to one dimensional or single directional form of hydraulic conductivities.

3.1.2 Transmissivity

Transmissivity *(T)*, which is a product of hydraulic conductivity and the saturated thickness of the aquifer *(D).* It is defined as the rate of flow under a unit hydraulic gradient through a cross-section of unit width over the whole saturated thickness of the aquifer. It is expressed as:

$$T = KD \qquad 3.5$$

3.1.3 Specific Storage

Specific Storage *(S_s)* of a saturated confined aquifer is the volume of water that a unit volume of aquifer releases from its storage under a unit decline in hydraulic head. Water released is due to the increase in effective compaction stress on the aquifer and expansion of water due to the decrease in pressure *(P).* It is expressed as:

$$S_s = \rho g(\alpha + n\beta) \qquad 3.6$$

3.1.4 Storativity

Storativity of a saturated aquifer of thickness, *D*, is the volume of water released from storage per unit surface area of the aquifer per unit decline of the hydraulic head. It is a

dimensionless parameter because it involves volume of water per volume of aquifer and its values range from 5×10^{-5} to 5×10^{-3}. It is expressed as:

$$S = \rho g D(\alpha + n\beta) \qquad 3.7$$

Where α and β are compressibility of an aquifer material and fluid respectively due to change in pressure. Compressibility of groundwater under the temperatures usually encountered can be taken as a constant 4.4×10^{-10} m^2/N. The parameter *n* is the porosity of the medium defined as the ration of the total volume of the solid portion of the medium to its void volume.

3.1.5 Specific Yield

Specific yield (S_y) is the volume of water release from an unconfined aquifer storage per unit surface area per unit decline in water table due to gravity. The values of specific storage range from 0.01 to 0.30.

3.2 PUMPING TEST THEORY: ESTIMATION OF HYDRAULIC CONDUCTIVITY IN A CONFINED AQUIFER

The flow of groundwater in a confined aquifer is investigated through well hydraulic tests called pumping tests. The principle of a pumping test relies on the fact that drawdown measurements performed in a production borehole (at known discharge) and nearby piezometers can be substituted into a fitting groundwater flow equation and calculate hydraulic parameters of the aquifer. Conversely, if the hydraulic characteristics are known, the solution to the flow equations towards a borehole can be used to estimate the drawdown of the potential surface or water table near the pumping well. In this dissertation, the analytical equations used to describe radial flow are adopted from Kruseman and De Ridder (1990) and are described in Sections 3.2.1 and 3.2.2

3.2.1 Groundwater Flow towards a Pumping Borehole

Groundwater flow influenced by pumping in a borehole is referred to as radial flow. There are two types of equations that are used to describe flow of groundwater in a confined aquifer. These equations are steady-state flow and unsteady-state flow. Steady-state flow is achieved when there is negligible change in water level in the borehole over time. However, in most cases it is difficult to attain steady state condition implying that within practical setting and finite period of most pumping tests in confined aquifers, the water

level may continue to drop with time. If the drop-in water level is uniform or attains a constant hydraulic gradient, the state of flow is referred to as pseudo state flow. This occurs mostly in confined porous aquifers. In a confined fractured aquifer, unsteady-state flow is adopted as long as the change in water level can still be measured.

Fetter (2001), showed that the general groundwater flow equation for a confined aquifer in two-dimensional flow is given by:

$$\frac{\partial^2 h}{\partial x^2} + \frac{\partial^2 h}{\partial y^2} = \frac{S}{T}\frac{\partial h}{\partial t} \qquad 3.8$$

In steady-state flow there is no change in head with time: $\frac{\partial h}{\partial t} = 0,$ then:

$$\frac{\partial^2 h}{\partial x^2} + \frac{\partial^2 h}{\partial y^2} = 0 \qquad 3.9$$

Equation 3.9 represents a **Laplacian groundwater flow equation** for a confined aquifer under steady-state condition.

When groundwater flows towards a pumping borehole as shown in Figure 3.1, the flow is referred as radial flow.

Kruseman and De Ridder (1990) highlighted assumptions guiding the evaluation of pumping test data for a confined aquifer under a steady-state condition as,

i. The aquifer is bounded on the bottom by a confining layer.
ii. The aquifer is horizontal and of seemingly infinite areal extent.
iii. The potentiometric surface of the aquifer is horizontal prior to the start of the pumping over the area of influence.
iv. The potentiometric surface remains unchanged with time prior to the start of the pumping and any changes in the position of the potentiometric surface are due to the effect of the pumping borehole alone.
v. The aquifer is homogeneous and isotropic.
vi. The pumping well and the observation well penetrates the entire thickness of the aquifer and all flow is radial and horizontal toward the well.
vii. Darcy's law is valid, meaning that the flow is laminar.
viii. The pumping well has an infinitesimal diameter and is 100% efficient.

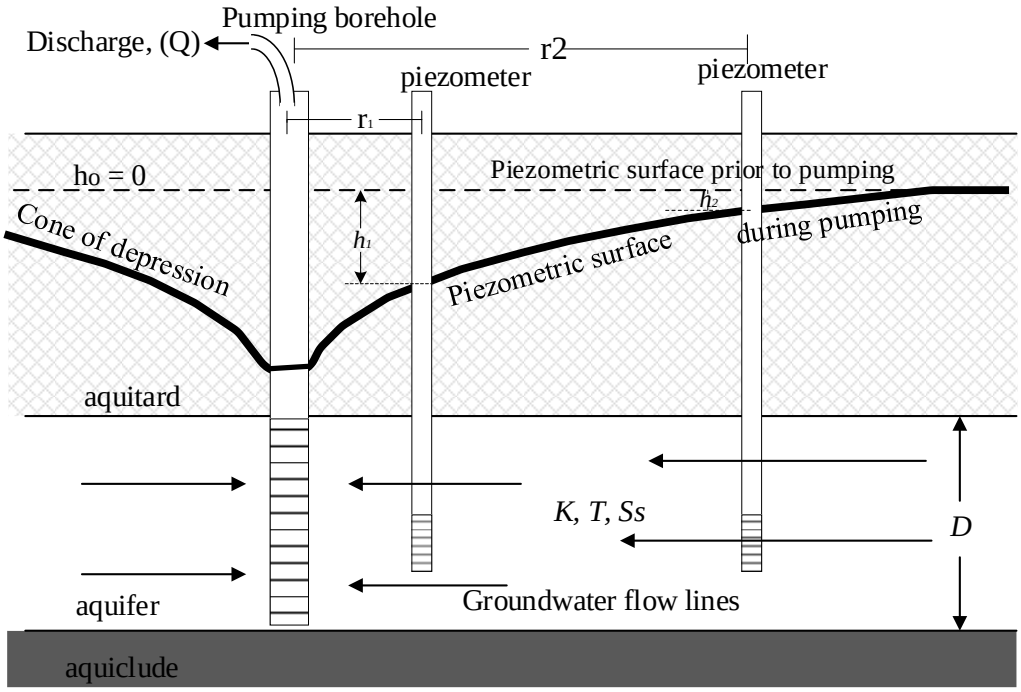

S = drawdown of piezometric surface,
K = hydraulic conductivity, T = Transmissivity, S_s = Specific storage

Modified Kruseman & De Ridder (1990)

Figure 3.1: Drawdown in the pumped confined aquifer

3.2.2 Stead-State Flow in a Confined Aquifer

Under steady-state radial flow towards a production well in a confined isotropic and homogeneous aquifer with radial symmetry, Equation 3.9 is expressed in polar coordinates as:

$$\frac{\partial^2 h}{\partial r^2} + \frac{1}{r}\frac{\partial^2 h}{\partial r^2} = 0 \qquad 3.10$$

Where, from Pythagoras theorem:

$$r = \sqrt{(x^2 + y^2)}, \qquad 3.11$$

Fitter (2001) showed that the solution of Equation 3.10 in terms of residual drawdown at a fixed point is:

$$dh = \frac{Q}{2\pi T}\frac{dr}{r}, \qquad 3.12$$

Considering a set-up where there are two observation wells as in Figure 3.1, giving the following boundary conditions;

At distance r_1 from the pumping well, the head is h_1, and at distance r_2 from the pumping well, the head is h_2.

A solution can be computed through integration of the Equation 3.12 with these boundary conditions,

$$\int_{h1}^{h2} dh = \frac{Q}{2\pi T} \int_{r1}^{r2} \frac{dr}{r} \quad 3.13$$

$$h_2 - h_1 = \frac{Q}{2\pi T} \ln(\frac{r_1}{r_2}) \quad 3.14$$

Rearranging Equation 3.14, yields the **Theim equation** for a stead state flow in a confined aquifer:

$$T = KD = \frac{Q}{2\pi(h_2 - h_1)} \ln(\frac{r_1}{r_2}) \quad 3.15$$

$$T = KD = \frac{2.30Q}{2\pi(h_2 - h_1)} \log(\frac{r_1}{r_2}) \quad 3.16$$

Where: $KD = T$ is aquifer transmissivity (m^2/d), D is the aquifer thickness (m), K is the hydraulic conductivity (m/d) and Q is the pumping discharge rate (m^3/d). For situations where there is only one observation borehole, r_1 is the diameter of the pumping borehole and h_1 is the drawdown in the pumping borehole.

Hydraulic conductivity can be calculated using semi-log time drawdown and semi-log distance drawdown curves. The limitation with Theim equation is that it is not able to calculate the storativity of an aquifer.

3.2.3 Unsteady-State Flow in a Confined Aquifer

3.2.3.1 Theis method

A further Pythagorean operation on Equation 3.8 by Fetter (2001), converted the two-dimensional groundwater flow equation under unsteady state condition to polar coordinates.

$$\frac{\partial^2 h}{\partial r^2} + \frac{1}{r}\frac{\partial^2 h}{\partial r^2} = \frac{S}{T}\frac{\partial h}{\partial t} \quad 3.17$$

The solution of groundwater flow Equation 3.17 under unsteady-steady condition in a confined aquifer when a borehole is pumped at constant rate was derived by Theis in

1935, (Fetter, 2001). Under unsteady-state condition the initial boundary condition for a horizontal piezometric surface is:

$$h(r,0) = h_0 \, for \, all \, r \tag{3.18}$$

and the boundary condition signifying an infinitely horizontal extent with no drawdown is:

$$h(\infty,t) = h_0 \, for \, all \, r \tag{3.19}$$

Then the solution of Equation 3.17 as provided by Theis (Kruseman & De Ridder, 1990) under the above boundary conditions in Equations 3.18 and 3.19 is expressed as:

$$h_0 - h = s = \frac{Q}{4\pi KD}\int_{\mu}^{\infty}\frac{e^{-a}}{a}da = \frac{Q}{4\pi KD}W(u) \tag{3.20}$$

Equation 3.20 is called **Theis equation,** where $s = h_0 - h$ is the drawdown measured in the field and since $T = KD$, Then from Equation 3.20:

$$s = \frac{Q}{4\pi T}W(u) \tag{3.21}$$

The term *W(u)* is referred to as the Well function, and is also referred to as dimensionless drawdown. It is given by:

$$W(u) = -0.5772 - lnu + u - \frac{u^2}{2.2!} + \frac{u^3}{3.3!} - \frac{u^4}{4.4!} + \cdots \tag{3.22}$$

Where the argument *u* also known as the dimensionless time is given by:

$$u = \frac{r^2\mathrm{S}}{4Tt} \tag{3.23}$$

Then from Equation 3.23:

$$\mathrm{S} = \frac{4Ttu}{r^2} \tag{3.24}$$

Where S is the storativity of an aquifer, *t* is the time since pumping began, *Q* is the constant discharge rate and *r* is the radial distance from the pumping well.

Estimation of hydraulic conductivity using Thesis equation is done by matching graphs of drawdown against r^2/t with *W(u)* against *(u)* and the coordinates of the matching points can be used to calculate transmissivity and storativity. The limitation of Theis is

that in fitting the curves to match, early drawdown data does not closely represent the theoretical drawdown equation on which the type curve is based.

3.2.3.2 Cooper Jacob method

Cooper Jacob further observed that the dimensionless time argument *u* in Equation 3.22 becomes small with prolonged pumping (increase in *t*) and decrease in the distance *r* from the pumping well (Kruseman & De Ridder, 1990). This implies that on distances very close to the pumping borehole after adequately lengthy pumping the terms after *ln u* in Theis equation can be neglected.

Therefore, for values of *u, (u<0.01):*

$$s = \frac{Q}{4\pi KD}(-0.5772 - ln\frac{r^2\mathrm{S}}{4Tt}) \quad 3.25$$

$$s = \frac{2.30Q}{4\pi T}\log(\frac{2.25Tt}{r^2\mathrm{S}}) \quad 3.26$$

Equation 3.26 represents **Cooper Jacob's equation** for unsteady-state flow in a confined aquifer.

Estimation of hydraulic parameters (*T, K and S)* using Cooper Jacob equation is achieved by plotting the time – drawdown and distance drawdown curves. Of interest to note is that, analysis using Cooper Jacob Equation 3.26 for two piezometers yields similar results to Theim equation in Equation 3.16. Kruseman and De Ridder (1990) highlighted that in addition to the assumptions in Section 3.2.1, the Cooper Jacob method applies for unsteady-state flow and for small *u <0.01 (small r and large t).* Though in practice values of *u<0.1* are acceptable.

3.2.4 Steady-State Flow in Unconfined Aquifer

Considering an unconfined aquifer as shown in Figure 3.2, water is being pumped under steady-state horizontal flow where the drawdown change is negligible or the change in drawdown is constant (a state when the time – drawdown graphs in piezometers are parallel). The Dupluit equation provides the analytical solution to Equation 3.9 as (Fetter, 2001)

$$Q = 2\pi rKh(\frac{\partial h}{\partial r}) \quad 3.27$$

Which is satisfied if the assumptions and conditions provided in Section 3.2.1 are met in addition of the flow throughout the vertical section of the aquifer being assumed to be horizontal and having a linear flow velocity which is tangent to the hydraulic gradient.

Then the integration of Equation 3.27 within the boundaries $r_1$and r_2 with ($r_2 > r_1$) is given by:

$$Q = \pi K \left[\frac{h_2^2 - h_1^2}{\ln(\frac{r_2}{r_1})} \right] \qquad 3.28$$

Equation 3.28 is referred to as the **Thiem Dupuit** method of an unconfined steady-state flow (Kruseman & De Ridder, 1990).

In the field we measure *s* rather than *h* therefore if the thickness of the aquifer is known as *D.* Then:

$$Q = \frac{2\pi KD(s_1 - s_2)}{\ln(^{r_2}/_{r_1})} \qquad 3.29$$

$$Q = \frac{2\pi KD(s_1 - s_2)}{2.30\log(^{r_2}/_{r_1})} \qquad 3.30$$

It is important to highlight that Equation 3.30 and Equation 3.17 are analogous.

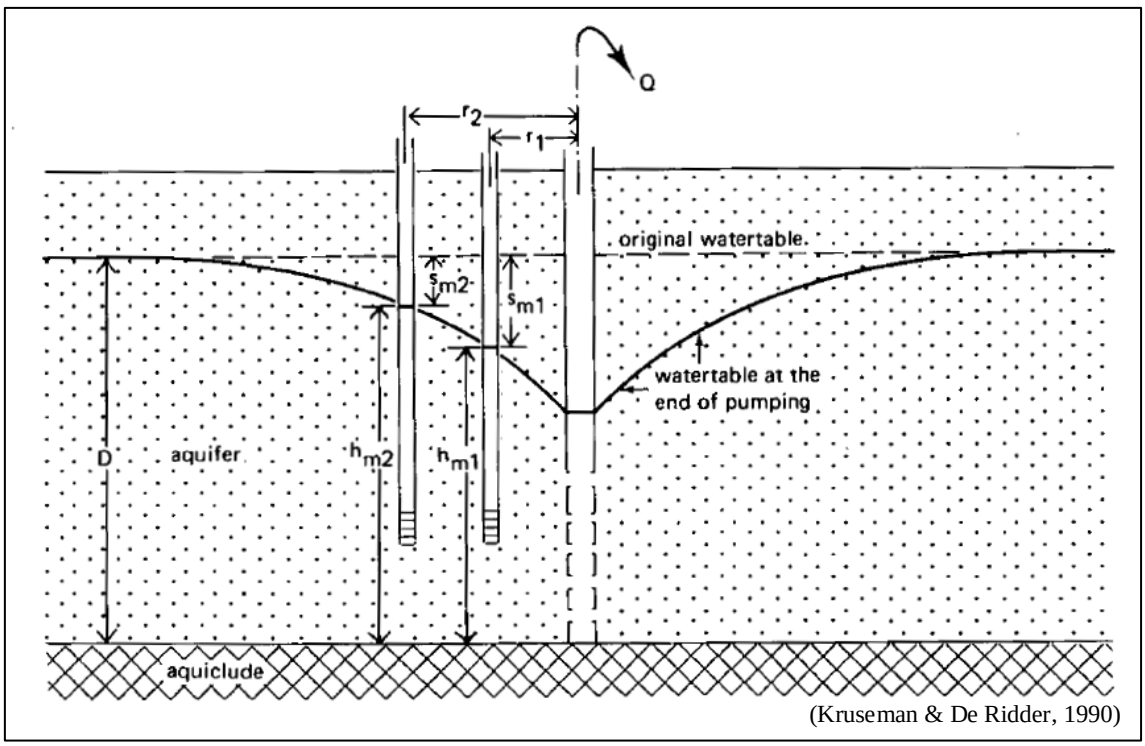

(Kruseman & De Ridder, 1990)

Figure 3.2: Drawdown in a pumped unconfined aquifer

Since Equations 3.17 and 3.30 are similar, Kruseman & De Ridder (1990) proposed that the analytical solutions of a confined aquifer under steady-state flow can be used to solve groundwater water flow problems in an unconfined aquifer.

3.3 STREAMING POTENTIAL THEORY

Self-potential method is a passive and non-invasive geophysical method which measures electrical response at the ground surface in order to infer the disturbances in the electrical currents of the conductive sub-surface material. The electrical response is measured as electrical potential at a set of measurement points or stations using non-polarizing electrodes connected to a voltmeter. The data obtained from self-potential survey can be analysed to determine the source causing the electrical current in the ground and obtain useful information on groundwater flow.

3.3.1 Emergence of Streaming Potential Method

Self-potential measurements began in 1830, when measurements were made across a mineralised sulphide vein in Cornwall (UK) using copper-plate electrodes and a string galvanometer as a detector (Telford *et al.,* 1976). His attempt successfully located the position of the mineralised sulphide. However, the data was sporous with compromised precision. The sporous nature of self-potential data was resolved in 1865, when Mattecucci (Telford *et al.*, 1976) developed the first non-polarizing pot electrode for use in self-potential measurements. This allowed the method to gain appreciation in mineral exploration (Revil & Jardani, 2013). Sato & Mooney (1960) developed a model called "Geo-battery model" which explained the occurrence of self-potential anomalies due to the interaction of an ore body with water as shown in Figure 3.3.

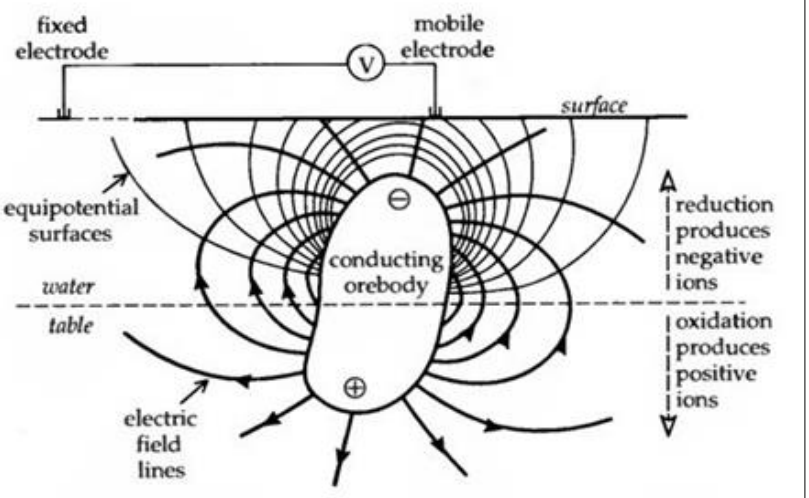

(Sato & Mooney, 1960)

Figure 3.3: Schematic geo-battery model of an ore body

3.3.2 Traditional Applications of Self-potential Method

In the 1990s, the famous geo-battery model was refined to a non-linear geo-battery model called the Butler-Volmer model, (Bigalke & Grabner, 1997). This paved a way for application of self-potential method in environmental investigations, mostly involving mapping of plumes. Within this decade, the use of the self-potential method gained momentum and found a key role of application to hydrothermal systems, water resources and geo-hazards. Some of the example of applications include delineation of geothermal source, mapping of leakage paths from dams, canals and buried pipelines, and mapping of detachment walls and lateral limits of landslide masses.

However, in most of all these applications, the results from self-potential surveys were used only for qualitative analysis (mapping objectives) that gave an indication of the presence of self-potential anomalies. Revil & Jardani (2013) attributed this to the complexity nature of the causative source of the self-potential signals.

Towards late 1990s, to the early millennium era, various researchers made effort to develop inverse problem algorithms to determine the source distribution responsible for the self-potential anomalies recorded at the ground surface, (Revil & Jardani, 2013). However, the inverse problem algorithms suffered from non-uniqueness of the solution.

This thesis emphasizes the contribution of self-potential signals related to groundwater flow often called streaming potential (S_tP). The work is motivated by Revil *et al.* (2003), Linde *et al.* (2007) and Fagerlund & Heinson (2002) who demonstrated the possibility of

using streaming potential signals for the quantitative estimation of the hydraulic parameters of a porous medium and have shown the existence of a correlation between the streaming-potential signals and the values of the hydraulic head.

3.3.3 Electrical Double Layer

The study of electro-kinematic signals starts with a good understanding of the electrical double layer associated with the interface between the solid medium and the liquid (Fourie, 2003). The term "electrical double layer" is a generic name describing the electrochemical system coating the surface of the minerals. In the case of groundwater, the solid medium is the mineral grain of the aquifer and the liquid is the water flowing within the aquifer.

The most occurring mineral in Karoo aquifers is Silica. If Silica interacts with water, the silanol groups (SiOH) of the surface of the mineral grain will become negatively charged as a result of proton loss resulting in SiO^- surface sites. On few occasions the silanol groups can gain a proton resulting in positively charged surface sites ($SiOH_2^+$), (Revil & Jardani, 2013). The process of ion-exchange *(proton gain and loss)* at the grain boundary, implies that the resulting mineral surface charge is pH dependant. However, interaction with water typically makes the mineral grain boundary to be negatively charged at near-neutral pH. Since water is electrolytic in nature, the negatively charged grain boundary attracts the H^+ ions of electrolytic water and repels the OH^- ions. The above phenomenon is illustrated in Figure 3.4.

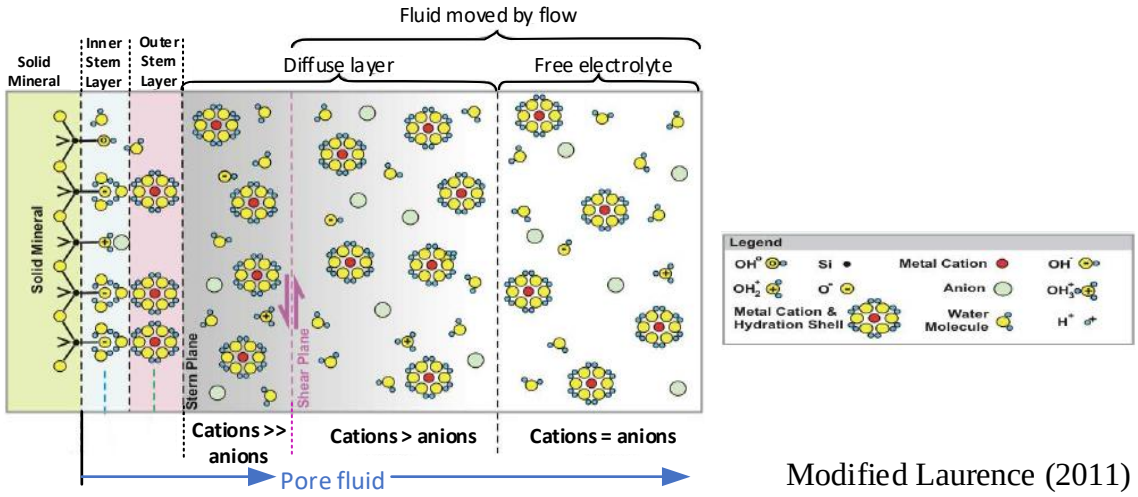

Modified Laurence (2011)

Figure 3.4: Schematic representation of mineral & pore water charges interaction

The resultant (charged capillary) is that, the zone within the liquid phase near the mineral grain boundary is dominantly positively charged forming an aggregation of excess charge (excess ions and/or electrons) at the interface of the two phases on each side as shown in Figure 3.5.

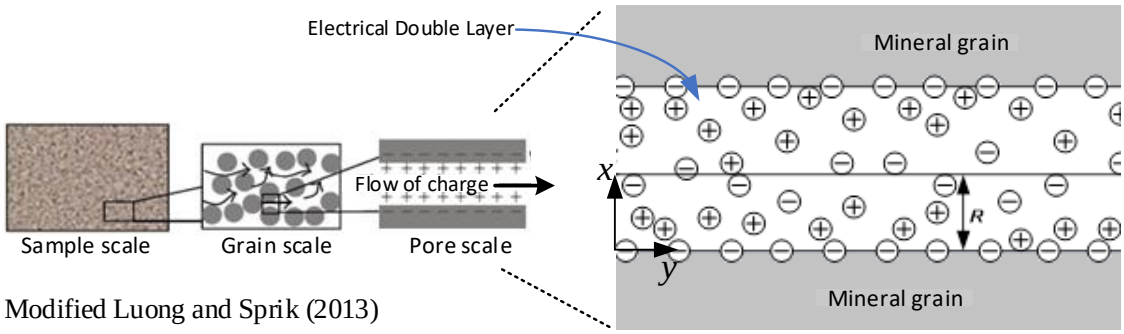

Figure 3.5: Schematic diagram of a charged capillary

A charged capillary exists at the boundary between the fluid and the surface of the mineral grain resulting in the generation of an electric potential. The charged capillary model was described in the Gouy-Chapman model (one-layer) as a uniform surface charge on the mineral grain, which is neutralized by a surplus of ions of opposite sign in the liquid phase resulting in diffuse layer where the ionic concentration, *N*, is greatest nearest the mineral grain wall and then decreases exponentially, (according to Boltzmann distribution of ions) approaching zero at some distance as described by and Fourie (2003) and Rathore et al (2005).

$$N_{+}(x) = N^{o}\exp(\frac{-ze\varphi(x)}{K_b T}) \qquad 3.31$$

$$N_{-}(x) = N^{o}\exp(\frac{ze\varphi(x)}{K_b T}) \qquad 3.32$$

Where N^{+} and N^{-} are cation and anion concentration at a distance x from the mineral grain surface, N^{o} is the ionic concentration far from the mineral grain surface, e is the electronic charge, z is the ionic valence, K_b is the Boltzmann constant, T is the temperature in Kelvin and $\varphi(x)$ is the electric potential at a distance x from the mineral grain surface until a distance $x = R$ is reached where charge is balanced.

A further improvement of the Gouy-Chapman model of a charged capillary resulted in the Stern model of the electrical double layer. According to the Stern model, there is an inner layer of ions more strongly adsorbed next to the mineral grain surface by electrostatic and Van der Waal's forces, called a Stern or Helmholtz layer (Fagerlund &

Heinson, 2002). Further from the mineral grain surface is the diffuse layer also called the Gouy layer. The Stern layer is usually one ion in thickness (Fourier, 2003). The existence of excess charge at the interface on each side in the Stern layer and the diffuse or Gouy layer constitutes an **electrical double layer (EDL)**. The electrical double layer is a term describing the electrochemical system coating the surface of the mineral grain, (Revil & Jardani, 2013).

3.3.4 The Zeta Potential

The mineral grain surface is usually negatively charged (Fagerlund & Heinson, 2002), this means that the electric potential φ is lowest at the grain surface. It increases linearly in the Stern layer and exponentially approaching zero as the remaining charge offset is balanced out in the diffuse layer. The zeta potential (ξ-potential) is defined as the potential in the fluid mobile phase, which is the hydrodynamic slipping plane (S-Plane). The S-plane separates the mobile and immobile phases of the fluid and usually close to H-plane which is separating the Stern and diffuse layers as shown in Figure 3.6.

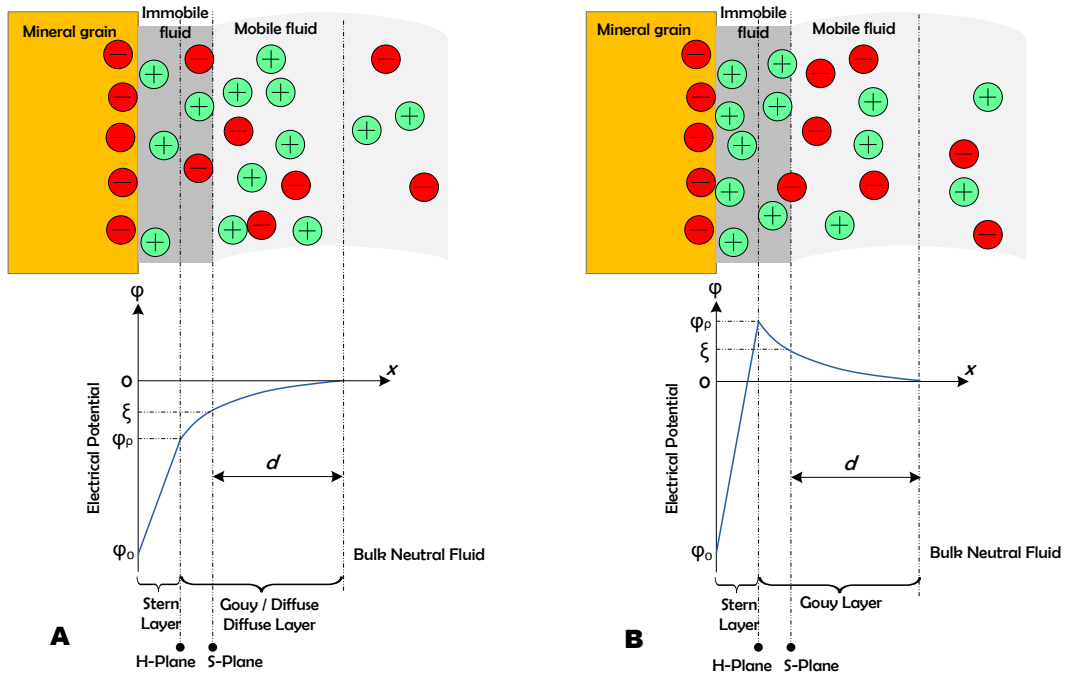

Adapted from Fagerlund & Heinson (2002)

Figure 3.6: Electrical double layer and electric potential,

Revil and Jardani (2013) referred the S-plane as the OHP, which stands for Outer Helmholtz Plane. The ξ-potential can be positive or negative depending on the intensity

of adsorption in the Stern Layer. For weak adsorption of ions, the potential will rise linearly within the stern layer and continue to rise exponentially towards zero in the diffuse layer as in the case of adapted from Fagerlund & Heinson (2002), Figure 3.6A. If the adsorption of ions in the stern layer is very strong, the potential will rise above zero and will decrease exponentially in the diffuse layer as it approaches zero, the case of adapted from Fagerlund & Heinson (2002), Figure 3.6B. The movement of groundwater causes a drag of charges in the mobile part of electrical double layer which intern results in the generation of a convective electric current or streaming potential gradient. There is a direct relationship existing between the magnitude of the ξ-potential, and the amount of charge transported. If the magnitude of the ξ-potential is more negative, it implies that more positive ions have been transported and if it is more positive, this implies that more negative charges/ ions have been transported. If there is no ξ-potential existing, it means there is no streaming potential gradient generated. In such a system constituting a liquid and a solid medium the net charge within the liquid and the charge on the surface of the solid medium has to be equal in magnitude and of opposite signs creating an electro-neutral medium (Revil & Jardani, 2013).

3.3.5 Streaming Current and the Coupled Flow Problem

The fluid always flows in the direction of negative pressure gradient ($-\nabla P$), this implies that the Zeta potential is negative. This causes a convective current which is positive in the direction of flow to generate an electric gradient (streaming potential) along the flow path. From classical electrical theory, the potential gradient will cause a current called the streaming current, to flow back through the fluid by conduction. Revil & Jardani (2013) defined streaming current as the quasi-static source current density associated with the drag of the excess of electric charge in the electric diffuse layer of a porous material.

In the absence of external current sources and in an isotropic porous material, Sill (1983) describes the total macroscopic electric current density *(J)* passing through a unit cross sectional surface area (in Am^{-2}) as the resultant of the summation of the conduction current density (J_c) and a convective current density *(J_s)*:

$$J = J_c + J_s \qquad 3.33$$

Assuming that the flow is laminar and the radius of curvature of the pore is much bigger than the thickness of the electrical double layer, Fagerlund & Heinson (2002) described the convective current J_s per unit area over a pore as:

$$J_s = \frac{\xi \varepsilon_r \varepsilon_o}{\mu} \overline{\nabla_n P} \qquad 3.34$$

Where ξ is the Zeta Potential (ξ-Potential), ε_r is the relative dielectric constant of the liquid and ε_o is the dielectric constant of the vacuum, μ is the viscosity of the fluid and $\overline{\nabla_n P}$ is the mean pressure gradient normal to the cross-section area.

And the conduction current per unit area, J_c, over a cross section is given by Ohm's law and taking note that $E = \overline{\nabla_n \varphi}$, Then:

$$J_c = -\sigma \overline{\nabla_n \varphi} \qquad 3.35$$

Where σ is the electrical conductivity of the bulk fluid and matrix (usually referred to as the d.c electrical conductivity of a porous material in Sm^{-1}, this can be obtained from field measurements of the electrical resistivity ($\sigma = \rho^{-1}$ where ρ [Ωm]), φ [V] is the streaming potential, which can be measured in the field using a voltmeter. Note $E = \overline{\nabla_n \varphi}$,

Substituting Equations 3.34 and Equation 3.35, in to Equation 3.33, the total electric current density *(J)* becomes:

$$J = -\sigma \overline{\nabla_n \varphi} + \frac{\xi \varepsilon_r \varepsilon_o}{\mu} \overline{\nabla_n P} \qquad 3.36$$

Since groundwater flow is driven by hydraulic head gradient, ∇h, we can write:

$$J = -\sigma \overline{\nabla_n \varphi} + \frac{\xi \varepsilon_r \varepsilon_o \rho g}{\mu} \overline{\nabla_n h} \qquad 3.37$$

Where using $P = \rho g h$, where ρ is the density of the fluid (in kg/m^3), g is the specific gravity and h is the hydraulic head. But $\varepsilon_r \varepsilon_o = k$, where k is the intrinsic permeability (in m^2), then Equation 3.37 becomes:

$$J = -\sigma \overline{\nabla_n \varphi} + \frac{\xi k \rho g}{\mu} \overline{\nabla_n h} \qquad 3.38$$

From groundwater flow theory, the flow of groundwater can be described by Darcy's law in Equation 3.2 and expressing it in terms of permeability the Darcy velocity becomes:

$$q = -\frac{k \rho g}{\mu} \overline{\nabla h} \qquad 3.39$$

Substituting Equation 3.39 into 3.38 yields a relationship between streaming potential and groundwater flow described by Revil & Linde (2006) as a **coupled-flow problem**:

$$J = -\sigma\overline{\nabla\varphi} - \overline{\mathbf{C_v}}q \quad 3.40$$

Where $\overline{\mathbf{C_v}}$ *[in Cm^{-3}]* is a coupling term that describes the excess charge of the pore water per unit volume, *C* = charge.

According to Linde *et al*. (2007), self-potential measurements are highly sensitive to changes in groundwater flow patterns, and hydraulic gradients as a function of permeability and groundwater flow velocity.

3.3.6 Poison Equation

Revil & Jardani (2013) showed that, in order to determine the field equation for the Electro-static potential (streaming potential), a continuity equation of the current density is formulated in the limit of the quasi-static regime of the Maxwell equations (Poisson relation) such that the total current equals zero:

$$\nabla \cdot \mathbf{J} = 0 \quad 3.41$$

Applying the condition over the elementary length of the domain to Equation 3.40 yields:

$$0 = -\sigma\nabla\varphi - \overline{\mathrm{C}_v}q \quad 3.42$$

$$-\sigma\nabla\varphi = \overline{\mathrm{C}_v}q \quad 3.43$$

This implies that in a steady-state of thermodynamic disequilibrium, the electric current caused by convection due to fluid flow is balanced over the length of the domain of the elementary volume by that caused by the conduction. The displacement current is neglected, meaning that the total current density is conservative (all the current entering a control volume must also exit in the absence of sources and sinks; there is no storage of electrical charges inside the control volume.

If we substitute, $q = -K\overline{\nabla h}$ (from Darcy law) Equation 3.43 becomes:

$$\left(\frac{\nabla\varphi}{\nabla h}\right)_{J=0} = \frac{-K\overline{\mathrm{C}_v}}{\sigma} \quad 3.44$$

Introducing the partial differentials Equation 3.43 can be written as:

$$\left(\frac{\partial\varphi}{\partial h}\right)_{J=0} = \frac{-K\overline{\mathrm{C}_v}}{\sigma} = C_S \quad 3.45$$

Where C_S is the streaming potential coupling coefficient. Equation 3.45 is the **fundamental equation** for interpreting streaming potential signals. Where in practical

terms φ (V) is the streaming potential field measured in the field and $\partial\varphi$ is the streaming potential gradient and ∂h is the hydraulic gradient or drawdown gradient.

3.3.7 Laboratory Procedure to Determine Streaming Potential Coupling Coefficient

The value of C_S plays a key role in controlling the magnitude of the streaming potential of a given fluid potential. It is usually determined experimentally from the laboratory for different fluid and rock types under controlled environment. Principally Equations 3.45 can be used to determine the value of the coupling term $\overline{\mathbf{C}_{\boldsymbol{v}}}$ and zeta potential (ξ-Potential) for different types of rocks on various environment parameters (Fagerlund & Heinson, 2002). The procedure presented below is an extract of Fagerlund & Heinson (2002), in which they determined streaming potential coupling coefficient form the laboratory. A typical instrument set-up is shown in the Figure 3.7.

Rock samples used in the set-up are crashed and tightly put in the sample tube to avoid any vacuum space. The pressure difference measured as hydraulic head, ΔH creates the driving force to force fluid flow through the sample and the voltage measured between the electrodes at the ends of the sample $V = V_{outlet} - V_{inlet}$ is the streaming potential. Voltage is continuously measure at changing H allowing a set of values of streaming potential for different hydraulic heads. A graph of V against H is plotted to determine the gradient which represent the streaming potential coupling coefficient.

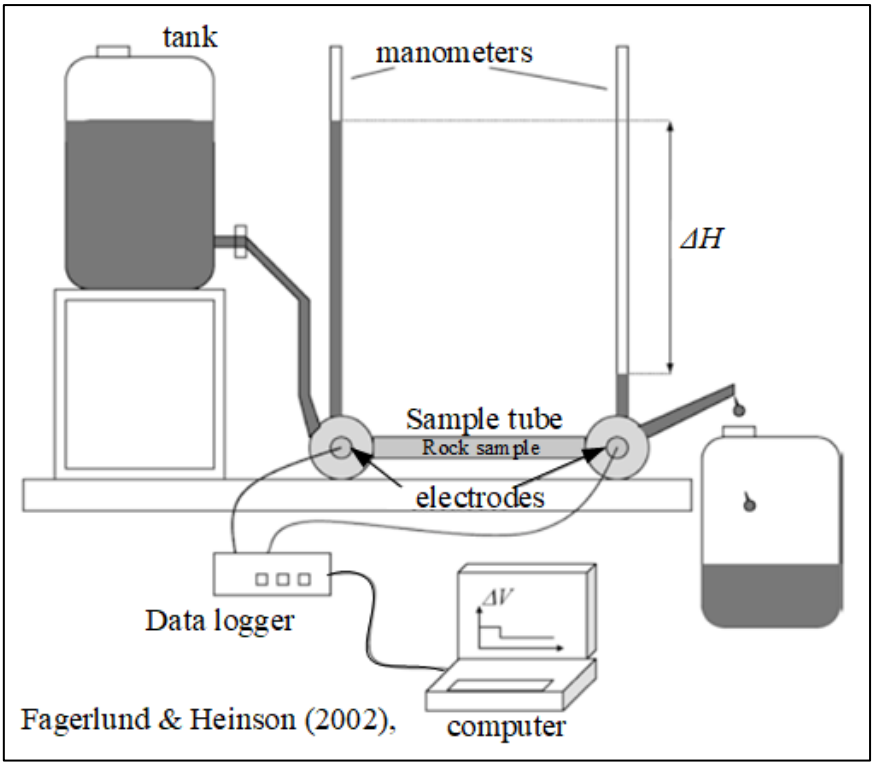

Figure 3.7: Laboratory set-up for determining zeta potential and streaming potential coupling coefficient (Cs)

The procedure is performed for different rock samples of different grain size and fluid permeability, electrolyte concentration, temperature and pH. The obtained value of *Cs* can be used through Equation 3.46 to determine the Zeta Potential:

$$C_S = \frac{\varepsilon_r \varepsilon_o \xi \rho g}{n\sigma} \qquad 3.46$$

Where σ is the fluid electrical conductivity, *n* is the viscosity of the fluid, $\mathcal{E}_r$ and $\mathcal{E}_o$ are the relative dielectric constant of the fluid and vacuum respectively.

However, what is useful in the field is the streaming potential coupling coefficient, *Cs*. In our field set-up at both test sites the arrangement of the observation boreholes allows a situation of calculating the value of streaming potential coupling coefficient by monitoring hydraulic head and streaming potential at the observation boreholes and using regression analysis.

3.3.8 Coupled Flow Solution for Pseudo-Steady State

This section illustrates the computation of an analytical solution for a **coupled radial groundwater flow** under steady state conditions as derived by Rizzo *et al*. (2004). Figure 3.8 represents an unconfined aquifer or partially confined aquifer as the case of Krudgerdrift dam site. However, Rizzo *et al*. (2004) showed that the same solution can

be used to estimate hydraulic conductivity in fractured aquifers as long as the pseudo state is reached. Meaning it is only applicable in the late times of pumping test

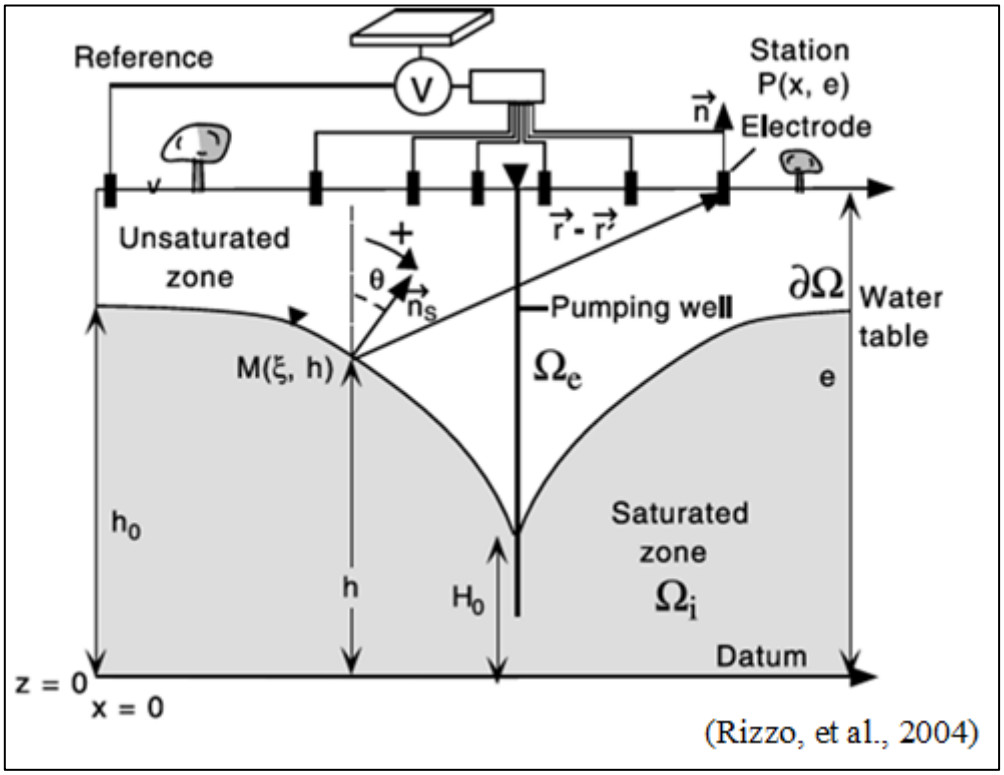

Figure 3.8: Schematic set-up for monitoring electrical response during pumping

Assume a three-dimension flow, the volumetric current density J_v is given by:

$$J_v = \rho g[\nabla C_V \cdot \nabla h + C_v \nabla^2 h] \qquad 3.47$$

where:

$$J_v = -\nabla \cdot \mathbf{J_s} = -\nabla \cdot (-\sigma \nabla \varphi) \qquad 3.48$$

Under steady state conditions where there is no change in piezometric head at late times, the first term in Equation 3.47 can be ignored, then:

$$J_v = \rho g C_v \nabla^2 h \qquad 3.49$$

According to Rizzo *et al*. (2004), under Dupuit's assumption (Section 3.2.4) for a homogeneous unconfined aquifer, the piezometric head *h(r)* at a distance *r* from the pumping borehole for steady-state flow is given by:

$$h(r) = ({H_0}^2 + \frac{Q}{\pi K} \ln(r/r_0))^{1/2} \qquad 3.50$$

Where r_0 is the radius of the pumping borehole and H_0 is the head in the pumping borehole.

Using Equations 3.49 and 3.50 yields:

$$J_v(r) = \frac{\rho g C_v Q^2}{4\pi^2 K^2 r^2 ({H_0}^2 + \frac{Q}{\pi K}\ln({}^{r}/_{r_0}))^{3/2}} \quad 3.51$$

In the geometry shown in Figure 3.8, the continuity Equation 3.42 becomes:

$$-\nabla \cdot (-\sigma \nabla \varphi) = \begin{cases} J_v(r), & r \in \Omega_i \\ 0, & r \in \Omega_e \end{cases} \quad 3.52$$

This is the fundamental field equation for interpreting (quasi-static) streaming potential signal.

Where the electrical potential is given by:

$$\mathbf{E} = -\nabla \varphi \quad 3.53$$

We assume a constant conductivity distribution in the conductive half space below the ground surface where the upper ground is assumed to be a good insulator meaning the electric field exist everywhere tangential to the ground surface where it is measure. Therefore, the boundary condition at the ground surface is $\boldsymbol{n} \cdot \nabla \varphi = 0$.

Considering the assumption above, Equation 3.52 becomes:

$$\nabla^2 \varphi = \begin{cases} -J_v(r)/\sigma, & r \in \Omega_i \\ 0, & r \in \Omega_e \end{cases} \quad 3.54$$

Any surface electrical conductivity discontinuity in the region Ω_e external to the source volume *(which is the region between the piezometric and ground surfaces)* is not accounted for. Ω_i and Ω_e are internal and external source volume in which the fluid flow is occurring. According to Equation 3.54, the electrical potential is harmonic outside the source volume. The solution being Green's function of the Poisson equation:

$$\nabla^2 G(r, r') = \delta(r') \quad 3.55$$

Where $\delta(r')$ is the Dirac Distribution at source point $M(r')$.

Rizzo *et al.* (2004), gives the Green's functions for any horizontal and homogeneous half space as,

$$G(r, r') = -\frac{1}{2\pi}\frac{1}{|r - r'|} \quad 3.56$$

$$G(r, r') = -\frac{1}{2\pi}\ln(r - r')^2 \quad 3.57$$

in three and two dimensions, respectively. Applying the boundary value problem in Equation 3.54 to the Green's Theorem yields:

$$\varphi(r) = -\frac{1}{\sigma_i}\int_{\Omega_i} G(r,r')J_v\,(r')dV \qquad 3.58$$

where *dV* is the elementary volume. If the problem in 3.58 is to have a solution then the necessary and sufficient condition is:

$$\int_{\Omega_i} J_v(r')dV = \int_{\Omega_i} \nabla^2 h(r')\,dV = 0 \qquad 3.59$$

which is obtained by the continuity equation for the mass of water in steady state conditions.

The following assumptions suffice:

1. The reference electrode is considered to be at infinity, where Ω∞=0, outside the electrical radius of influence due to the cone of depression therefore the electrical potential at surface is measured to a reference electrode.
2. The only contributors to the electrical potential are pressure head variations
3. The electrical potential is only dependent on the distance, r from the borehole.
4. The borehole walls have an infinity conductivity.

Integrating Equation 3.58, taking into consideration the condition in Equation 3.59 and the above assumptions, yields:

$$\varphi(r) = -\frac{1}{2\pi}\int_{\Omega_i} \frac{\rho g C_v Q^2 r' dr' d\theta dz}{4\pi^2 K^2 \sigma_i r'^3 \left[{H_0}^2 + \frac{Q}{\pi K}\ln\left({r'}/{r_0}\right)\right]^{3/2}} \qquad 3.60$$

$$\varphi(r) = \int_{R_b}^{r}\int_{Z-h(r')}^{z}\left[\frac{C'Q^2 dr' dz}{4\pi^2 K^2 r'^2 \left[{H_0}^2 + \frac{Q}{\pi K}\ln\left({r'}/{r_0}\right)\right]^{3/2}}\right] \qquad 3.61$$

$$\varphi(r) = \left(\frac{C'Q^2}{4\pi^2 K^2}\right)\int_{R_b}^{r}\left[\frac{dr'}{r'^2\left[{H_0}^2 + \frac{Q}{\pi K}\ln\left({r'}/{r_0}\right)\right]}\right] \qquad 3.62$$

Where R_b, is the borehole radius and $C' \equiv \left(\frac{\partial \varphi}{\partial h}\right)_{J=0} = \frac{-\rho g C_v}{\sigma}$ as provided by Equation 3.45, which is the electro-kinematic coupling coefficient associated with pressure head variations (in Vm^{-1}) and, H_o is the hydraulic head in the pumping well.

For relatively small drawdowns the electrical potential response is given by:

$$\varphi(r) \approx -\frac{1}{r}\left(\frac{C'Q^2}{4\pi^2 K^2 {H_0}^2}\right) \qquad 3.63$$

Equation 3.63 is a **first-order approximation electrical response for a steady-state radial flow**. This expression will be used to calculate K in Krugersdrift Dam test site.

The following observations can be drawn from this method (Equation 3.63):

i. The streaming potential anomaly around a pumping well is positive because the electro-kinematic coupling coefficient is generally negative as afforded by Equation 3.45.

ii. The streaming potential is inversely proportional to the square of hydraulic conductivity therefore, the analytical solution is quite sensitive to the equivalent permeability of the aquifer.

3.3.9 Coupled Flow Power Law Relationship

The hydraulic conductivity can be calculated from Equation 3.63. The equation can be presented as:

$$\varphi(r) = Ar^{-1} \qquad 3.64$$

Where the distance *r* is referenced from the pumping borehole and:

$$A = -\frac{C'Q^2}{4\pi^2 K^2 {H_0}^2} \qquad 3.65$$

Straface *et al*. (2011) named Equation 3.64 as the **coupled flow power law relationship**. The significance for the power law is that, a plot of electrical potential data as a function of distance and obtaining he value of *A* from linear regression analysis (best fitting curve) provide a means of computing the mean aquifer hydraulic conductivity. Its resultant will be compared to estimations obtained from Cooper Jacob, Theis and Thiem-Dupuit methods.

3.3.10 Coupled Flow Solution During Relaxation Phase

A recovery test involves hydraulic head or streaming potential measurements performed during the relaxation of the phreatic surface after the pump is shut down. When in the relaxation state, Birch (1998) and Revil *et al* (2003) showed that the electrical potential observed at point P is:

$$\varphi(r) \approx -\frac{C'}{2\pi}\int_{\partial\Omega} h(r')\left(\frac{n_s(r')\cdot(r-r')}{|r-r'|^3}\right)ds \qquad 3.66$$

This implies that each element of the piezometric surface can be seen as a small dipole with strength proportional to the piezometric level (Rizzo *et al.,* 2004). If the changes in pressure head is small and the solid angle θ from which the source surface as seen at point P is 2π, then Equation 3.66 becomes:

$$\delta\varphi(r) \approx C'(h(r) - ho) \qquad 3.67$$

Which is a **first order linear approximation electrical response for a coupled radial flow problem in an aquifer relaxation mode.** Where h_o is the hydraulic head at the reference electrode. This means that after shutdown of the pump, according to Equation 3.67, the streaming potential is directly proportional to the piezometric level.

In transient condition we consider our aquifer to be confined, therefore the residual drawdown at a fixed point is given by:

$$\delta s \equiv h_0 - h = \frac{2.3Q}{4\pi T} log\left(\frac{t}{t'}\right) \qquad 3.68$$

Where h_o is the initial hydraulic head, T is the aquifer transmissivity, t' is the time since pumping stopped, $\delta t = t + t'$ is the duration of the pumping test. Therefore, under the validity of the assumptions underlying Equations 3.67 and 3.68, the electrical potential is given by:

$$\delta\varphi(r) = \frac{C'2.3Q}{4\pi T} log\left(\frac{t}{t'}\right) \qquad 3.69$$

It implies that Equation 3.69 can be used as a proxy for the direct measurement of the piezometric surface.

CHAPTER 4:
METHODS AND MATERIALS

4.1 INTRODUCTION

This chapter highlights the materials, approach, and methods used in conducting the research experiments. It explains how the experimental data was collected and instruments used, highlighting all precautions taken and challenges encountered. It lastly scripts the processing and interpretation techniques that were adopted to facilitate the computation of the hydraulic structure from the measured streaming potentials. The method adopted for the study experiments and interpreting the results is summarised in the flow chart below in Figure 4.1and explained in the sections of this chapter.

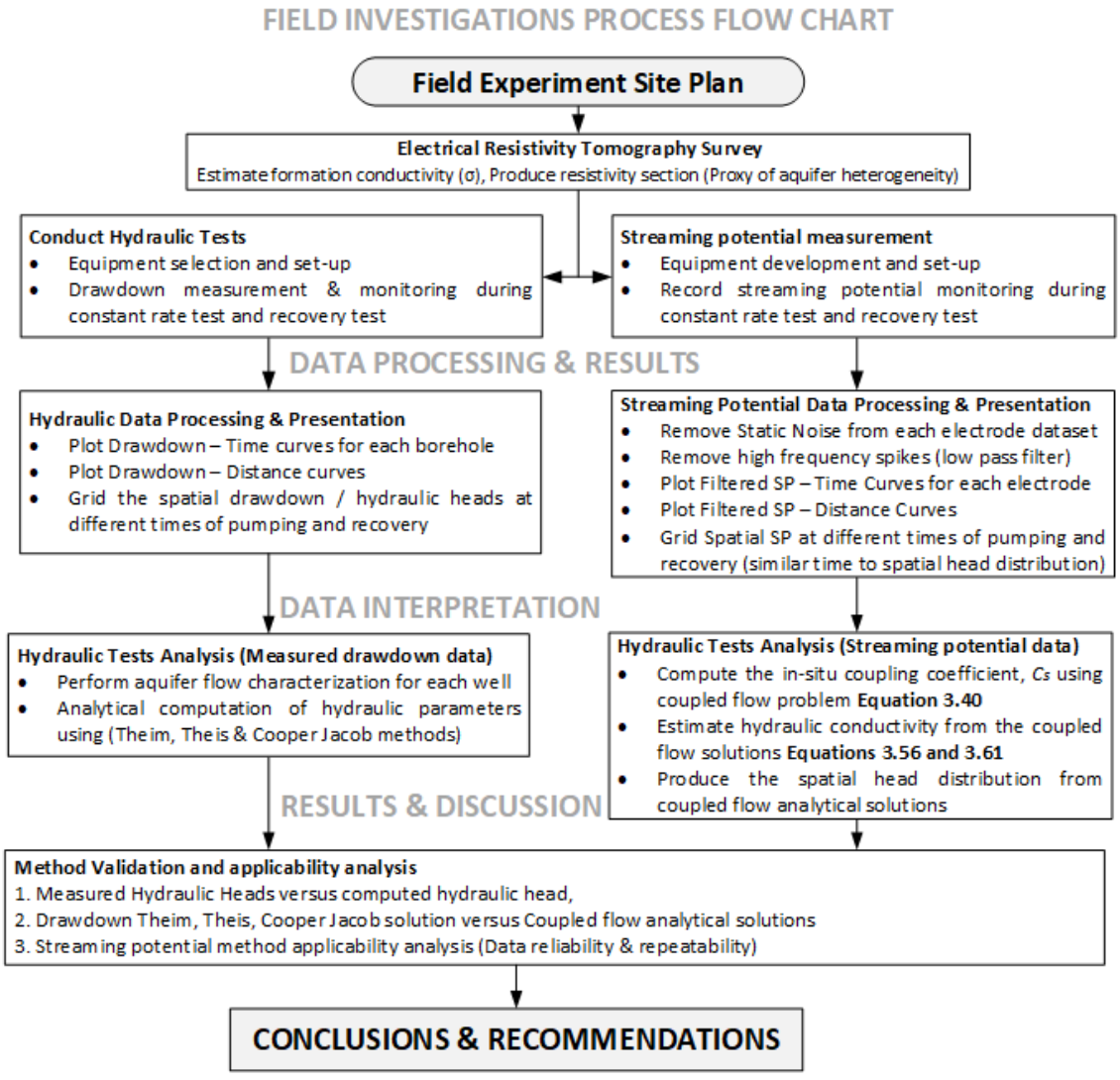

Figure 4.1: Adopted methodology for study field investigations and data interpretation

4.2 SITE CHARACTERISATION

The aim of this study activity was to characterise each test site in terms of its known hydraulic and physical properties. In general, highly fractured aquifers and porous aquifers are usually assumed to be homogeneous when interpreting hydraulic parameters (Kruseman & De Ridder, 1990). However, Zappa *et al.* (2006) emphasised that groundwater flow is greatly influenced by the physical properties of the aquifer. The effect of these physical properties on spatial variation of the geohydrological properties is referred to as heterogeneity. Work performed under this activity sort to discuss such occurrences and lay a conceptual understanding of the test sites geohydrology. This was achieved in two steps:

4.2.1 Conceptual Geohydrological Review of The Test Site

Specific review of the test site is important in this study because the interpretation framework of streaming potential signals strongly depend on the knowledge of existing geohydrological model. The hydraulic condition of the two test sites is well known as supported by the literature available, for example Botha *et al.* (1998), Woodford and Chevallier (2002), Fourie (2003) and Gomo (2011). Therefore, the first step was to closely review the literature available for each test site and select a model from which the interpretation framework of the results is set. In-depth discussion on the conceptual hydrogeological framework of the two test sites is presented in Chapter 5.

4.2.2 Hydro-Census

Most hydrogeological and geophysical investigations are initialised by field reconnaissance visits where the researcher familiarises him or herself to the site conditions. This helps in planning for the field work. During hydro-census static water levels, coordinates and depths of each borehole and piezometer were measured and recorded. The depth of the borehole and static water level were measured using Solinst water level meter and a Solinst TLC which is a temperature, level and conductivity meter while a Garmin hand held Etrex-30 was used for recording coordinates of each borehole. At both test sites some boreholes and piezometers are either blocked or collapsed such that measurement cannot be taken. Hence the visit afforded a way of planning for the experiments in selecting measurement points.

For example, Gomo (2011) reported that Boreholes BH7 and BH8 are 12 m and 6 m deep respectively but at the time of hydro-census, the depth of boreholes BH7 and BH8 were 7.9 m and 4.97 m respectively. At the time the site was developed, these two boreholes had fully penetrated the porous aquifer satisfying the assumption of horizontal flow. After realising such limitations, it became critical to establish if the boreholes at Modder River test sites were still usable for the experiment. Hence an electrical conductivity profiling technique was chosen as the method to check if there are still horizontal inflows into the borehole or not (Figure 4.2).

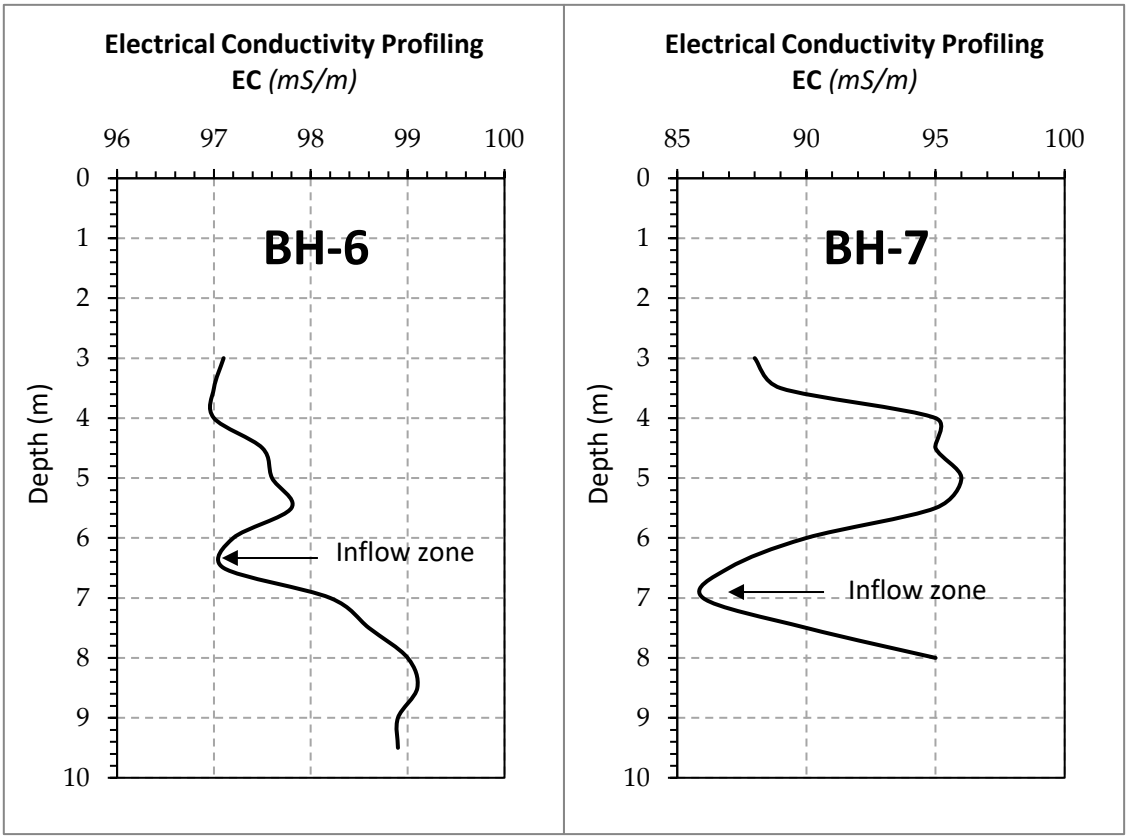

Figure 4.2: Electrical conductivity profiling showing water inflow zones for BH6 and BH7

The profiling was conducted using a Solinst TLC, which is a temperature, level and conductivity meter. The results of EC profiling showed that the main flows are between 6.5 m and 7 m which meant that both BH6 and BH7 were still usable for the experiment. The information collected during hydro-census survey is presented in Chapter 5.

4.3 FIELD INVESTIGATIONS

The output of site characterization activity is a Conceptual geological understanding of each site and a field experiment plan. A field experiment plan entails identifying the data

and all parameters to be collected on site, equipment to be used, assembling the equipment, preparing a specific site instrument configuration layout, preparing data collection forms, developing a method statement for each type of measurement to be made on site and finally choosing the right time for conducting the experiment.

The experiment is a combination of hydraulic tests (pumping tests) and geophysics measurements (Streaming potential and resistivity surveys), therefore the measurements performed during the research experiments consisted of three datasets which are:

- Apparent electrical resistivity (electrical conductivity) measurements for the unsaturated subsurface.
- Drawdown measurements during a constant rate and recovery test.
- Measurement of streaming potentials during the constant rate and recovery test.

This section of the chapter describes how the measurements were done and the equipment used in performing the measurements. It also documents the precautions taken during measurements in order to reduce the noise and eliminate errors associated with drawdown and streaming potential measurements.

4.3.1 Timing of Field Investigations

The first experiments at the Campus Test Site and Modder River test site were conducted in July 2015. A repeat experiment was conducted at the Campus in February 2016. Due to limited funding and resources only one experimental trial was effectively considered for the purpose of this research study. The experiments were conducted during the time when there was no rainfall activity because, in rainy season the overburden is usually saturated. This creates a muting effect to electrical signals and distorts the true value of sub-surface electrical property of the unsaturated zone and aquifer. Also streaming potential signals are very sensitive to any form of subsurface flow. The experiment relies on the assumption that the only contribution to groundwater flow is hydraulic pressure difference induced by pumping the borehole. In the rainy season, production is slowed down and carries a risk of equipment damage, which may frustrate the whole program. Rainy events accompanied by lightning and thunderstorms will induce electromagnetic noise in to the near subsurface which will affect the self-potential readings recorded on surface.

4.3.2 Selection of Measurement Points

Based on the review of existing geohydrology data and hydro-census the measurement points for each investigation method were selected. The test site layout map showing the location and orientation of electrical resistivity survey line, positioning of streaming potential electrodes and the location of drawdown monitoring boreholes at Campus Test Site and Krugersdrift Test Site is shown in Figure 4.3 and Figure 4.4 respectively.

4.3.2.1 Campus Test Site measurement points

Boreholes UO20, UO3, UO18, UP15, UO19 were chosen as measurement points for both drawdown and streaming potentials because of their locations relative to the orientation of the parallel bedding fracture orientation. Woodford and Chevallier (2002) revealed that boreholes UO20, UO3, UO18, UP15 and UP16 intercepted the bedding parallel fracture and UO19 did not intercept the same fracture. Hence UO19 is considered to be in a different hydraulic system to the rest of the boreholes. This implies that the progression of the cone of depression affects UO19 differently than the rest of the boreholes. The concept shall be investigated and confirmed with results of both drawdown and streaming potentials presented in Chapters 5 and 6.

Campus Test Site has over 24 boreholes drilled and developed, it would have been appropriate to monitor drawdown and streaming potentials at each borehole. However, the number of monitoring points was limited by the number of electrodes acquired and water level loggers available. The researcher could only afford to procure eight porous pots electrode *(7 monitoring and 1 used as reference electrode)*. At the time of field investigations only five level loggers were available for use. The most ideal approach would have been to place the monitoring points around the pumping borehole (at least at each sector angle). The layout in Figure 4.3 shows that the cone of depression was investigated only in the eastern side of pumping borehole UP16. Measurements in the western side of UP16 were restricted by lack of access in the meteorology station yard whose boundary is very close to UP16.

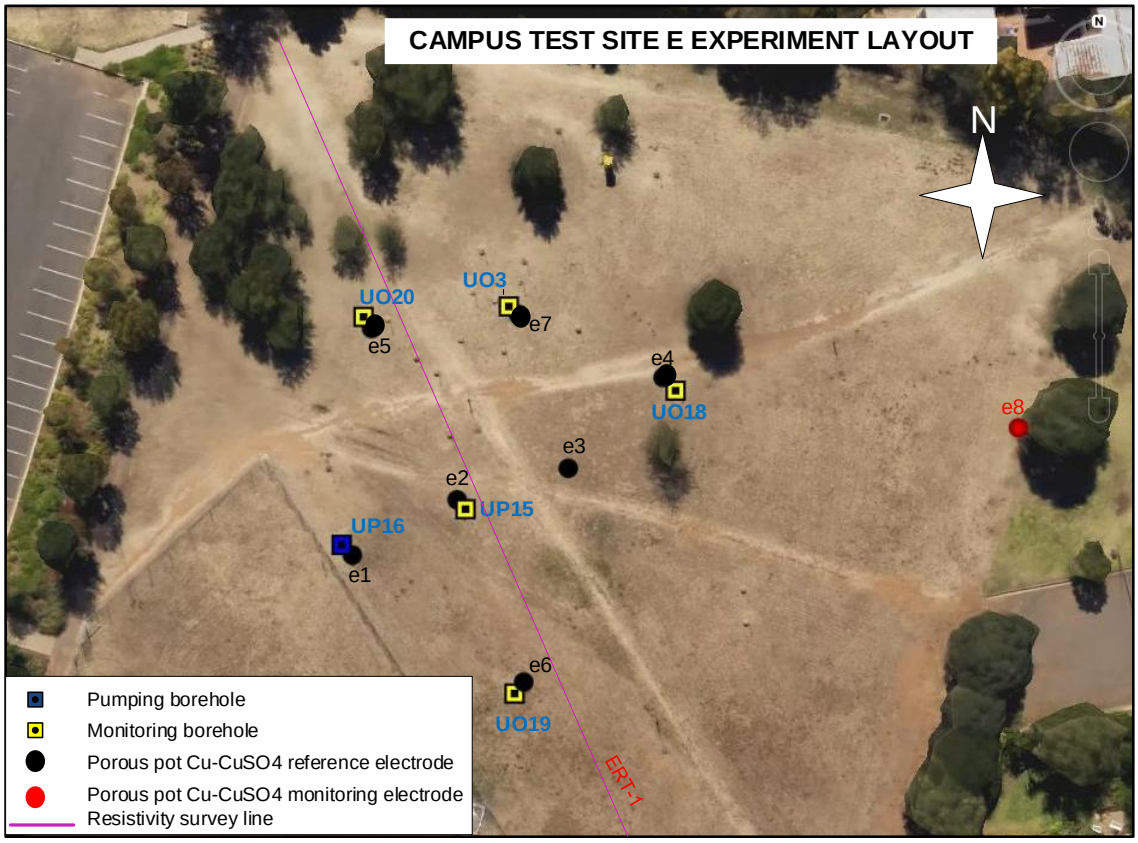

Figure 4.3: Campus Test Site plan showing drawdown and streaming potential measurement points

4.3.2.2 Krugersdrift Test Site experiment layout

According to Gomo (2011) nine boreholes (boreholes BH1 – BH9) were constructed at Krugersdrift Test Site within the alluvium porous aquifer. Only boreholes BH3, BH5 BH6, BH7, BH8 and BH9 were chosen as the measurement points with for both drawdown and streaming potential. BH7 was chosen as the pumping borehole as it is located centrally on the test site allowing for monitoring of streaming potential around the borehole. Logically it would have been ideal to monitor drawdown on borehole BH4 instead of BH9 but at the time of the experiment, but bees had colonised borehole BH4. However, SP electrodes were positioned to monitor the signals around the borehole even on BH4.

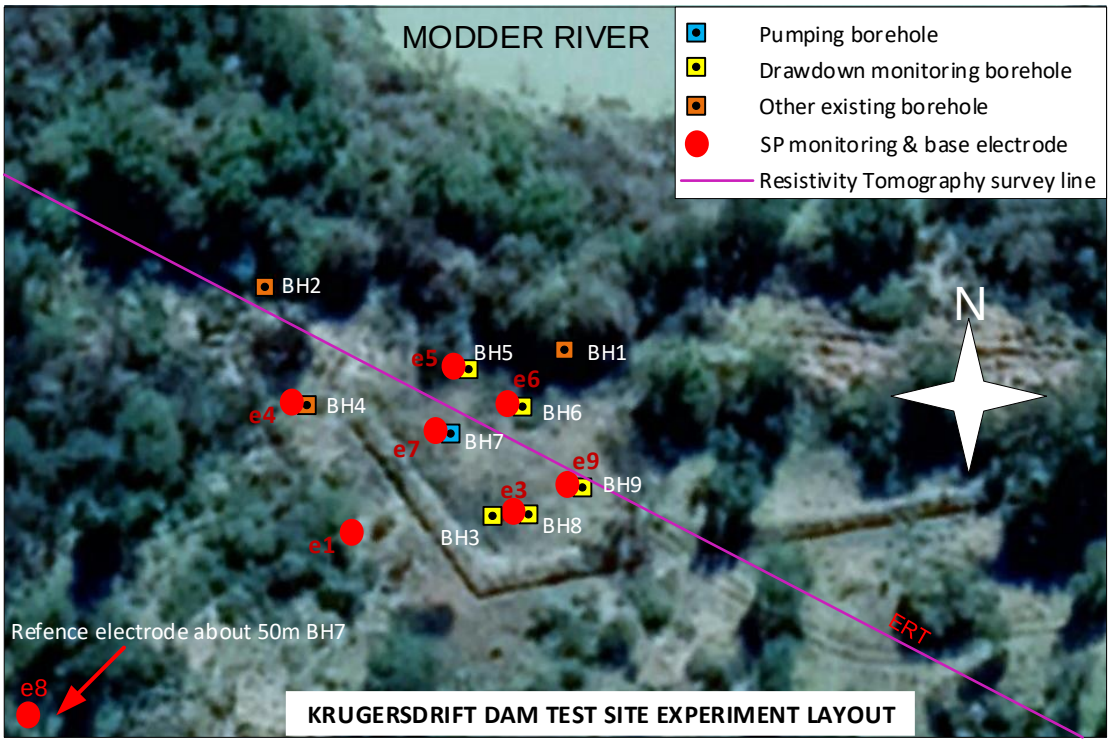

Figure 4.4: Krugersdrift dam test site plan showing drawdown and streaming potential measurement points

4.3.3 Resistivity Tomography Survey

A resistivity survey (electrical resistivity tomography) was conducted with the main of investigating if the resistivity of the unsaturated zone is homogeneous (Kirsch, 2006). The coupled flow problem is sensitive to resistivity variations (Fagerlund & Heinson, 2002), if the resistivity of the unsaturated zone is completely homogeneous then the change in SP due to pumping is essentially a mirror image to drawdown. Coupling coefficient described in Equation 3.45 is dependent on the formation electrical conductivity, therefore it became essential to also estimate the sub-surface electrical conductivity value.

Two profiles of electrical resistivity tomography (ERT) were conducted in total, one at each site. ABEM Terrameter SAS4000 imaging set with an ES10-64C Electrode selector belonging to the Institute of Groundwater Studies, with 2.5 m take-outs over 150 m spread was used (Figure 4.5). The spread achieved an effective exploration depth of 20 mbgl, sufficient to cover delineate the subsurface and the aquifer thicknesses of both sites. Data were collected using Schlumberger array because it is sensitive to both vertical and lateral variations in the subsurface conductivity and it has a good signal to noise ratio. A robust, least square inversion was performed using RES-2D Inversion software used to

develop models of sub-surface heterogeneity. The results of ERT are presented in Chapter 5 under geo-electric properties of the test sites.

Figure 4.5: Photographs of resistivity survey at Campus and Krugersdrift Test Sites

4.3.4 Drawdown and Recovery Measurements

4.3.4.1 Equipment and pumping test procedure

The constant discharge drawdown and recovery tests (CRT) were performed for 2 to 6 hours by recording the drawdown during pumping. Recording of the drawdown during the test was done using SOLINST Level Loggers model 30001. The level logger is immersed in water completely during the measurement and it measures the total (absolute) pressure. When submerged, it records the combination of barometric pressure and the water pressures. The actual pressure of just the water above the sensor is obtained by subtracting the barometric pressure from the total pressure. A Barologger was installed on the ground level next to the pumping borehole and its readings were used to compensate the barometric pressure. The drawdown in the borehole was computed finally using the resultant water pressure after barometric pressure compensation. Level loggers were set to record throughout the period of the test at an interval of 1 minute.

At the pumping borehole the water levels were recorded manually using a Solinst Temperature Level and Conductivity meter model 107. Time intervals were monitored

using a digital stop watch. After 300 minutes of pumping, recovery readings were monitored for 60 minutes in the pumping borehole and observation boreholes.

Pumping at both test sites was performed using submersible pumps. A submersible pump is a non-positive displacement pump, its discharge varies with pressure exerted by the water column above it. As the water level in the borehole drops, the discharge rate of the pump reduces. Therefore, to avoid much variations discharge rates were monitored at 20 minutes intervals through-out the duration of the test by recording time taken to fill a 20 L bucket.

4.3.4.2 Drawdown measurements at Campus Test Site

Pumping was conducted on borehole UP16 at a constant discharge rate of 2 L/s using a 3 hp submersible pump. During the constant rate test drawdown was monitored in the observation boreholes UO19, UO3, UP15, UO18, and UO20. In order to avoid recharging the aquifer with water being pumped from the borehole, water was discharged at the storm water drainage channel in the nearby car park. Test started at 1730 hours and was completed 2330 hours. The test was conducted for 360 minutes (5 hours of pumping and 1 hour of recovery).

4.3.4.3 Drawdown measurements at Krugersdrift Test Site

At Krugersdrift Test Site the water being pumped from the borehole was discharged directly in the river channel. Pumping was done in borehole BH7 using a 0.5 Hp submersible pump at a discharge rate of 0.7 L/s. Drawdown and recovery was monitored boreholes BH3, BH5, BH6, BH8 and BH9. The total time for the test was 200 minutes (2 hours of pumping and 1 hour and 20 minutes of recovery).

4.3.5 Streaming Potential Measurements

4.3.5.1 Streaming Potential Equipment

Streaming potential measurements are performed using non-polarizing electrodes connected to a voltmeter. A non-polarizing electrode is formed by a metal in contact with its own salt (Telford *et al.,* 1976). In this experiment non-polarizing electrodes were made of copper electrodes in a copper sulphate solution (Figure 4.7). The electrodes used were custom made by Geotron Systems (Pty) Ltd. The difference of the electric potential between the two electrodes was measured by voltmeters with high sensitivity of at least

0.01 mV and high internal impedance of approximately 100 MΩ. Figure 4.6 shows the seven voltmeters used to read the streaming potentials.

Figure 4.6: Voltmeters used to measure streaming potentials at each electrode station.

For accurate measurements of self-potentials, the resistance of the voltmeter must be 10 times higher than the resistance of the ground between the two electrodes (Revil & Jardani, 2013). This is done to avoid leakage of current in the voltmeter when surveying in areas with very resistive rock of the order of >100 000 Ωm. Resistivity survey at both sites show that in general the subsurface resistivity values vary in the range of 5 to 100 Ωm. At each electrode station the contact resistance was measured between the electrode and the ground before the start of the survey.

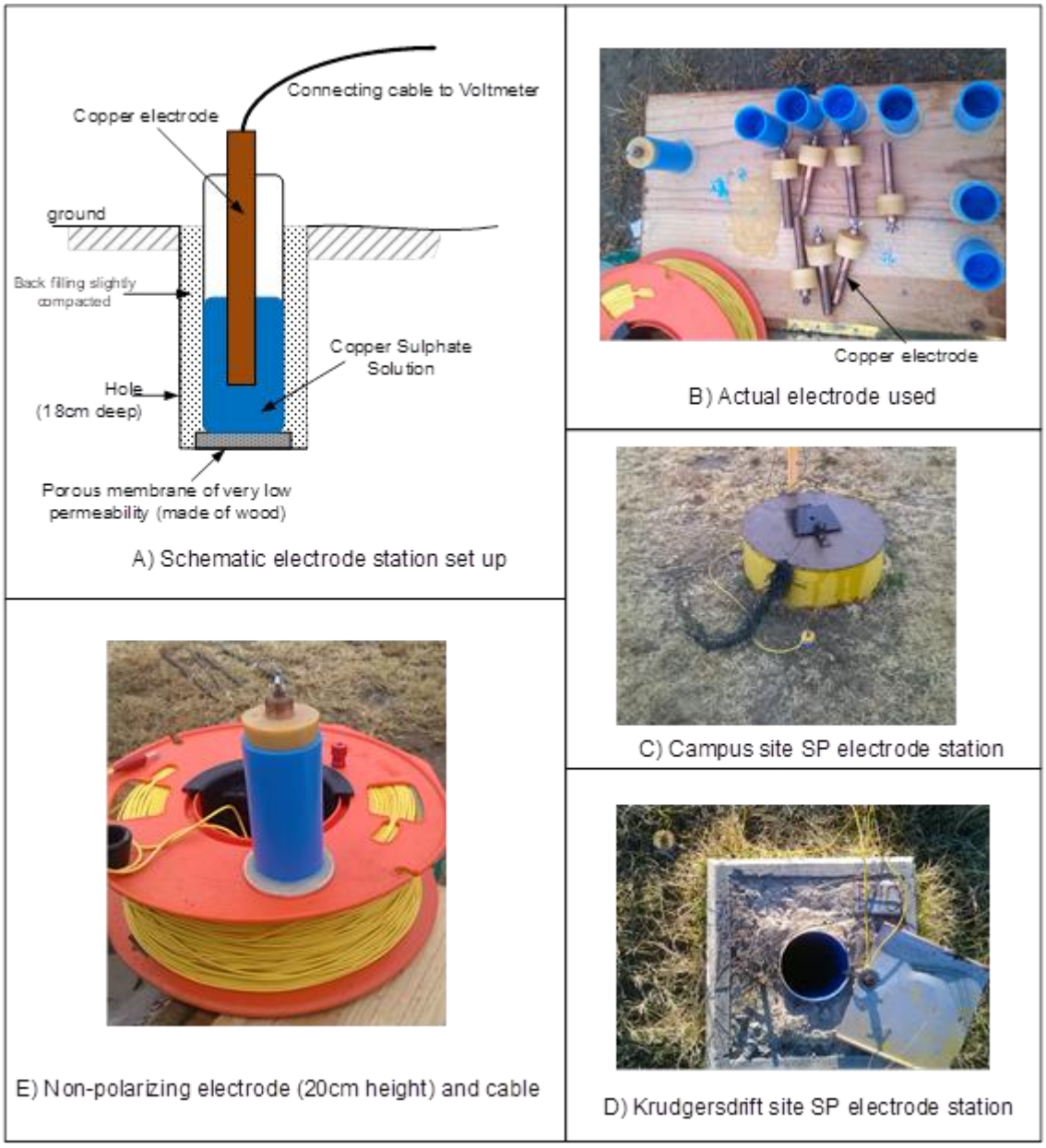

Figure 4.7: Non-polarizing electrode used at each site

Figure 4.7A shows the typical schematic non-polarizing electrode installed in the ground. Figure 4.7C and Figure 4.7D are showing the actual electrode installed at the measurement stations at Campus and Krugersdrift Test Sites, respectively.

4.3.5.2 Streaming Potential Measurement Procedure

To avoid errors in streaming potential readings as highlighted by Revil & Jardani (2013) the following precautions were taken into consideration:

i. The electrodes were installed about 20 cm into the ground, as shallower depth is usually affected by diurnal temperature variations which in-turn affect the readings. Burying of the electrode has advantages in that the sensitivity of the

electrode to external electromagnetic noise reduces with depth and also avoids sporous electrical signals associated with grass cover.

ii. The hole prepared for the electrode station is dug until moisture is seen and at the porous test site the stations were prepared with Bentonite and allowed to stabilize for 15 minutes before taking readings. This keeps the potential drop between the electrode and the ground (membrane potential) constant in space and time.

Seven porous – pot Cu-CuSO4 electrodes were placed around the pumping borehole and a reference electrode was placed approximately 100m from the pumping well where it was not affected by the depression cone (Figure 4.3 and 4.4). The field set up of SP equipment is in principle similar to the schematic diagram in Figure 3.8.

Streaming Potentials (SP) were measured at each electrode as the difference in electric potential between the reference electrode and the monitoring electrodes. SP values were recorded manually, at 1-minute interval within the first 10 minutes and at 2 minutes interval between 10 and 30 minutes and finally at 5 minutes interval until shut down of the pump.

The limitations in recording of streaming potentials were that only a single value was recorded at each electrode within each time interval. The normal practise in data collection especially for manually collected data is to get at least 3 to 4 measurements within each time interval and calculate the average for that interval in order to improve the signal to noise ratios.

At the Campus Test Site streaming potentials were measured at station located on boreholes UP16, UO19, UO3, UP15, UO18, and UO20 (Figure 4.3) during the same period as the duration of the pumping test. An extra electrode was placed in between boreholes UP15 and UO18. At the Krugersdrift Test Site, streaming potential measurements were performed at stations located at boreholes BH3, BH4, BH5, BH6, BH7, BH9 and BH8. An extra electrode (e_1) was placed between further southwest of borehole BH7.

4.4 DATA PROCESSING AND INTERPRETATION

Two primary datasets exist for these two experiments (drawdown and streaming potential data sets) and these have different processing and interpretation procedures. However, the effort of using streaming potential measurement for estimating hydraulic conductivity are done to try and simulate the common practice of using drawdown data.

4.4.1 Processing and Interpretation of Pumping Test Drawdown Data

The study adopts a procedure of interpreting pumping test data using Theis and Cooper Jacob analytical equations for radial flow towards a production borehole (Kruseman & De Ridder, 1990).

- The first stage of hydraulic test data interpretation is identifying the groundwater flow regimes using derivative curves (time -drawdown log- log plots and semi log plots). This involves identifying different kind of groundwater flow phases and characteristics in the aquifer as the cone of depression progresses outwards from the pumping borehole.
- An attempt will be made to plot the spatial head and spatial drawdown distribution of the test site in-order to identify the preferential flow paths.
- The second stage of pumping test data interpretation is estimation of aquifer hydraulic parameters such as hydraulic conductivity (*K*), transmissivity (*T*) and storativity (*S*).
- Parameters at Campus Test Site will be estimated using the Cooper Jacob method and the parameters at Krugersdrift Test Site will be estimated using Theis, Cooper Jacob.
- Gomo (2011) highlighted a possibility that the aquifer at Krugersdrift Test Site has some characteristics of a semi-confined aquifer. The writer of this dissertation identified some similarities of the semi log-plot to those of unconfined aquifer. Hence the second attempt of parameter estimation will be to use Thiem-Dupuit's condition for small changes in drawdown at the Krugersdrift Test Site.

4.4.2 Processing and Interpretation of Streaming Potential Data

Unlike drawdown data, streaming potential data contains static noise and are sporous in nature, which in most cases distorts the trend of the main signal. Processing of streaming potential data is performed by removing these forms of noise from the raw data before it is interpreted in-terms of groundwater flow parameters as shown in Figure 4.8.

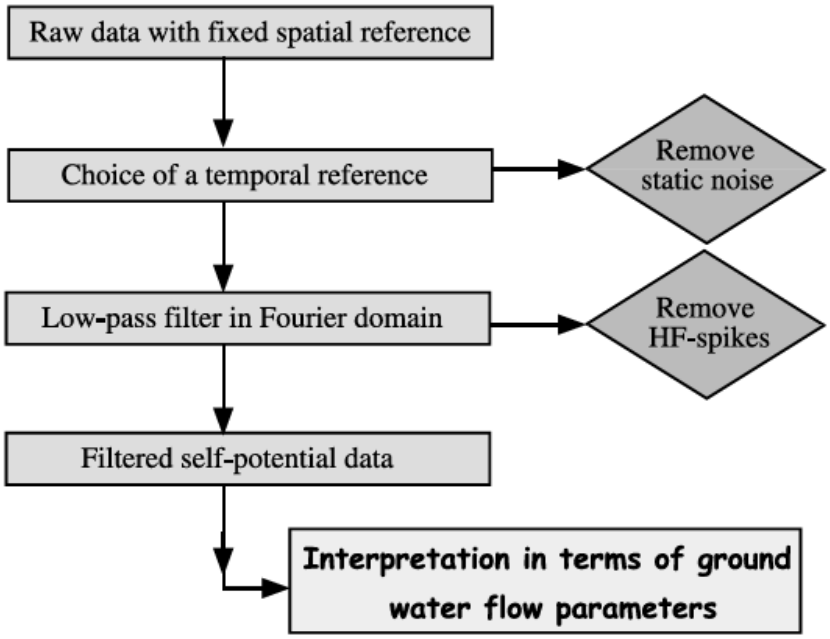

Figure 4.8: Processing procedure for streaming potential data.

4.4.2.1 Pre-processing procedure for streaming potential data

Pre-processing procedure is the step of preparing streaming potential data for interpretation. This is achieved by filtering off noise from the data and producing a best fit curve which will be adopted for interpretation purpose. Pre-processing involved:

i. **Removing static or background noise:** Static noise on self-potential data is the background and naturally occurring first order self-potential response recorded by the voltmeter, which is mostly due to some form subsurface redox reactions or background natural groundwater flow. Removing of static noise was achieved by selecting a reference or base station outside the influence of the cone of depression and reference every reading to that point.

   The background trend of self-potential signal was observed throughout the duration of the test and is subtracted from measured values (Figure 4.9). However, the background static noise was of the order of 0.3 mV as compared to the streaming potential anomaly of minimum magnitude of 1.5 mV. Therefore, the data was considered to have little to negligible static noise as not much difference is notice between the raw data and the data that have static noise removed as illustrated in Figure 4.9. Monitoring of background potential was only performed at Krugersdrift Test Site.

ii. **Removing High frequency Spikes:** High frequency spikes are medium to high amplitude and narrow oscillations observed in experimental data collected over time (in time domain). Streaming potential data is very sensitive and susceptible to that. A Gaussian Regression Low Pass Frequency Filter (GAUS-LPF) with a standard deviation of 60 was applied to the measure data and the resultant is a smooth measured data used for interpretation.

There are some low to high amplitude noise with long periods anomalies (that have no meaning to the conceptualised flow system) which cannot be removed by Gaussian regression. If these anomalies occur on a readout time interval selected for interpretation then manual fitting of the data profile was done across the anomaly as illustrated in Figure 4.11.

Also, some noise exists due to electrode shift over time because of change of contact potentials and temperature variations but these were observed to be of the order of less than 10-4 mV during the equipment development stage.

4.4.2.2 Interpretation of Streaming potential data in-terms of groundwater flow

The fundamental equation of interpreting streaming potential data as discussed in Chapter 2 is guided by Equation 3.45 which describes the relationship of streaming potential gradient from the pumping well to the change in hydraulic head. Interpretation of streaming potential data involved the following steps:

Step 1: **Plotting of Time – Potential graphs:** The filtered streaming potential data for each electrode is plotted against time.

Step 2: **Producing spatial streaming potential gradient maps:** Streaming potential theory, and findings from Fagerlund & Heinson (2002) and Rizzo *et al* (2004) show that streaming potential signal are more stable in the late times of pumping test especially under steady state or pseudo-steady state conditions. Therefore, the data used for preparing the spatial streaming potential gradient maps was selected from late times (same times similar those earlier used for preparing spatial drawdown maps).

Step 3: **Calculation of apparent or in-situ streaming potential coupling coefficient:** The normal procedure of determining streaming potential is through laboratory experiments (Fagerlund & Heinson, 2002) where the samples, but this study follows the procedure of Ball *et al* (2010) in which

he estimated the streaming potential coupling coefficient by using Equation 3.45. The arrangement of boreholes and piezometers on the test sites allows for determination of in-situ streaming potential since drawdown was also monitored at each electrode station.

Step 4: **Computation of hydraulic head from streaming potential data:** Using the coupling coefficient and Equation 3.45 a straight forward computation of drawdown around the pumping well is performed at different times of the test selected on the bases of the flow phases. This is done for each test site. The spatial computed drawdown map is produced. With the knowledge of the final water levels in the pumping well the hydraulic head is also computed and a spatial computed hydraulic head map is also produced.

Step 5: **Estimation of aquifer hydraulic conductivity:** The computed drawdown and hydraulic head are used in the normal groundwater solutions provided by Cooper Jacob methods for estimation of hydraulic conductivity or Thiem-Dupuit method, which are the two methods that allow for distance – drawdown analysis.

Step 6: **Estimation of hydraulic conductivity using coupled flow power relationship:** As earlier highlighted, Krugersdrift Test Site is a confined aquifer which at times during the flow phases exhibits noticeable semi confined and unconfined aquifer characteristics. Therefore, coupled flow solutions (coupled power relationship) provided by Rizzo, *et al.*, (2004) in Equation 3.64 and Equation 3.69 for both pumping and relaxation phases under the conditions of Thiem-Dupuit for small drawdown changes in unconfined aquifers will be used to estimate average hydraulic conductivity of the aquifer.

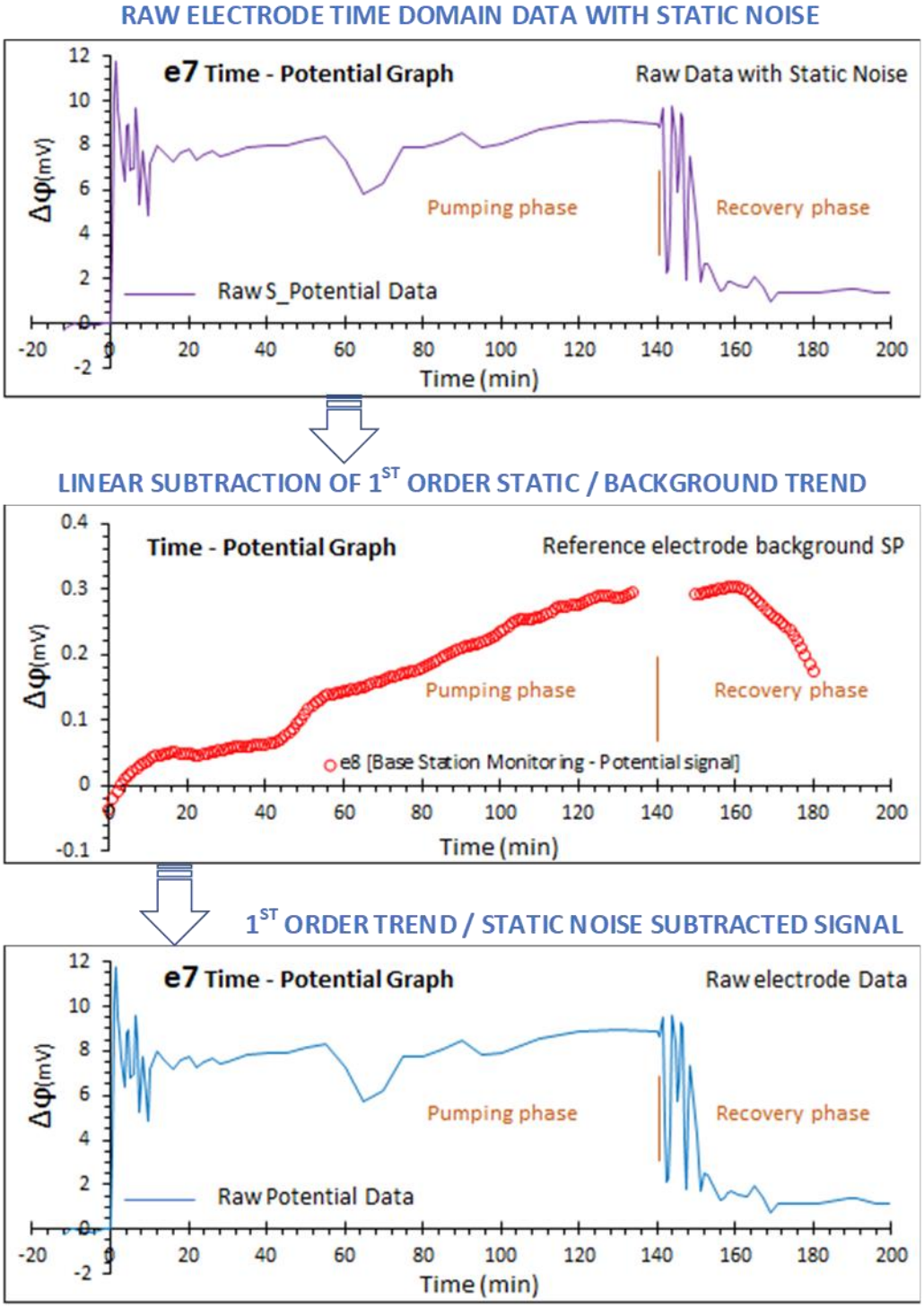

Figure 4.9: Example of static first order trend removal procedure performed on Krugersdrift Test Site potential data.

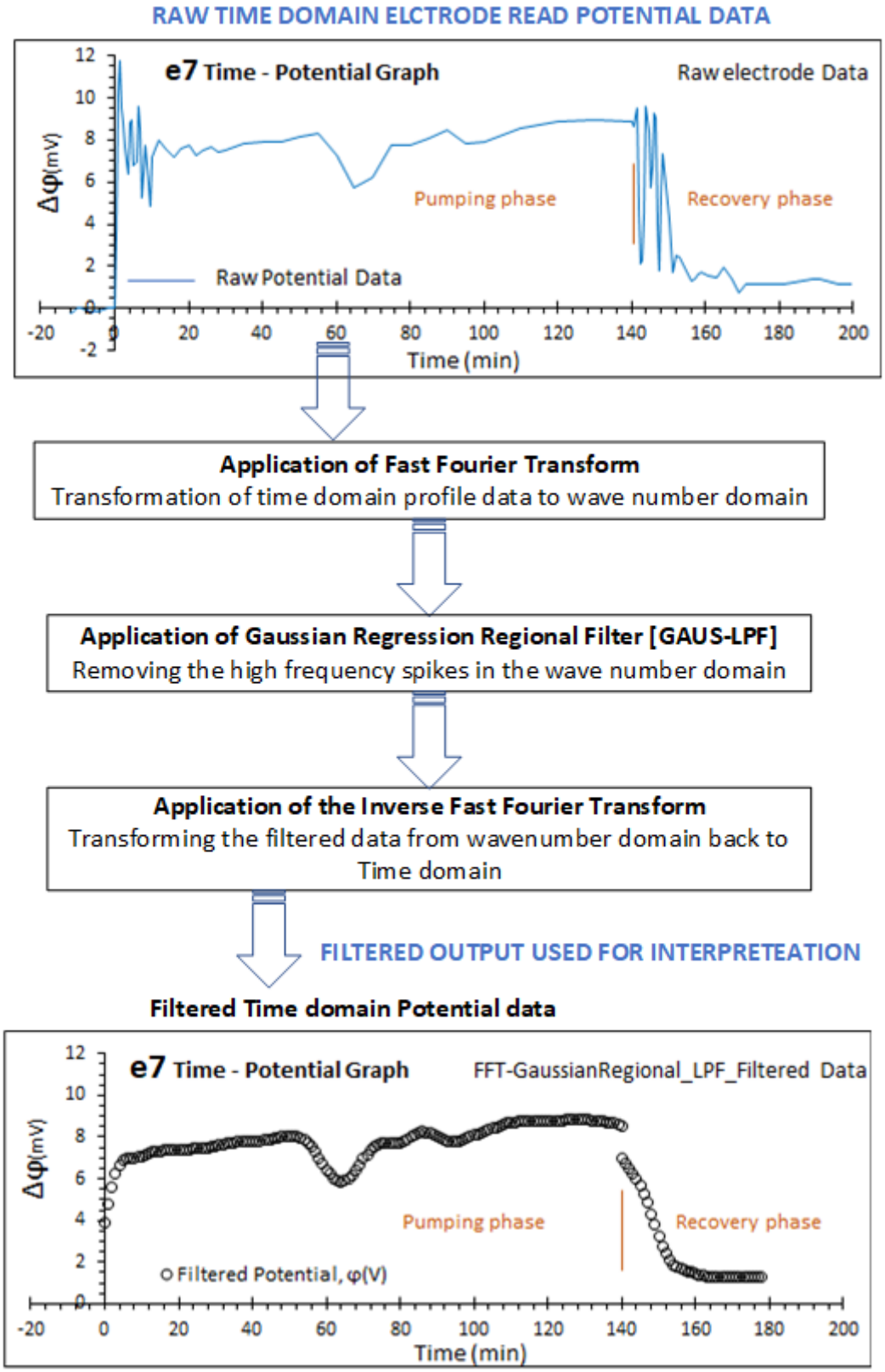

Figure 4.10: Illustration of Gaussian filtering procedure applied on electrode (e7) data for Krugersdrift Test Site experiment

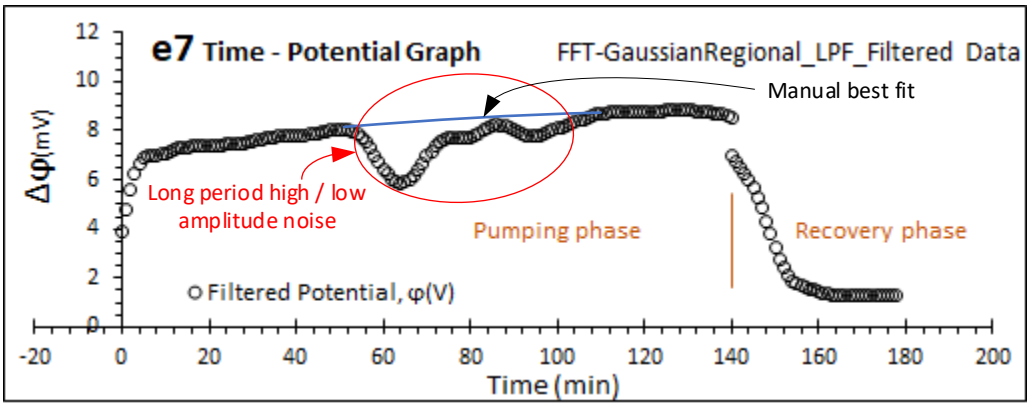

Figure 4.11: Manual best fitting technique to eliminate long period noisy anomalies

4.5 VALIDATION OF STREAMING POTENTIAL METHOD

It is acknowledged that traditional hydraulic test involving drawdown measurements have been widely used to successfully provide reliable estimations of aquifer parameters such as hydraulic conductivity. Therefore, in this study, the results from streaming potential method are compared to estimations from measured drawdown pumping test analysis. The following steps will be performed in the validation process:

Step 1: **Inspection of the mirror image rule:** Radial flow **s**treaming potential theory (Coupled flow problem) reveals that streaming potential gradient is a mirror image of change in hydraulic head (drawdown). Time - Streaming potential graphs and spatial distribution maps are compared against Time - Drawdown graphs to check the inverse or mirror image relationships.

Step 2: **Validation of computed drawdown:** The computed drawdown is compared against measured drawdown through a correlation graphing analysis.

Step 3: **Validation of computed hydraulic conductivity:** In this study hydraulic parameter estimations from measured drawdown analysis (pumping tests) are considered to be the true and exact characteristic values of the system. The validation process of the estimated hydraulic conductivity from streaming potential method will be achieved by computing the closeness of the estimation to the exact value.

4.6 EVALUATION OF STREAMING POTENTIAL METHOD APPLICABILITY

Validation process explained above, in its own right is a profound evaluation of the use of the streaming potential method in estimation of hydraulic conductivity. However, the step will be a concluding statement laid in Chapter 6, highlighting if streaming potential method is usable or not for the purpose of estimating hydraulic conductivity.

CHAPTER 5:
CASE STUDY SITES CHARACTERISATION

5.1 INTRODUCTION

The research was performed in two case study sites representing a fractured Karoo aquifer and a porous Karoo aquifer. A discussion of the geology and geohydrology of the selected case study sites was performed as part of understanding the test sites geohydrology models. Streaming potential readings are sensitive to subsurface heterogeneity variations and so resistivity imaging results for each test sites are also presented as preliminary evaluation of the level of electrical conductivity homogeneity of the unsaturated subsurface. The chapter finalises by discussing the flow characteristics of each test site using the drawdowns measurements acquired during the field experiments.

5.2 CAMPUS TEST SITE AQUIFER CHARACTERISTICS

5.2.1 Introduction

The Campus Test Site is one of the famous research test sites that was used to characterize the geohydrological properties of fractured Karoo aquifers (Woodford & Chevallier, 2002). It covers an area of approximately 34 560 m^2. The site was initially developed by the Institute of Groundwater Studies for research purposes and many postgraduate students have used it for their master's and doctoral study research. However, the key literature used to develop a conceptual geohydrological understanding of the Campus Test Site is from Botha *et al* (1998), Woodford and Chevallier (2002) and Fourie (2003).

5.2.2 Geology of the Campus Test Site

The geology of the Campus Test Site is relatively uniform and is situated partially on a basal outcrop of the Spitskop Sandstone, but mainly on the underlying Campus Sandstone which are part of the upper beds of the Adelaide Subgroup (Figure 5.1). The stratigraphy is divided into five different rock units namely, mudstone, carbonaceous shale, cross laminated mudstone and siltstone, cross laminated rhythmite sequence and cross bedded sandstone. The lithofacies of the Campus Test Site lithological units from 3 core boreholes and the profile of the campus geology from 24 percussion boreholes drilled by the year 2003 are shown in Figure 5.2 and Figure 5.3 respectively.

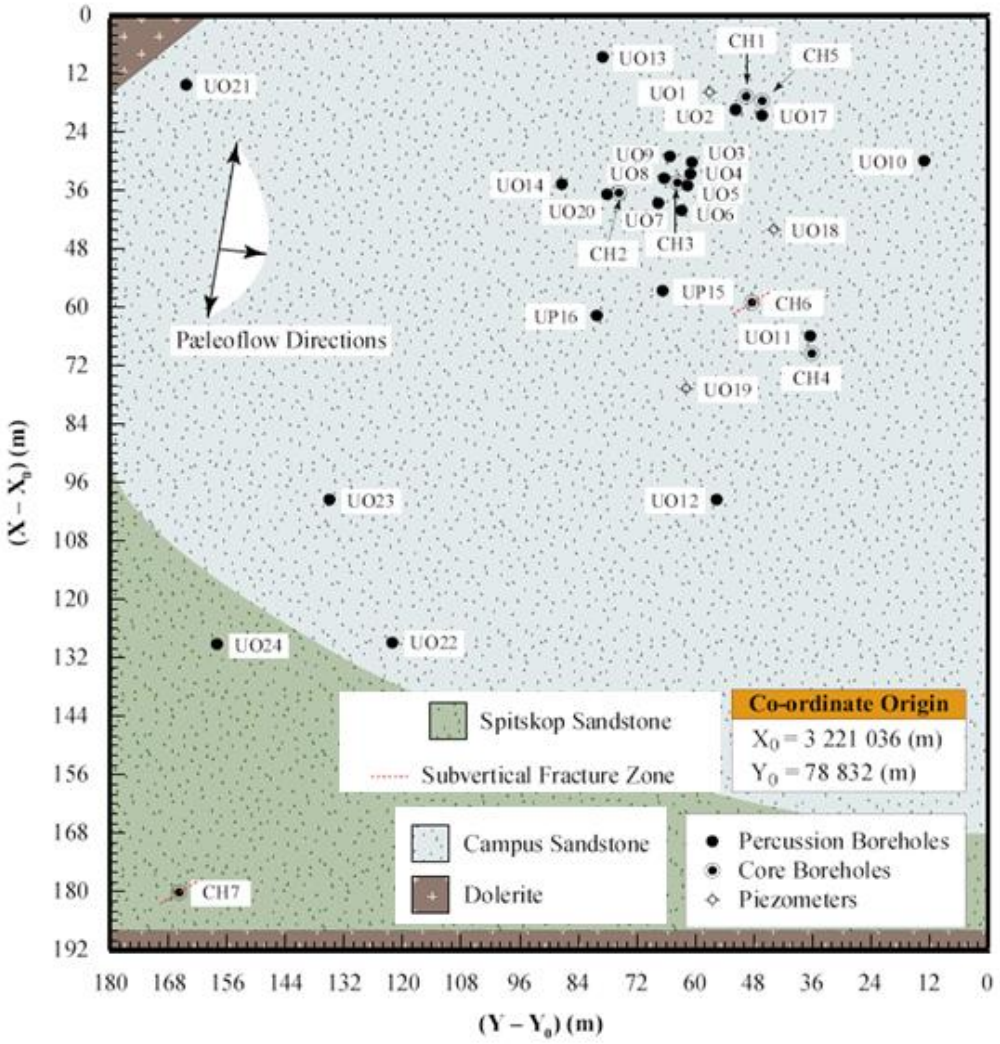

Figure 5.1: Plan view of Campus Test Site geology and location of test boreholes.

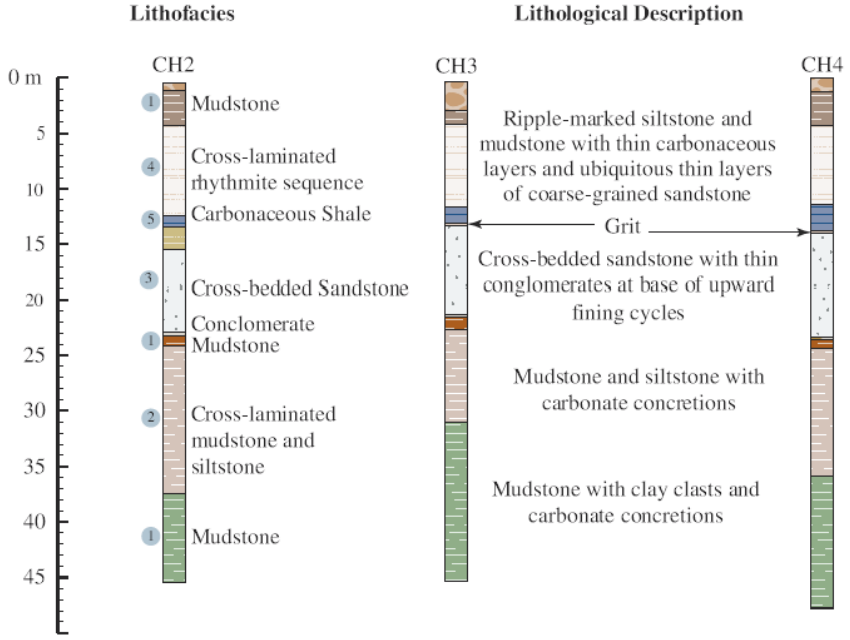

Figure 5.2: Lithofacies of the lithological units for the Campus Test Site (3 core boreholes).

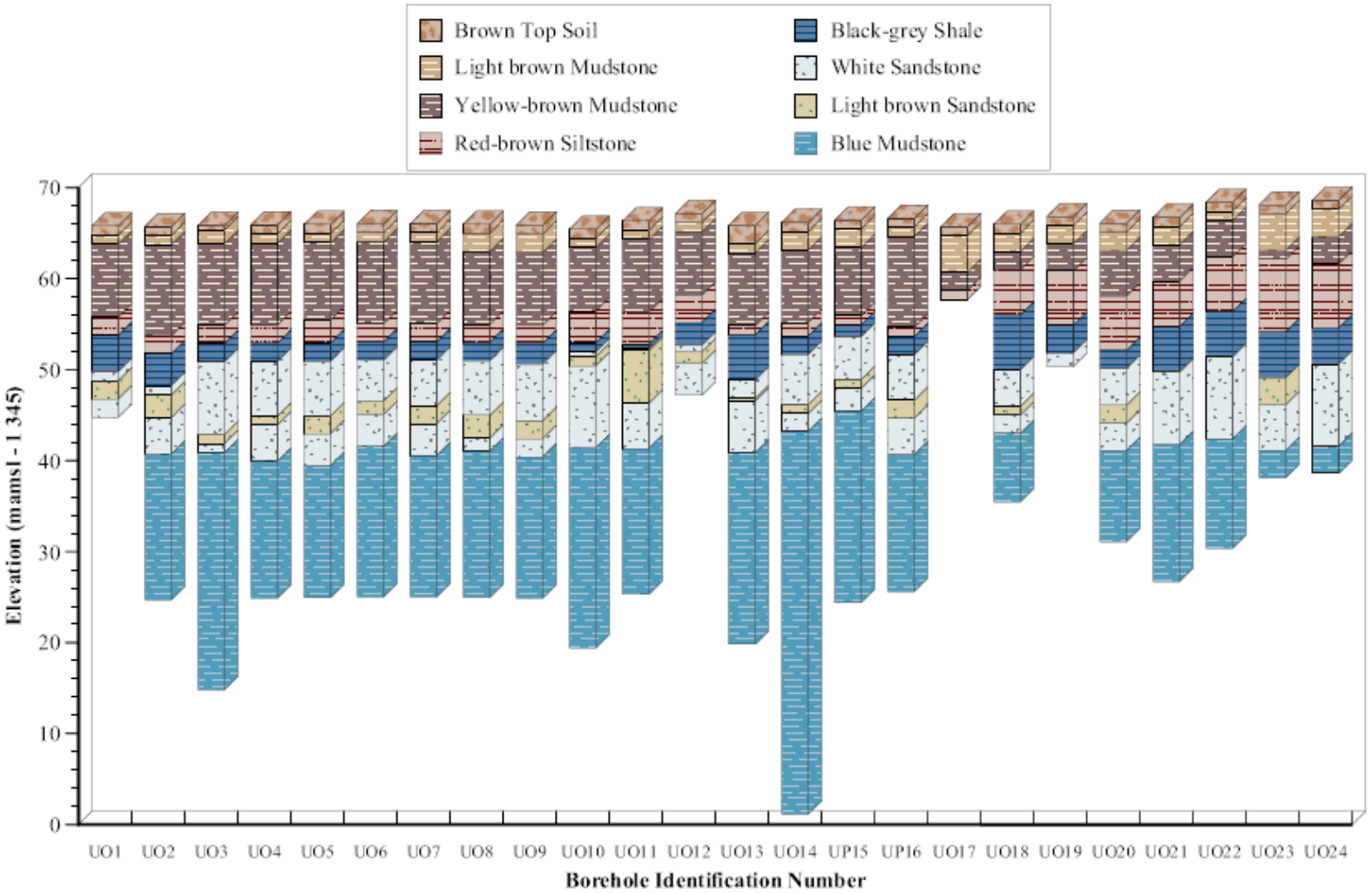

Figure 5.3: Geological logs of 24 percussion boreholes drilled by 2003 at the Campus Test Site.

5.2.3 Geometry of the Campus Test Site Aquifer

Three aquifers exist on the Campus Test Site as shown in Figure 5.4. The upper most aquifer is a phreatic aquifer that occurs in a laminated alternation of mudstones and siltstones with thicknesses of 6 to 9 m and a fine-grained, cross-laminated rhythmite sequence of thicknesses varying between 1 and 6 m. The first and second aquifer are separated by a black carbonaceous shale layer of varying thickness between 0.5 and 4 m. The second aquifer is the main campus aquifer comprising of thick (8 – 11 m) Campus Sandstone layer and is confined. The third aquifer is also confined and occurs in a succession of interbedded mudstone, siltstone and a fine-grained sandstone.

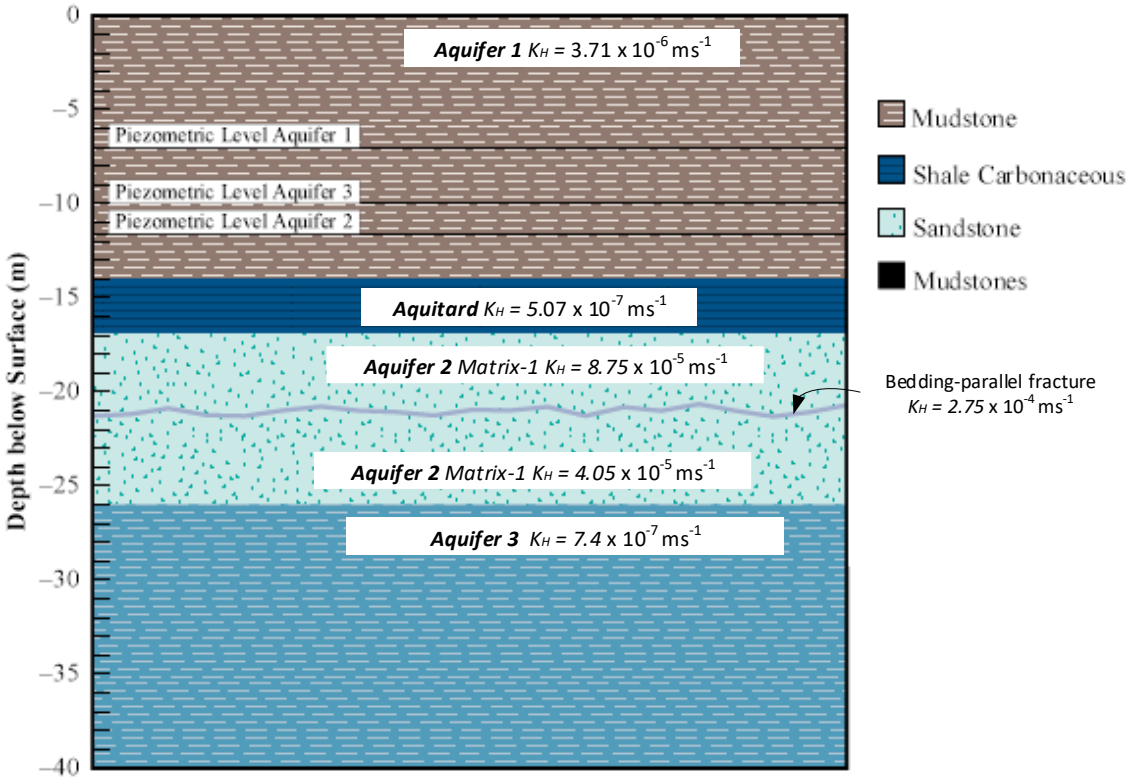

Modified from Woodford & Chevallier, (2002)

Figure 5.4: Schematic presentation of Campus geological section and aquifer present

Figure 5.4 reveals that a mode 1 bedding parallel fracture exists within the main aquifer matrix at around 22 m in depth. Botha *et al.* (1998) observed that yield of the boreholes on the campus depend on the presence of this prominent bedding-plane fracture. All high yielding boreholes intersect this fracture while all low yielding boreholes did not intersect the fracture. It also shows the average horizontal hydraulic conductivities of each aquifer unit determined by a series of double packer tests (Woodford & Chevallier, 2002). It

shows that the hydraulic conductivities decrease in depth even within the same main aquifer matrix.

Results of pumping test data analysis for boreholes UO26, UO28 and UO29 performed by Van der Voort & Van Tonder (2000) using Barker method showed that the prominent fracture has a fractal dimension of approximately 1.5. The key observation was that the occurrence of the fracture is likely to be localised. Figure 5.5 shows the fractal representation of the geometry of the prominent fracture on Campus Test Site giving an indication of its aerial extent.

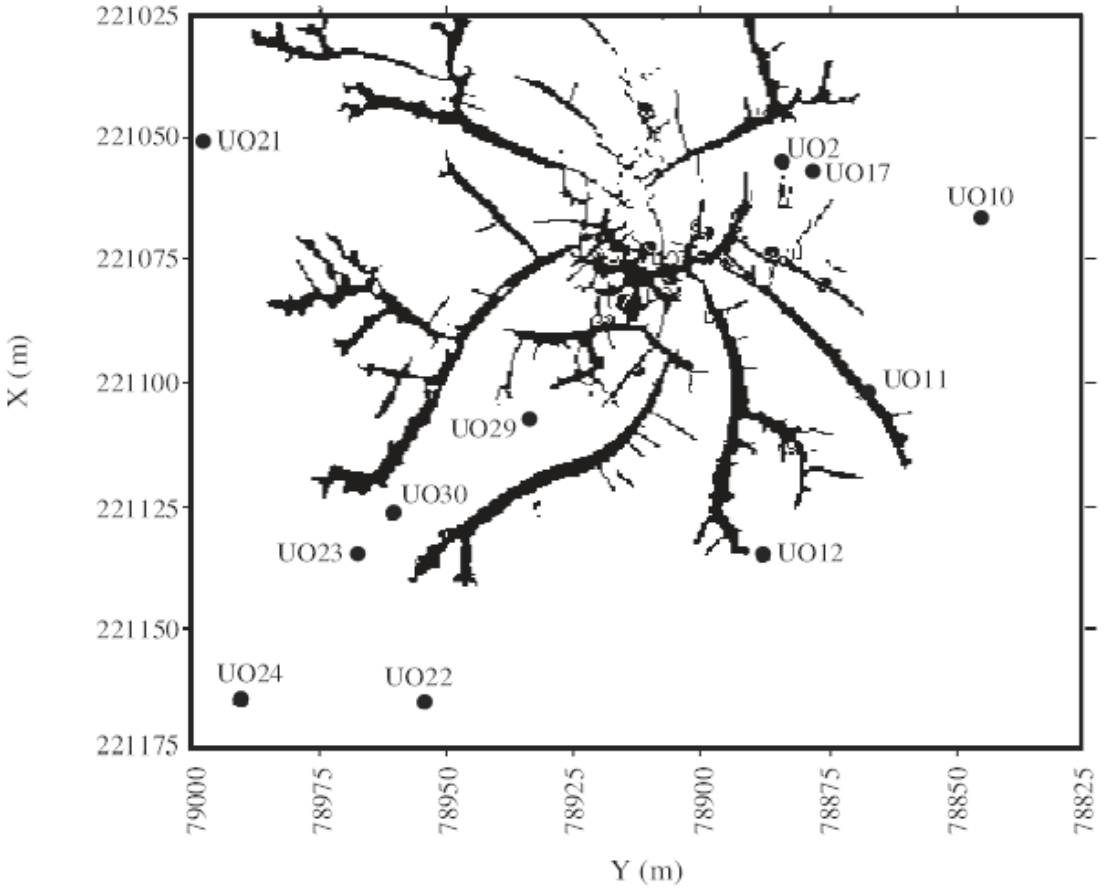

Figure 5.5: Fractal representation of the geometry of the prominent fracture on Campus Test Site

5.2.4 Aquifer Flow Characteristic at the Campus Test Site

The Campus aquifer is classified as a multi-layered and multi-porous aquifer in which the bedding parallel fractures form the main conduits of water and the matrix formation forms main storage of water. Therefore, two types of flow exist namely matrix flow and bedding

parallel fracture flow. The pumping test data were used to identify these types of groundwater flow at the Campus Test Site (Figure 5.6)

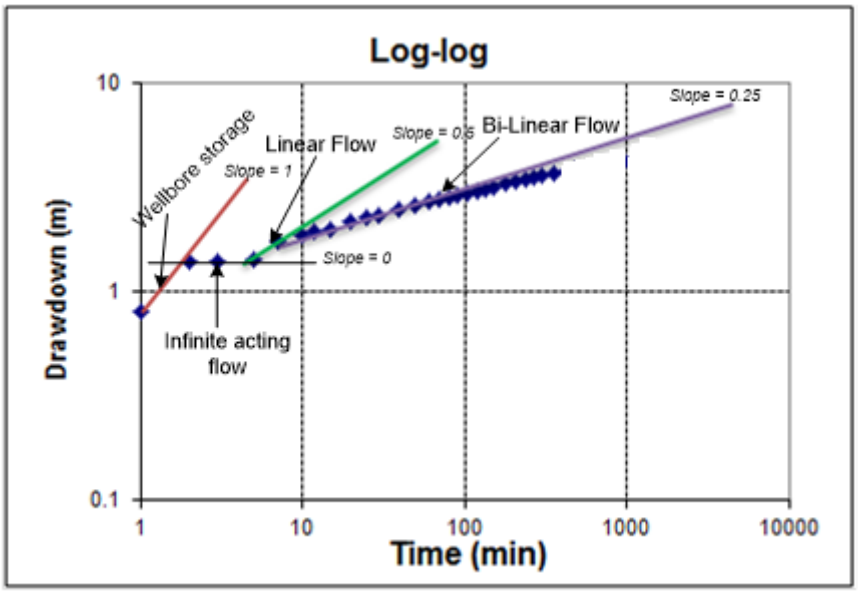

Figure 5.6: Log-log diagnostic time drawdown plot for UP16 at Campus Test Site

The flow phases present at the Campus Test Site are identifiable using log-log diagnostic plots and the phases are described below:

- **Wellbore storage:** Wellbore storage is defined as the water in the borehole column that is immediately drained within the first few seconds of pumping before a hydraulic gradient is created within the aquifer. It is identified by a slope of 1 on the log-log plot. This occurred within the first two minutes of pumping.
- **Infinite acting flow:** When the borehole that has intersected the fracture is pumped, the drop in the piezometric pressure will cause the water from the aquifer matrix to leak into the fracture. This type of matrix flow is vertical in nature. Flow within the fracture is horizontal towards the borehole. It is identified as the horizontal line with a slope of zero after well bore storage representing Theis model. The dominant flow is fracture flow. It occurred between the 2nd and 7th minute of pumping.
- **Linear flow:** This is identified by a slope of 0.5 and it occurred between the 7th and 10th minute of pumping. Due to the limited storage in the fracture, linear flow only lasted for 3 minutes of pumping.

- **Bi-linear flow:** It is represented by linear flow from matrix to the fracture and linear flow from fracture to the borehole. It is identified by a slope of 0.25 from 10th minute to 200 minutes. This is the dominant flow.

The derivative plot was used to identify the position of fractures in the matrix (Figure 5.7)

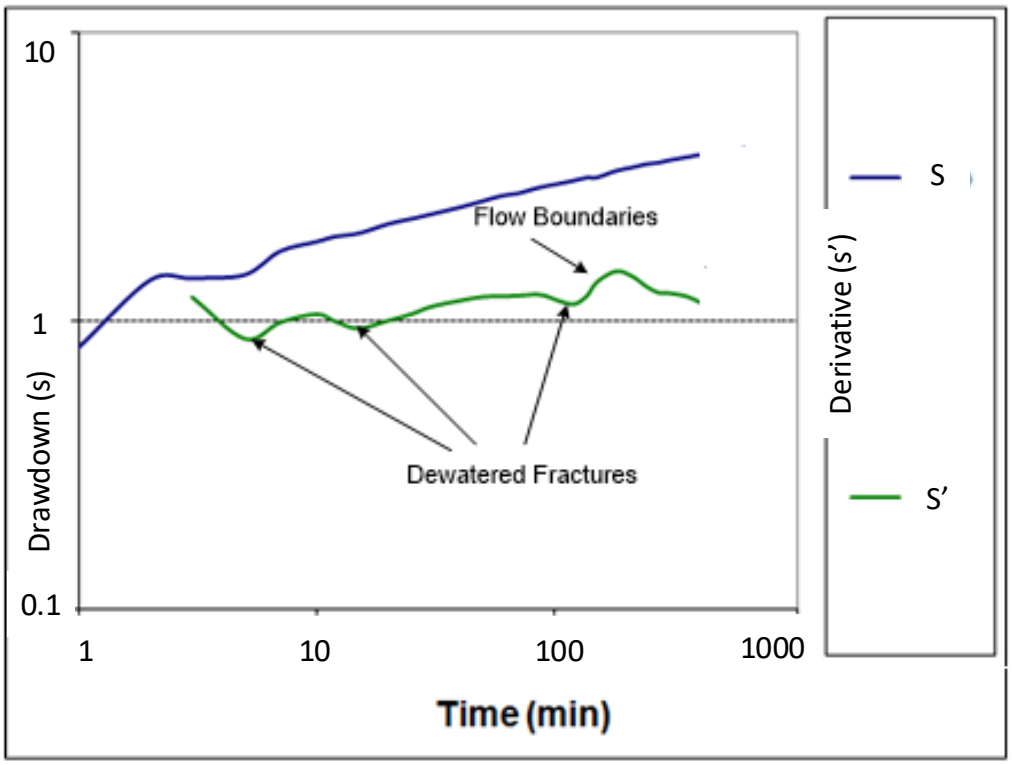

Figure 5.7: Log-log diagnostic time-drawdown / derivative plot for UP16 at Campus Test Site

5.2.5 Geoelectric Property of the Campus Test Site Aquifer

An electrical resistivity tomography (ERT) was performed on the Campus Test Site along one profile in the north-west to south-east direction as part of the study activity using a Terrameter SAS4000 Imaging set with 2.5 m take-outs over 150 m spread. Only one profile section was conducted due to limitation in space as a result of buildings and paved roads. Limitation of space also reduced length of spread to 150 m, as a result affected the maximum depth of investigation. However sufficient data was collected, which gave an indication of unsaturated zone resistivity heterogeneity.

The aim of conducting the resistivity profile was an attempt to use electrical resistivity property in delineating the lithofacies and assign an average electrical resistivity value to the aquifer matrix and other lithofacies. The maximum depth of exploration achieved for this ERT was 20 mbgl. Therefore, it also scanned the main aquifer which lies between 15

and 25 mbgl. Demarcation of lithological facies was done by correlating it with geological logs for boreholes UO13, UO20, UO27, UP15 and UO19 with the depth space of 20 m.

The following observation were made for the electrical resistivity section (Figure 5.8):

i. Resistivity image shows that the unsaturated sub-surface is considered to be homogeneous with respect to electrical properties. It also confirms that the hydrogeological units of the Campus Test Site are uniform.

ii. Lowest resistivity values averaging 11 Ωm were recorded within the upper phreatic aquifer unit comprising of mudstone and siltstone. Since electrical conductivity is a reciprocal of electrical resistivity, this unit was assigned an electrical conductivity value of 0.091 Sm^{-1}.

iii. The main aquifer is characterised by resistivity values beyond 50 Ωm and a characteristic formation electrical conductivity value of 0.02 Sm^{-1}.

iv. The Campus sandstone aquifer shows a dome shape this agrees with the observation by Woodford and Chevallier (2002).

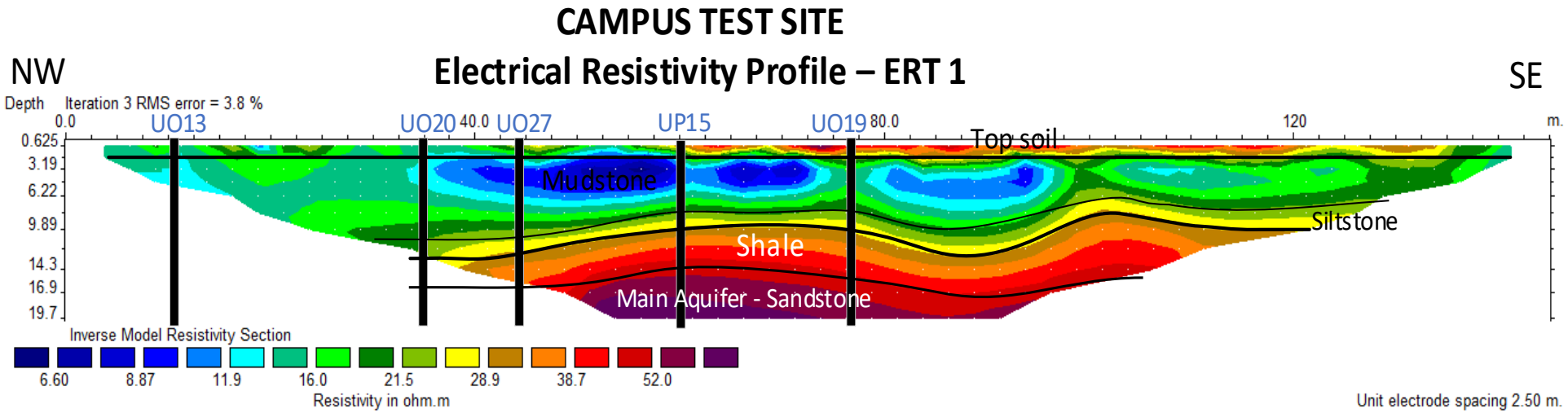

Figure 5.8: Electrical resistivity tomography for Campus Test Site

5.3 KRUGERSDRIFT TEST SITE AQUIFER CHARACTERISTICS

5.3.1 Introduction

The literature presented in this dissertation on the geology and geohydrology is extracted from Gomo (2011). However, interpretation of pumping test and electrical resistivity data collected complimented the conceptual understanding of the Krugersdrift Test Site.

Krugersdrift Test Site is a porous alluvial channel aquifer located on the riparian zone between the terrestrial land (terrestrial aquifer) and the river bank of the Modder River as illustrated in Figure 5.9. It was developed as a research site by Gomo (2011). The river channel at the test site is a bedrock river channel. Outcrops of shale bedrock are visible on the river bank.

This study limits its discussion to the characteristics of the alluvial aquifer in the riparian zone, the geology and geohydrological behaviour of the terrestrial aquifer was not cover.

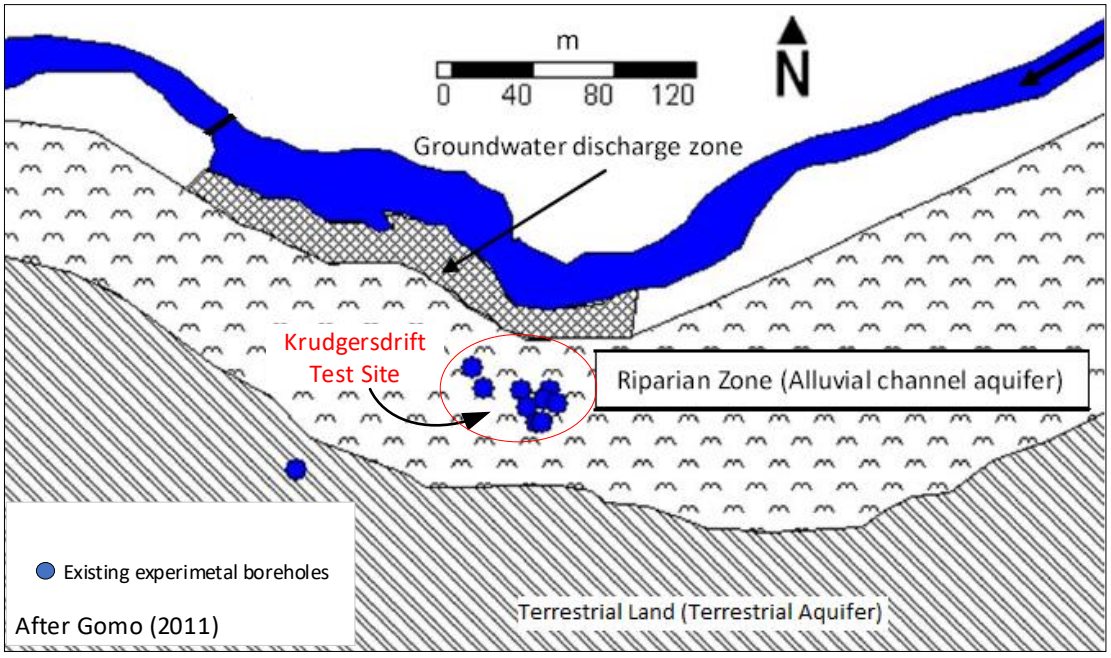

Figure 5.9: Location of the Krugersdrift Test Site on the alluvial channel

5.3.2 Geology of the Krugersdrift Test Site

Krugersdrift Test Site is characterised by an alluvial cover overlying the impermeable shale bedrock. The alluvial cover comprises of a thin layer of calcareous soils and calcrete underlain by a succession of clay, silt and gravel-sand channel deposits. The lithology of the boreholes drilled and developed within the test site are shown in Figure 5.10.

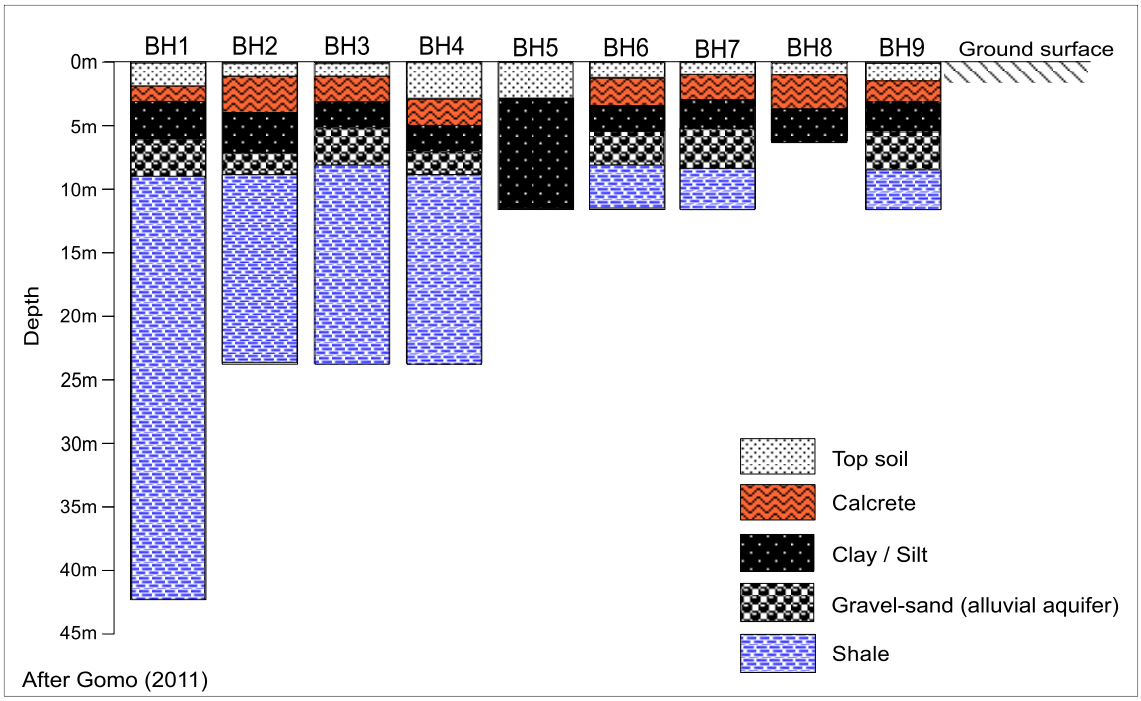

Figure 5.10: Lithology of the boreholes drilled at Krugersdrift alluvial aquifer site

Figure 5.10 shows a group of boreholes drilled to depths of 12 m, 24 m and 42 m. These boreholes confirm that the geological units occur uniformly across the area of the test site. Gomo (2011) conceptualised the fine-grained clay-silt layer to have been deposited through a flood deposition process, while the gravel and medium to coarse grained layer is perceived to have been deposited by a river channel deposition process. The calcareous soil is as a result of geological chemical interactions.

5.3.3 Geohydrology Model of Krugersdrift Test Aquifer

The Krugersdrift Test Site is conceptualised to have two aquifers classified by Gomo (2011) as shallow and deep aquifers (Figure 5.11). The shallow aquifer is referred to in this study as the "porous alluvial aquifer" within 10 m of the subsurface. Gravel and sand channel deposits with average thickness of 3.5 m form the main part of this aquifer with high hydraulic conductivity properties. Its water levels range between 2.5 mbgl to 3.5 mbgl. The fine-grained clay and silt create semi-confining conditions for this aquifer. Aquifer transmissivity values ranging from 17 m^2/d to 120 m^2/d were estimated by Gomo (2011).

The deep aquifer is a fractured shale bedrock aquifer with hydraulic heads around 6.5 mbgl. It is characterised by very low transmissivity values varying between 0.1 to 0.9 m/d. Boreholes 1, 2 and 4 were developed only in this aquifer and are very low yielding.

Groundwater discharges into the river via the bedding parallel fractures at the interface of the shallow and deep aquifer.

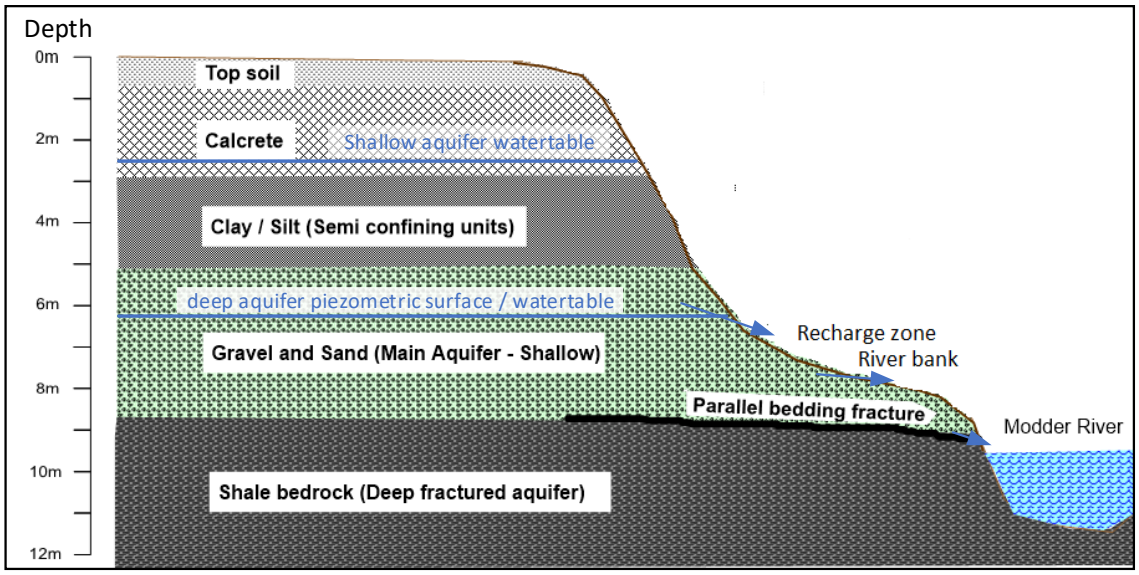

Figure 5.11: Conceptual aquifer for Krugersdrift Test Site

5.3.4 Aquifer Flow Characteristics

Aquifer flow characteristics are usually determined using derivative drawdown plots (either log-log plots or semi-log plots). Drawdown in BH7 is not satisfactory smooth therefore BH3 is chosen to illustrate the characteristic flows in the Krugersdrift Dam Test site aquifer (Figure 5.12). However, the shape of their time – drawdown graphs are similar.

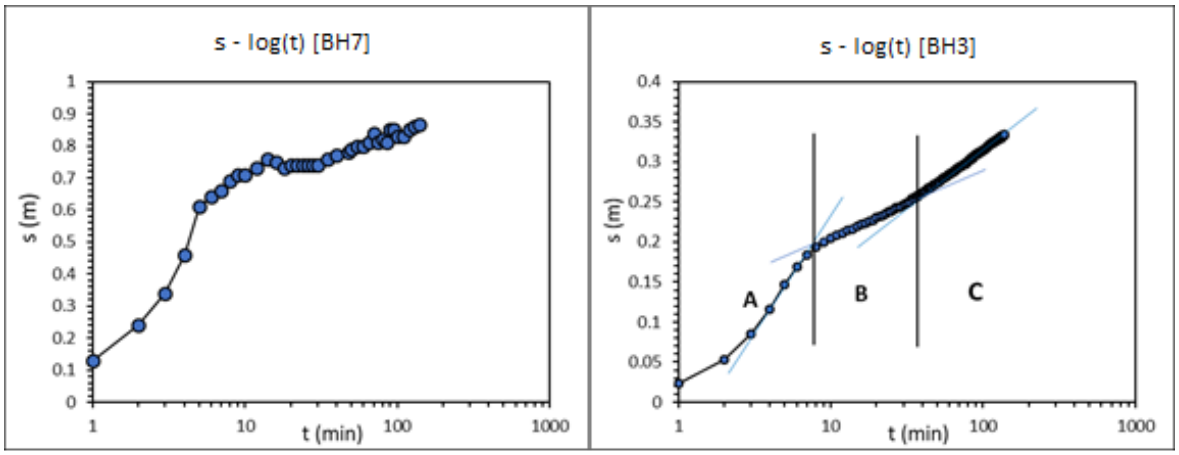

Figure 5.12: Semi-log plot of drawdown (linear scale) against time (log scale) showing the three flow phases at Krugersdrift Test Site

In general, the drawdown behaviour of the boreholes is characterised by three flow phases and the duration of these phases is dependent on the aquifer heterogeneity. The phases are described below:

- **Flow Phase A (Theis response):** In this stage, the aquifer conforms to the confined behaviour where Theis response is the dominant flow. It occurred within the first 10 minutes of pumping. The water is instantaneously released from the aquifer storage (gravel sand layer) due to aquifer compaction and groundwater expansion.
- **Flow Phase B:** Flow in this phase is mainly characterised by horizontal groundwater flow from the aquifer. This stage is usually unlikened to contribution of delayed drainage which is typical of unconfined aquifers. This usually noticed by the flattening of the semi-log plot in the medium times soon after Theis response. Gomo (2011) argued that, although there is some deviation from the confined straight line plot the current plots are far from flattening to justify unconfined delayed or gravity drainage. The flow was dominant until the 40^{th} minute of pumping where the system entered into a pseudo-steady state.
- **Flow Phase C (Radial Acting Flow):** This phase is the most dominant flow referred to as radial acting flow (RAF) characterized by the release of groundwater from the gravel-sand layer. On a derivative plot it is identified by a horizontal line. It is within this time period that estimations of hydraulic parameters representing the aquifer matrix are performed. The system is observed to have reached the pseudo-steady state in the flow phase.

5.3.5 Geoelectric Property of Krugersdrift Test Site

An electrical resistivity tomography was performed on the Krugersdrift Test Site along one profile in the north-west to south-east direction with 2.5 m take-outs over 150 m spread. Only one profile section was conducted. As earlier highlighted in Section 5.2.4, the main aim of conducting the resistivity profile was to investigate the level of electrical homogeneity of the unsaturated subsurface. Demarcation of lithological facies was done by correlating it with geological logs for boreholes BH2, BH7, BH3 and BH9.

The following observations were made for the electrical resistivity section (Figure 5.13):

1. The resistivity section shows that the alluvial cover units consisting of soil, clay silt and gravel-sand are uniformly layered throughout the aquifer with no

electrical resistivity or conductivity discontinuities suggesting a fairly homogeneous subsurface.

2. Lowest resistivity values below 8 Ωm were recorded within the layer delineated as the soil horizon suggesting either high silt content or moisture levels in that zone. However, it is worth noting that the lowest resistivities were recorded on the areas covered with dense vegetation cover, hence the low resistivities might be attributed to moisture retained by the vegetation within the vadose zone.
3. The clay-silt layer was assigned an electrical resistivity character between 10 and 15 Ωm. It also seats uniformly above the gravel-sand aquifer across the test site.
4. The main groundwater flow horizon referred to as the shallow aquifer zone between 15 Ωm and 25 Ωm.
5. The bedrock is characterised by resistivity values more than 25 Ωm and occurs uniformly across the entire test site.
6. In general, the electrical resistivity image gave an indication that subsurface is homogeneous in nature and assumption laid by Kruseman & De Ridder (1999) about horizontal and homogenous aquifer are applicable. No vertical hydraulic boundaries are conceptualised along the ERT profile.

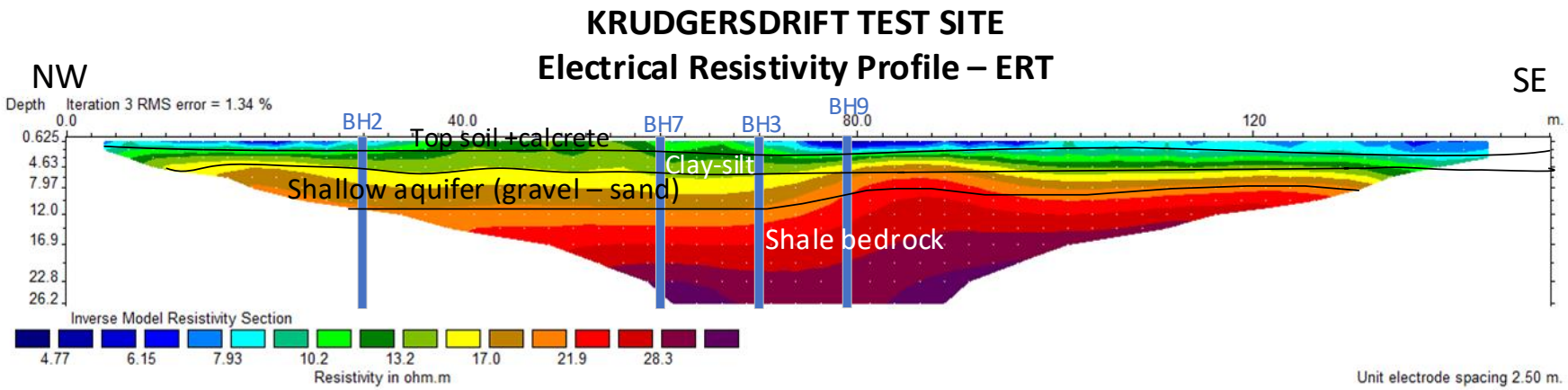

Figure 5.13: Electrical resistivity tomography for Krugersdrift Test Site

CHAPTER 6:
RESULTS AND DISCUSSION

6.1 INTRODUCTION

The results for the field experiments conducted are presented in this chapter. The pumping test results and discussion for the Campus Test Site (CTS) and Krugersdrift Test Site (KTS) is performed in Sections 6.2 and 6.4 respectively. The discussion is limited to hydraulic parameter estimation. Hydraulic parameters estimated are transmissivity (*T),* hydraulic conductivity (*K*) and storativity. These are estimated using both Theis and Cooper Jacob methods for both experimental sites.

Sections 6.3 and 6.5 follow up with the presentation of streaming potential results, analysis and discussion for Campus Test Site and Krugersdrift Test Site respectively. Estimation of hydraulic parameters using streaming potential method is performed using the coupled flow problem provided by Equation.

The chapter concludes by performing a validation procedure on the streaming potential method in hydraulic parameter estimation. Validation of the streaming potential is performed against the results of the parameters estimated by use of measured drawdown.

6.2 CAMPUS TEST SITE PUMPING RESULTS

Pumping test at campus was performed on UP16 as a pumping borehole and boreholes UP15, UO20, UO3, UO18 and UO19 were used as observation boreholes and measurement point for both drawdown and streaming potentials because of their locations relative to the orientation of the parallel bedding fracture orientation. Figure 6.1 shows the location of the boreholes and position with respect to the bedding plane fracture.

Figure 6.1 is important for this study because it provides a precondition of the expected behaviour of each borehole during pumping test. This is because the presence of the parallel bedding fracture controls the behaviour of the borehole and hence influence the transmissivities of these boreholes at different times of pumping (Woodford & Chevallier, 2002).

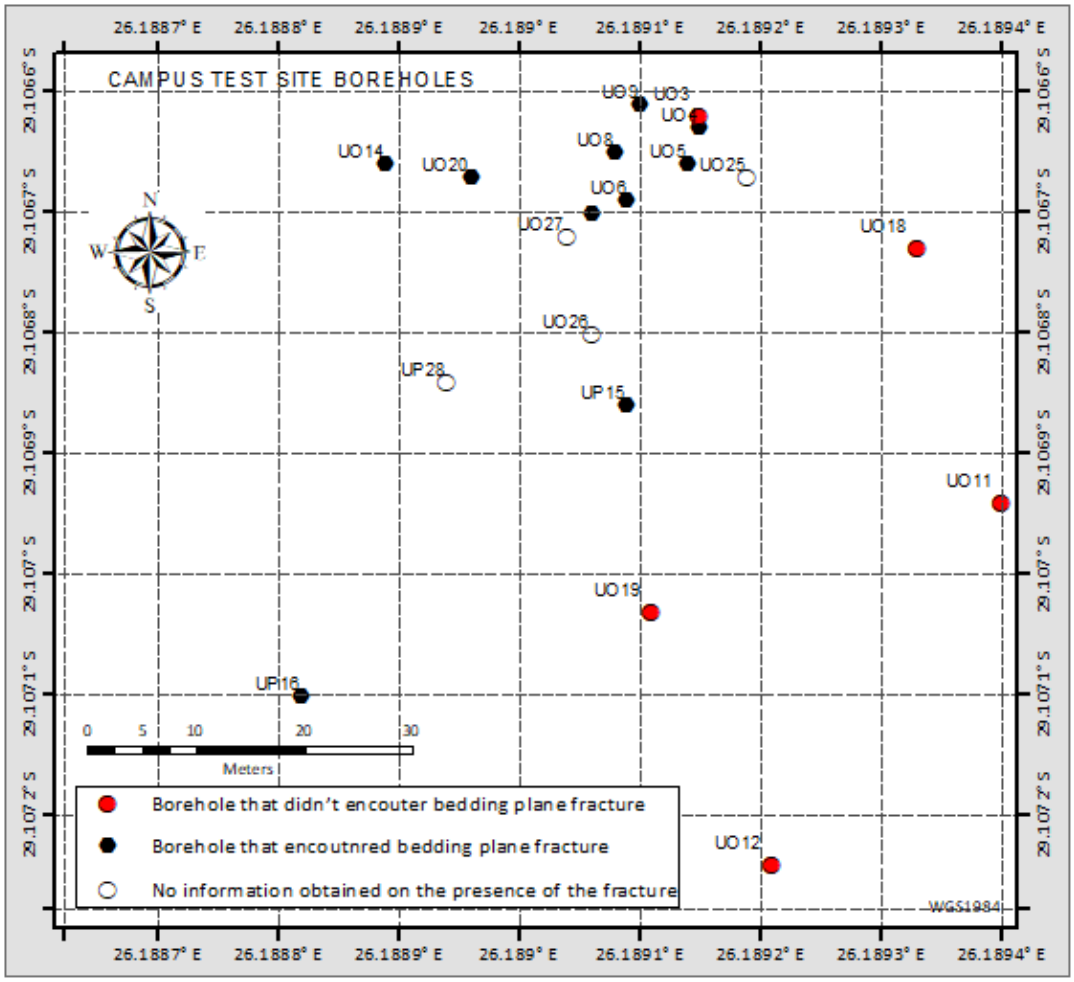

Figure 6.1: Campus Test Site boreholes and their relative location with respect to the bedding plane fracture

Figure 6.1 is important for this study because it provides a precondition of the expected behaviour of each borehole during pumping test. This is because the presence of the parallel bedding fracture controls the behaviour of the borehole and hence influence the transmissivities of these boreholes at different times of pumping (Woodford & Chevallier, 2002).

6.2.1 Baseline Details for the Experimental Boreholes

Prior to test pumping at Campus Test Site (CTS), a hydro-census survey was performed with the aim of recording the baseline information of the boreholes. Table 6.1 shows the baseline details of the boreholes that were used for the experiment.

Table 6.1: Baseline borehole details recorded prior to pumping for CTS

Borehole ID	Longitude WGS84	Latitude WGS84	Elevation (m.amsl)	SWL (m.bgl)	BH Depth (m.bgl)	Hydraulic Head (Ho) (m.amsl)
UP16	26.18882	-29.10710	1411.5	17.25	38.50	9.3
UP15	26.18909	-29.10686	1411.0	16.75	42.00	9.3
UO20	26.18896	-29.10667	1411.0	16.33	29.00	9.7
UO19	26.18911	-29.10703	1411.0	16.42	36.00	9.6
UO3	26.18892	-29.10662	1411.0	14.81	51.00	11.2
UO18	26.18933	-29.10673	1411.0	16.90	28.00	9.1

An elevation of 1385 metres above mean sea level was chosen as the reference point for calculations of hydraulic head. The hydraulic head values shown in Table 6.1 are the hydraulic heads at time t = 0 min prior to pumping test. This agrees with the borehole logs which were presented in Section 5.3.2. Borehole UO19 was only drilled to 28 mbgl and developed in upper aquifer.

6.2.2 Time-Drawdown Curves for Campus Test Site

A discussion of the Campus Test Site aquifer was performed in Section 5.2.3. Botha *et al.* (1998) conceptualised the aquifer as a typical confined and fractured Karoo aquifer.

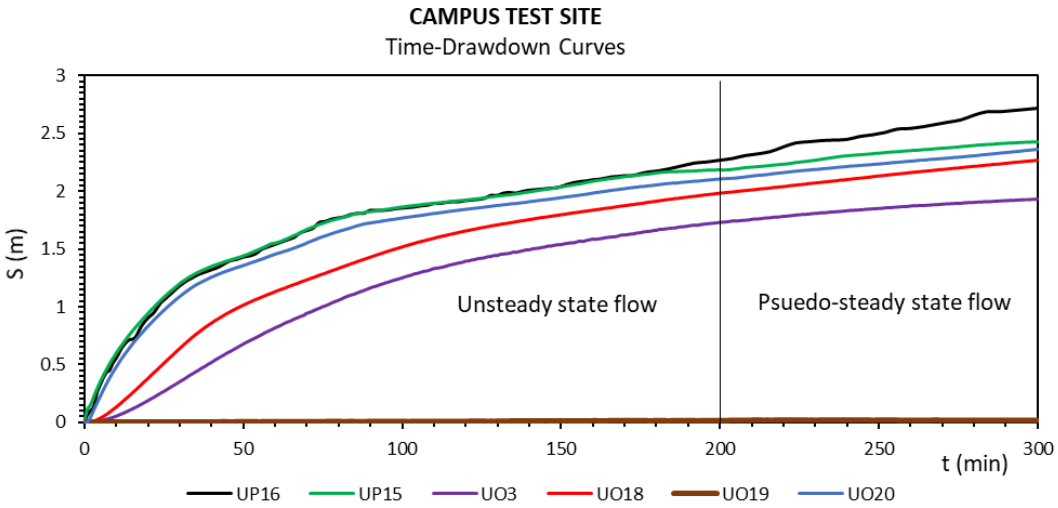

Figure 6.2: Time – drawdown graphs for a constant rate test performed on UP16 with UP15, UO3, UO18, UO19 and UO20 used as observation wells.

Figure 6.2 shows that groundwater flow did not reach steady-state condition because the measured drawdown kept on increasing with time until the time when the pump was

switch off. Rather a pseudo-steady-state flow environment was reach after 200 min of pumping. Pseudo-steady state condition is observed as the state at which the time-drawdown curves in the observation boreholes are parallel to each other. In this time period the hydraulic gradient is considered constant throughout the aquifer.

From 0 to 200 min of pumping the drawdown measured in UP16 and UP15 are of comparable magnitude hence follow the same path. However, at 190 min the change in drawdown in UP16 increases sharply separating from the drawdown of UP15. The sharp increase is as a result of either dewatering of local fractures or a hydraulic boundary.

The most important observation is that the drawdown in UO19 did not change noticeably with time. In Figure 6.2, the graph of UO19 drawdown cannot be seen because it is lying along the horizontal time axis. As explained earlier UO19 is a piezometer developed in a different aquifer system to that in the rest of the boreholes, hence the behaviour is expected to be different.

Unlike UP15, the drawdown curve for UO18 and UO3 show delayed response in water level decline when pumping resumed, which is defined as having longer response time. The response time is defined as the time taken for quantifiable drawdown to be measured in the observation borehole after resuming pumping in the test well. It gives an indication of the rate of spread of the cone of depression. The delayed response is because UO18and UO3 did not encounter a bedding parallel fracture, although they were developed in the same aquifer system as UP16 and UP15. The long response time is more significant in UO3. At late times the drawdown profile for UO18 follows a similar path to the one in UO20 and UP15, this is because UO18 is also developed in the same aquifer as UP16 and UP15. It gives an indication that at these late times the dominant flow is matrix flow unlike in the early times were fracture flow plays an influential role.

6.2.3 Recovery Phase – Aquifer relaxation mode

The recovery phase is the time when the aquifer is naturally recharged to its initial water level after the pump is switched off. This is referred to as the relaxation mode and the drawdown measured during this time is often called residual drawdown ($s`$). In this discussion the terms recovery and residual drawdown will be used interchangeably. The time – residual drawdown graphs for the Campus Test Site are shown in Figure 6.3.

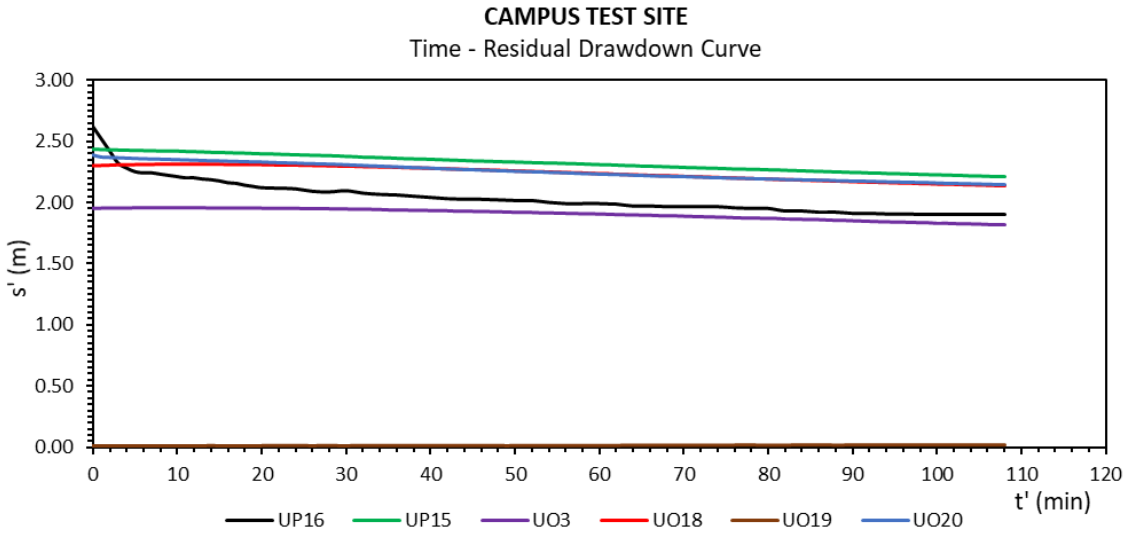

Figure 6.3: Time – recovery graphs at UP16, UP15, UO3, U018, UO19 and UO20

Over a period of 120 min of recovery phase monitored the observation boreholes only recovered about 0.2 m. However, during this phase, the recovery path in in all the observation boreholes except UO19 became parallel to each other after 55 min of recovery monitoring. Very small residual drawdown changes of the order of 0.2 m approximating a steady-state flow condition after 55 min of relaxation mode. Hence this phase will be use to solve the coupled flow steady state problem for the relaxation mode derived by Rizzo *et al.* (2004).

6.2.4 Spatial Drawdown and Hydraulic Head Maps for the Campus Test Site

Spatial drawdown and hydraulic head maps were constructed from the measured drawdown in the pumping and monitoring boreholes (Figure 6.4 and Figure 6.7) at time t = 300 min. The hydraulic heads were computed by taking elevation 1385 m.amsl as the datum level. Therefore, all hydraulic heads are referenced from this datum level. Time t =300 min was chosen to represent the aquifer drawdown because in this time period the groundwater flow towards the borehole is radial linear flow dominated by matrix flow.

The spatial drawdown and hydraulic head distribution maps reveal the distribution and shape of the cone of depression. A wider cone of depression suggests that the entire system is responding to pumping and which is prominent in more transmissive zone. A steeper cone of depression or drawdown gradient may reveal a flow barrier or a less transmissive environment.

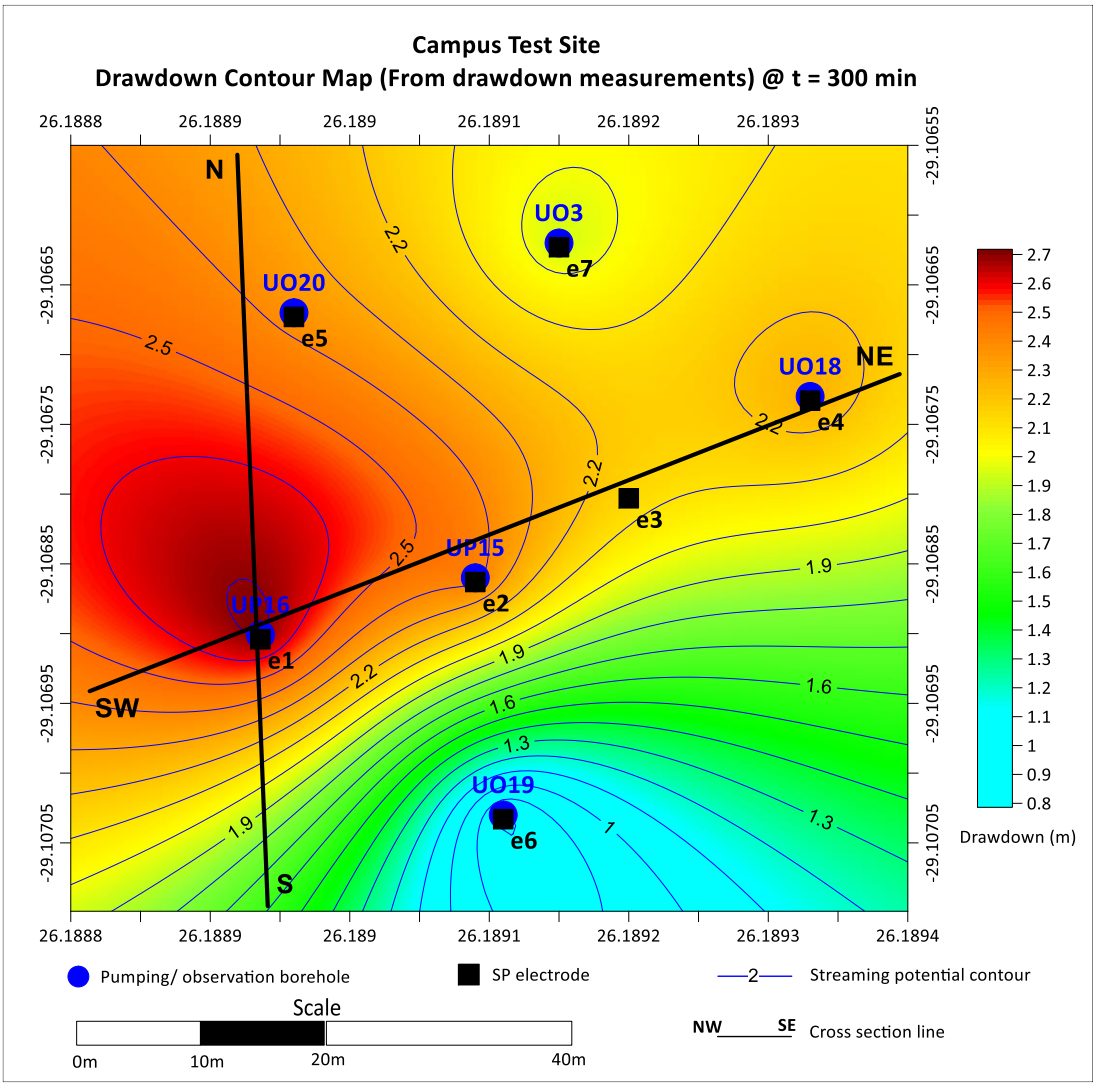

Figure 6.4: Spatial drawdown map of the Campus Test Site at time *t*=300 min

Figure 6.4 shows that the spatial drawdown is highest on the pumping borehole and decreases away from the borehole. Less drawdown was recorded on borehole UO19. This is primarily because the borehole is developed in an aquifer which is not directly linked to the aquifer being pumped by UP16.

Drawdown cross-sections showing the shape of the drawdown cone were produced along section lines S-N and SW – NE showing in Figure 6.4. The drawdown cones along these section lines are shown in Figure 6.5 and Figure 6.6.

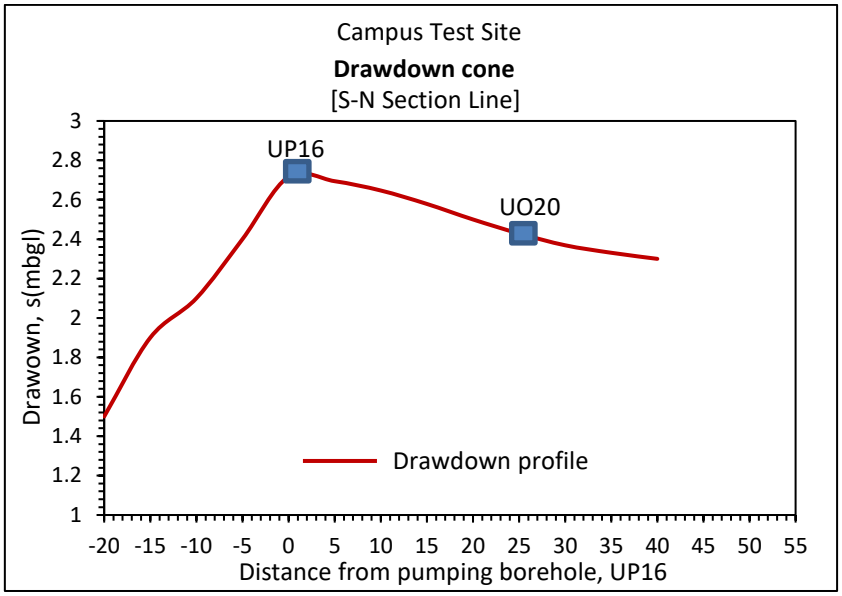

Figure 6.5: South -north drawdown cone across the pumping well (UP16) at Campus Test Site at time *t* = 300 min

The drawdown cone shown in Figure 6.5 shows near symmetry across the pumping well UP16. In the south of borehole UP16, the drawdown gradient is 0.06 and 0.01 in the north of UP16 towards UO20. The progress of the cone in the north is more pronounced that in the south of UP16 (i.e. boreholes UO20 has short response time than UO19). Beside the fact that these boreholes are in different aquifer system, the discussion from Section 5.2.3 reveals that the presence of a parallel bedding fracture influences the behaviour of the aquifer, and hence the drawdown distribution at the Campus Test Site.

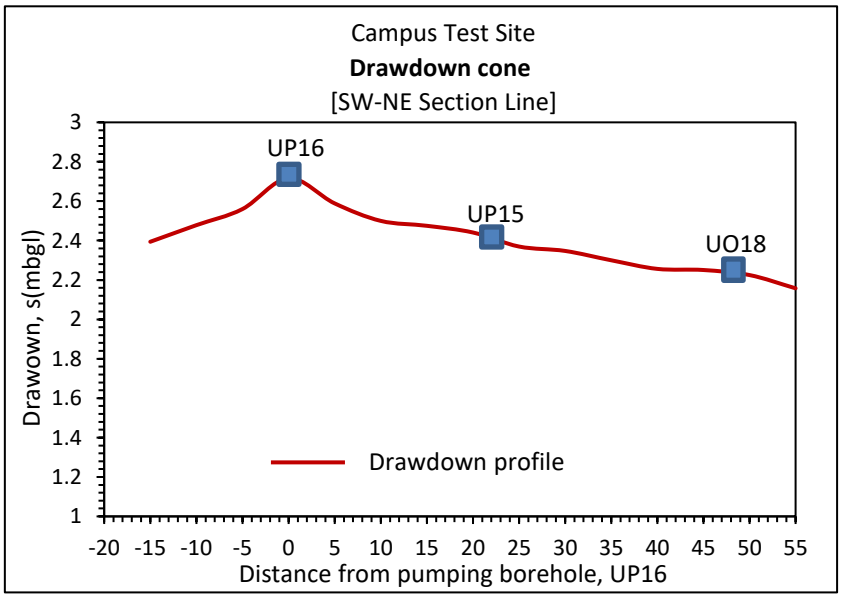

Figure 6.6: South west -north east drawdown cone across the pumping well (UP16) at Campus Test Site at time *t* = 300 min

The drawdown cone shown in Figure 6.6 shows near symmetry across the pumping well UP16. In the west of borehole UP16, the drawdown gradient is 0.08 and 0.02 in the first 30m west of UP16 and reduces further to flattening onwards.

Using elevation 1385 mamsl as the arbitrarily chosen datum line, hydraulic head distribution at the end of pumping was also produced. Kriging point contouring technique with a slope of 1 and slope angle of 30^{o} in combination with nugget effect exterminator. The slope of 30 degrees was chosen to follow the orientation angle of the measurement line, UP16 to UO18 which in principle coincides with the orientation of the bedding plane at the Campus test site. Figure 6.7 shows the hydraulic head distribution at the Campus Test Site.

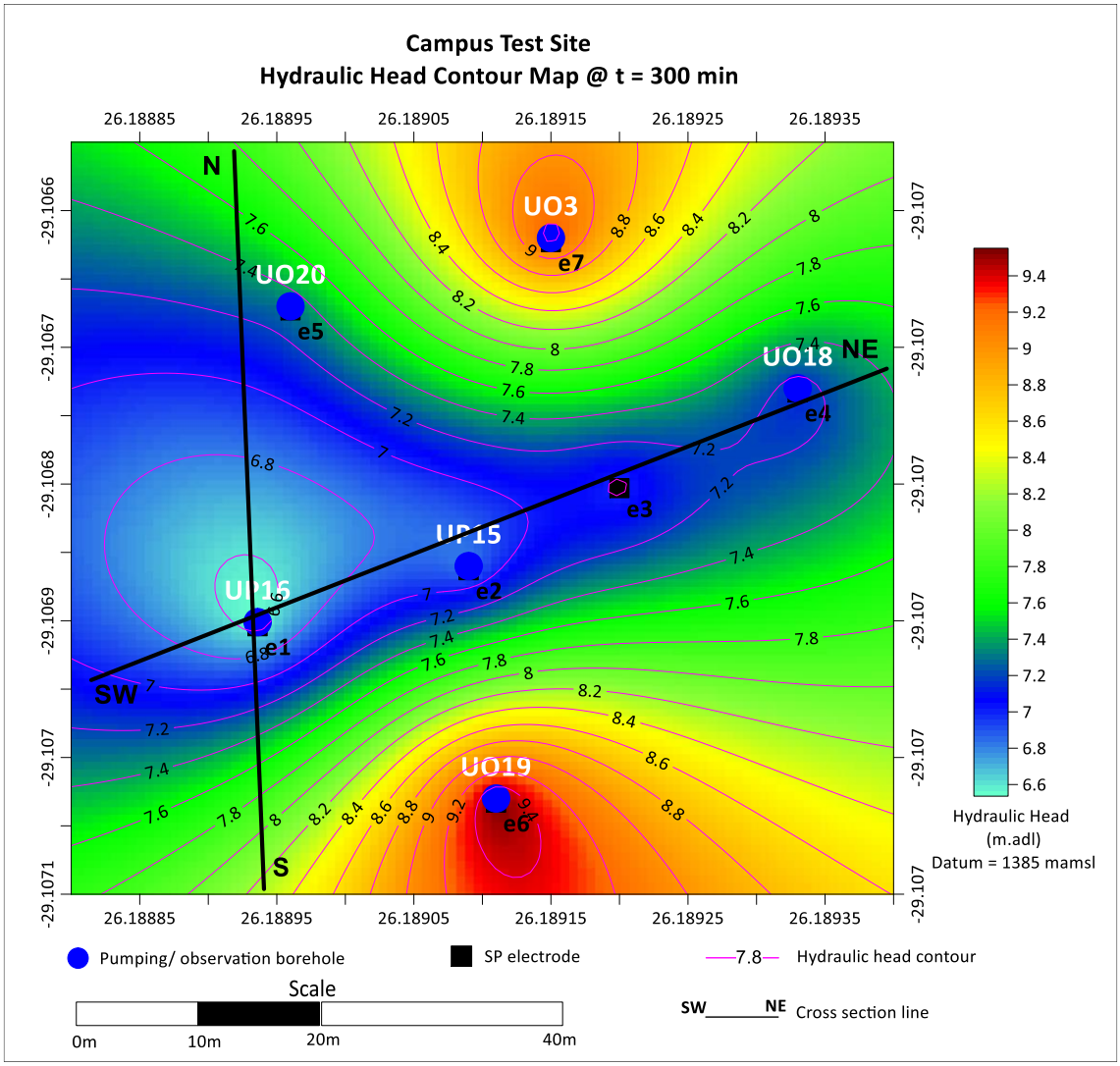

Figure 6.7: Spatial hydraulic head map of the Campus Test Site at time *t*=300 m

Figure 6.7 shows that the hydraulic head distribution for the Campus Test Site at time *t* = 300 min just before switching off of the pump is highest on the pumping borehole and decreases away from the borehole. Less drawdown was recorded on borehole UO19. This primarily because the borehole is developed in any aquifer which is not directly linked to the aquifer being pumped by UP16.

The dark blue region shown in Figure 6.7 is the areas of maximum drawdown or least hydraulic head. Review of the geometry of the campus aquifer reveals that this area coincides with the area mapped by Woodford & Chevallier (2002) as being influenced by the parallel bedding fracture. The two cones of depression are shown in Figure 6.8 and Figure 6.9

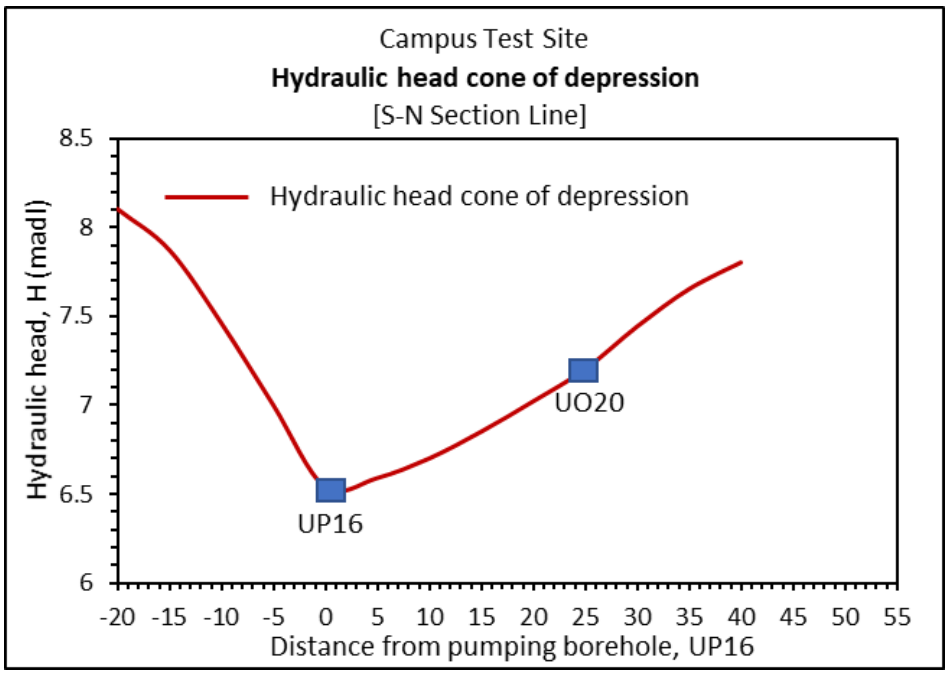

Figure 6.8: South – north hydraulic head cone of depression across the pumping well (UP16) at Campus Test Site at *t* = 300 min

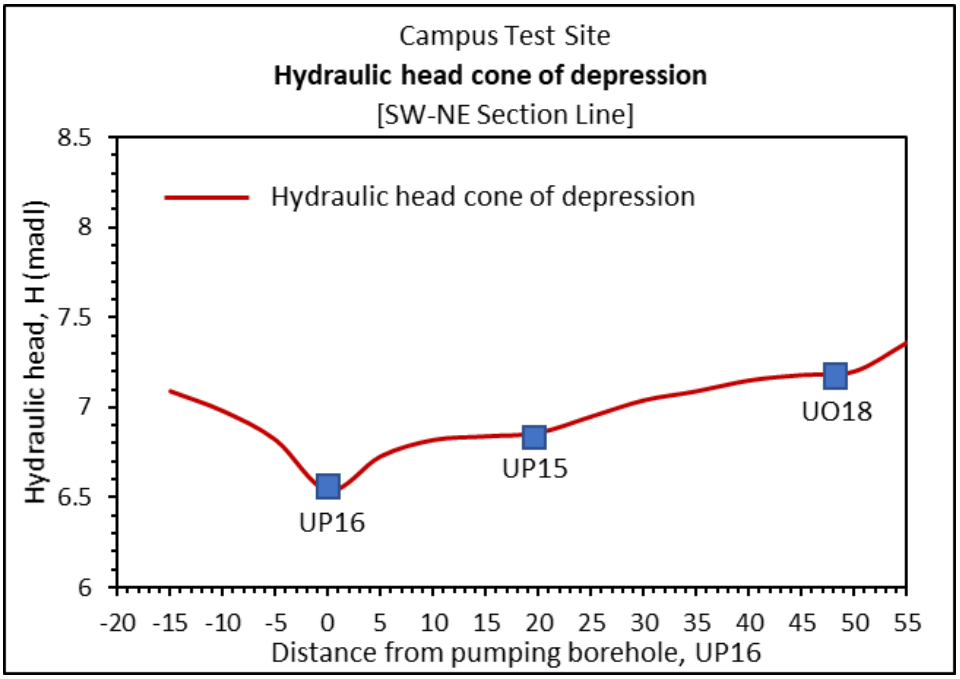

Figure 6.9: South west – north east hydraulic head cone of depression across the pumping well (UP16) at Campus Test Site at *t* = 300 min

Figure 6.8 and Figure 6.9 represent the cone of depression across borehole UP16 in the south to north and southwest to north east directions. Their implication to groundwater flow characterisation is similar to the explanation given under drawdown cones. However, it is apparent to mention that the drawdown cone is a mirror reflection image of the cone of depression for the hydraulic head.

6.2.5 Hydraulic Parameters Estimation for the Campus Test Site

Hydraulic parameter estimation was achieved by using Theis curve matching and Copper Jacob methods for a confined aquifer under unsteady-state flow condition. Since Cooper Jacob method is based on Theis method the estimation from these two methods should have comparable magnitudes of *K* and *T*. The estimated parameters are compared and a mean aquifer hydraulic conductivity is determined. The objective of the study is to estimate the hydraulic parameters of the aquifer matrix. As discussed in Section 5.2.4, matrix flow (infinity radial acting flow) is dominant in the late times. Hence Theis and Cooper Jacob methods were applied in the late times.

6.2.5.1 Theis curve matching

FC pumping test analysis software was used to determine transmissivity and storativity at all the observation boreholes whose drawdown was monitored and the results of the estimated values of transmissivity and hydraulic conductivity are shown in Table 6.2

Figure 6.10 shows borehole UP15 as an example of Theis curve matching performed. The rest of Theis curve matching on other observation boreholes is presented in Appendix A.

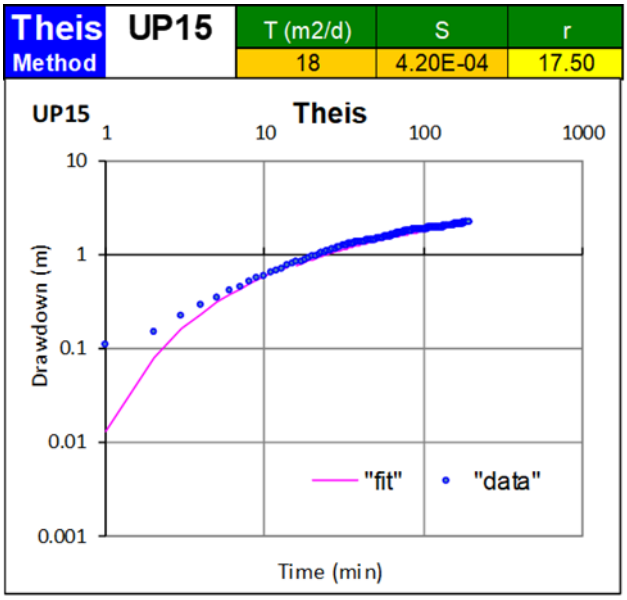

Figure 6.10: Theis late time curve matching on a semi log time – drawdown graph on UP15

Theis curve matching at UP15 estimated Transmissivity *(T)* of 18 m^2/d and Storativity *(S)* of 4.2×10^{-4} m^2/d at late times. Borehole logs show that the average aquifer thickness at Campus Test Site is 9 m. Since, $T = KD$, it follows that:

$$K = T/D \tag{6.1}$$

$$K(UP15) = \frac{18\ m^2/d}{9\ m} = \mathbf{2\ m/d} \tag{6.2}$$

A similar operation was conducted on all observation boreholes and the calculated hydraulic conductivity values are shown in Table 6.2.

6.2.5.2 Cooper Jacob Method

Unlike Theis method, Cooper Jacob is applicable even on the pumping well. Cooper Jacob analysis was applied on all the monitored boreholes including the pumping borehole. Illustration of Cooper Jacob method application on pumping borehole UP16 is shown in Figure 6.11.

From Equation 3.26, it can be seen that a graph of drawdown *(s)* against *log t* (semi log plot) is a straight line. According to Kruseman and De Ridder (1990) if the straight line

crosses the time axis (i.e. at s = 0 and time t_0 is read), the slope of the straight line over a unit log time can be used to calculate transmissivity using the following equation:

$$T = \frac{2.30Q}{4\pi\Delta s} \qquad 6.3$$

Where, Δs is the change in drawdown per unit log time (slope per unit log time).

However, in this dissertation FC pumping analysis software was used under the same principle to estimate T and S of the pumping borehole. Figure 6.11 shows the time – drawdown semi log plot for UP16 and the output of Copper Jacob estimation in the late time of infinite radial acting flow (IRAF).

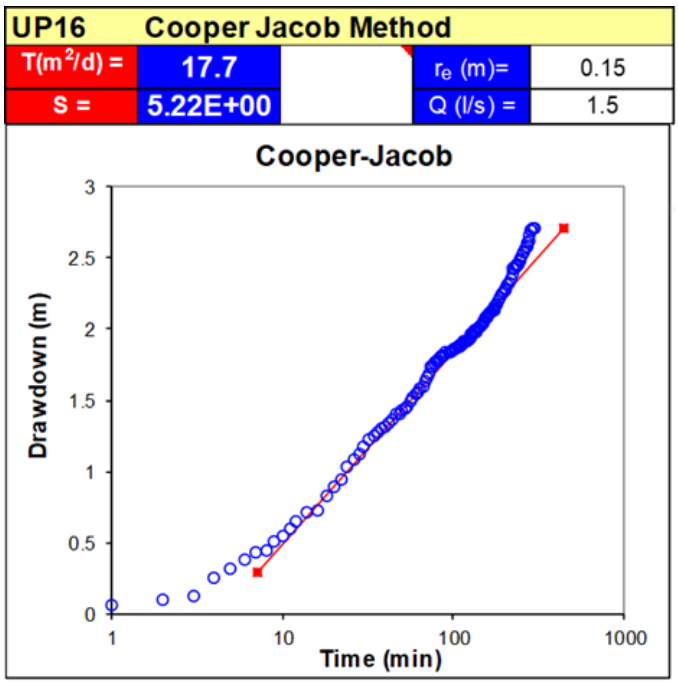

Figure 6.11: Application of Cooper Jacob method for pumping borehole UP16 during infinite Radial Flow in the late times using FC pumping test analysis software

Transmissivity of 17.7 m^2/d was obtained and the hydraulic conductivity is calculated using Equation 6.1 with aquifer thickness (D) of 9 m, to give K of 1.97 m/d.

The same procedure was performed on all monitored observation boreholes except UO19 (which is in a completely different aquifer system) and the output time – drawdown plots are shown in Appendix A and Table 6.2 shows the values of estimated T, K and S.

6.2.6 Discussion on Pumping Test Data Analysis for the Campus Test Site

The results of the estimated values of hydraulic parameters for the two methods above are summarised in Table 6.2.

The following views can be drawn from the estimated values of hydraulic parameter T, K and S using Theis and Cooper Jacob methods.

1. Transmissivity values ranging between 10 and 20 m^2/d were obtained and hydraulic conductivity values ranging between 1.0 and 2.1 m/d (*K* approximately in the order of 10^{-4} m/s). These values obtained are in agreement with the hydraulic conductivity values presented in Figure 5.4 as provided by Botha *et al.* (1998), Woodford & Chevallier (2002) and Van Tonder *et al.* (2000). The values obtained are typic parameters for the Karoo sandstone aquifer matrix.
2. The Campus aquifer has great potential for good storage of groundwater evidence by the estimated storativity values of the order 10^{-4}.
3. All values estimated from the two methods chosen, that is Theis and Cooper Jacob methods are comparable to each other. Therefore, for the case of campus aquifer any one of the two methods can be used to estimate the matrix hydraulic parameters.

   However, it is observed that as we move away from the pumping borehole the estimated values of *T* and *K* using Theis method decrease in magnitude fast than those estimated by Cooper Jacob method. In other words, Copper Jacob gives lager values of *K* and *T* as compared to Theis. The explanation for this observation was not pursued in this study.
4. The value of storativity obtained by Cooper Jacob on the pumping well is not representative of the aquifer storativity, hence it was discarded from the summary.
5. Boreholes UO3 and UO18 are developed in the same sandstone aquifer as UO20, UP15 and UP16 but did not intersect the parallel bedding fracture. This is evidence by lower values of transmissivity and hydraulic conductivity obtained.

Table 6.2: Summary of estimated hydraulic parameter values (*T*, *K* and *S*) from Theis and Cooper Jacob methods for CTS

Borehole ID	Theis			Cooper Jacob		
	T (m^2/d)	K (m/d)	S	T (m^2/d)	K (m/d)	S
UP16				17.7	2.0	
UP15	18.0	2.0	4.20E-04	19.1	2.1	3.31E-04
UO3	10.0	1.1	3.80E-04	13.6	1.5	2.80E-04
UO18	11.0	1.2	1.60E-04	14.6	1.6	1.20E-04
UO20	16.0	1.8	2.40E-04	14.6	1.6	1.83E-04
Arithmetic Mean	**13.8**	**1.5**	**3.00E-04**	**15.9**	**1.8**	**2.3E-04**
Geometric Mean	**13.3**	**1.5**	**2.80E-04**	**15.8**	**1.8**	**2.1E-04**

6.3 CAMPUS TEST SITE STREAMING POTENTIAL RESULTS

The streaming potential measurements were made concurrent with the constant rate tests in which drawdown measurements were taken. This section presents results of streaming potential data collected for the Campus Test Site and use the dataset to estimate hydraulic parameters of the aquifer.

6.3.1 Raw Data and Digitally Filtered Time Potential Graphs

The recorded raw and filtered streaming potentials were plotted on a time – potential graph for each electrode as illustrated in Figure 6.12 with electrode e_2 as an example. The measured raw data from streaming potential electrodes was digitally filtered using a Gaussian regional filter and standard deviation of 60, which is a low pass filter that eliminates high frequency spikes as explained in Section 4.4.2.

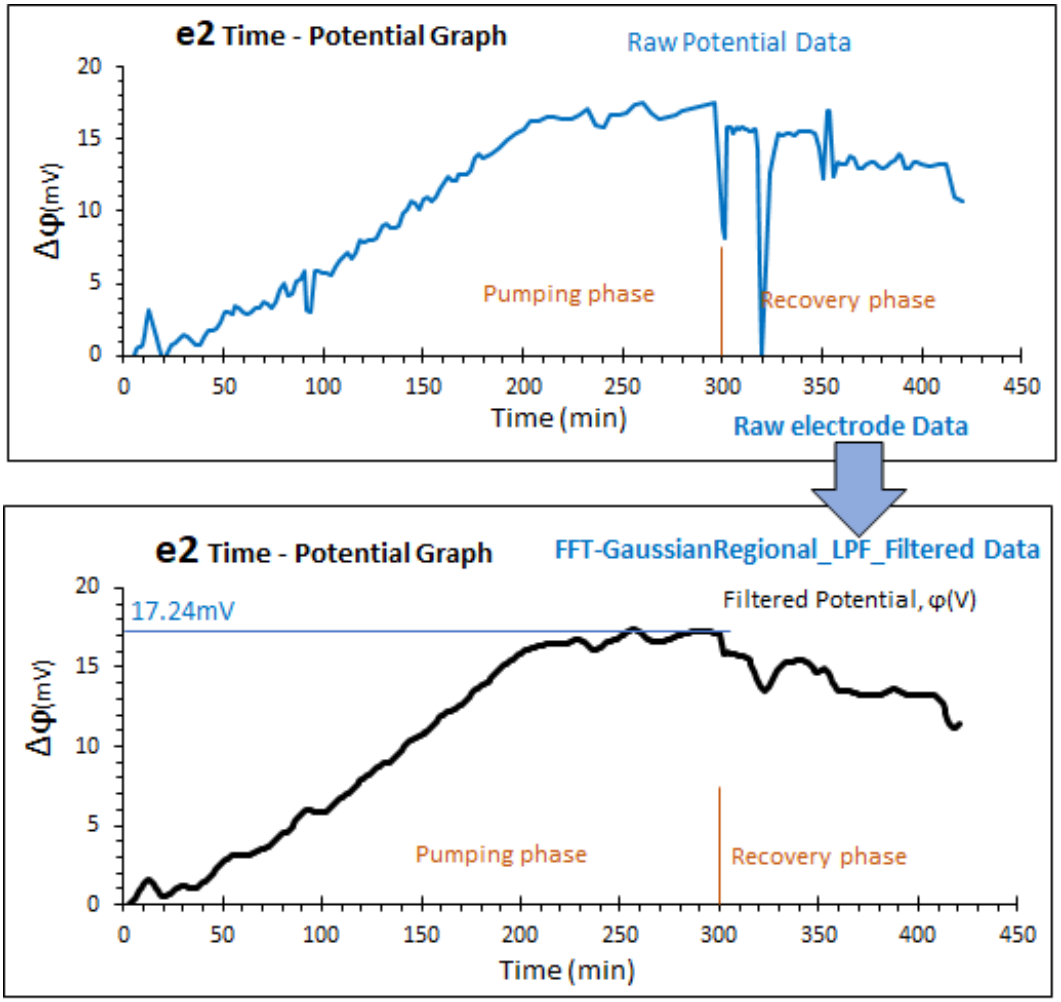

Figure 6.12: Raw and filtered time – potential graph for self-potential signals recorded at electrode e_2 (UP15) at Campus Test Site

The figure shows that the maximum streaming potential $\varphi(r)$ recorded for electrode e_2 is 17.24 mV. The is the value of potential at maximum drawdown just before the pump was switched off (t = 300 min). Streaming potential signals recorded were erratic, especially in the first 10 minutes of pumping, this might be attributed to wetting of electrodes due to sudden vertical drain of water from the matrix. This erratic behaviour was more noticeable in the observation boreholes that were near to the fracture or intersected the fracture. The same erratic noise is notice in the first time of recovery period, this is because of the sudden change in ground water flow direction and velocity which eventually disturbs the equilibrium potential gradient that would have been created on the porous electrode between the porous membrane and the electrolyte boundary. However, the Gaussian low-pass filter was successful in eliminating the noise.

The interesting observation is how the streaming potential signals stabilized in the time period identified as the state were groundwater flow was in pseudo-state (after t =

200 min). In this time period the streaming potential profile became a near replica of the drawdown profile.

6.3.1.1 Time – potential graphs during pumping phase

The filtered time potential signals recorded during the pumping phase are shown for all the seven monitoring stations in Figure 6.13. The individual plots for each electrode are presented in Appendix C.

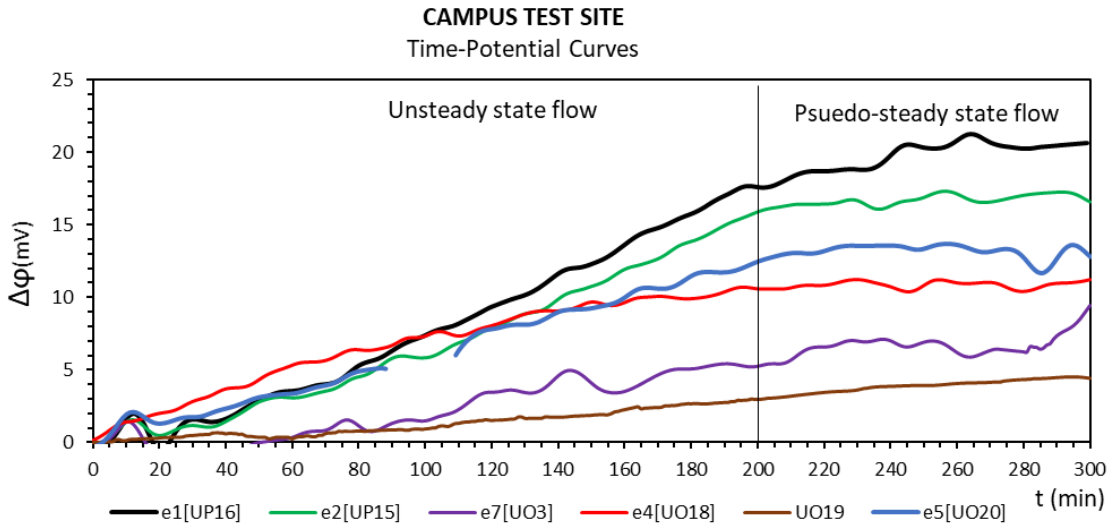

Figure 6.13: Time – potential graphs for filtered streaming potential signals recorded on electrodes, e1, e2, e3, e4, e5, e6 and e7 during pumping phase at CTS

The following was observed on the time-potential graphs during pumping phase:

i. Long period anomalies (similar to the one observed between 140 and 160 minutes could not be eliminated because of their long wavelengths. However, with the theory existing to date of streaming potential interpretation, only the final potentials are the ones important for quantitative interpretation.

ii. In general, the trends and shapes of the streaming potential signals recorded replicate the drawdown measurements shown in Figure 6.2.

iii. The time t=200min was earlier identified as the transition zone when the system entered into pseudo state, this behaviour is clearly noticed on the time-potential graphs in Figure 6.13 with the flattening of potential signals. The signals from the stations located on the observation boreholes are observed to be running parallel to each other.

iv. The time drawdown graph for UO19 did not show any change in hydraulic head throughout the duration of the pumping test. In contrary to that behaviour a significant potential change was recorded on electrode e_6 which was located next to observation boreholes UO19. The presumed explanation is that the source of potential signals is the response of the matrix as a whole and since the method is non-intrusive it implies that, the signals recorded are a summation of flow in all the aquifers as opposed to a piezometer which only gives the dedicated aquifer response.

6.3.1.2 Time – potential graph during relaxation phase

The potentials recorded during relaxation phase are also called residual potential in this dissertation. Figure 6.14 shows the filtered time potential signals recorded during the recovery phase. The use the terms recovery and aquifer relaxation state are often interchanged in this dissertation.

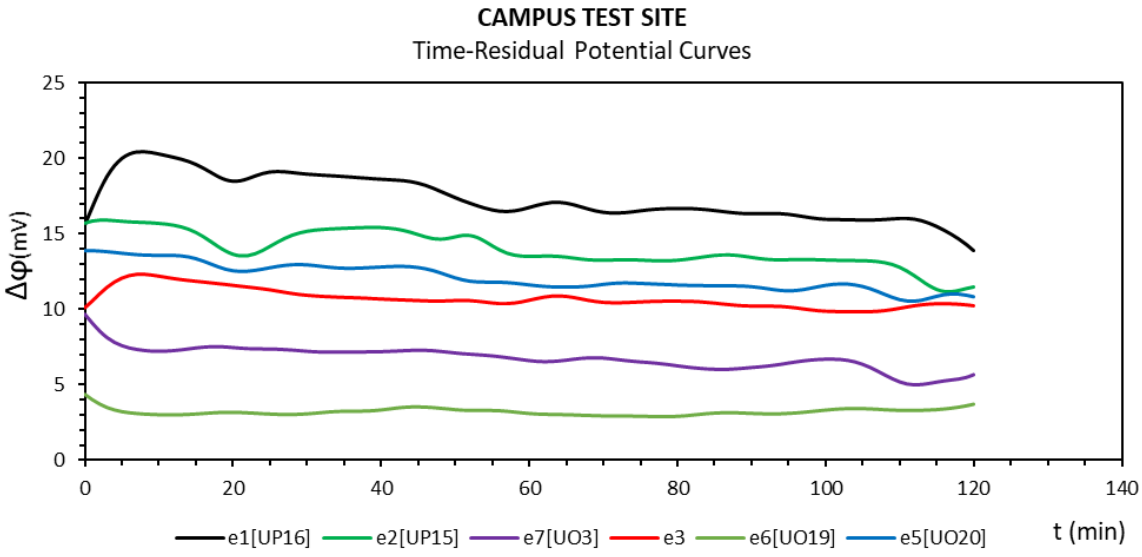

Figure 6.14: Time – potential graph for self-potential signals recorded on electrodes, e1, e2, e3, e4, e5, e6 and e7 during pumping phase at CTS

From the time – residual potential graphs it can be observed that:

i. The filtered signals show a near replica of residual drawdown recorded during recovery shown in Figure 6.3.

ii. Both streaming potential signals recorded during the pumping and recovery phases form a positive anomaly around the pumping well, similar to the trend of

drawdown. The highest positive anomalies are recorded near to the pumping borehole and reduce as we move away from the borehole.

6.3.2 Spatial Streaming Potential Gradient Maps for CTS

As earlier discussed in Section 4.4.2, streaming potential theory, and findings from Fagerlund & Heinson (2002) and Rizzo *et al.* (2004) it is shown that streaming potential signals are more stable in the late times of pumping test. Therefore, the late time streaming potential signals were used for the estimation of hydraulic conductivity. The late time chosen for drawdown analysis (t = 300 min) is the same coincides with the same late time chosen for the plotting and gridding of streaming spatial distribution maps.

Table 6.3 shows the magnitude of streaming potential signals at time *t*=300 min selected which were gridded using Kriging gridding method for the entire spatial domain of the test site.

Table 6.3: Streaming potentials at time *t* = 300 min for each monitoring electrode at the Campus Test Site

Electrode ID	Change in Streaming Potential at t=300 min $\Delta\varphi$ (mV)	Description of the location
e_1	20.4	Located about 0.5 m from pumping borehole UP16
e_2	17.2	Located 30 cm next to UP15
e_3	13.7	Located in between UO18 and UP15
e_4	11.2	Located 30 cm next to UO18
e_5	13.9	Located 30 cm next to UO20
e_6	4.5	Located 30 cm next to UO19
e_7	6.8	Located next to UO3

The grid map showing streaming potential gradient / spatial streaming potential at time *t* =300 min is shown in Figure 6.15 while Figure 6.16 and Figure 6.17 reveals the shape of the cone of increment along cross-section lines S-N and SW-NE, respectively.

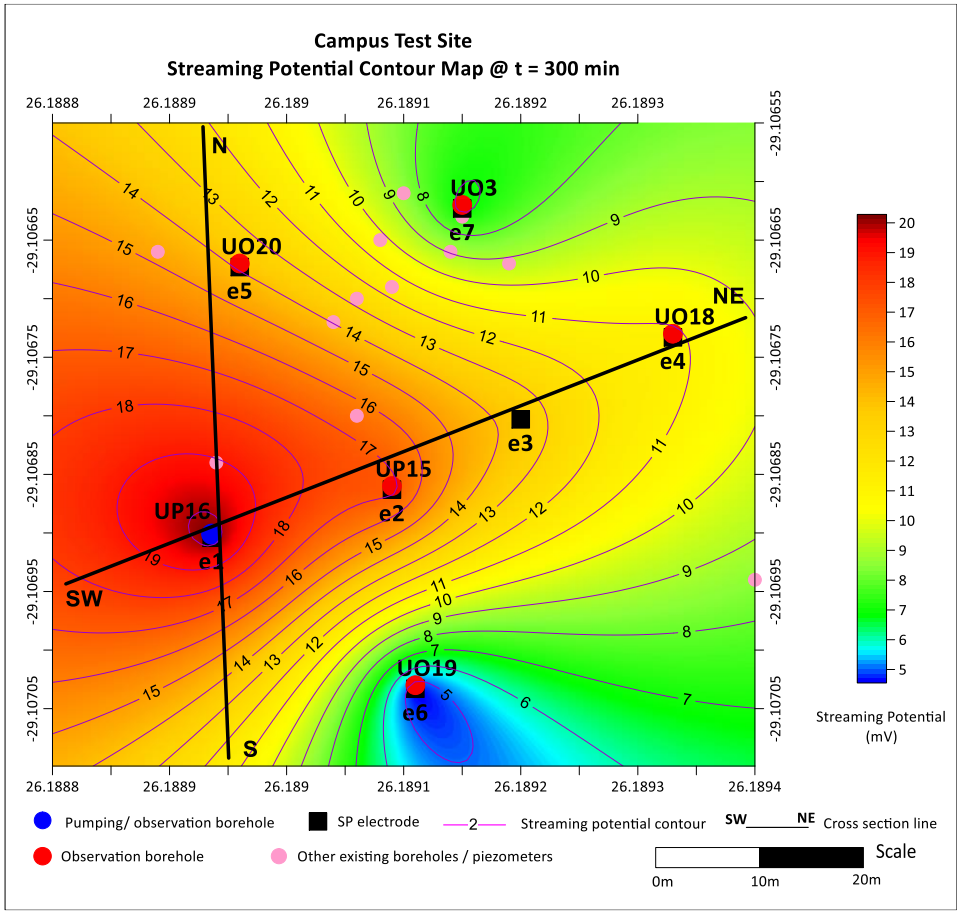

Figure 6.15: Spatial streaming-potential map (SP gradient map) at *t* = 300min for the Campus Test Site

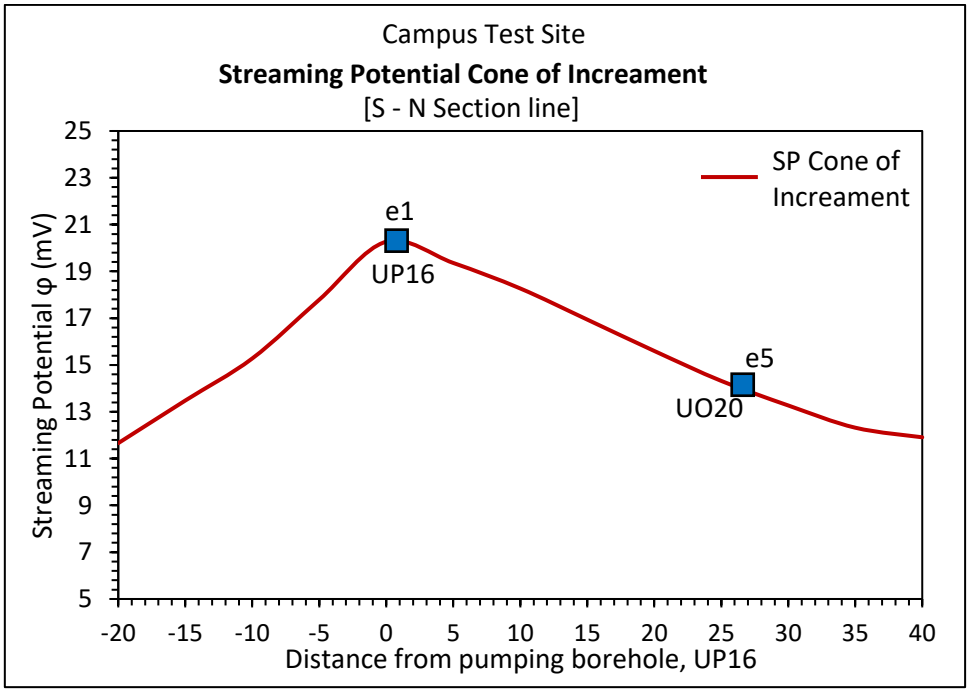

Figure 6.16: Streaming potential gradient / cone of increment at *t* = 300 min across pumping borehole UP16 along S-N section line at the Campus Test Site

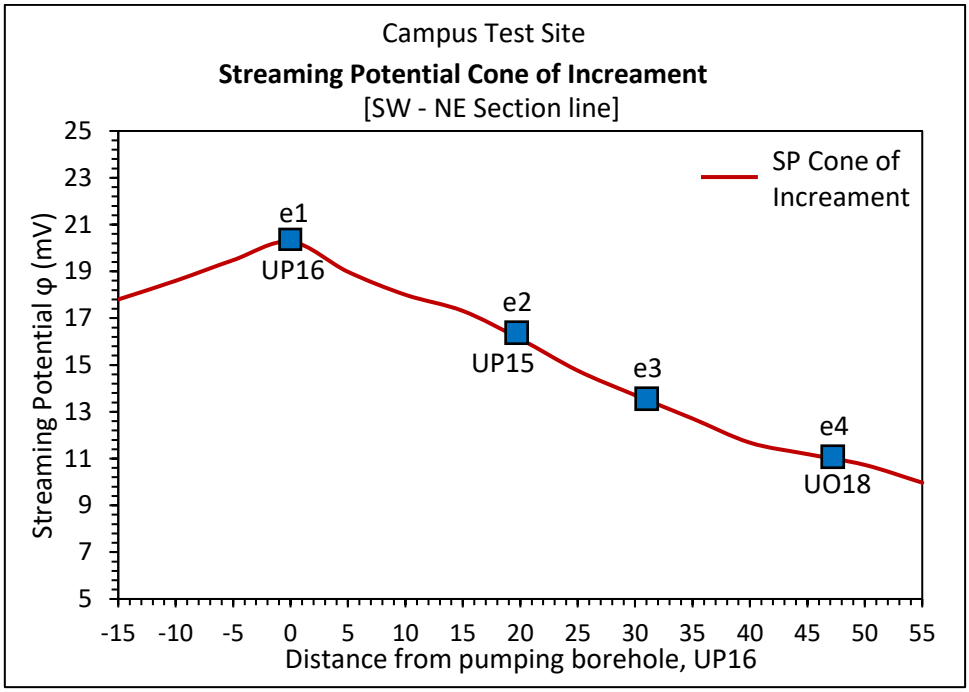

Figure 6.17: Streaming potential gradient / cone of increment at *t* = 300 min across pumping borehole UP16 along SW-NE section line at the Campus Test Site

The following observation were made from the streaming potential gradient map and sections:

i. Streaming potential signals form a positive anomaly around a pumping well. The positive anomaly, herein named the cone of increment, is a mirror image of the cone of depression formed by the hydraulic head during pumping around the well (it exhibits similar contour distribution as the one for drawdown). This agrees with the coupled flow problem which relates the streaming potential gradient to the hydraulic gradient linearly through a negative coupling coefficient of proportionality.

ii. The spatial distribution of streaming potentials reveals the closeness of the aquifer to homogeneity property as the streaming potential signal cone of increment is near symmetric around the pumping well.

6.3.3 In-situ Streaming Potential Coupling Coefficient for the Campus Test Site

The streaming potential coupling coefficient for the test site was calculated using an in-situ method suggested by Ball *et al.* (2010). Streaming potentials and drawdown data recorded at t = 0 and t = 300 min (which are the times at start and end of pumping) for

boreholes that were monitored both for drawdown and streaming potential change were used to calculate the streaming potential gradient and hydraulic gradient between each measurement station at pumping borehole. However, drawdown and streaming potential measurements from UO19 were not considered for computation of the streaming potential coupling coefficient because the behaviour of UO19 is different from other boreholes. The procedure is illustrated in Table 6.4.

Table 6.4: Streaming potential and hydraulic head gradient measured *t* = 300 min for each monitoring station at CTS

BH	Electrode	$\varphi_{1(300)}$	$\varphi_{0(300)}$	$\delta\varphi_{(300)}$	$s_{1(300)}$	$H_{o(300)}$	$H_{1(300)}$	$\delta H_{(300)}$
UP16	e1	20.4	20.4	0.0	2.72	6.53	6.53	0.0
UP15	e2	17.2	20.4	-3.1	2.43	6.53	6.82	0.3
UO18	e4	11.2	20.4	-9.2	2.27	6.53	7.13	0.6
UO20	e5	13.9	20.4	-6.5	2.36	6.53	7.31	0.8
UO3	e7	6.8	20.4	-13.6	1.93	6.53	9.26	2.7

In Table 6.4 the different parameters have the following meanings:

- $\varphi_{1(300)}$ and $\varphi_{o(300)}$ are the magnitudes of streaming potential signal recorded at the observation and pumping borehole at time t = 300 min respectively and $\delta\varphi$ is the linear change in streaming potential between the pumping borehole and the observation borehole at the time t = 300 min.

- $s_{1(300)}$ and $s_{o(300)}$ are the drawdown measurements taken at the observation and pumping borehole at time t = 300 min respectively. Using the hydraulic head in each borehole prior to pumping (calculated in Table 6.1) and drawdown value, the at each borehole at t = 300 min the hydraulic head at t = 300 min was computed using the relationship:

$$H_{(t=300)} = H_{(t=0)} - s_{(t=300)} \qquad 6.4$$

- For the pumping borehole, the hydraulic head at time t = 300 min is labelled as $H_{o(300)}$ while for the observation borehole it is labelled as $H_{1(300)}$.

- $\delta\varphi_{(300)}$ and $\delta H_{(300)}$ are the linear change in streaming potential and hydraulic head between the pumping borehole and any the observation borehole.

From the coupled flow problem relationship provided in Equation 3.45, the values of $\delta\varphi_{(300)}$ and $\delta H_{(300)}$ were used to plot a straight line graph of $\delta\varphi_{(300)}$ against $\delta H_{(300)}$ with

(zero; zero) intercept as shown in Figure 6.18. The gradient of the straight line is defined as the in-situ streaming potential coupling coefficient, *Cs*.

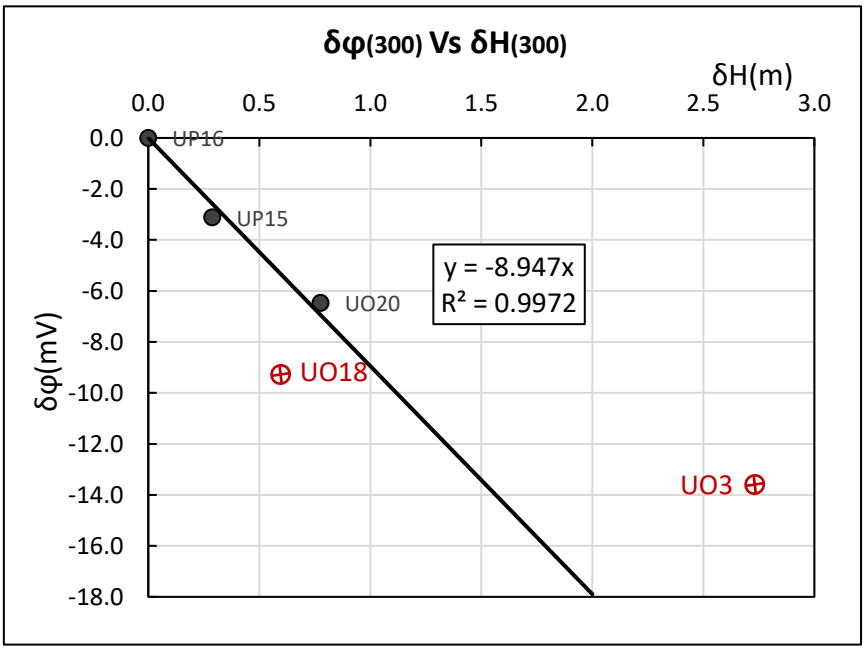

Figure 6.18: Graph of linear change in streaming potential (δφ) against linear change in hydraulic head (δH) at time *t* = 300 min at CTS

From the graph, the streaming potential coupling coefficient (*Cs*) is approximately equal to **-8.95 mV/m**. The effect of UO3 and UO18 was masked because UO3 is developed in a different aquifer system and UO18 was just considered as an outlier.

6.3.4 Computation of Hydraulic Head using Streaming Potential Data at CTS

To compute the hydraulic head using streaming potential, it is assumed that one borehole exists at the test site (which is our pumping borehole as in the case of most groundwater projects). The hydraulic heads in the half space around the borehole are computed by direct approach using Equation 3.45.

An illustration of the dimensions, layout and labelling of quantities used to calculate hydraulic head is shown in Figure 6.19.

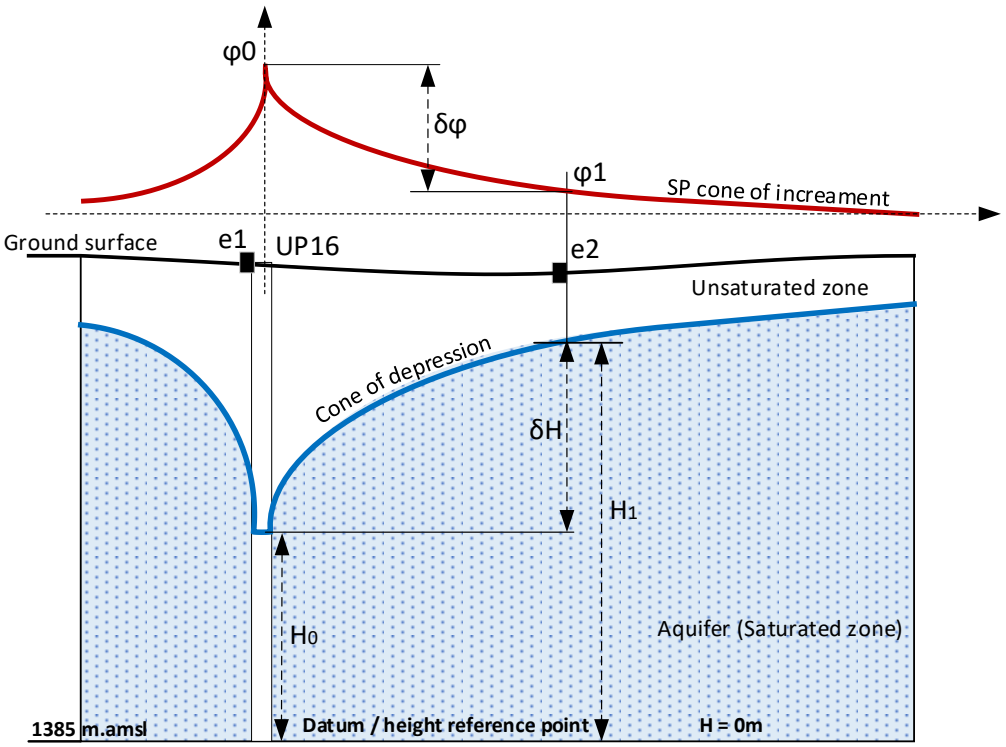

Figure 6.19: Illustration of computing hydraulic head using the measured streaming potential at surface at CTS

From measured streaming potential, the linear change in streaming potential between the pumping borehole and electrode is computed as:

$$\delta\varphi = \varphi_1 - \varphi_0 \qquad 6.5$$

H_0, which is our hydraulic head in the pumping borehole is known through the drawdown measurements and taking 1 385 mamsl as the datum point where the hydraulic head is zero through-out the half space of the aquifer as:

$$H_o = Z_{UP16} - Z_{DATUM} - h_0 - s_0 \qquad 6.6$$

$$H_o = 1411.5\,m - 1385\,m\ - 17.25\,m - 2.72\,m = 6.53\text{ m} \qquad 6.7$$

Where Z_{UP16} is the surface elevation at UP16 collar, Z_{DATUM} is the datum elevation = 1 385 m, h_0 is the water level in UP16 at start of pumping and s_0 is the measured drawdown in UP16.

Our problem is to find H_1 on any point on the surface where streaming potentials have been measured. From Figure 6.19, it can be seen that the linear change in hydraulic head (δH) is given by:

$$\delta H = H_1 - H_0 \qquad 6.8$$

From Equation 3.45:

$$\delta H = \frac{\delta\varphi}{C_s} = \frac{\delta\varphi}{-8.95} m \qquad 6.9$$

Where C_s is the streaming potential coupling coefficient computed in Section 6.3.3, which is -8.95 mV/m. Using electrode e_2 as an example, then:

$$\delta H = \frac{\varphi_1 - \varphi_0}{-11.986} = \frac{17.24 - 20.36}{-8.95} = 0.349 \text{ m} \qquad 6.10$$

From Equation 6.34, it follows that:

$$H_1 = H_0 + \delta H \qquad 6.11$$

$$H_1 = 6.53\, m + 0.349\, m = 6.88 \text{ m}$$

Drawdown at e_2 is computed from equation:

$$s_1 = (H_0 + s_0) - H_1 \qquad 6.12$$

$$s_1 = (6.53 + 2.72)\, m - 6.88\, m = 2.4 \text{ m}$$

The same procedure is performed for all the streaming potential monitoring station and Table gives the computed hydraulic heads and drawdown from streaming potential method for each electrode station.

Table 6.5: Table showing computed hydraulic heads and drawdown from streaming potential measurements at Campus Test Site

Electrode	$\varphi_{1(300)}$	$\varphi_{0(300)}$	$\delta\varphi_{(300)}$	$\delta H_{(300)}$	$H_{0(300)}$	$H_{1(300)}$	$s_{1(300)}$
e_1	20.4	20.36	0.0	0.000	6.53	6.53	2.72
e_2	17.2	20.4	-3.1	0.349	6.53	6.88	2.37
e_3	13.7	20.4	-6.7	0.746	6.53	7.28	1.97
e_4	11.2	20.4	-9.2	1.024	6.53	7.55	1.70
e_5	13.9	20.4	-6.5	0.723	6.53	7.25	2.00
e_6	4.5	20.4	-15.9	1.775	6.53	8.31	0.94
e_7	6.8	20.4	-13.6	1.517	6.53	8.05	1.20

6.3.5 Estimation of Hydraulic Conductivity from Streaming Potential

Section 6.3.3 discussed the procedure of calculating hydraulic parameters from direct drawdown measurements through the application of the analytical solution provided by

Theis and Copper Jacob methods. The conclusion was that at Campus Test Site all two methods give similar approximation of *K* and *T*.

Streaming potential method in a confined aquifer only give the value of drawdown at a particular time in pseudo-steady state. The late time *t* = 300 min was chosen. The estimation of transmissivity is performed by using a distance – drawdown graph from Cooper Jacob method.

From Equation 3.26, it can be seen that:

$$T = KD = \frac{2.30Q}{4\pi\Delta s} \qquad 6.13$$

and:

$$S = \frac{2.25KDt}{{r_0}^2} \qquad 6.14$$

where Q is the pumping discharge = 129.6 m^3/d and Δs is the change in drawdown per unit log distance r of the observation point from pumping well (slope per unit log distance).

Kruseman & De Ridder (1990), provided a solution of estimating transmissivity by means of plotting a graph of drawdown *(s)* against distance *(r)* of the observation borehole from the pumping borehole, with *r* in a log scale and *s,* on linear scale. The graph is a straight line whose horizontal axis *r* (log scale) intercept represent a value r_0 for drawdown equal to zero. The gradient of the line, change in drawdown per log distance (Δs) can be determined.

The determined values of Δs and r_0 substituted into Equations 6.13 and 6.14 to obtain the mean value of aquifer transmissivity and storativity.

The procedure is demonstrated below as follows:

A distance – drawdown graph was plotted on a semi-log plot with drawdown on the vertical linear scale and distance on the horizontal log scale as shown in Figure 6.20 using the values of drawdown computed form streaming potential method provided in Table 6.5.

The horizontal intercept r_0 at $s = 0$ is read out as 180m. The gradient Δs per change in log distance is read from the graph as:

$$\Delta s = 2.52 - 0.48 = 2.04 \text{ m} \qquad 6.15$$

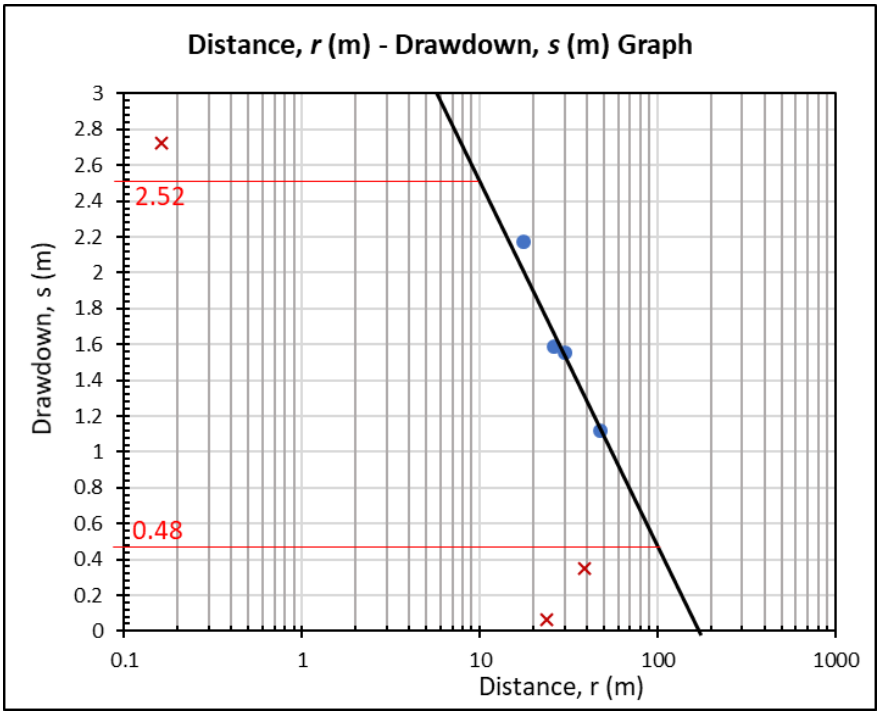

Figure 6.20: Illustration of computing hydraulic head using the measured streaming potential at surface at CTS

- The value of Δs is substituted in Equation 6.13 to obtain the estimate value of aquifer transmissivity as:

$$T_{mean} = KD = \frac{2.30 \times 129.6\, m^3/d}{4\pi \times 2.04\, m} = 11.627 \text{ m}^2/\text{d} \qquad 6.16$$

The estimated mean aquifer transmissivity is of comparable magnitude to the values of *T* estimated in Section 6.2.5 by Theis and Copper Jacob. This validates streaming potential method as a valid tool in estimating transmissivity. The value of hydraulic conductivity is obtained from the relationship *T* = *KD* as follows:

$$K_{mean} = \frac{T}{D} = \frac{11.627}{9} m/d = 1.29 \text{ m/d} \qquad 6.17$$

Storativity is then obtained from Equation 6.14 as:

$$S = \frac{2.25 \times 11.627 \times 300 \times (6.94 \times 10^{-4})}{180^2} = 8.07 \times 10^{-4} \qquad 6.18$$

This value of storativity is in the order of *S* estimated from Theis and Copper Jacob methods.

6.3.6 Estimation of Hydraulic Conductivity Using the Relaxation Mode

Rizzo *et al.* (2004) provided a coupled flow analytical solution in recovery / aquifer relaxation mode in Equation 3.69, it follows that transmissivity *T* is given as:

$$T = = \frac{C'2.3Q}{4\pi\delta\varphi(r)} log\left(\frac{t}{t'}\right) \qquad 6.19$$

Where the values of *C'* and *Q* are known and $t^{'}$ is the duration of pumping test and *t'* is the recovery period after switching off the pump and $\delta\varphi(r)$ is the potential gradient at each station at the end of recovery. The values of $\varphi(r)$ are the measured streaming potential values at the end of pumping test. For the Campus Test Site, the duration of the test was 420 min. Therefore *t'* at the end of the pumping test is 120 min and *t* is 300 min.

Using these known quantities, the value of *T* for each electrode position was calculated using Equation 6.19. Table 6.6 provides the values of estimated transmissivity and hydraulic conductivity.

Table 6.6: Values of transmissivity and hydraulic conductivity estimated using the relaxation mode coupled flow solution provided by Rizzo *et al.* (2004)

Electrode	$\varphi_{2(420)}$	log(t/t')	Q (m^3/d)	C' (mV/m)	$\delta\varphi_{2(420)}$	T (m^2/d)	K (m/d)
e_1	13.855	-0.146	129.6	-8.947	0		
e_2	11.487	-0.146	129.6	-8.947	2.37	13.10	1.46
e_3	10.218	-0.146	129.6	-8.947	3.64	8.53	0.95
e_4	8.279	-0.146	129.6	-8.947	5.58	5.56	0.62
e_5	10.811	-0.146	129.6	-8.947	3.04	10.19	1.13
e_6	3.727	-0.146	129.6	-8.947	10.13	3.06	0.34
e_7	5.688	-0.146	129.6	-8.947	8.17	3.80	0.42
					Arithmetic mean	7.37	0.82
					Geometric mean	6.47	0.72

The estimated values in Table 6.6 by use of coupled flow solution for transient recovery in a confined aquifer provided by Rizzo *et al*. (2004) in Equation 3.69 are lower as compared to the mean transmissivity estimated from direct application of the coupled flow problem. This may imply that the analytical solution of solving for *T* using recovery data requires verification and should be used with caution.

The method estimates lower hydraulic conductivities on stations located at UO19, UO3 and UO18, with the lowest at UO19 followed by UO3. This agrees with geohydrological

setting of the Campus Test Site in that these boreholes did not encounter the bedding plan fracture. Although the estimations for UP15 and UO20 are lower than the true values obtained from measured drawdown analysis using Copper Jacob, their values are near to the order of 10^0 which is the order of the true value.

6.4 KRUGERSDRIFT TEST SITE PUMPING RESULTS

Prior to test pumping a hydro-census was performed to record the baseline information of the boreholes. Table 6.7 shows the baseline records of the boreholes.

Table 6.7: Baseline borehole details recorded prior to pumping for KTS

Borehole ID	**Longitude** WGS84	**Latitude** WGS84	**Elevation** (m.amsl)	**SWL** (m.bgl)	**BH Depth** (m.bgl)	**Hydraulic Head (Ho)** (m.amsl)
BH3	28.88943	-25.95134	1241.8	2.70	19.07	9.07
BH4	28.88931	-25.95130	1241.6	3.66	22.00	7.89
BH5	28.88927	-25.95130	1241.3	2.42	10.17	8.91
BH6	28.88931	-25.95137	1241.3	2.42	11.35	8.92
BH7	28.88934	-25.95128	1241.6	2.53	7.89	9.05
BH8	28.88943	-25.95137	1241.8	2.79	4.97	8.98
BH9	28.88940	-25.95144	1241.5	2.63	11.62	8.89

An elevation of 1230 metres above mean sea level was chosen as the reference point for calculations of hydraulic head. The hydraulic head values shown in Table 6.7 are the hydraulic heads at time $t = 0$ min.

6.4.1 Time-Drawdown Curves for Krugersdrift Test Site

Krugersdrift Test Site (KTS) is conceptualised to be a semi-confined aquifer (Gomo, 2011). As discussed in Chapter 5, the time-drawdown curves show that the system reached a pseudo-steady state condition after 60 minutes of pumping with drawdown changes of the order of 0.00015 m/min (Figure 6.21).

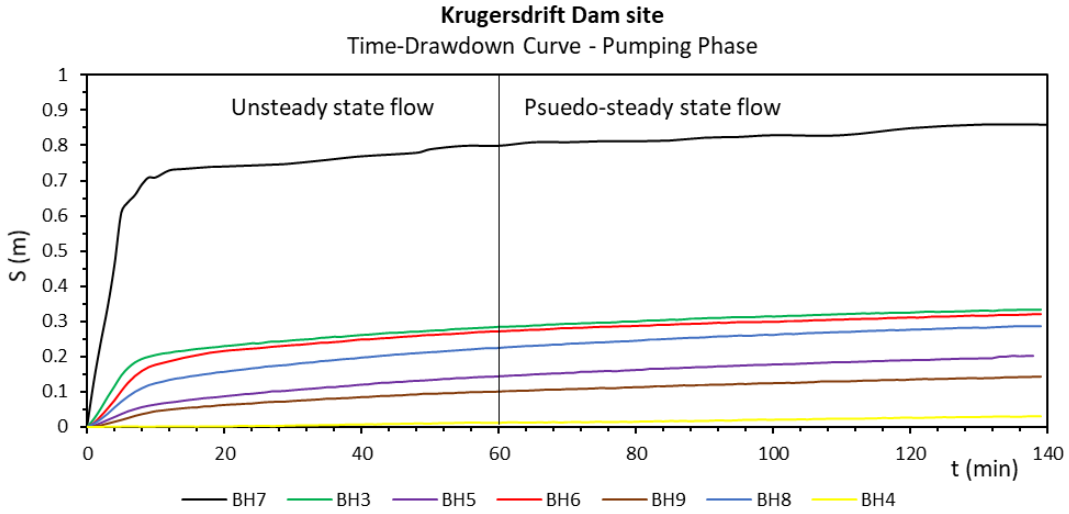

Figure 6.21: Time – drawdown graphs for a constant rate test performed at BH7 with BH3, BH4, BH5, BH6, BH8 and BH9 used as observation wells.

The drawdown measurements from the observation boreholes show that the system has high horizontal hydraulic conductivity evidenced by the quick response time. The response time varied from 1 minute to 2 minutes and is affected by the hydraulic properties of the media through which groundwater is being transmitted and the distance from the pumping well.

6.4.2 Recovery Phase – Aquifer relaxation mode

The recovery phase is the time when the aquifer is naturally recharged to its initial water level after the pump is switched off. This is referred to as the relaxation mode and the drawdown measured during this time is often called residual drawdown *(s`).* In this discussion the terms recovery and residual drawdown will be used interchangeably. The time-recovery curves show that the aquifer has good recharge observed by the quick recovery. All the boreholes recovered to 80% of the original water level at about 40 minutes recovery time mark (Figure 6.22).

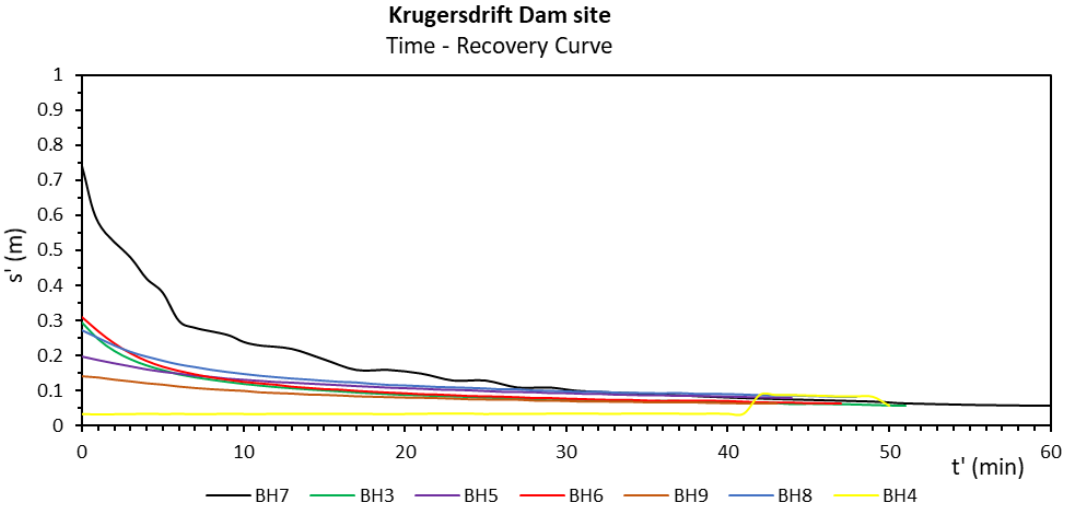

Figure 6.22: Time – recovery graphs at BH7, BH3, BH4, BH5, BH6, BH8 and BH9

6.4.3 Spatial Drawdown and Hydraulic Head Maps

Spatial drawdown and hydraulic head maps were constructed from the measured drawdown in the pumping and monitoring boreholes (Figure 6.23 and Figure 6.24) at time t = 140 min. The hydraulic heads were computed by taking elevation 1 230 m.amsl as the datum level. Therefore, all hydraulic heads are referenced from this datum level.

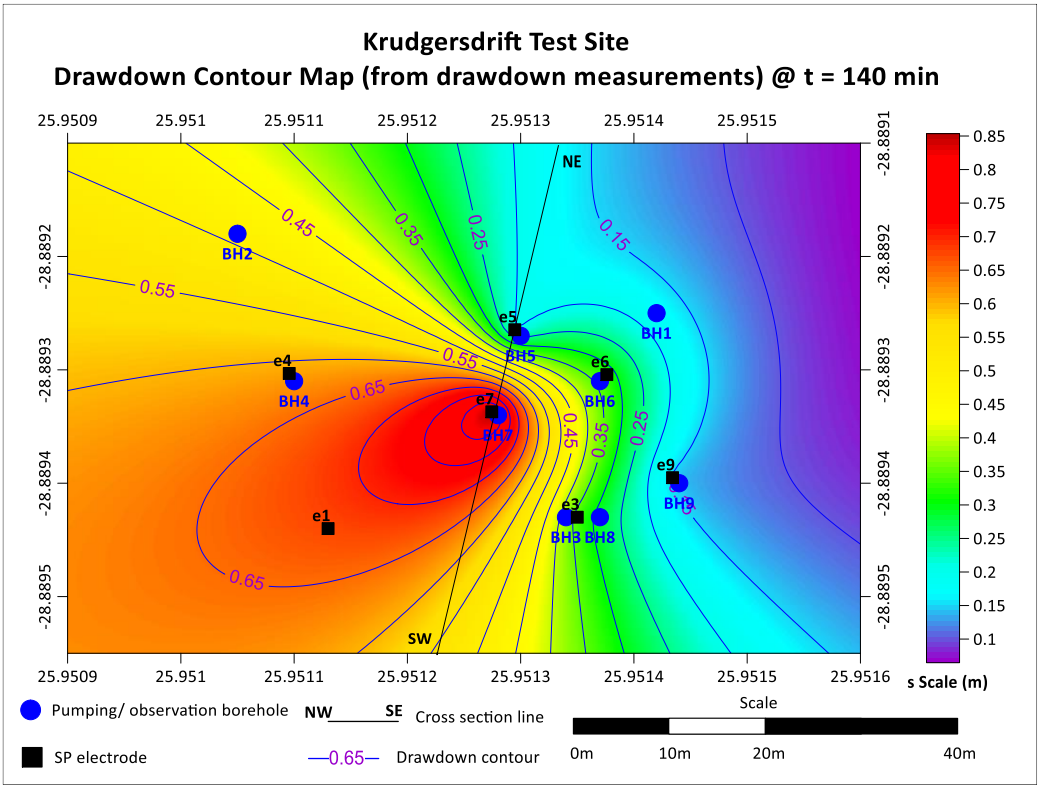

Figure 6.23: Spatial drawdown map of the Krugersdrift Test Site at time t=140 m

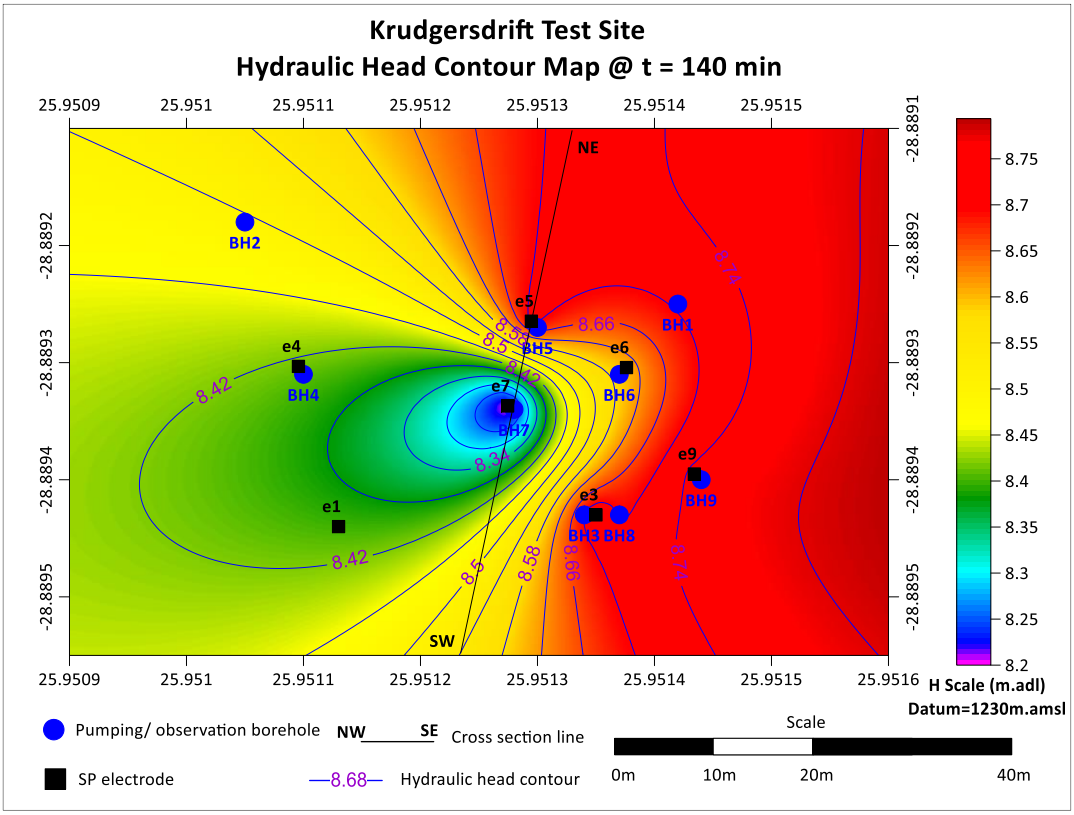

Figure 6.24: Spatial hydraulic head map of the Krugersdrift Test Site at *t* = 140 min

Both spatial drawdown and hydraulic head distribution maps show that the piezometric surface is near symmetrical around the pumping borehole with a skewness towards in the southwestern direction. However, such skewness occurred because the drawdown from boreholes BH4 and BH2 were neither included nor monitored and so the software interpolated the left half space.

However, an important observation is the near symmetry of the drawdown cone and piezometric surface around the borehole suggesting aquifer homogeneity conditions. According to Gomo (2011), the drawdown cone only deviates from the symmetrical image if there are spatial variations of physical and hydraulic parameters within the space domain of the test site.

6.4.4 Drawdown Cone and Piezometric surface across BH7

Cross-section lines in the direction NE to SW were selected in Figure 6.23 and Figure 6.24 for the generation of the drawdown and piezometric surface (hydraulic head) section as a function of distance r from the pumping well.

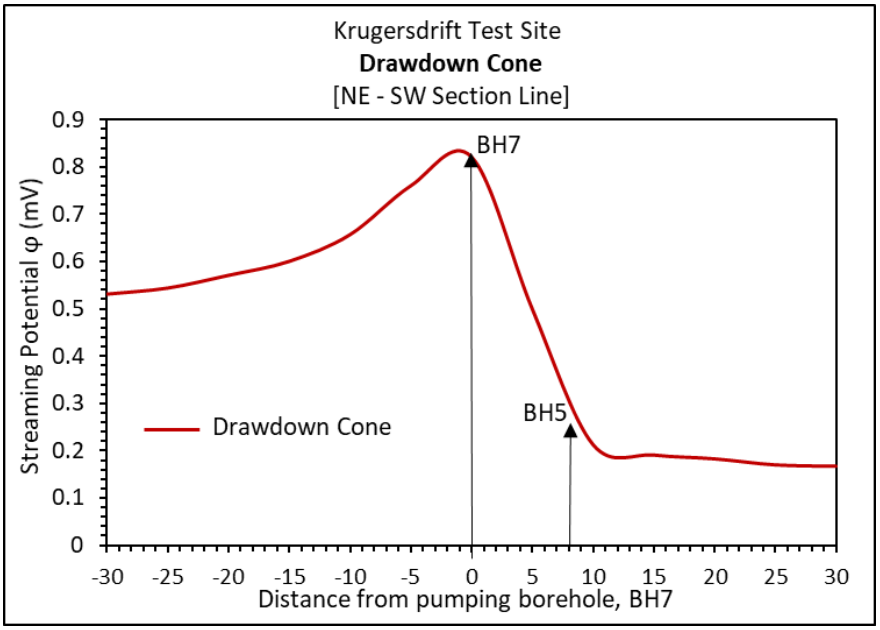

Figure 6.25: Drawdown cone across the pumping well (BH7) at Krugersdrift Test Site at *t* = 140 min

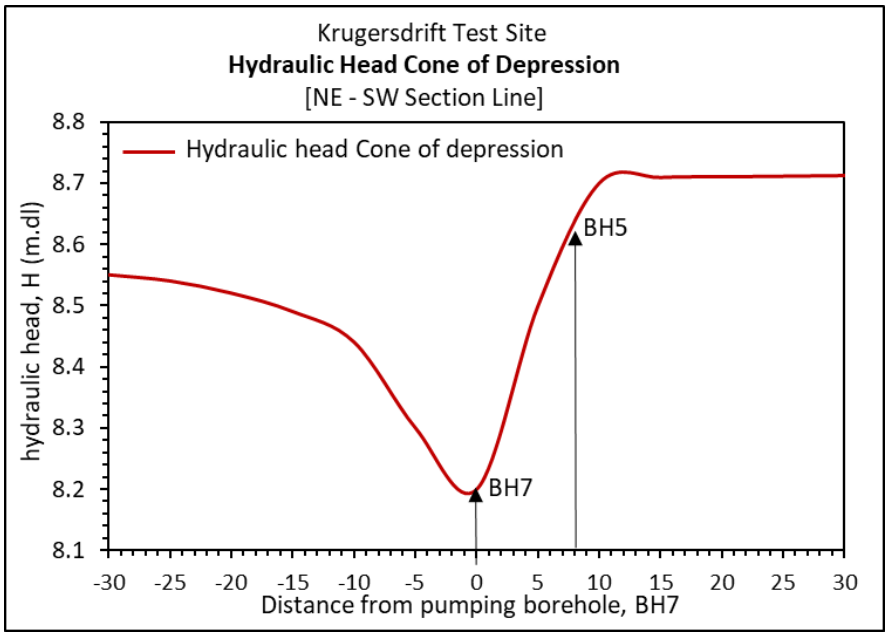

Figure 6.26: Hydraulic head cone of depression or piezometric surface across the pumping well (BH7) at Krugersdrift Test Site at *t* = 140 min

Figure 6.25 and Figure 6.26 show that drawdown cone and hydraulic heads are mirror images of each other. The drawdown decreases with distance from the pumping well while the hydraulic head increases away from the pumping well. The section line chosen show the deviation from symmetry of the cone of depression around the pumping borehole. Gomo (2011) postulated that BH5 encountered a thicker layer of clay-silt from the flood deposits. These have a lower transmissivity which limits the progression of the cone of depression outwards. Figure 6.26 agrees with this phenomenon.

6.4.5 Hydraulic Parameters Estimation for Krugersdrift Test Site

Hydraulic parameter estimation is achieved using Theis curve matching method, Copper Jacob and Thiem-Dupuit method. The estimated parameters are compared and a mean aquifer hydraulic conductivity is determined. Pumping test data analysis was performed firstly using Theis and Cooper Jacob Method for a confined aquifer under unsteady-state groundwater flow condition. And lastly using Theim-Dupluit method for steady state conditions in an unconfined aquifer.

It is apparent that steady state was not reached as there was still measurable drawdown change in the observation boreholes. Therefore, the first attempt will be to use unsteady state conditions and assumptions. However, the discussion in Section 6.4.1, pointed out that a pseudo state groundwater flow condition was reached after 60 min of pumping, hence an attempt to estimate hydraulic parameters using Dupluit assumptions was made. It is not hypothetically incorrect because if the expression of Coper Jacob method for Distance-drawdown analysis is performed with two observation boreholes, it will yield a similar expression as Thiem-Dupuit.

As discussed in Section 5.3.4, the main flow characterising groundwater flow in Krugersdrift Test Site aquifer is Radial Acting Flow (RAF) which occurs in the late times of the time-drawdown curve. Hence Theis and Cooper Jacob methods were applied in the late time data after 60 min of pumping and Thiem-Dupuit method was applied in the late time t =140 min.

6.4.5.1 Theis curve matching

FC pumping test analysis software was used to determine transmissivity and storativity at all the observation boreholes whose drawdown was monitored and the results of the estimated values of transmissivity and hydraulic conductivity are shown in Table 6.8. Figure 6.27 shows Borehole BH3 as an example of Theis curve matching performed. The rest of Theis curve matching on other observation boreholes is presented in Appendix B.

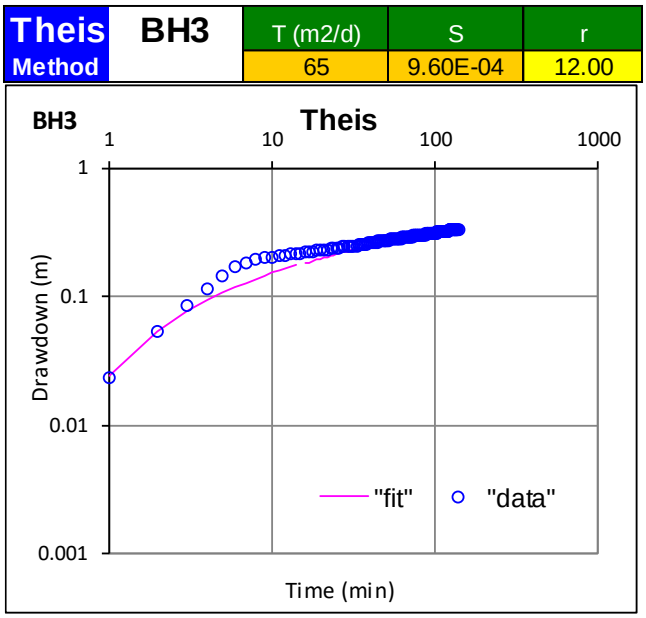

Figure 6.27: Theis curve matching on a semi log Time at late times – Drawdown graph on BH3

Theis curve matching at BH3 estimated Transmissivity *(T)* of 67 m^2/d and Storativity *(S)* of 9.5×10^{-4} m^2/d at late times. Borehole logs show that the average aquifer thickness at Krugersdrift Test Site is 6.5 m. Since, $T = KD$, it follows that:

$$K(Bh3) = \frac{67\ m^2/d}{6.5\ m} = 10.3\ \text{m/d} \qquad 6.20$$

A similar operation was conducted on all observation boreholes and the calculated hydraulic conductivity values are shown in Table 6.8 on page 132.

6.4.5.1 Cooper Jacob Method

The parameters for the aquifer at Krugersdrift Test Site can be estimated by using Cooper Jacob method of confined or semi-confined aquifer in unsteady-state flow. The use of Cooper Jacob in estimation of parameters was discussed in Section 3.2.3.2. Two approaches are used here to get representative values of transmissivity and hydraulic conductivity at each observation borehole (or even the abstraction borehole) and on the aquifer as a whole. Illustration of Cooper Jacob method application on pumping borehole BH7 is shown in Figure 6.28.

From Equation 3.26, it can be seen that a graph of drawdown *(s)* against *log t* (semi log plot) is a straight line. According to Kruseman and De Ridder (1990) if the straight line crosses the time axis (i.e. at $s = 0$ and time t_0 is read), the slope of the straight line over a unit log time can be used to calculate transmissivity using the following equation:

$$T = \frac{2.30Q}{4\pi\Delta s} \qquad 6.21$$

Where, Δs is the change in drawdown per unit log time (slope per unit log time).

However, in this dissertation FC pumping analysis software was used under the same principle to estimate T and S of the pumping borehole. Figure 6.28 shows the time – drawdown semi log plot for BH7 and the output of Copper Jacob estimation in the late time of Radial Acting Flow (RAF). An aquifer transmissivity value of 64.6 m^2/d was obtained which gives hydraulic conductivity of 9.94 m/d. This is comparable to the value obtained for observation borehole BH3 using Theis method.

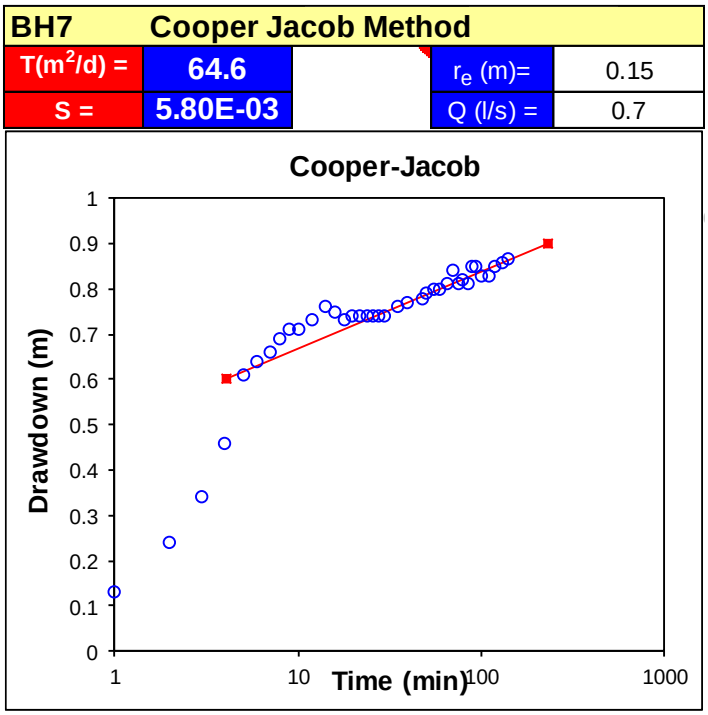

Figure 6.28: Application of Cooper Jacob method for pumping borehole BH7 during RAF using FC pumping test analysis software

The same procedure was performed on all monitored observation boreholes except BH4 and the output time – drawdown plots are shown in Appendix B and Table 6.8 shows the values of estimated T, K and S.

6.4.5.2 Thiem-Dupuit Method

Thiem-Dupuit method as provided by Equation 3.30 assumes that the aquifer is unconfined and the system reached a pseudo-steady state. Since the aquifer is conceptualised to be semi-confined an attempt to interpret the hydraulic test data using

Thiem-Dupuit method according to the procedure of Kruseman and De Ridder (1990) was done using Equation 3.30.

i. **Direct approach of Thiem-Dupuit method**

Firstly the value of T was calculated by direct application of Equation 3.30 between the pumping borehole BH7 and observation borehole. For example application of Equation 3.30 on BH3 as observation borehole yields at time *t* = 140 min:

$$T_{140} = \frac{2.30 \times \log(\frac{r_2}{r_1}) \times Q}{2\pi \times (s_1 - s_2)} \quad 6.22$$

$$T_{140}(BH3) = \frac{2.30\log(\frac{12}{0.15}) \times 60.48\ m^3/d}{2\pi \times (0.865 - 0.3336)\ m} = 79.3\ \mathrm{m^2/d} \quad 6.23$$

$$K_{140}(BH3) = \frac{79.3\ m^2/d}{6.5\ m} = 12.2\ \mathrm{m/d} \quad 6.24$$

Where, r_1 is the radius of the pumping borehole in metres, r_2 is distance of the observation borehole BH3 from the pumping well, s_1 is the drawdown in the pumping borehole at time *t* = 140 min, s_2 is the drawdown in the observation borehole BH3 at *t* = 140 min and Q is the constant rate discharge is equal to 60.48 m^3/day.

A similar procedure was performed for each observation borehole (BH5, BH6, BH8 and BH9). BH4 was not used because its time – drawdown curve does not replicate that of the pumping borehole and is not parallel to other time-drawdown graphs for the observation boreholes (meaning its in a different system). The calculated *T* values for other observation boreholes are shown in Table 6.8.

ii. **Indirect (Graphying) approach of Thiem-Dupuit method**

Equation 3.30 can be rearranged to the form:

$$\log(\frac{r_2}{r_1}) = \frac{2\pi T}{2.30 \times \mathrm{Q}}(s_1 - s_2) \quad 6.25$$

Equation 6.25 represents a linear equation of the form $y = ax$. Therefore the average aquifer transmissivity (*T*) can be obtained from the gradient of the linear graph of $\log(r_2/r_1)$ versus $(s_1 - s_2)$. This gradient is given by:

$$\mathrm{Gradient} = \mathrm{a} = \frac{2\pi T}{2.30 \times \mathrm{Q}} \quad 6.26$$

Rearranging Equation 6.26 in terms of T yields:

$$T = \frac{2.30aQ}{2\pi} = 22.14a \qquad 6.27$$

Figure 6.29 demostrates the graphical approach of calculating hydraulic parameters using the Thiem-Dupuit method.

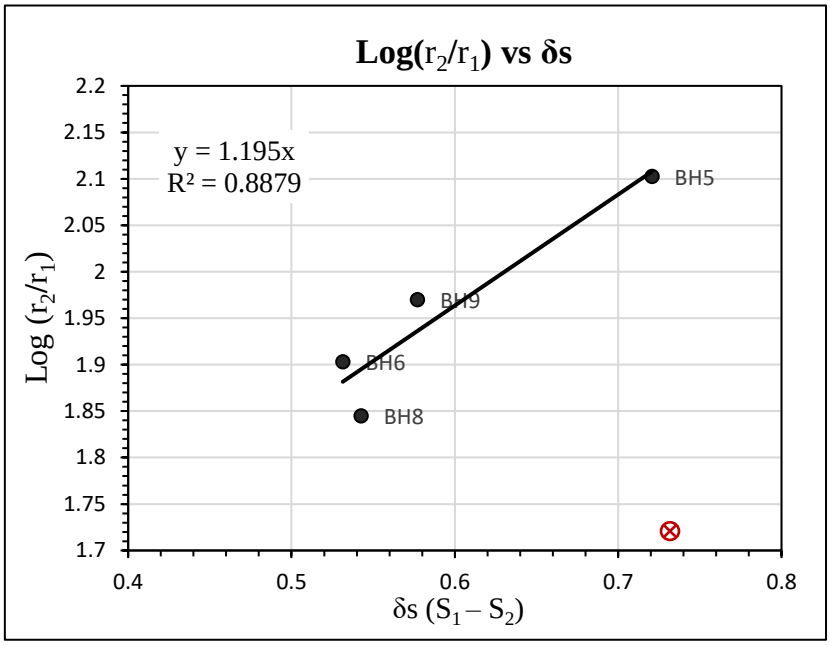

Figure 6.29: Thiem-Dupuit Log(r_2/r_1) versus (s_1-s_2) graph for KTS

From Figure 6.29 the gradient of the graph, a = 1.195, therefore using Equation 6.27, the mean transmissivity and mean hydraulic conductivity are:

$$T_{mean} = \frac{2.30 \times 1.195 \times 60.48}{2\pi} = 26.46 \text{ m}^2/\text{d} \qquad 6.28$$

$$K_{mean} = \frac{26.46}{6.5} = 4.1 \text{ m}^2/\text{d} \qquad 6.29$$

T_{mean} and K_{mean} represent the average aquifer transmissivity and hydraulic conductivity computed from the Thiem-Dupuit indirect method.

6.4.1 Discussion on Pumping Test Data Analysis for Krugersdrift Test Site

The results of the estimated values for the three methods above are summarised in Table 6.8.

Table 6.8: Summary of estimated hydraulic parameter values (T, K and S) from Theis, Cooper Jacob and Thiem-Dupuit methods for KTS

Borehole ID	Theis			Cooper Jacob		Thiem-Dupuit	
	T (m^2/d	K (m/d)	S	T (m^2/d	K (m/d)	T (m^2/d	K (m/d)
BH3	65.0	10.0	0.00096	77.6	11.9	79.3	12.2
BH5	70.0	10.8	0.00381	68.0	10.5	57.7	8.9
BH6	53.0	8.2	0.00260	76.4	11.8	75.3	11.6
BH8	68.0	10.5	0.00157	68.0	10.5	75.6	11.7
BH9	68.0	10.5	0.00710	68.0	10.5	64.6	9.9
A. Mean	**64.8**	**10.0**	**0.00321**	**71.6**	**11.0**	**70.5**	**10.8**
G. Mean	**64.5**	**9.9**	**0.00264**	**71.5**	**11.0**	**70.1**	**10.8**

The following views can be drawn from the estimated values of hydraulic parameter *T*, *K* and *S* using three methods chosen.

1. Transmissivity of the order $5 \text{ to } 8 \times 10^1\ m^2/d$ and hydraulic conductivity values ranging between 8 m/d and 12 m/d were calculated using all the methods. Such values agree with the submission of Gomo (2011), that the aquifer is high transmissive and has high hydraulic conductivities typical of gravel-sand porous aquifers. The values agree with range of values published by other researchers. This makes the drawdown measurements valid to act as validating tool for streaming potential method.
2. Alluvial channels have great potential for good storage of groundwater evidence by the estimated storativity values of the order 10^{-3}.
3. According to Gomo (2011) aquifer test in an ideal homogeneous aquifer media should yield comparable aquifer parameters, however heterogeneous conditions attributed by the physical and chemical differences in geology properties of the aquifer material result in spatial variation in these hydraulic properties. The pumping test conducted showed great similarities and comparability of

transmissivity and hydraulic values for all the observation boreholes and pumping borehole.

However, a method which gives only the mean value of the hydraulic parameter is will not give a true reflection of the hydraulic properties surrounding observation and pumping boreholes because in principle obtaining a mean value assumes that the aquifer is homogeneous *(i.e. The mean value of T and K is the equivalent T and K of a homogeneous aquifer).* Such an approach will under-estimate the hydraulic properties of Krugersdrift test site (i.e. T_{mean} and K_{mean} calculated in Equations 6.28 and 6.29 are less than the values obtained in Table 6.8 by an order of 3).

4. The ability to obtain similar estimation using Cooper Jacob, Theis and Thiem-Dupuit methods suggest a fair degree of homogeneity of the aquifer. Although steady state condition was not achieved, the changes in drawdown were so small to allow pseudo state flow conditions to be applied. It also implies that the aquifer is not completely unconfined as confined assumptions of Theis and Cooper Jacob gave similar results comparable to Thiem-Dupuit method. Hence the conceptualisation of it being semi-confined holds.
5. A comprehensive knowledge review on the underlying geological conditions and spatial level of heterogeneity of the aquifer deposits is a fundamental tool for analysing aquifer test in alluvial channel beds. Therefore, site characterisation and resistivity imaging activities played an impact role in revealing the nature and conceptualised behaviour of the aquifer.

6.5 KRUGERSDRIFT TEST SITE STREAMING POTENTIAL RESULTS

Streaming potential measurements were made concurrent with the constant rate tests in which drawdown measurements were taken. This section presents results of streaming potential data collected and the procedures for estimating hydraulic conductivity.

6.5.1 Raw Data and Digitally Filtered Time - Potential Graphs

The recorded raw and filtered streaming potentials were plotted on a time – potential graph for each electrode as illustrated in Figure 6.30 with electrode e_3 as an example.

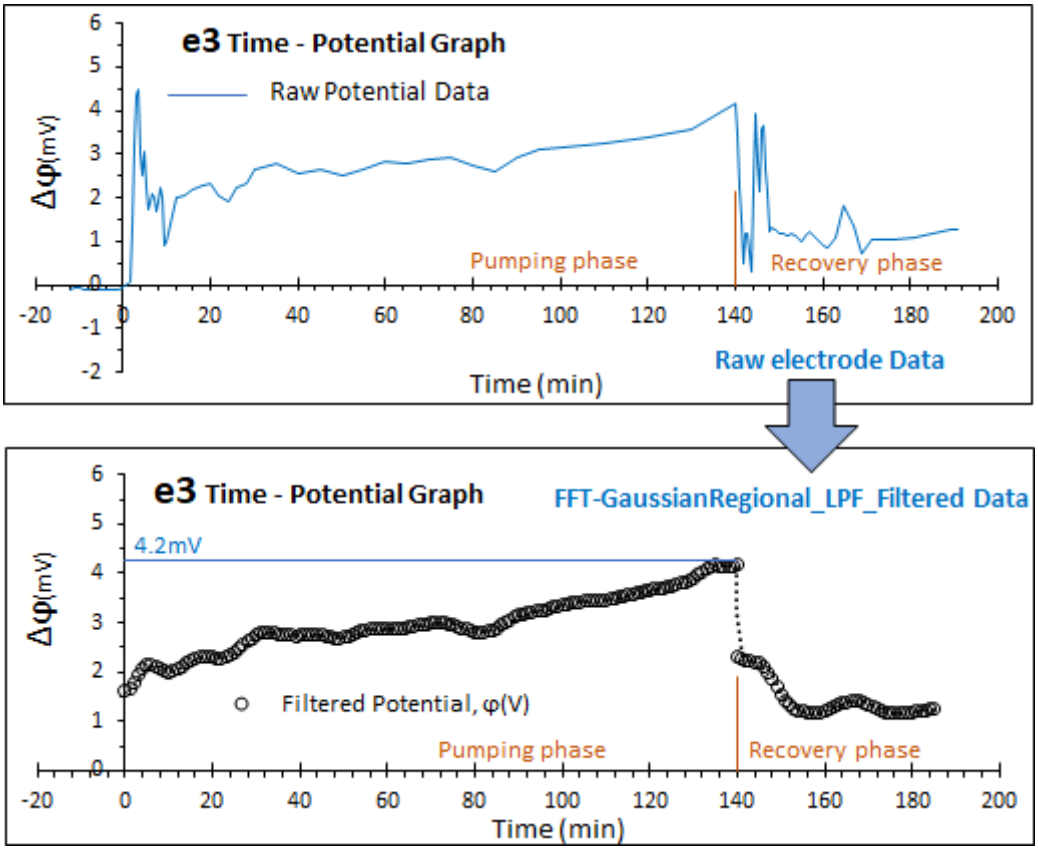

Figure 6.30: Raw and filtered time – potential graph for self-potential signals recorded at electrode e_3 at Krugersdrift Test Site

The measured raw data from streaming potential electrodes was digitally filtered using a Gaussian regional filter and standard deviation of 60, which is a low pass filter that eliminates high frequency spikes as explained in Section 4.4.2.

6.5.1.1 Time – potential graphs during pumping phase

The raw and filtered time potential signals recorded during the pumping phase is shown at all the seven monitoring stations is shown in Figure 6.31 The individual plots for each electrode are presented in Appendix D.

The following was observed on the time-potential graphs during pumping phase:

i. Streaming potential signals recorded were erratic, especially in the first 10 minutes of pumping, this might be attributed to the fact that during this phase groundwater flow is rapid and an instant hydraulic pressure is created making sporous potential differences on the non-polarising electrodes. The noise in the initial 10 minutes is consistent an all electrodes. However, the Gaussian low-pass filter was successful in eliminating the noise.

ii. Long period anomalies (similar to the one observed between 60 and 80 minutes could not be eliminated because of their long wavelengths. However, with the theory existing to date of streaming potential interpretation, only the final potentials are the ones important for quantitative interpretation.

iii. In general, the trends and shapes of the streaming potential signals recorded replicate the drawdown measurements shown in Figure 6.21.

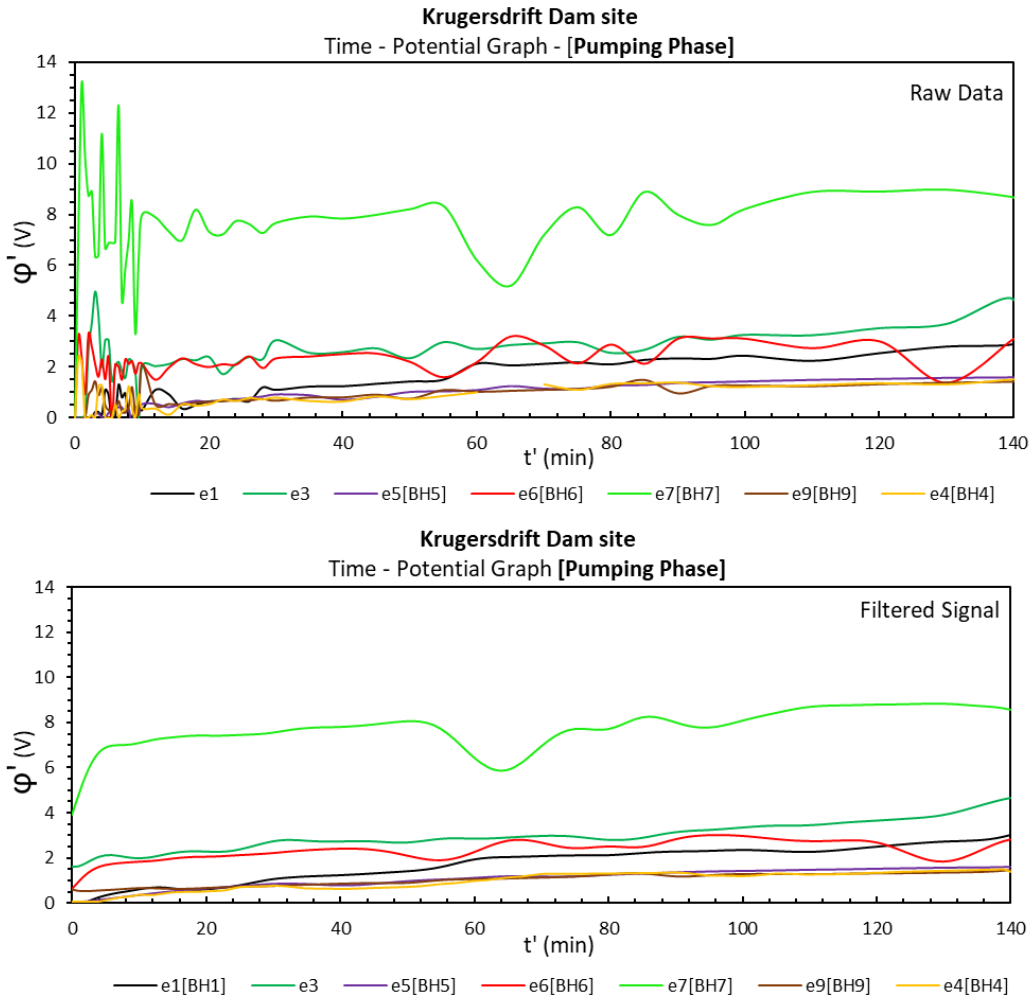

Figure 6.31: Raw and filtered time – potential graph for self-potential signals recorded on electrodes, e_1, e_3, e_4, e_5, e_6, e_7 and e_9 during pumping phase at KTS

6.5.1.2 Time – potential graph during relaxation phase

The potential s recorded during relaxation phase are also called residual potential in this dissertation. Figure 6.32 show the raw and filtered time potential signals recorded recovery phase also referred to as the aquifer relaxation state.

From the time – residual potential graphs shown in Figure 6.32, it can be observed that:

i. Unlike the pumping phase, the recovery signals are noisy throughout the time period when the recovery phase was being recorded. It is actually the opposite of what would have been expected. We expected to have more streaming potential noise when the system is under stress. However, the Gaussian regional filter was effective enough to eliminate these high-frequency spikes in the data.

ii. The filtered signals show a near replica of residual drawdown recorded during recovery shown in Figure 6.22.

iii. Both streaming potential signals recorded during the pumping and recovery phases form a positive anomaly around the pumping well, similar to the trend of drawdown. The highest positive anomalies are recorded near to the boreholes and reduce as we move away from the borehole.

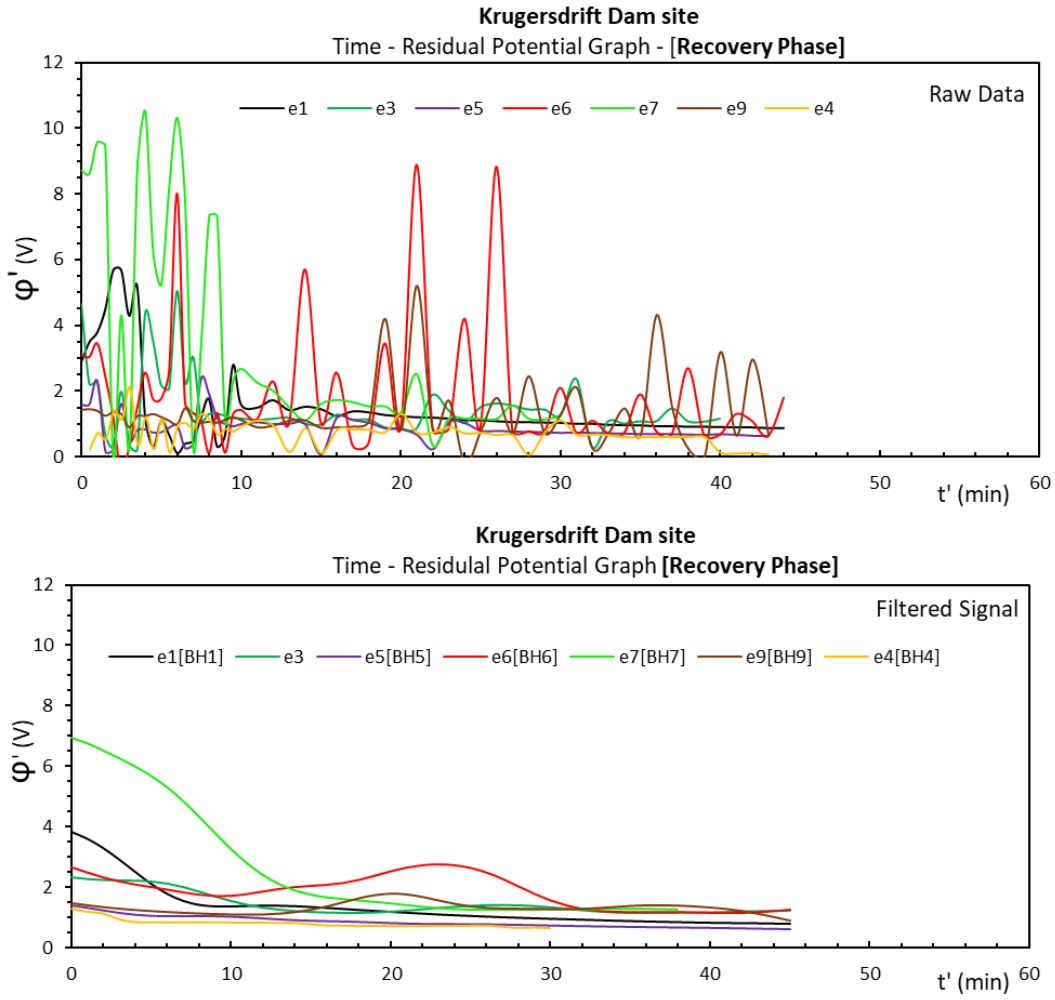

Figure 6.32: Time – potential graph for self-potential signals recorded on electrodes, e_1, e_3, e_4, e_5, e_6, e_7 and e_9 during pumping phase at KTS

6.5.2 Spatial Streaming Potential Gradient Maps

The streaming potentials at time *t*=140 min were selected to represent the final potential gradient due to pumping for each electrode. Table 6.9 shows the magnitude of streaming potential signals at time *t*=140 min selected which were gridded using Kriging gridding method for the entire spatial cover of the test site.

The grid map showing streaming potential gradient / spatial streaming potential at time *t* =140 min is shown in Figure 6.33. Figure 6.30 illustrates the reading procedure for the streaming potential value at time *t* = 140 min with example of electrode, e_3. The streaming potentials at time *t* = 140 min. Figure 6.34 and Figure 6.35 represent the shape of the cone of increment along cross-section lines NW-SE and NE-SW, respectively.

Table 6.9: Streaming potentials at time *t* = 140 min for each monitoring electrode at KTS

Electrode ID	Change in streaming potential at t = 140 min Δφ (mV)	Description of the location
e1	3	Location 20 m south west of pumping borehole BH7
e3	4.2	Location between BH3 and BH8
e4	1.5	Location 30 cm from BH4
e5	1.6	Location 30 cm from BH5
e6	2.9	Located 30 cm form BH6
e7	8.8	Location near pumping borehole (1m form BH7)
e8	1.5	Location 30 cm form BH9

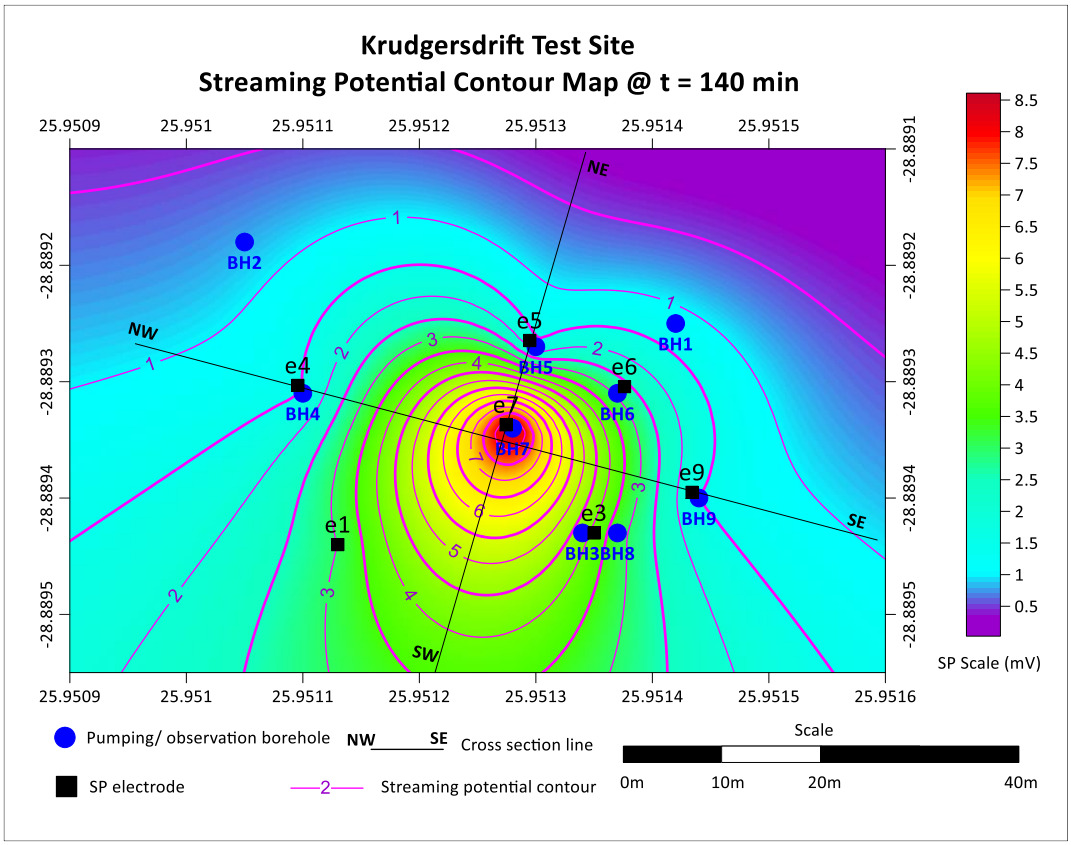

Figure 6.33: Spatial streaming-potential map (SP gradient map) at *t* = 140min for KTS

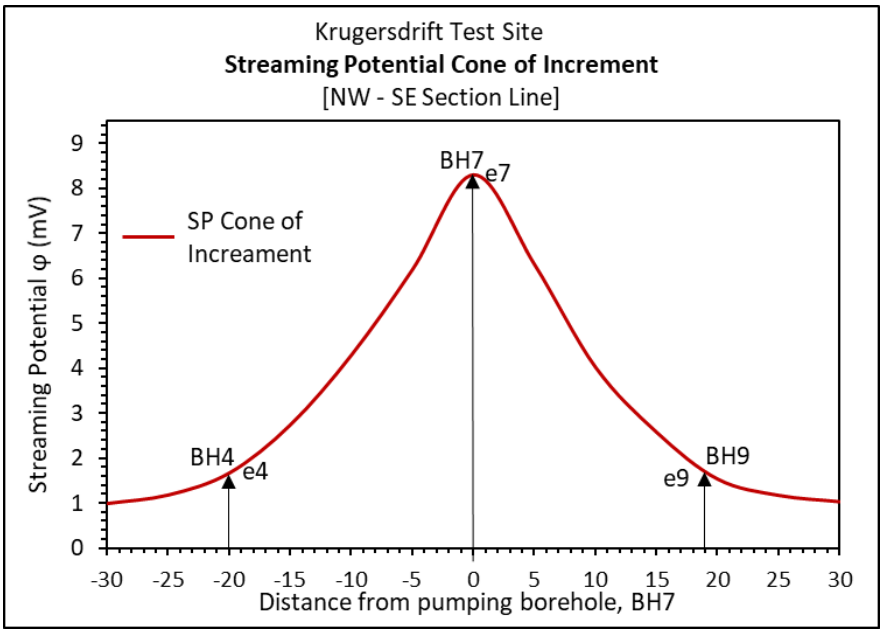

Figure 6.34: Streaming potential gradient / cone of increment at *t* = 140 min across pumping borehole BH7 along NW-SE section line at KTS

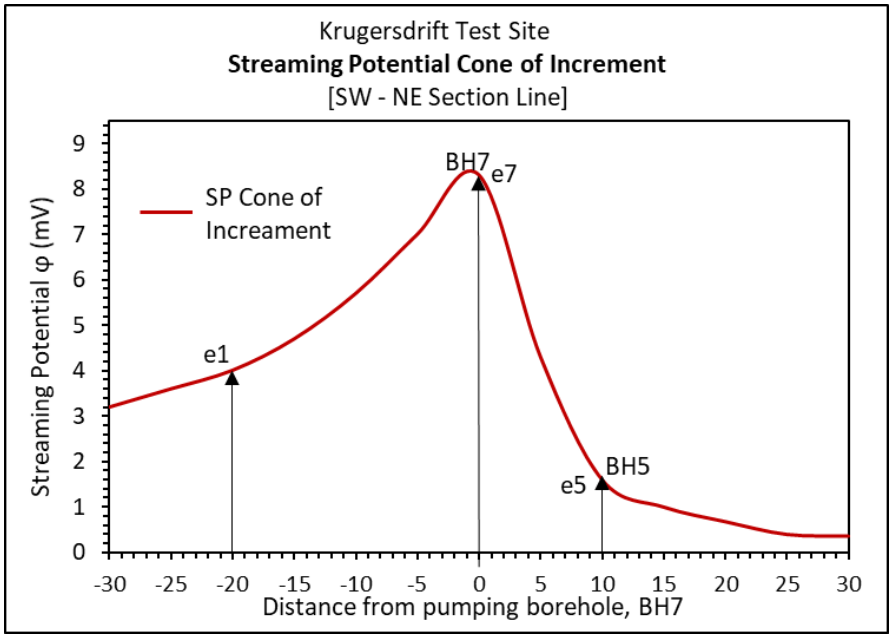

Figure 6.35: Streaming potential gradient / cone of increment at *t* = 140 min across pumping borehole BH7 along SW-NE section line at KTS

The following observation were made from the streaming potential gradient map (Figure 6.33).

i. An early observation from Figure 6.33, Figure 6.34 and Figure 6.35 is that the streaming potential signals form a positive anomaly around a pumping well. The positive anomaly, herein named the cone of increment, is a mirror image of the cone of depression formed by the hydraulic head during pumping around the well (also illustrated in Figure 6.34 and Figure 6.35). This agrees with the coupled flow problem which relates the streaming potential gradient to the hydraulic gradient linearly through a negative coupling coefficient of proportionality

ii. The spatial distribution of streaming potentials reveals the closeness of the aquifer to homogeneity property as the streaming potential signal cone of increment is near symmetric around the pumping well (also illustrate in Figure 6.34). The slight deviation biased towards e_3 and e_1 is interpreted as an indication of the preferential flow path (the signals increase more where there is more groundwater flow). This suggest that the aquifer is more transmissive towards e_1 and e_3 in the south west direction.

iii. An early indication of a less transmissive zone (that distorts the symmetry) is observed at e_5 and e_6, as it limits the progressive spread of streaming potential cone of increment (illustrated in Figure 6.35). This may be attributed to the flood

deposit layer deposited around BH5 comprising of very fine-grained sediments. It may also be as a result of a flow boundary as a result of sudden vertical drop in height towards the river bank.

6.5.3 In-situ Streaming Potential Coupling Coefficient

The streaming potential coupling coefficient for the test site was calculated using an in-situ method suggested by Ball *et al.* (2010). Streaming potentials and drawdown data recorded at t = 0 and t = 140 min (which are the times at start and end of pumping) for boreholes that were monitored both for drawdown and streaming potential change were used to calculate the streaming potential gradient and hydraulic gradient between each measurement station at pumping borehole. The procedure is illustrated in Table 6.10.

Table 6.10: Streaming potential and hydraulic head gradient measured t = 140 min for each monitoring station at KTS

BH	Electrode	$\varphi_{1(140)}$	$\varphi_{0(140)}$	$\delta\varphi_{(140)}$	$s_{1(140)}$	$H_{0(140)}$	$H_{1(140)}$	$\delta H_{(140)}$
3	e3	4.6	8.8	4.2	0.33	8.19	8.74	-0.55
5	e5	1.6	8.8	7.2	0.20	8.19	8.71	-0.52
6	e6	2.9	8.8	5.9	0.32	8.19	8.60	-0.41
7	e7	8.8	8.8	0.0	0.87	8.19	8.19	0.00
9	e9	1.5	8.8	7.3	0.14	8.19	8.75	-0.56

Where:

- $\varphi_{1(140)}$ and $\varphi_{o(140)}$ are the magnitudes of streaming potential signal recorded at the observation and pumping borehole at time t = 140 min respectively and $\delta\varphi$ is the linear change in streaming potential between the pumping borehole and the observation borehole at the time t = 140 min.

$s_{1(140)}$ and $s_{o(140)}$ are the drawdown measurements taken at the observation and pumping borehole at time t = 140 min respectively. Using the hydraulic head in each borehole prior to pumping (calculated in

- Table 6.7) and drawdown value, the at each borehole at t = 140 min the hydraulic head at t = 140 min was computed using the relationship:

$$H_{(t=140)} = H_{(t=0)} - s_{(t=140)} \qquad 6.30$$

- For the pumping borehole, the hydraulic head at time t = 140 min is labelled as $H_{o(140)}$ while for the observation borehole it is labelled as $H_{1(140)}$.
- $\delta\varphi_{(140)}$ and $\delta H_{(140)}$ are the linear change in streaming potential and hydraulic head between the pumping borehole and any the observation borehole.

From the coupled flow problem relationship provided in Equation 3.45, the values of $\delta\varphi_{(140)}$ and $\delta H_{(140)}$ were used to plot a straight line graph of $\delta\varphi_{(140)}$ against $\delta H_{(140)}$ with (zero; zero) intercept as shown in Figure 6.36. The gradient of the straight line is defined as the in-situ streaming potential coupling coefficient, *Cs*.

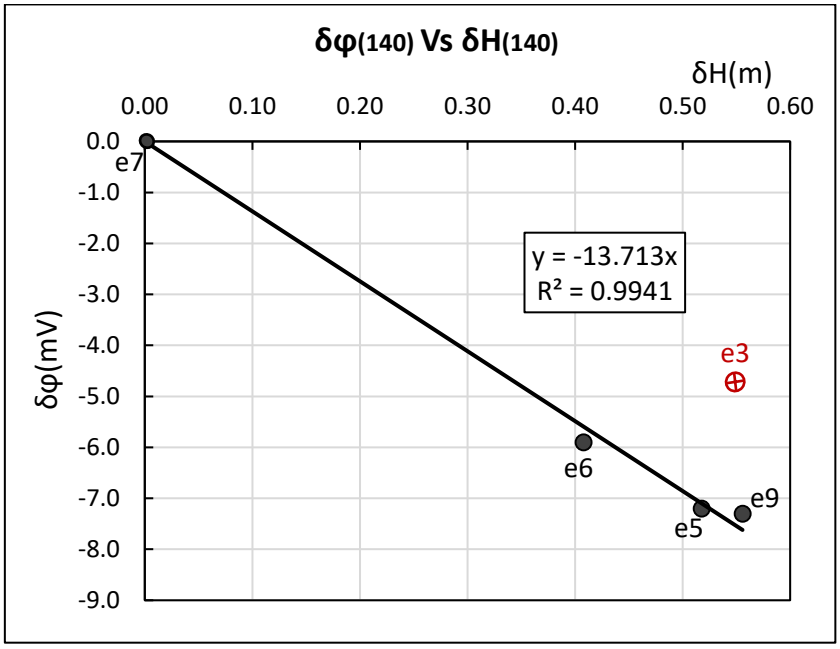

Figure 6.36: Graph of linear change in streaming potential (δφ) against linear change in hydraulic head (δH) at time t = 140 min at KTS

From the graph, Streaming potential coupling coefficient *(Cs)* = -13.713 mV/m.

6.5.4 Computation of Hydraulic Head using Streaming Potential Data

To compute the hydraulic head using streaming potential data, it is assumed that one borehole exists at the test site (which is our pumping borehole as in the case of most groundwater projects). The hydraulic heads in the half space around the borehole are computed by direct approach using Equation 3.45.

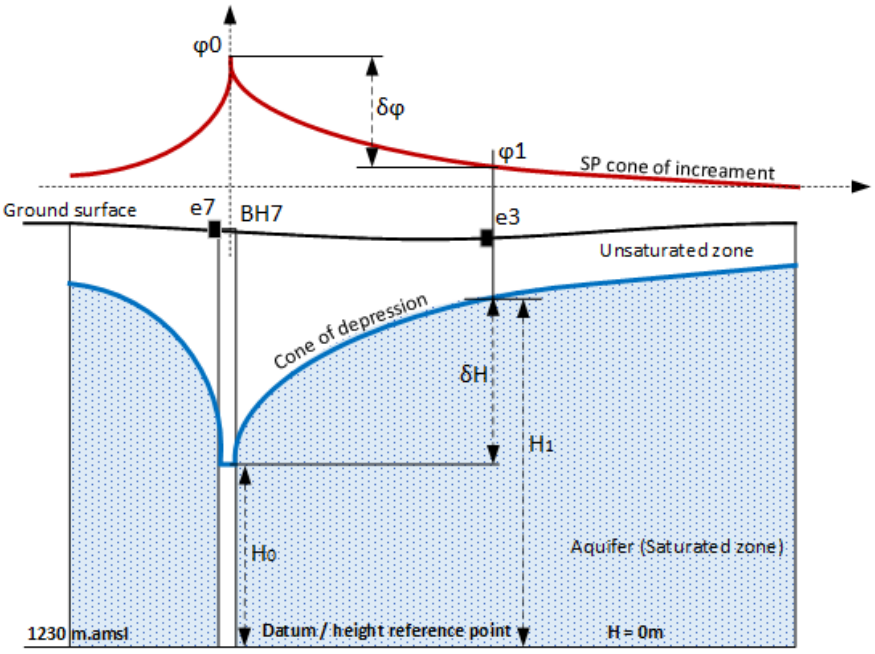

Figure 6.37: Illustration of computing hydraulic head using the measured streaming potential at surface at KTS

From measured streaming potential, the linear change in streaming potential between the pumping borehole and electrode is computed as:

$$\delta\varphi = \varphi_1 - \varphi_0 \qquad 6.31$$

H_0, which is our hydraulic head in the pumping borehole is known through the drawdown measurements and taking 1230 m.amsl as the datum point where the hydraulic head is zero through-out the half space of the aquifer as:

$$H_o = Z_{BH7} - Z_{DATUM} - h_0 - s_0 \qquad 6.32$$

$$H_o = 1241.58\,m - 1230\,m\ - 2.53\,m - 0.865\,m = 8.185\ \text{m} \qquad 6.33$$

Where Z_{BH7} is the surface elevation at BH7 collar, Z_{DATUM} is the datum elevation = 1230 m, h_0 is the water level in BH7 at start of pumping and s_0 is the measured drawdown in BH7.

Our problem is to find H_1 on any point on the surface where streaming potentials have been measured. From Figure 6.37, it can be seen that the linear change in hydraulic head (δH) is given by:

$$\delta H = H_1 - H_0 \qquad 6.34$$

From Equation 3.45:

$$\delta H = \frac{\delta\varphi}{C_s} = \frac{\delta\varphi}{-13.713} m \quad 6.35$$

Where C_s is the streaming potential coupling coefficient computed in Section 6.5.3, which is -13.713 mV/m. Using electrode e_3 as an example, then:

$$\delta H = \frac{\varphi_1 - \varphi_0}{-13.713} = \frac{4.6 - 8.8}{-13.713} = 0.3063\ m \quad 6.36$$

From Equation 6.34, it follows that:

$$H_1 = H_0 + \delta H \quad 6.37$$

$$H_1 = 8.185\ m + 0.3063\ m = 8.491 \text{ m}$$

Drawdown at e_3 is computed from equation:

$$s_1 = (H_0 + s_0) - H_1 \quad 6.38$$

$$s_1 = (8.185 + 0.865)\ m - 8.491\ m = 0.559 \text{ m}$$

The same procedure is performed for all the streaming potential monitoring station and Table gives the computed hydraulic heads and drawdown from streaming potential method for each electrode station.

Table 6.11: Table showing computed hydraulic heads from streaming potential measurements at Krugersdrift Test Site

Electrode	$\varphi_{1(t=140)}$	$\varphi_{0(t=140)}$	$\delta\varphi_{(t=140)}$	$\delta H_{(t=140)}$	$H_{o(t=140)}$	$H_{1(t=140)}$	$s_{1(t=140)}$
e1	3.0	8.8	-5.8	0.4230	8.19	8.6130	0.3811
e3	4.6	8.8	-4.2	0.3063	8.19	8.4963	0.5146
e4	1.5	8.8	-7.3	0.5323	8.19	8.7223	0.2560
e5	1.6	8.8	-7.2	0.5250	8.19	8.7150	0.2643
e6	2.9	8.8	-5.9	0.4302	8.19	8.6202	0.3728
e7	8.8	8.8	0.0	0.0000	8.19	8.1900	0.8650
e9	1.5	8.8	-7.3	0.5323	8.19	8.7223	0.2560

6.5.5 Estimation of Hydraulic Conductivity from Streaming Potential

Section 6.4.5 discussed the procedure of calculating hydraulic parameters from direct drawdown measurements through the application of the analytical solution provided by Theis, Copper Jacob and Thiem-Dupuit methods. The conclusion was that at Krugersdrift Test Site all three methods give similar approximation of *K* and *T*. Hence for the sake of demonstrating the applicability of streaming determining *K* and *T* from streaming

potential method a direct application of Thiem-Dupuit Equation 3.28 is performed. In principle when Cooper Jacob distance – drawdown method is performed the two will yield the same result.

From Equation 3.30 it follows that:

$$Q = \frac{2\pi T(s_0 - s_1)}{2.30\log(r_1/r_0)} \qquad 6.39$$

Where Q is the pumping discharge = 60.48 m^3/d, r_1 is the linear distance between the electrode station and pumping borehole, r_2 is the radius of the pumping borehole = 0.15 m and s_0 and s_1 have already been defined in Section 6.5.3.

Taking electrode e_3 for example of illustration, the transmissivity at electrode e_3 is:

$$T(e_3) = \frac{60.48 \times 2.30 \log\left(\frac{12}{0.15}\right)}{2\pi(0.865 - 0.515)} m/d \qquad 6.40$$

$$T(e_3) = 120.4\, m^2/d \qquad 6.41$$

Then it follows that:

$$K(e_3) = \frac{120.4}{6.5} = 18.5 \text{ m/d} \qquad 6.42$$

The same procedure is repeated for all electrodes, and Table 6.12 gives the values of estimated hydraulic conductivity from streaming potential measurements.

Table 6.12: Table showing computed hydraulic conductivity and transmissivity values using streaming potential measurements at the Krugersdrift Test Site

Electrode	r_1	r_0	s_1	s_0	T	K
e_1	20.00	0.15	0.3811	0.8650	97.2193	14.9568
e_3	12.00	0.15	0.5146	0.8650	120.239	18.4983
e_4	20.00	0.15	0.2560	0.8650	77.2427	11.8835
e_5	8.00	0.15	0.2643	0.8650	63.6493	9.7922
e_6	10.50	0.15	0.3728	0.8650	82.9854	12.7670
e_9	19.00	0.15	0.2560	0.8650	76.433	11.7589
				Arithmetic mean	**86.2947**	**13.2761**
				Geometric mean	**84.5191**	**13.0029**

6.5.6 Estimation of Mean Hydraulic Conductivity using Coupled Flow Power Law

The application of Coupled Flow Power law was discussed in Section 3.3.9 which states that under steady-state conditions the streaming potential signals decreases with distance from the pumping well (Rizzo *et al.*, 2004). In principle the Coupled Flow Power law is an approach that calculates the mean hydraulic parameters of an aquifer directly from the measured streaming potential. This implies that it should give a similar or comparable result to the mean hydraulic parameters estimated form Thiem-Dupuit method under section 6.4.5.2. In this section the Coupled power law Equation 3.64 was applied on streaming potential data with the intent of estimating K. From Equation 3.64 it follows that the coefficient of the power law *(A)* can be obtained by plotting a graph of the measure streaming potential $\varphi(r)$ at t = 140min in terms of reciprocal of distance r from the pumping well ($\varphi(r)$ versus $1/r$) and a best fitting graph is obtained (Figure 6.38).

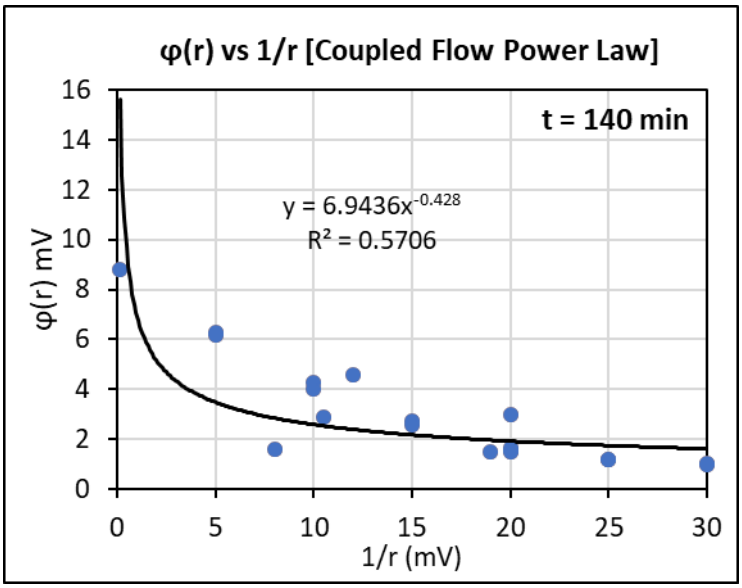

Figure 6.38: Illustration of coupled power law for estimating hydraulic conductivity at KTS

Additional data used $\phi(r)$, for plotting the power law were obtained from Figure 6.34 along the axis of perfect symmetry. From Figure 6.38 the coefficient of the power law A is obtained as 6.936 with a fitting coefficient of correlation, R^2 = 0.57.

Substituting the values of *A* into Equation 3.65 yields:

$$K = \sqrt{\frac{-C_s Q^2}{4\pi^2 A {H_0}^2}} = \frac{Q}{2\pi H_0}\sqrt{\frac{-C_s}{A}} \quad 6.43$$

$$K = \frac{60.48}{2\pi \times (8.19)}\sqrt{\frac{-(-13.713)}{6.936}} = 1.653 \text{ m/d} \quad 6.44$$

It follows that:

$$T = KD = 2.03 \times 6.5 = 10.7 \text{ m}^2/\text{d} \quad 6.45$$

Application of the Coupled power law Equation 3.65 by Rizzo *et al.* (2004) estimates a mean hydraulic conductivity of 1.65 m/d, which is in the same order as the mean value of K estimated from Equation 6.29. This validates the reliability of the Coupled power law in estimating the mean hydraulic parameters. However, when compared to *K* estimated from directly application of the Coupled flow problem Equation 3.45, it appears that the result is less by an order of 10^1. Straface *et al.* (2011) also made the same observation when he applied the coupled flow power law which utilizes Boussinesq linearization and concluded that it under-estimates *K*.

6.6 VALIDATION OF STREAMING POTENTIAL METHOD

As discussed in Section 4.5, the validation process compares the estimation of *K* from streaming potential method to that estimated from the drawdown measurements and performs an inspection of the mirror image relationship between streaming potential signals recorded around a pumping well and the hydraulic head.

6.6.1 Inspection of the Streaming Potential – Hydraulic Head Mirror Image Reflection

Results from both experiments at Krugersdrift and Campus Test Sites as illustrated by Figure 6.15, Figure 6.16 and Figure 6.17 for the Campus site and Figure 6.33, Figure 6.34 Figure 6.35 for Krugersdrift site show that streaming potential signals form a cone of increment around the pumping well. This cone of increment is a complete mirror reflection of the piezometric surface formed as a result of pumping. It is apparent to note that the shape of drawdown and streaming potential signals across a pumping borehole are similar and both form a cone of increment.

The ability of the streaming potential signals to give a reflection of the piezometric surface and cone of depression during pumping validates the approach as useful to hydraulic tests and agrees with the fundamentals of coupled flow theory for streaming potential signals around a pumping well.

6.6.2 Validation of Computed Drawdown

A straight forward validation process is performed by plotting the measured drawdown against the computed drawdown for the stations were both drawdown and streaming potential signals were recorded. In principle if the method is 100% valid or they both correlate to perfection a straight-line graph of slope of 1 is supposed to be obtained with a correlation of 1. This kind of validation process reveals the closeness of the two quantities (measured and computed) to each other.

Figure 6.39 reveals that for the Campus Test Site, the computed drawdown values from streaming potential method have a correlation level of 95% to the measured drawdown.

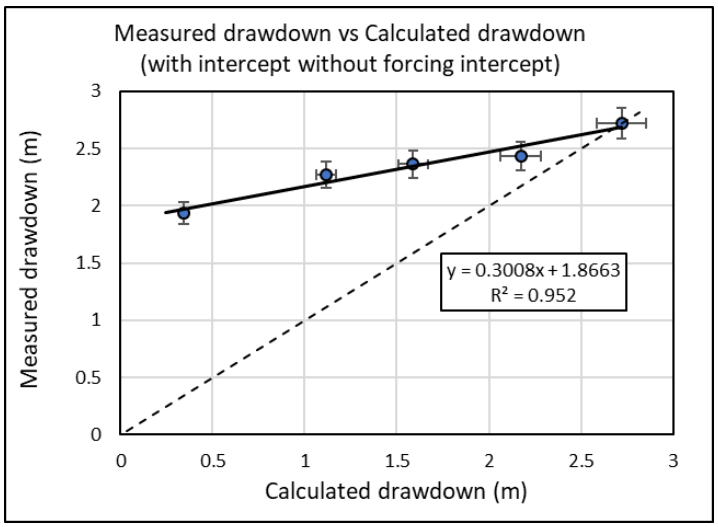

Figure 6.39: Correlation of measured drawdown and drawdown calculated form streaming potential method at *t*=300 min at CTS

For the Krugersdrift Test Site data, correlation analysis was performed under two scenarios. First by forcing the best fit line to cross the origin (0;0 cartesian coordinates) and secondly when it is not forced to cross the origin. The broken lines shown in both Figure 6.40a and b are the lines of ideal correlation. However, from the analysis it can be observed that the coefficient of correlation (R^2) is high with 88% and 95% levels of co-relation between the measured and calculated drawdowns.

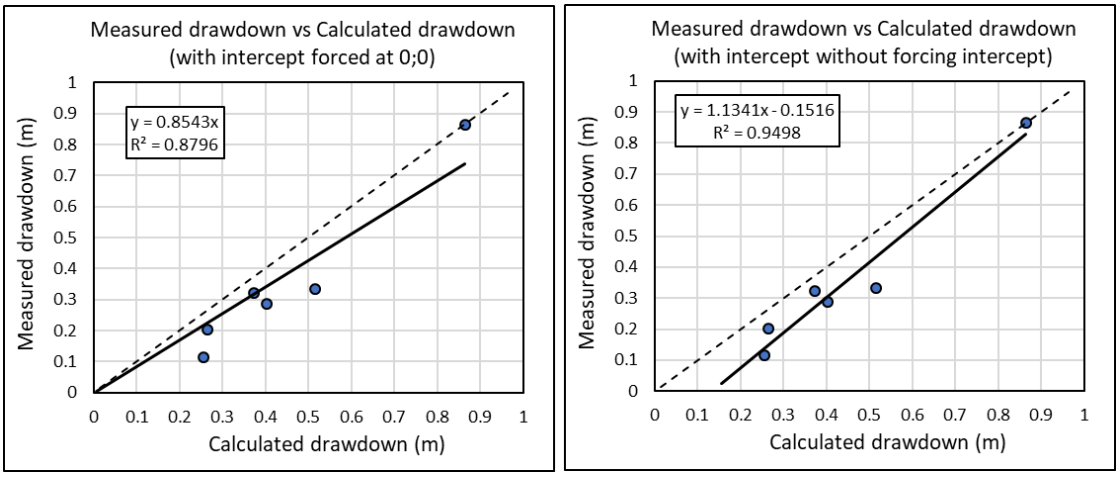

a.) With intercept forced at origin **b.)** With intercept not forced at origin

Figure 6.40: Correlation of measured drawdown and drawdown calculated form streaming potential method at t=140 min at KTS

The high level of correlation validates streaming potential method as a valid tool for computing drawdown around a pumping borehole.

6.6.3 The Validation of Computed Hydraulic Parameters

As earlier highlighted, the traditional and common practice of determining the in-situ hydraulic parameters is through drawdown measurements during a constant rate test. The results from analysis of the measured drawdown have been providing reliable point estimations of the hydraulic parameters. It follows that in this study the determined values from analysis of pumping test data using the measured drawdown data are used as the true values of the aquifer system. Therefore, the computed *K* values from streaming potentials are in this section compared to the *K* values determined from pumping test method.

6.6.3.1 Validation of hydraulic conductivity estimations at Campus Test Site

At the Campus Test Site, the hydraulic conductivities at boreholes UP15, UO3, UO18 and UO20 were estimated using both Theis and Cooper Jacob methods. From the estimated value a mean *K* for the aquifer was computed. The two methods gave out point estimations of hydraulic conductivities that are comparable to each other.

Streaming potential method was used to estimate the mean hydraulic conductivity using method 1 of direct coupled relationship as provided by Equation 3.45, and also hydraulic conductivities at boreholes UP15, UO3, UO18 and UO20 were estimated using the

analytical solution provided by Rizzo *et al*. (2004) for a system in transient environment under confined conditions. The summary of the estimation is given in Table 6.13.

Table 6.13: Summary of measured hydraulic conductivities and their relative error at the Campus Test Site

Borehole / electrode ID	**Hydraulic conductivity estimations from drawdown measurements, *K* (m/d)**		**Hydraulic conductivity estimations from streaming potential measurements, *K* (m/d)**	
	Theis	Copper Jacob	Coupled flow problem **(Equation 3.45)** plus Copper Jacob *(r vs s)*	Coupled flow power law **(Equation 3.69)**
UP15 / e_2	2	2.1	-	0.9
UO3 / e_7	1.1	1.5	-	0.4
e_3	-	-	-	0.6
UO18 / e_4	1.2	1.6	-	0.7
UO19 / e_6	-	-	-	0.2
UO20 / e_2	1.8	1.6	-	0.3
A. Mean	**1.5**	**1.7**	**1.3**	**0.5**
Relative error (against Copper Jacob)			**0.24**	**0.67**

In-order to evaluate the level of confidence of self-potential method, a relative error value was computed for each *K* value estimation. Table 6.13 shows that the mean estimated hydraulic conductivity of Campus aquifer had a relative error of 0.24 (24%) to Copper Jacob method. The error margin of 24% is acceptable and quite minimal. However, the use of the Coupled flow analytical solution provided by Rizzo *et al.,* (2004) estimated K values for each borehole with a mean relative error of 0.67 (67%) when compared to Copper Jacob method. The error is too large.

Based on the error analysis it shoes that a direct application of the Coupled for problem of Equation 3.45 provides estimation which are comparable to those determined from either Copper Jacob or Theis methods.

The solution suggested by Rizzo *et al.* (2004) for transient system under confined environment in relaxation mode through Boussinesq linearization, provides values of under estimated *K* by the order of 1/3. However, this does not discredit the application of the analytical solution Equation 3.69 provided by Rizzo *et al.* (2004). The under estimation might be because of pre-streaming potential signal filtering procedure before

extraction of the final potential used for interpretation. One would therefore not completely ignore the possibility of filtering a true representative value which might have yielded a close approximation. Also, though this analytical solution in this case was used for pseudo-state flow, Rizzo *et al.* (2004) during his derivation assumed a steady-state scenario. This cross application might have influenced the resultant increase in the relative error.

6.6.3.2 Validation of the hydraulic conductivity estimations for the Krugersdrift Test Site

At the Krugersdrift Test Site, the hydraulic conductivities at boreholes BH7, BH6, BH3, BH9 and BH5 were estimated using Theis, Cooper Jacob and Thiem-Dupuit methods. From the estimated value a mean *K* for the aquifer was computed. The three methods provided comparable point estimations of hydraulic conductivities. Streaming potential method was used to estimate the mean hydraulic conductivity using the coupled power law, Equation 3.64 by Rizzo *et al*. (2004) and a simple direct estimation of hydraulic conductivity around each monitoring station through the coupled relationship provided by Equation 3.45. Table 6.14.

Table 6.14: Summary of measured hydraulic conductivities and their relative error at the Krugersdrift Test Site

Borehole / electrode ID	**Hydraulic conductivity estimations from drawdown measurements, *K* (m/d)**			**Hydraulic conductivity estimations from streaming potential measurements, *K* (m/d)**	
	Theis	Copper Jacob	Theim-Dupluit	Coupled flow problem **(Equation 3.45)** plus Theim-Dupluit	Coupled flow power law **(Equation 3.64)**
e_1	-	-	-	14.96	-
BH3 / e_3	10.0	11.9	12.2	18.5	-
BH4	-	10.5	8.8	11.88	-
BH5 / e_5	10.8	11.8	11.6	9.79	-
BH6 / e_6	8.2	11.6	11.6	12.77	-
BH8	10.5	9.9	9.9	-	-
BH9 / e_9	10.5	10.8	10.8	11.76	-
A. Mean	**10.0**	**11.1**	**10.8**	**13.3**	**2.0**
Relative error (against Copper Jacob)				**0.20**	**0.82**

The relative errors computed for each streaming potential hydraulic conductivity estimation against Copper Jacob estimations from drawdown measurements show that a direct application of the coupled flow problem (Equation 3.45) gives better estimations of both spatial point estimations of *K* and mean hydraulic conductivity of the aquifer than the use of the couple flow power law (Equation 3.64). The estimations by use of Equation 3.45 plus Theim Dupluit solution gave estimations with a low relative error of 0.2 (20%) (20%) when compare relative to presumed true values of Cooper Jacob estimate while estimation of mean hydraulic conductivity using the power law had a huge relative error of 0.82 (82%) when compared to the mean value of hydraulic conductivity determined from Cooper Jacob method.

As in the case of Campus Test Site the application of analytical solutions provided by Equations 3.64 and 3.69 derived from Boussinesq linearization are misleading. The estimations in both cases give values of a lower order with a relative error between 60% and 85%. It will be wrong to conclude that the analytical solutions provided by Rizzo et al are wrong and should be discarded, but the occurrence of such variance might be a result of cumulative errors or assumptions which may not be exposed in this dissertation. It is apparent to mention that Straface *et al.* (2011) made the same observation that the coupled power law under estimates the values of hydraulic conductivities when compared to the idealised true values. He however proposed a numerical solution which utilizes a non-least square method for inverting hydraulic conductivity.

CHAPTER 7
CONCLUSSIONS AND LIMITATIONS OF THE STUDY

7.1 APPLICABILITY OF STREAMING POTENTIAL METHOD

The expositions made by this research study evaluate the streaming potential method as a useful tool in characterizing groundwater flow through estimation of hydraulic conductivity from measurements done during pumping test. It is evidenced that as afforded by theory, the streaming potential signals form a positive anomaly around a pumping well and are a direct mirror image of the hydraulic head cone of depression. This validated the method as key additional tool for detailed volumetric and spatial estimating of hydraulic parameters.

As earlier mentioned, many hydrogeology projects cannot afford the installation of piezometers, hence the results often used are extrapolated and do not represent the spatial variation of hydraulic parameters. In contrary if a single pumping test is complimented with streaming potential measurements a better resolution and presentation of the spatial hydraulic structure of the aquifer may be obtained. This is evidenced by the correction of drawdown estimations performed on stations located on UO19 at Campus Test Site and BH4 at Krugersdrift Test Site. The measured drawdown from these observation boreholes were not truly reflect the aquifer response to pumping because the boreholes or piezometers are installed in a different aquifer. The use of potential measurements at these observation point resolved a closer estimation of the aquifer matrix hydraulic parameters.

7.2 LIMITATION OF STREAMING POTENTIAL METHOD

The method has limitations in the sense that the approach used in this study to determine the streaming potential coupling coefficient relied on the availability of observation boreholes, which defeats the whole primary purpose of a non-invasive approach. Though Fagerlund & Heinson (2002), Rizzo *et al.* (2004) and Straface *et al.* (2011) determined streaming potential coupling coefficient from laboratory experiments of representative aquifer formations under varrying enviroments. In their submissions the results from application of these laboratory determined streaming potential coupling coefficient gave estimations of hydraulic heads and hydraulic conductivities which were of the same order comparable to the direct drawdown measurements. Hence in which ever approach

streaming potential method has to be coupled with either representative laboratory studies for determing streaming potential coupling coefficient or in-situ correlation with observed drawdown in observation boreholes if they are available.

The other limitation of streaming potential method application is its non-uniqueness in the analytical solution and the occurrence of noisy signals which require extensive digital filtering before processing. Digital filtering takes away the primary and local character of any dataset. Also, in terms of the easiness of measuring streaming potential signals, the use of porous pots is unfriendly to a layman and manual recording is tiresome because the signals are erratic. Recording of streaming potential therefore require a trained expert. This is why up to date self-potential method as a whole is unpopular and hence qualifying the labelling of it being, "the ugly duckling of geophysics". However, data collection of streaming potential can be improved by the use of analogue data loggers, therefore future work would be to design a measuring system which utilises automatic and multi-station logging of signals. If developed, this has potential of great economic value.

Up to date the researcher is not aware of any universally computed analytical solution or program for interpreting streaming potentials. Different researchers are still attempting to formulate a standard interpretation procedure for streaming potentials to a level where such procedures would be as user-friendly as the procedures used for the analysis of drawdown data collected during pumping tests. There is no standardised analytical solution and numerical solution that directly relates the measured streaming potential to hydraulic parameters.

The final observed limitation of streaming potential method with regard to compounded groundwater flow characterization (though it was not part of the objective of this study) is that signals obtained from streaming potential measurements are very unstable in the early and middle time of pumping test. This means that streaming potential signals are not usable in determining the groundwater flow regimes and the use of streaming potential signals is more reliable only in the steady-state or pseudo-state flow.

7.3 RELIABILITY OF HYDRAULIC CONDUCTIVITY VALUES ESTIMATED FROM STREAMING POTENTIAL METHOD

As discussed in Section 7.1 direct application of the coupled flow problem Equation 3.45 provided estimations which are comparable to values of both transmissivity, and hydraulic conductivity determined from the Theis and Copper Jacob methods by using

measured drawdown with relative errors of the magnitude of 0.2. This level of closeness to the presumed trues values qualifies the method as reliable.

Streaming potential method is repeatable in the sense that it was applied to two different sites with different properties and yet in both trials it gave comparable estimation with relative errors of the same order.

In conclusion this study qualifies streaming potential method as a useful and reliable tool in complimenting single well pumping tests and providing a spatial representation of hydraulic parameters. In this study the extent of spatial imaging of hydraulic parameters using streaming potential method was limited by the number of electrodes used, mainly because of financial constraints in procuring more electrodes. However, it is important to highlight that the assembly of streaming potential method field set up is way cheaper than the cost of installation of piezometers.

Though, it is in its initial development phase the experiments gave an interesting insight on the ability of streaming potential in resolving spatial heterogeneity of the aquifer and estimating the mean value of hydraulic conductivity.

REFERENCES

Ball, L. et al., 2010. Constraining fault-zone hydrogeology through interagted hydrogeological and geo-electrical analysis. *Hydrogeology Journal,* Issue 18, pp. 1057-1067.

Bigalke, J. & Grabner, E. W., 1966. The geobattery model: A contribution to large-scale electrochemistry. *Electrochemica Acta 42,* pp. 3443-3452.

Birch, F. S., 1993. Testing Fournier's method for finding water table from. *Groundwater,* pp. 50-56.

Birch, F. S., 1998. Imaging the Water Table by Filtering Self-Potential Profiles. *Groundwater,* September, 36(5), pp. 779-782.

Botha, J F; Verwey, J P; Van der Voort, I; Vivier, J JP; Bays, J; and Colliston, W P., 1998. *Karoo Aquifers: Their Geology, Geometry and Physical Properties,* Pretoria: Water Research Commission.

Catuneanu, O. & Bowker, D., 2001. Sequence stratigraphy of the Koonap and Middleton fluvial formations in the Karoo foredeep, South Africa.. *Journal of African Earth Sciences, ,* Issue 33, pp. 579-595.

Catuneanu, O; Wopfner, H; Eriksson, P.G; Cairncross, B; Rubidge, B.S; Smith, R.M.H; and Hancox, P.J., 2005. The Karoo basins of south-central Africa. *Journal of African Earth Sciences,* 18 July, 43(1-3), pp. 2111-253.

Denis, Ingrid; Denis, Rainier; Fourier, Fanus; Veltman, Sonia; Parsons, Roger; Titus, and Rian., 2008. *The Groundwater Dictionary: A comprehensive reference of groundwater related terminology,* s.l.: Department of Water Affairs and Forestry.

Dennis, I. & Dennis, R., 2012. *Climate change vulnerability index for Souht African aquifers.* South Africa, Water Research Commission.

Doussan, C., Jouniaux, L. & Thony, J. L., 2002. Variations of self-potential and unsaturated water flow with time in sandy loam and clay loam soils. *Hydrology,* Volume 267 , p. 173–185..

Fagerlund, F. & Heinson, G., 2002. Detecting subsurface groundwater flow in the fractured rock using self-potential (SP) methods. *Environmental Geology,* 22 October.pp. 782-794.

Fetter, C. W., 2001. *Applied Hydrogeology.* 4th ed. New Jersey: Merrill Publish Company.

Fitts, C. R., 2002. *Groundwater Science.* Imprint Edition ed. London: Acadermic Press.

Fourie, F. D., 2003. *Application of Electroseismic Techniques to Geohydrological Investigations in Karoo Rocks,* Bloemfontein: University of Free State, Institute of Groundwater Studies.

Geel, C., 2014. *Brief geologic overview of the Cape Fold Belt and Karoo Basin: Field excursion to Matjiesfontein, 10th Inkaba yeAfrica conference.* Matjiesfontein, Inkba yeAfrica.

Golder Associates, 2011. *Groundwater Report in support of the EMP for the South Western Karoo Basin Gas Exploration Application Project - Western Precinct,* Midrand: Golder Associates Pty (Ltd).

Gomo, M., 2011. *A groundwater surface wtare interaction study of an alluvial channel aquifer,* Bloemfontein: UFS.

Jardani, A; Revil, A; Barrash, W; Crespy, A; Rizzo, E; Straface, S; Cardiff, M; Malama, B; Miller, C; and Johnson, T., 2008. Reconstruction of the Water Table from Self-Potential Data: A Bayesian Approach. *Ground Water Journal.*

Johnson, M.R; Van Vuuren, C.J; Visser, J.N.J; Cole, D.I; Wickens, H; Christie, A.D.M; Roberts, D.L; and Brandl, G., 1997. The Karoo Basin, South Africa. *African Basins: Sedimentary basins of the World,* Volume 3.

Kruseman, G. P. & De Ridder, N. A., 1990. *Analysis and Evaluation of Pumping Test Data.* Second ed. Netherlands: International Institute for Land Reclamation and Improvement.

Linde, N; Revil, A; Bolève, A; Dagès, C; Castermant, J; Suski, B; and Voltz, M., 2007. Estimation of the water table throughout a catchment using self-potential and piezometric data in a Bayesian framework. *Journal Hydrology,* Volume 334 , pp. 88-98..

Maineult, A., Bernabe, Y. & Ackerer, P., 2005. Detection of advected concentration and pH fronts from self-potential measurements,. *J. Geophysics Research,* p. 110.

Makwiza, C., Fuamba, M., Houssa, F. & Jacobs, E. H., 2018. A conceptual theoretical framework to integrally assess the possible impacts of climate change on domestic irrigation water use. *Water SA,* 41(5), pp. 586-593.

Malama, B., Revil, A. & Kuhlman, K., 2009. A semi-analytical solution for transient streaming potentials associated with confined aquifer pumping tests. *Geophysics Journal International,* Volume 176, p. 1007–1016.

Manninen, T; Eerola, T; Makitie, H; Vuori, S; Luttinen, A; Senvano, A & Manhica, V., 2008. The Karoo volcanic rocks and related intrusions in southern and central Mozambique. *Geological Survey of Finland,* Issue Special paper 48, pp. 211-250.

McCathy, T. & Rubidge, B., 2005. The Story of Earth & Life. A Southern African Perspective on a 4.6-Billion-Year Journey. *Geological Magazine - Douglas Palmer,* 145(4), p. 334.

Nutting , P. G., 1930. Physical analysis of oil sands. *American Association of Petroleum Geologists,* Volume 14, pp. 1337-1334.

Pitman, W. V., Midgley, D. C. & Middleton, B. J., 1998. *Surface water resources of South Africa 1990.*

Rathore, A. S. & Guttman, A., 2005. *Electrokinetic Phenomena: Principles and Applications in Analytical Chemistry and Microchip Technology.* New York: Taylor & Francis e-Library.

Revil, A. & Jardani, A., 2013. *The Self Potential Method: Theory and Applications in Environmental Geoscience.* London: Cambridge University Press.

Revil, A. & Linde, N., 2006. Chemico-electromechanical coupling in microporous media.. *J Colloid Interface Scientific Journal,* Volume 2, pp. 682-694.

Revil, A., Naudet, V., Nouzaret, J. & Pessel, M., 2003. Principles of electrography applied to self-potential electrokinetic sources and hydrogeological applications. *Water Resour. Res.,* Volume 39, p. 5.

Rizzo, E; Suski, B; Revil, A; Straface, S & Troisi, S., 2004. Self-potential signals associated with pumping-tests experiments, J. Geophys. Res., 109. *Journal Geophysics Research,* Volume 109.

Roberts, J., 2010. SA water demand 'will exceed supply by 2025. *https://mg.co.za/article/2010-02-04-sa-water-demand-will-exceed-supply-by-2025,* Johanesburg: Mail and Guardian.

Rowsell, D. & De Swardt, A., 1976. Diagenesis in Cape and Karroo sediments, South Africa, and its bearing on their hydrocarbon potential. *Geological Society of South Africa,* January, 79(1), pp. 81-145.

Sato, M. & Mooney, H. M., 1960. The electrochemical mechanism of sulphide self-potentials. *Geophysics,* Volume 25, pp. 226-249.

Sill, W. R., 1983. Self-potential modelling from primary flows, Geophysics. *Geophysics,* Volume 48, pp. 76-85.

Straface, S., Rizzo, E., Gianpaolo, V. & Chidichimo, F., 2011. *Estimation of Hydraulic Conductivity in a Large Scale Laboratory Model by Means of the Self-Potential Method.* Alexandra, Egypt, s.n.

Suski, B; Revil, A; Titov, K; Konosavsky, P; Voltz, M; Dage`s, C & Huttel , O., 2006. Monitoring of an infiltration experiment using the self-potential. *Water Resources Research,* Volume VOL 42.

Tankard, A J; Jackson, MPA; Erickson, K A; Hobday, D K; Hunter, D R & Minter, W E L., 1982. *Crustal Evolution of Southern Africa: 38 Billion Years of Earth Histrory.* 1st ed. New York: Springer-Verlag.

Telford, W. M., Geldart, L. P., Sheriff, R. E. & Keys, D. A., 1976. *Applied Geophysics.* 1st ed. Cambridge: Cambridge University Press.

Titov, K. et al., 2005. Numerical modelling of self-potential signals associated with pumping test experiment. *Geophysics Journal International,* 5 May, Volume 162, pp. 641-650.

Turner, B. R., 1981. *Revised Stratigraphy of the Beaufort Group in the Southern Karoo Basin,* Newcastle: University of Newcastle.

Van der Voort, I. & Van Tonder , G. J., 2000. *Analysing the geometry of South african Fracture Rock Aquifers: Past Achievements and Future Challenges.* Cape Town, s.n., pp. 349-353.

Van Tonder, Gerit J; Botha, J F; Chiang, W H; Kunstman, H & Xu, Y., 2000. Estimation of sustainable yields of boreholes in fractured rock formations. *Journal of hydrology,* January, Volume 241, pp. 70-90.

Vegter, J. R., 1992. *An evaluation of groundwater exploration and its potential for urban use: A hydrogeological consulting report to the Directorate of Geohydrology,* Pretoria, South Africa: Department of Water Affairs and Forestry.

Wickens, H. d. V., 1994. *Basin Floor Fan Building Turbidites of the southwestern Karoo Basin, Ecca Group, South Africa,* Port Elizabeth, South Africa: s.n.

Woodford, A. C. & Chevallier, L., 2002. *Hydrogeology of Main Karoo Basin: Current Knowledge and Future Research Needs,* Pretoria: Water Research Commision.

Zappa, G., Bersezio, R., Felletti, F. & Guidici, M., 2006. Modeling heterogeneity of gravel sand, braided stream alluvial aquifers at the facies scale. *Journal of Hydrology,* 325(1-4), pp. 134-153.

ABSTRACT

The hydraulic parameters of heterogeneous aquifers are often estimated by conducting pumping (and recovery) tests during which the drawdown in a borehole intersecting the aquifer is measured over time, and by interpreting the data after making a number of assumptions about the aquifer conditions. The interpreted values of the hydraulic parameters are then considered to be average values that represent the properties of the bulk aquifer without taking into account local heterogeneities and anisotropies. An alternative and more economic approach is to measure streaming potentials in the vicinity of the borehole being tested. The streaming potential method is a non-invasive geophysical method that measures electrical signals generated by groundwater flow in the subsurface through a process known as electrokinetic coupling. This method allows data to be recorded at a high spatial density around the borehole. The interpretation of streaming potential data in terms of aquifer hydraulic parameters is facilitated by a coupled flow relationship which links the streaming potential gradient to the hydraulic gradient through a constant of proportionality called the electrokinetic coupling coefficient. In the current study, field measurements of streaming potentials were taken during the pumping and recovery phases of pumping tests conducted at two sites with dissimilar geological and geohydrological conditions. The recorded streaming potential data were interpreted by calculating the hydraulic head gradient from the streaming potential gradient, and by using the potential field analytical solution for the transient mode, which relates the streaming potential field directly to the average hydraulic conductivity. Hydraulic conductivity values estimated from the streaming potential method were of the same order as values determined from the analysis of drawdown data, with a relative error of 0.2. This study demonstrates that the streaming potential method is a viable tool to compliment pumping tests and provide a spatial representation of the hydraulic parameters.

APPENDIX A: PUMPING TEST THEIS AND COPPER JACOB ANALYISIS FOR CAMPUS TEST SITE

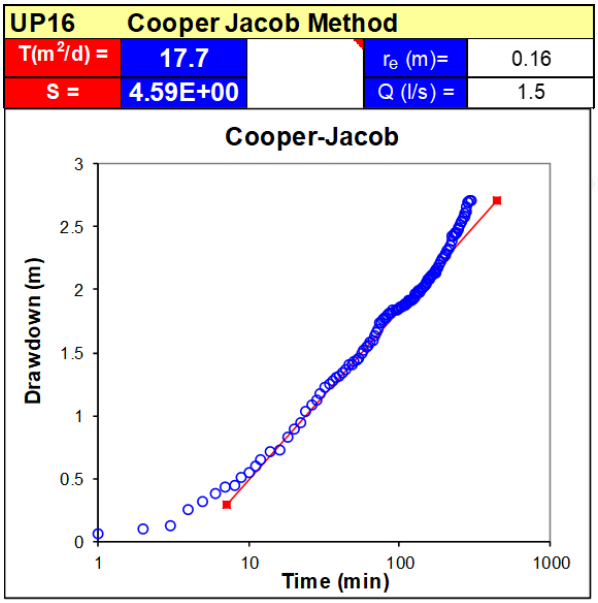

Cooper Jacob curve analysis for UP16

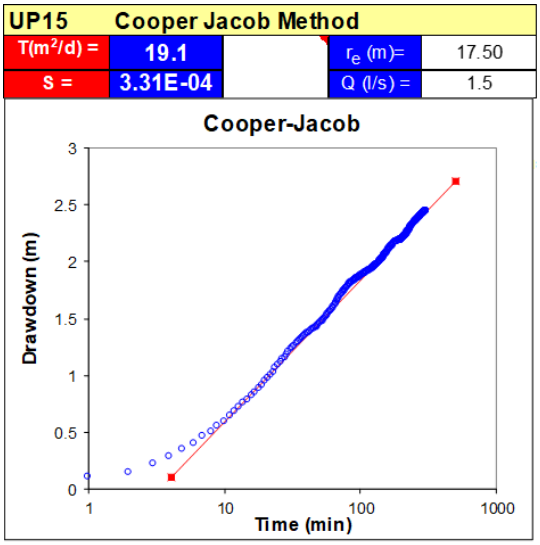

Cooper Jacob curve analysis for UP15

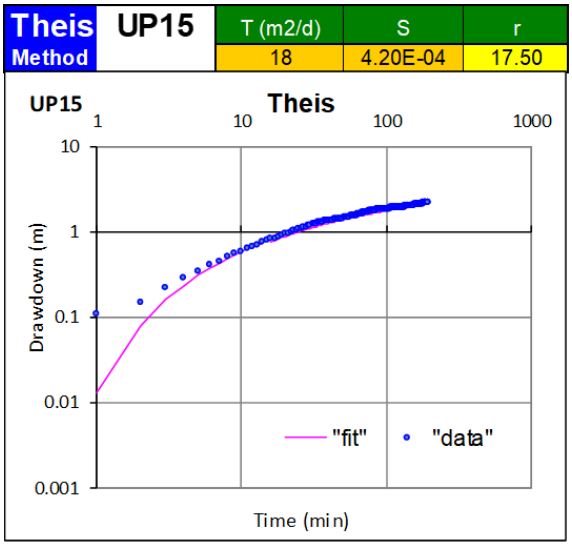

Theis curve analysis for UP15

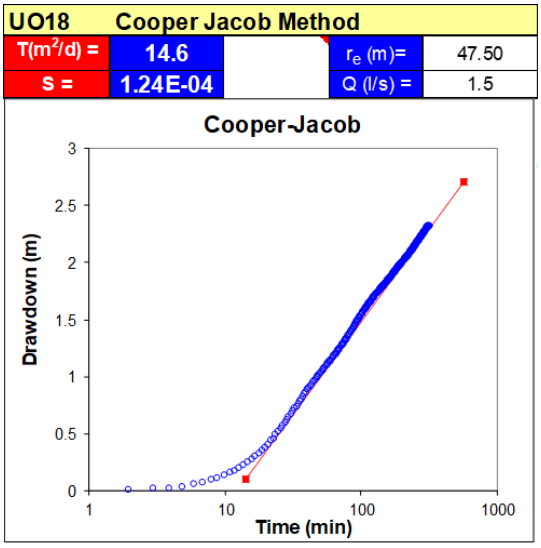

Cooper Jacob curve analysis for UO18

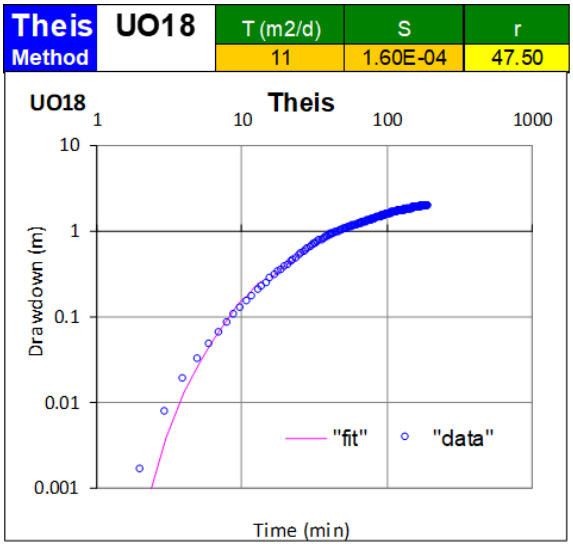

Theis curve analysis for UO18

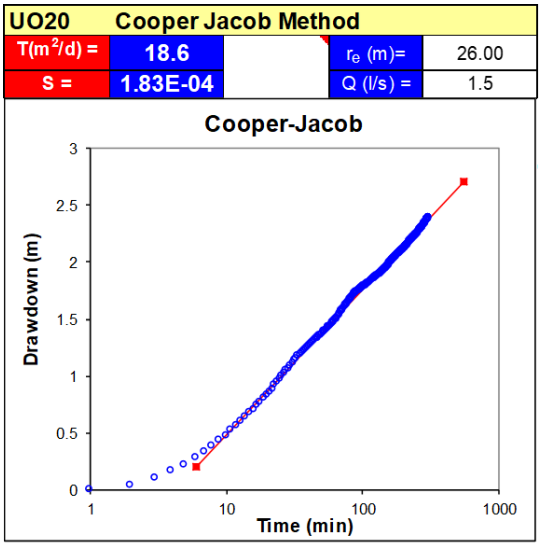

Cooper Jacob curve analysis for UO20

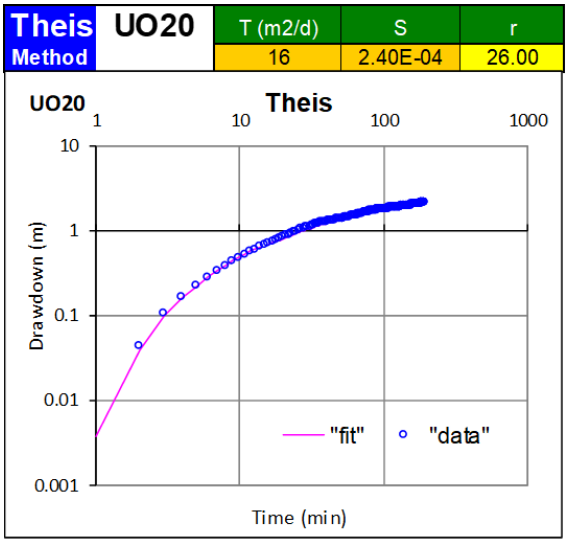

Theis curve analysis for U20

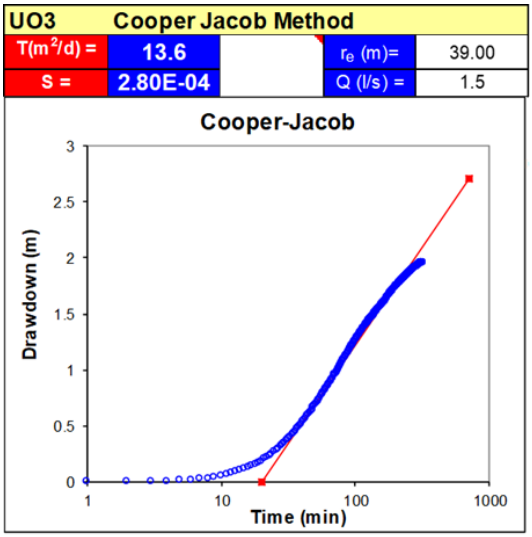

Cooper Jacob curve analysis for UO3

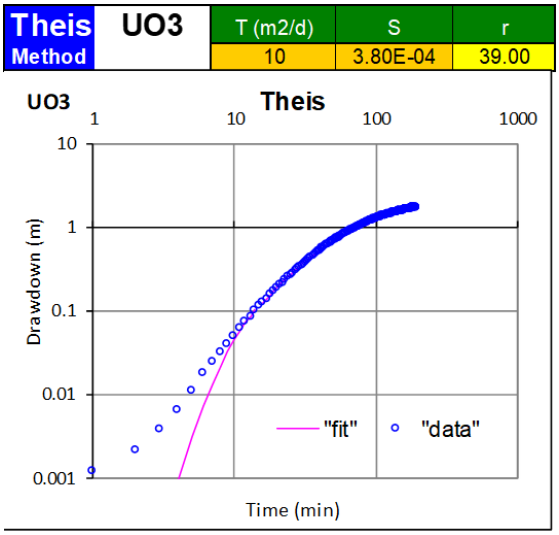

Theis curve analysis for UO3

APPENDIX B: PUMPING TEST THEIS AND COPPER JACOB ANALYISIS FOR THE KRUGERSDRIFT TEST SITE

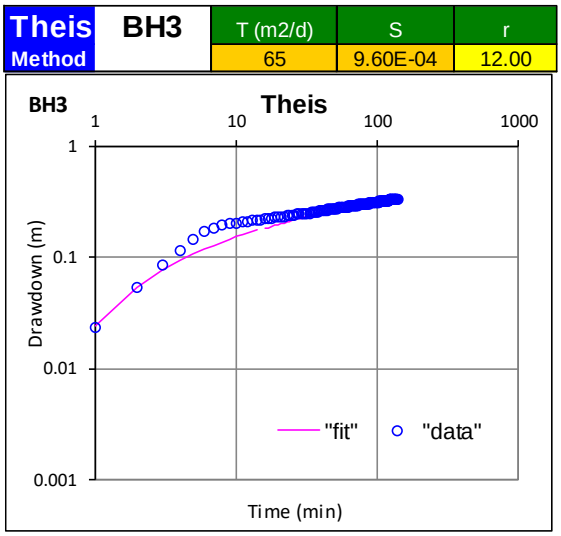

Theis curve fitting for BH3

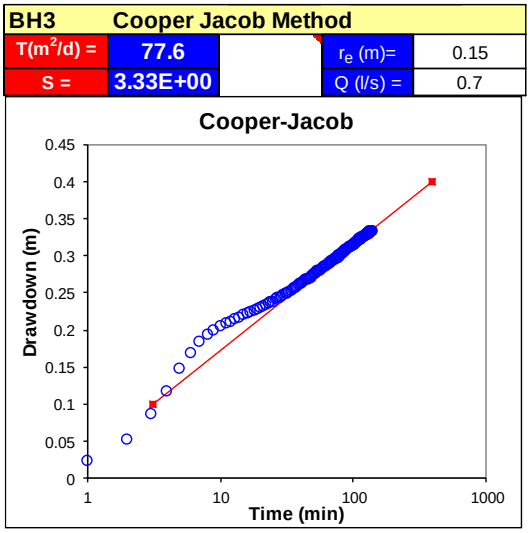

Cooper Jacob curve analysis for BH3

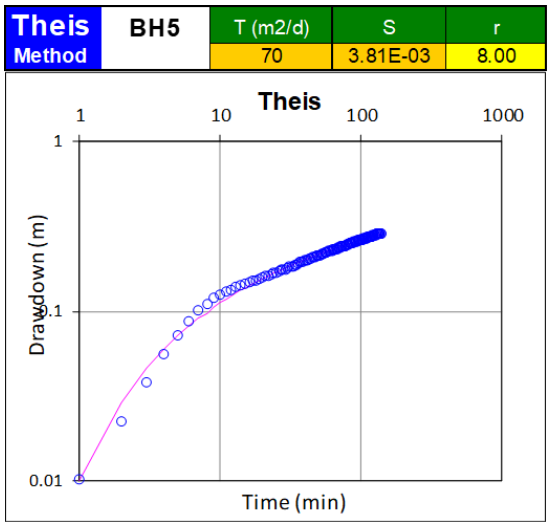

Theis curve fitting for BH5

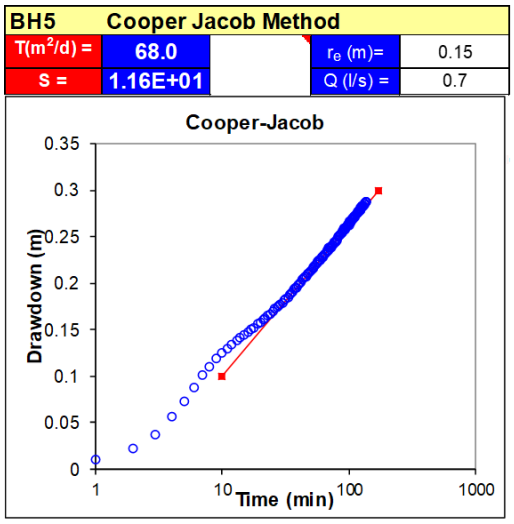

Cooper Jacob curve analysis for BH5

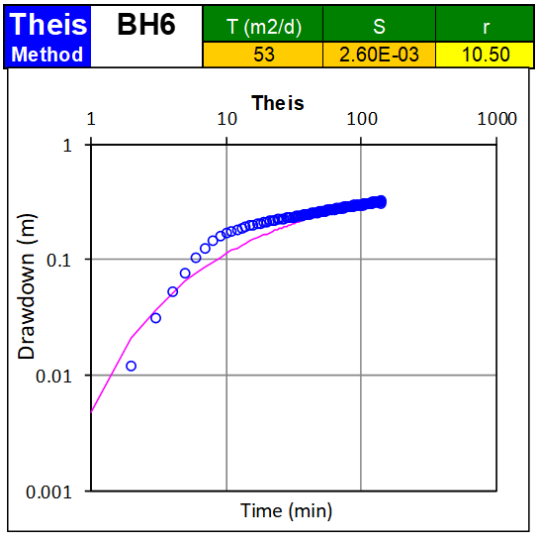

Theis curve fitting for BH6

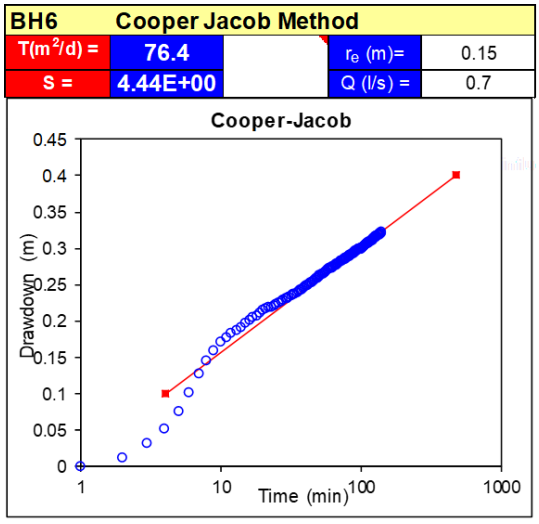

Cooper Jacob curve analysis for BH6

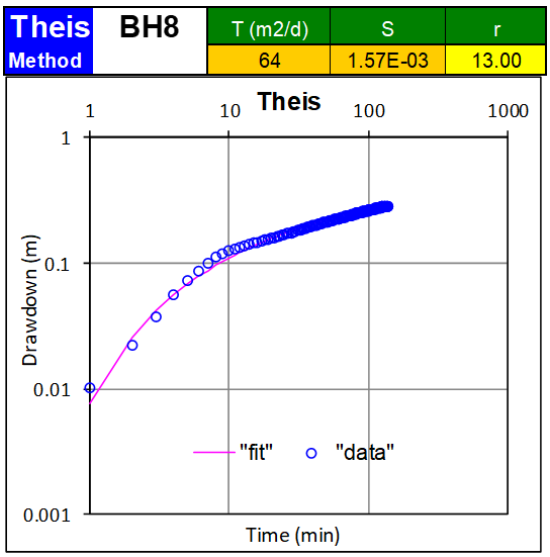

Theis curve fitting for BH8

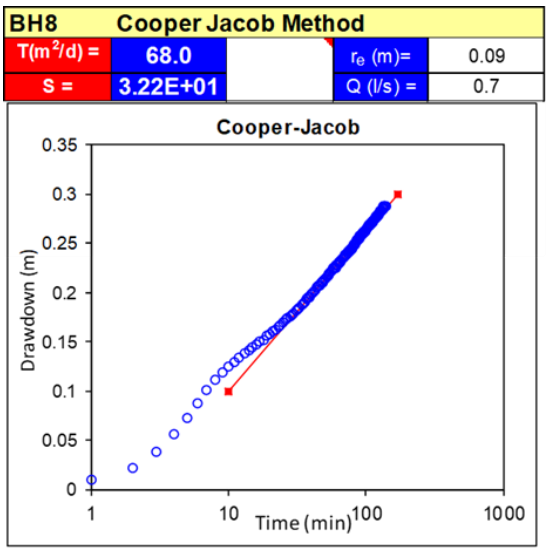

Cooper Jacob curve analysis for BH8

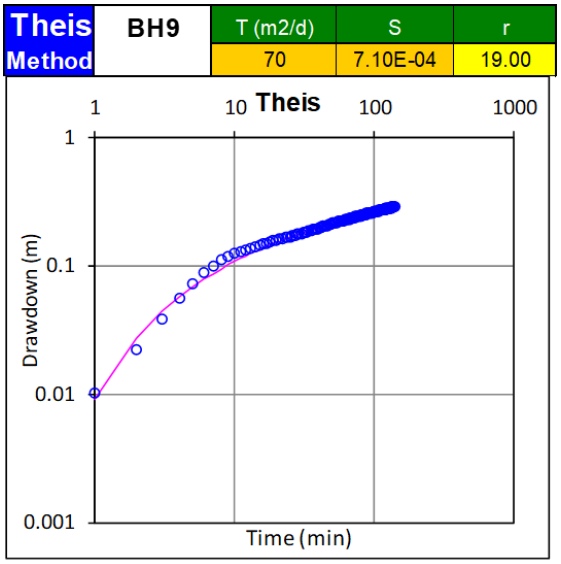

Theis curve fitting for BH9

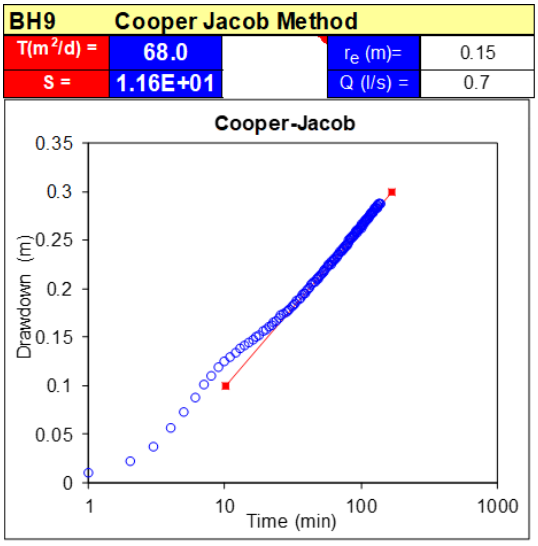

Cooper Jacob curve analysis for BH9

APPENDIX C: STREAMING POTENTIAL TIME – POTENTIAL PLOTS FOR CAMPUS TEST SITE

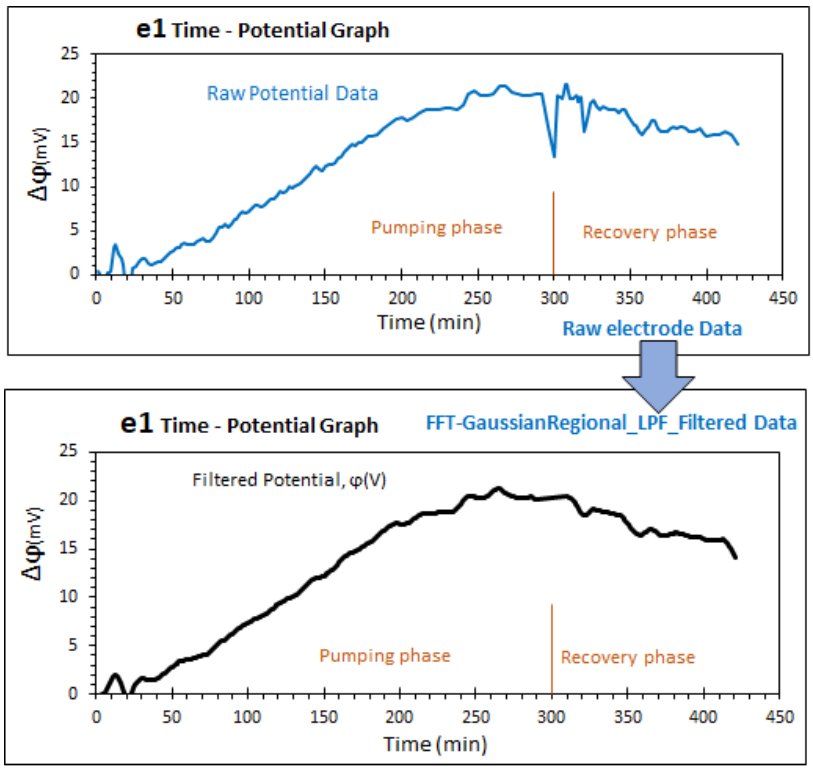

Potential- time graph for electrode *(e_1)* located at borehole UP16

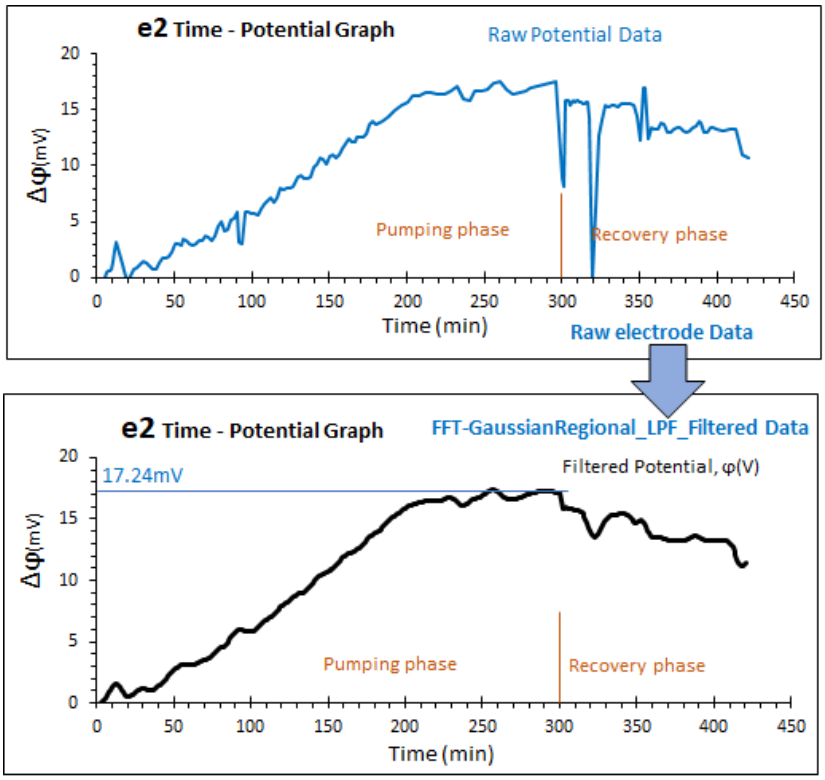

Potential- time graph for electrode *(e_2)* located at borehole UP15

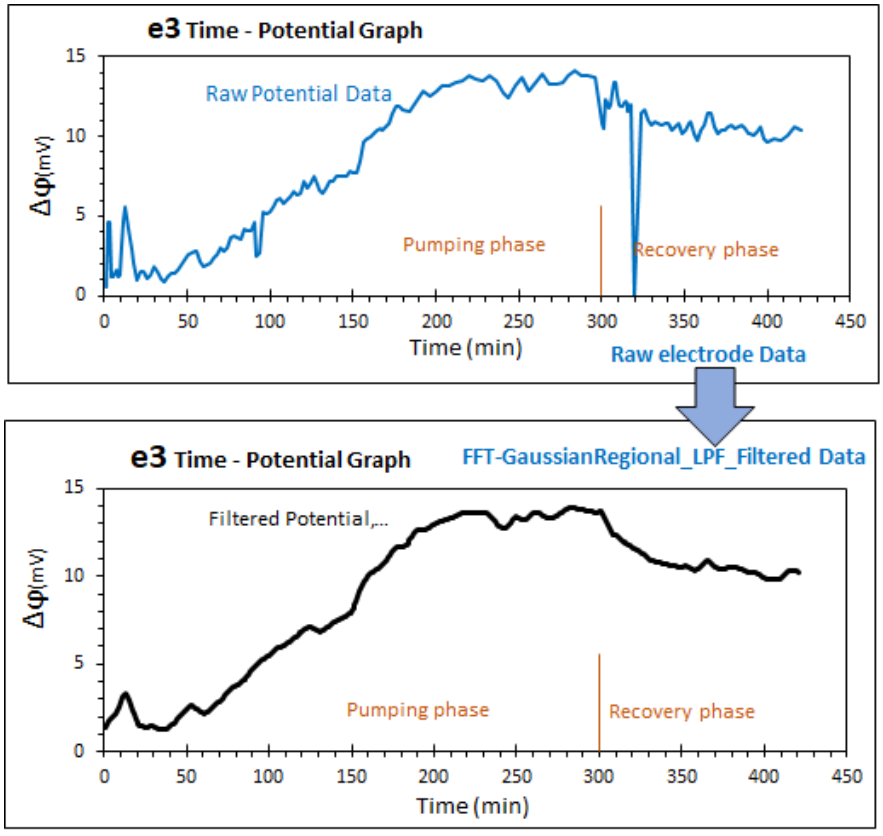

Potential- time graph for electrode *(e_3)*

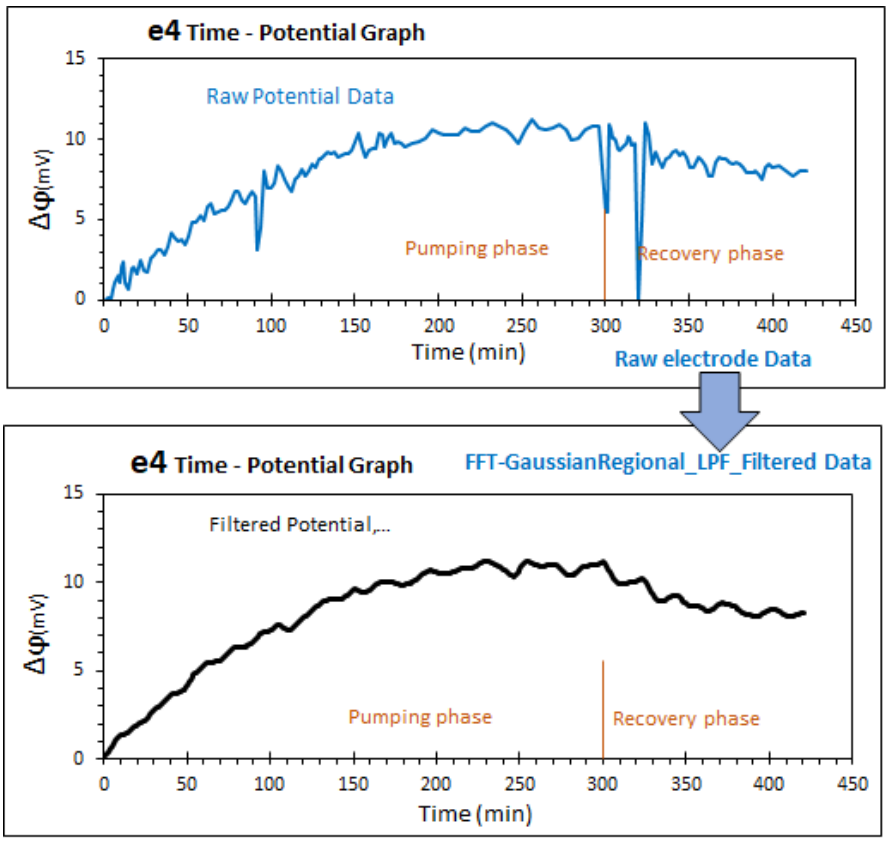

Potential- time graph for electrode *(e_4)* located at borehole UO18

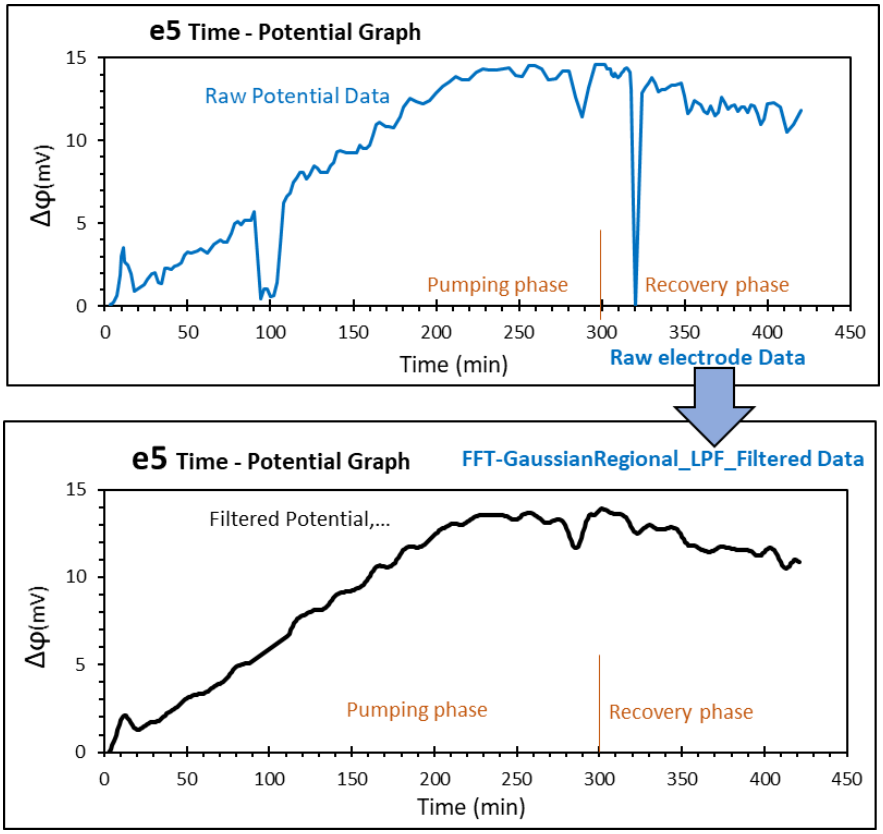

Potential- time graph for electrode *(e_5)* located at borehole UO20

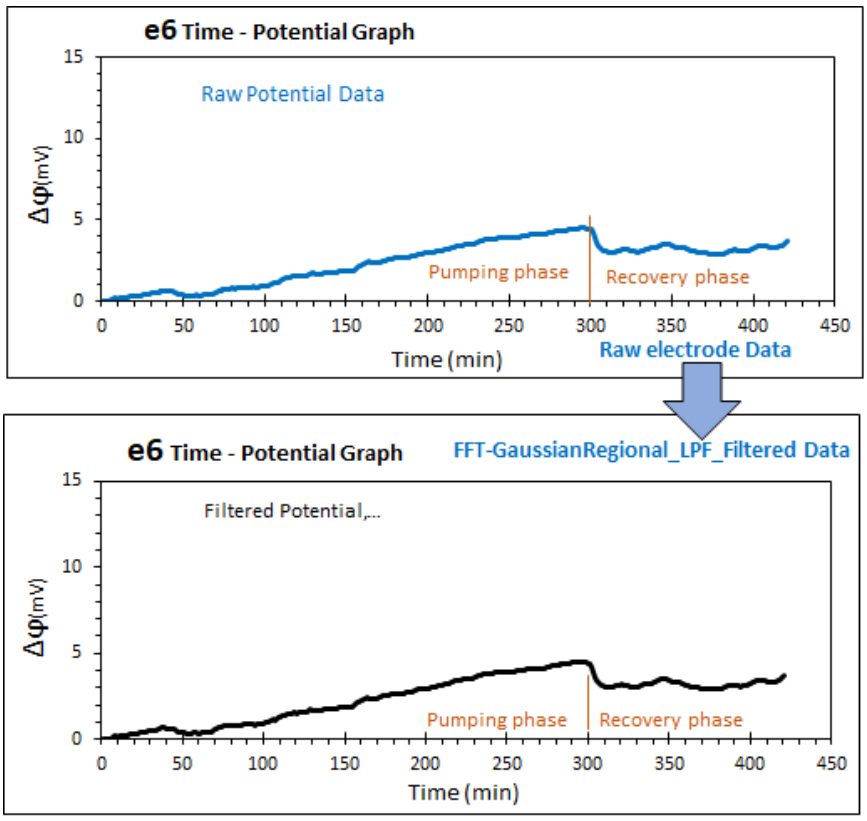

Potential- time graph for electrode *(e_6)* located at borehole UO19

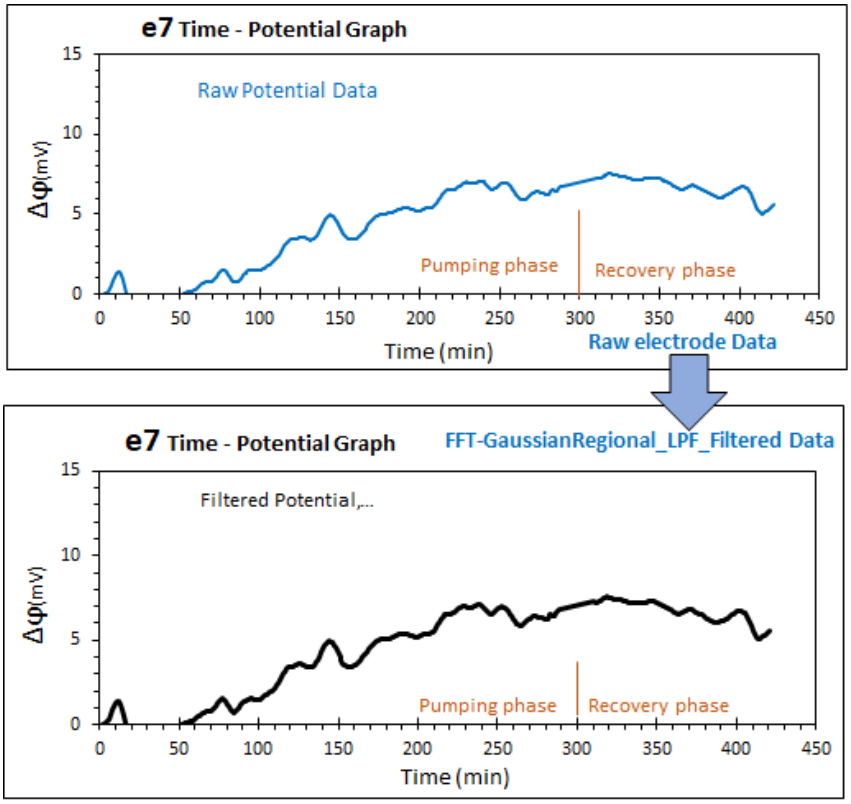

Potential- time graph for electrode *(e_7)* located at borehole UO3

APPENDIX D: STREAMING POTENTIAL TIME – POTENTIAL PLOTS FOR KRUGERSDRIFT TEST SITE

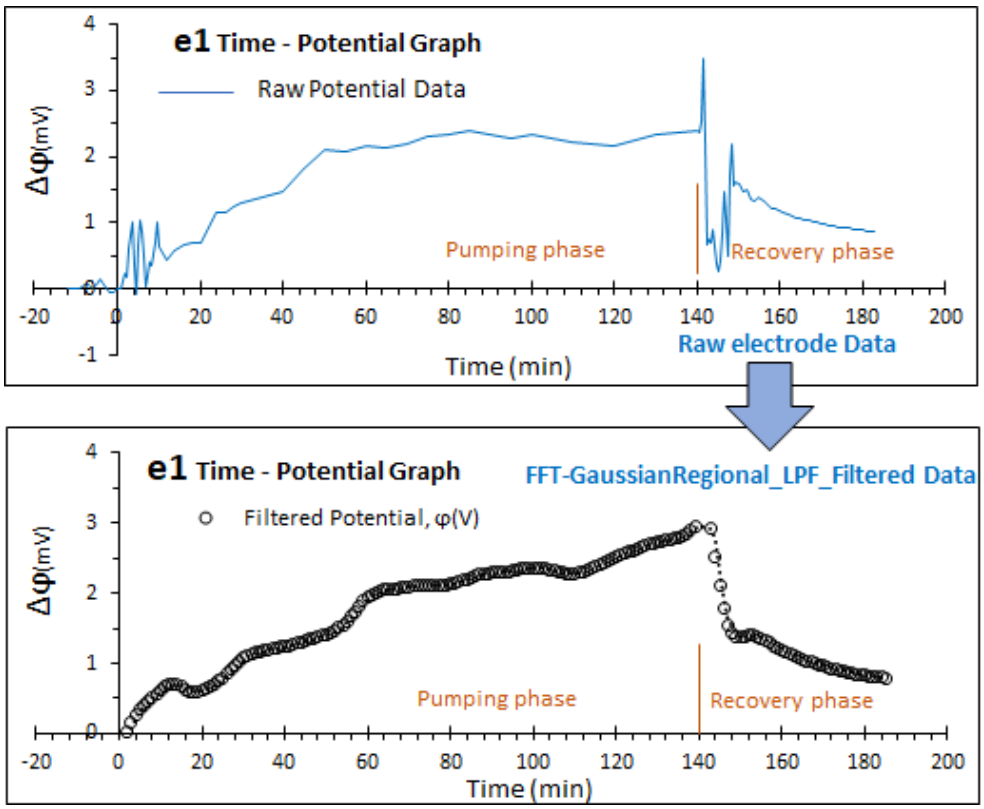

Potential- time graph for electrode *(e_1)*

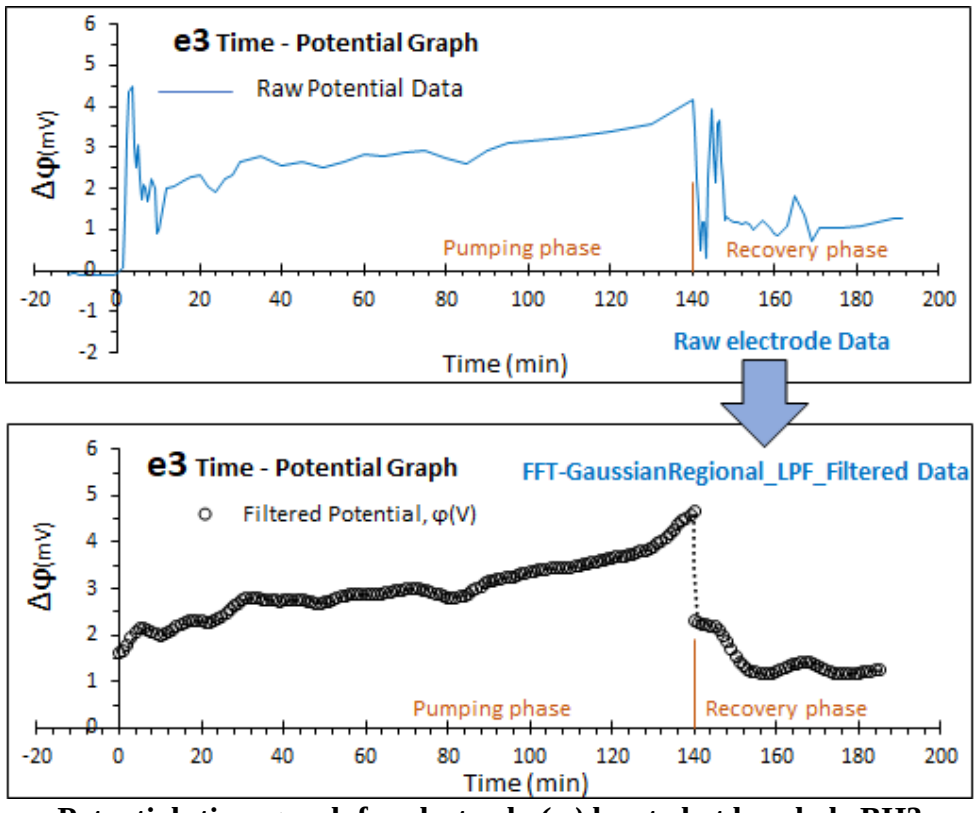

Potential- time graph for electrode *(e_3)* located at borehole BH3

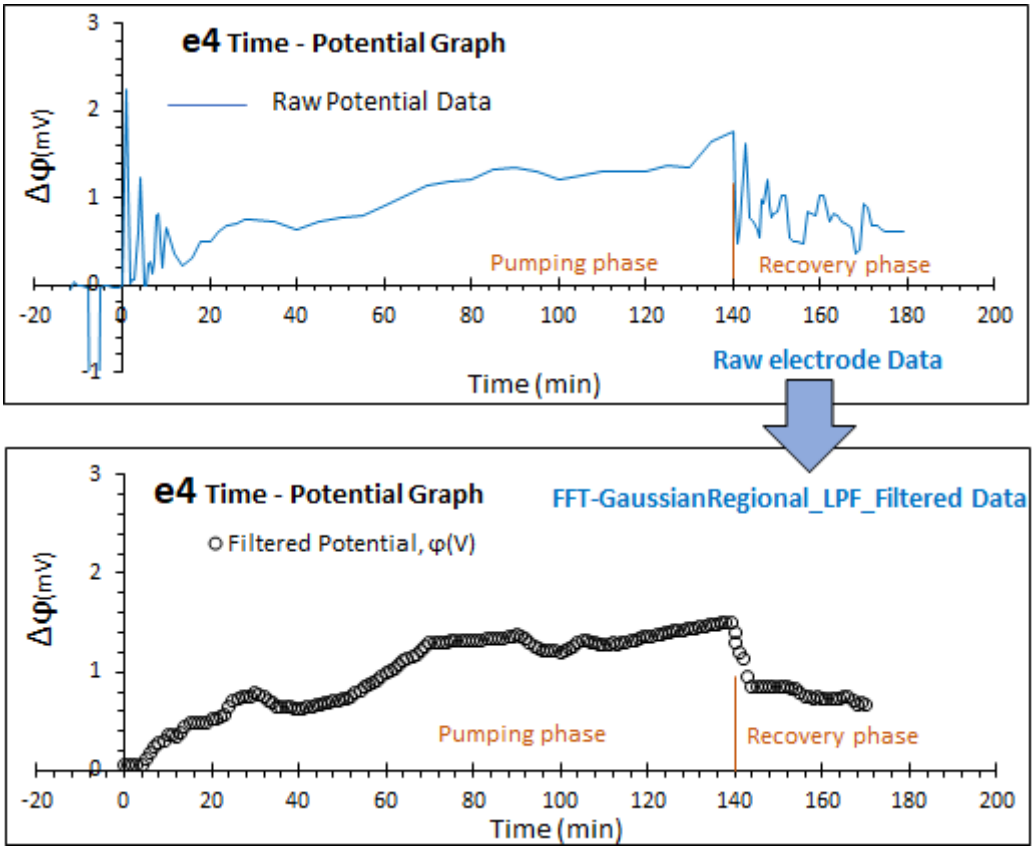

Potential- time graph for electrode *(e_4)* located at borehole BH4

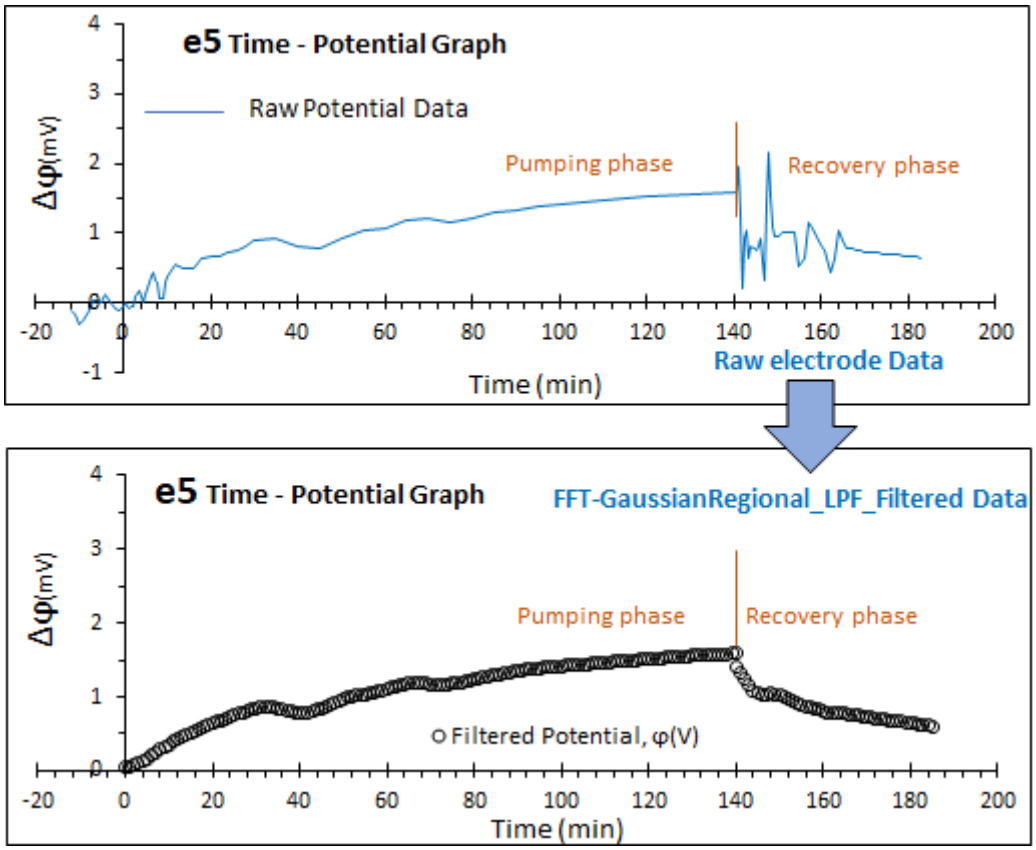

Potential- time graph for electrode *(e_5)* located at borehole BH5

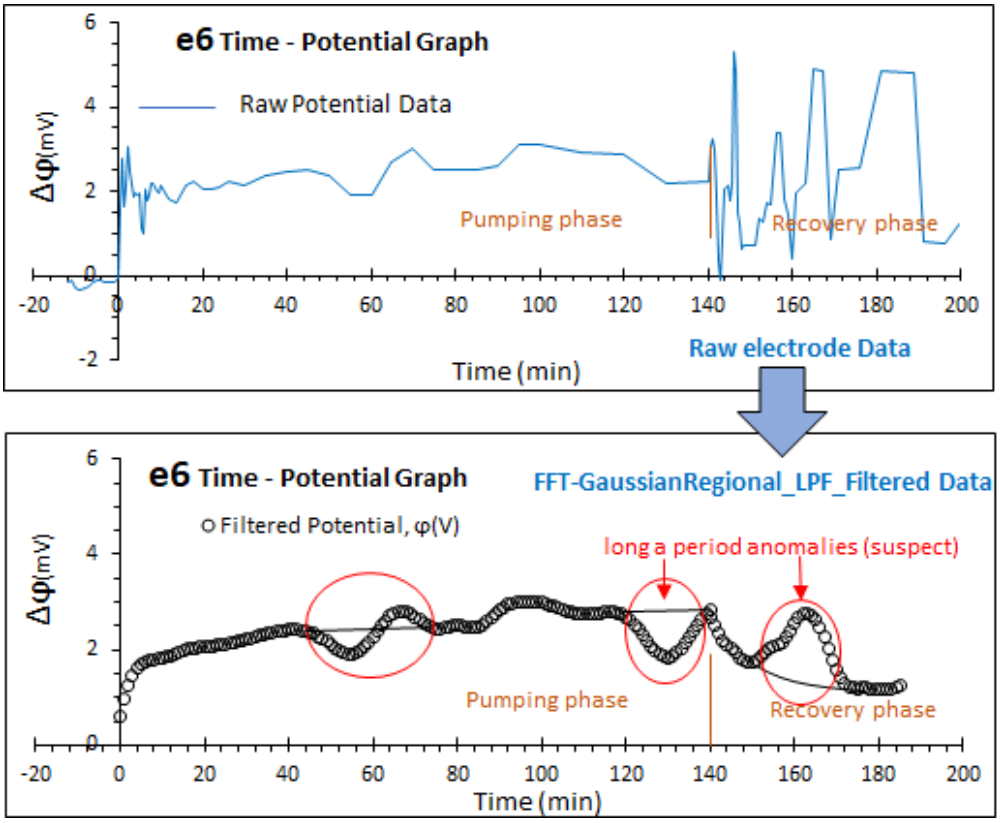

Potential- time graph for electrode *(e_6)* located at borehole BH6

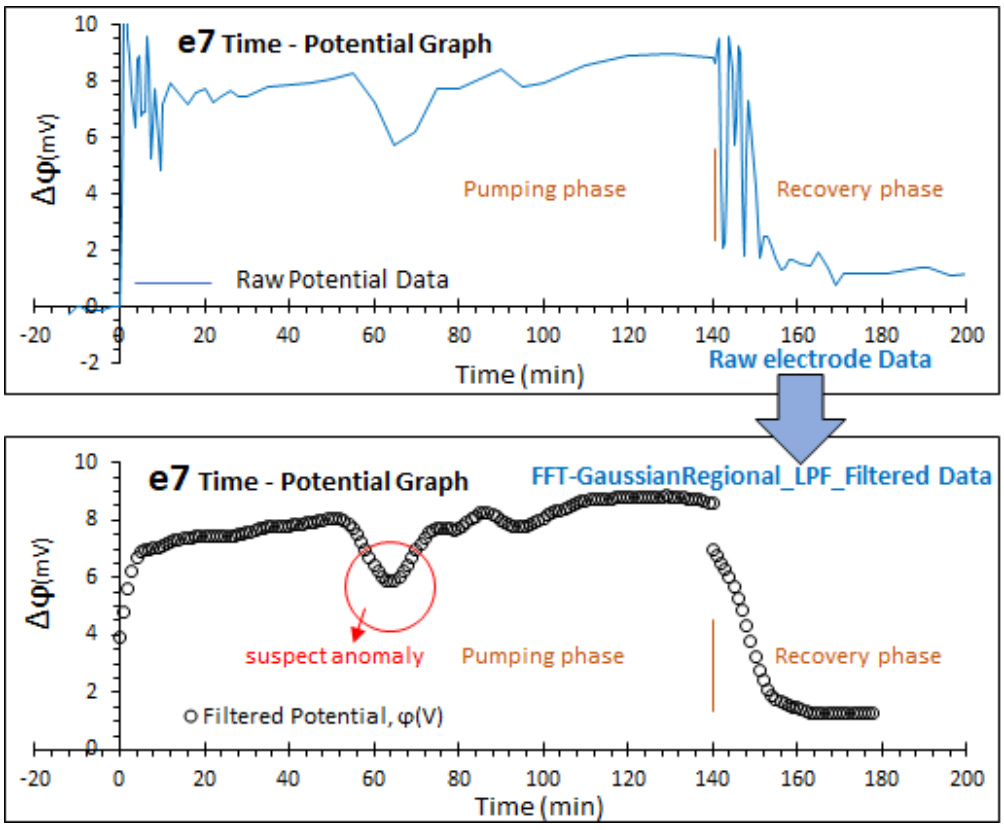

Potential- time graph for electrode *(e_7)* located at borehole BH7